**Universidade de Aveiro** Departamento de Biologia
**2013**

**ELIANA SOUSA CRUZ FERREIRA ALVES**

# INATIVAÇÃO FOTODINÂMICA DE BACTÉRIAS POR PORFIRINAS CATIÓNICAS

## Os seus alvos celulares e potenciais aplicações ambientais

# PHOTODYNAMIC INACTIVATION OF BACTERIA BY CATIONIC PORPHYRINS

## Their cellular targets and potential environmental applications

**Universidade de Aveiro** Departamento de Biologia
**2013**

**ELIANA SOUSA CRUZ FERREIRA ALVES**

# PHOTODYNAMIC INACTIVATION OF BACTERIA BY CATIONIC PORPHYRINS

## Their cellular targets and potential environmental applications

Tese apresentada à Universidade de Aveiro para cumprimento dos requisitos necessários à obtenção do grau de Doutor em Biologia, realizada sob a orientação científica da Doutora Maria Adelaide de Pinho Almeida, Professora Auxiliar do Departamento de Biologia da Universidade de Aveiro, e co-orientação científica da Doutora Maria Helena de Almeida Gonçalves Nadais, Professora Auxiliar do Departamento de Ambiente e Ordenamento da Universidade de Aveiro, e da Doutora Maria da Graça de Pinho Morgado da Silva Neves, Professora Associada com Agregação do Departamento de Química da Universidade de Aveiro

Apoio financeiro da Fundação para a Ciência e a Tecnologia e do Fundo Social Europeu no âmbito do III Quadro Comunitário de Apoio (bolsa de doutoramento SFRH/BD/41806/2007).

*A ti, eternamente amado irmão, Daniel*

**o júri**

presidente

Prof. Doutor António Manuel Melo de Sousa Pereira
Professor Catedrático do Departamento de Electrónica, Telecomunicações e Informática da Universidade de Aveiro

Prof. Doutor António Carlos Matias Correia
Professor Catedrático do Departamento de Biologia da Universidade de Aveiro

Prof. Doutora Maria da Graça de Pinho Morgado Silva Neves
Professora Associada com Agregação do Departamento de Química da Universidade de Aveiro

Prof. Doutora Maria Filomena Ribeiro Alcobia da Silva Trabucho Caeiro
Professora Auxiliar da Faculdade de Ciências da Universidade de Lisboa

Prof. Doutor João Maia Silva
Professor Auxiliar da Faculdade de Medicina da Universidade de Lisboa

Prof. Doutora Helena Maria Neto Ferreira de Sousa
Professora Auxiliar da Faculdade de Farmácia da Universidade do Porto

Prof. Doutora Maria Helena Gomes de Almeida Gonçalves Nadais
Professora Auxiliar do Departamento de Ambiente e Ordenamento da Universidade de Aveiro

Prof. Doutora Maria do Amparo Ferreira Faustino
Professora Auxiliar do Departamento de Química da Universidade de Aveiro

Prof. Doutora Maria Adelaide de Pinho Almeida
Professora Auxiliar do Departamento de Biologia da Universidade de Aveiro

**agradecimentos**

Ao longo dos últimos cinco anos, muitos foram os que contribuíram para a concretização do trabalho que aqui apresento. O percurso que culminou na defesa desta tese foi realizado com a ajuda de pessoas e entidades que não poderiam nunca ficar esquecidas.

À Professora Doutora Adelaide Almeida, orientadora, por ter sido e por continuar a ser muito mais do que orientadora. Pela confiança e incentivo, por acreditar no meu valor, por ser a supervisora que escolhi quando decidi mudar de rumo profissional.

À Professora Doutora Graça Neves, co-orientadora, pela forma entusiástica como sempre acompanhou o desenvolvimento da tese. Pelo rigor científico, pelo incentivo e pela disponibilidade.

À Professora Doutora Helena Nadais, co-orientadora, pela parceria que aceitou estabelecer connosco, pela disponibilidade mesmo perante trabalho nem sempre frutífero, pelas sugestões e comentários pertinentes.

À Professora Doutora Amparo Faustino, Professora Doutora Ângela Cunha e Doutor João Tomé. Pela proximidade que tiveram deste trabalho, pelo interesse, ajuda, exigência e rigor. Além disso, por me incluírem e considerarem a experimentar novos contextos, como o contato com universidades estrangeiras, os seminários, a Academia de Verão e o empreendedorismo.

Aos co-autores do trabalho científico publicado ou em processo de conclusão, pelo seu valioso contributo: Professor Doutor José Cavaleiro, Professor Doutor Augusto Tomé, Professor Doutor António Correia, Professora Doutora Rosário Domingues, Professora Doutora Ivonne Delgadillo, Professor Doutor Pedro Domingues, Doutor Zhi Lin, Doutor Newton Gomes e Doutora Luisa Helguero.

À Professora Doutora Rosário Domingues, uma palavra de especial apreço, por ter sido fundamental quando parte do plano inicialmente previsto tomou outra direção. O seu ânimo e espírito positivo são, para mim, uma inspiração. Obrigada por nos ter mostrado novos caminhos.

À Doutora Ana Cristina Esteves, não só pela preciosa colaboração, mas por ter feito a pergunta certa no momento exato.

Aos também co-autores, e colegas, com quem trabalhei de forma mais próxima, pela inestimável ajuda e cooperação: Doutora Carla Carvalho, Mestre Anabela Tavares, Mestre Tânia Melo, Mestre Ana Catarina Fernandes, Mestre João Rodrigues, Mestre Nuno Santos, Doutora Cláudia Simões, Mestre Luísa Dória e Mestre Elisabete Maciel.

Aos meus colegas de doutoramento que estiveram presentes, senão em todo, na maior parte deste período. Porque se tornaram companheiros de viagem e com quem estabeleci laços de amizade: Doutora Liliana Costa, Doutora Ana Luísa Santos, Doutora Luísa Santos, Mestre Inês Baptista, Mestre Carla Pereira, Mestre Catarina Prata, Mestre Vanessa Oliveira, Mestre Francisco Coelho, Mestre Clara Gomes, Licenciada Yolanda Silva e Licenciado António Pinto.

**agradecimentos**

Aos colegas que entre 2008 e 2012 desenvolveram os seus trabalhos no Laboratório de Microbiologia Ambiental e Aplicada, pela entreajuda, apoio, ou simplesmente partilha de vivências que nos marcaram. À Mestre Cátia Arrojado e ao Mestre Carlos Mendes. Não me esquecerei de quão amigos foram sempre, mas principalmente nos momentos mais difíceis.

Aos Técnicos Helena Dias e Armando Costa, e à D. Conceição Carvalho, cujo apoio técnico e logístico foram fundamentais, e que são muitas vezes o nosso SOS. Muito obrigada pela dedicação, disponibilidade e paciência.

À Professora Doutora Paula Gonçalves pela cedência do luminómetro e à Professora Doutora Virgília Silva que sempre foi disponível e incansável.

À Doutora Andreia Cruz e Doutora Tânia Caetano do Laboratório de Genética Molecular. Assim como há seis anos, agradeço-vos pela disponibilidade constante, pela ajuda solicitada, pela valiosa troca de ideias, sempre com um sorriso.

Aos colegas das Ciências Fotobiológicas, espalhados um pouco por toda a Europa, que conheci e com quem tive o prazer de conviver, que me fizeram ver, de uma forma muito mais abrangente, como toda a dedicação vale a pena e é recompensada.

A todos os que se cruzaram neste meu percurso, e que pelo seu pequeno contributo me ajudaram de alguma forma, expresso o meu profundo agradecimento.

Ao CESAM, por me ter acolhido nos primeiros passos na investigação científica.

Ao QOPNA, minha segunda casa, que sempre tão bem me recebeu.

À Universidade de Aveiro, porque me permitiu encontrar um caminho. Por me dar uma mão cheia de oportunidades. Por criar profissionais de valor, dos quais me orgulho de fazer parte.

À FCT, por financiar o meu trabalho.

Às minhas meninas, Daniela, Guida, Mónica, Rita, Sara e Sofia. Obrigada pela vossa amizade.

Aos familiares e amigos que fazem parte da minha vida, que estiveram mais próximos e me acompanharam nesta aventura, vivida intensamente. Por todo o vosso apoio e encorajamento, pelos momentos que partilhamos e por tudo o que me permitiram aprender, vos agradeço.

À “minha equipa”. Ser-vos-ei eternamente grata.

Aos meus pais, por serem os meus maiores Mestres.

Ao meu irmão, a quem dedico este trabalho.

**palavras-chave**

*Escherichia coli*, *Staphylococcus warneri*, porfirinas catiónicas, espécies reativas de oxigénio, inativação fotodinâmica, stress oxidativo, peroxidação lipídica, ácidos nucleicos, oxidação proteica, espetroscopia de infravermelho, bioluminescência, *Vibrio fischeri*, aquacultura, nanopartículas magnéticas

**resumo**

A inativação fotodinâmica (IF) é definida como o processo de destruição celular por stress oxidativo, causado pela interação entre uma fonte de luz, um fotossensibilizador (FS) e oxigénio molecular. A IF de bactérias tem sido extensivamente estudada nos últimos anos, demonstrando ser uma alternativa promissora aos agentes antimicrobianos convencionais para o tratamento de infeções superficiais e localizadas. Além disso, a aplicabilidade da IF vai muito para além do âmbito clínico, estando em estudo o seu potencial uso na desinfeção de águas recorrendo a FS imobilizados em suportes sólidos.

A primeira parte deste trabalho teve como objetivo estudar as modificações oxidativas nos fosfolípidos, nos ácidos nucleicos e nas proteínas da bactéria Gram-negativa *Escherichia coli* e da bactéria Gram-positiva *Staphylococcus warneri*, sujeitas ao tratamento fotodinâmico com porfirinas catiónicas. A segunda parte do trabalho teve como principais objetivos estudar a eficiência da IF em águas de aquacultura e a influência de diferentes parâmetros físico-químicos neste processo, usando como modelo celular a bactéria Gram-negativa bioluminescente *Vibrio fischeri* e por fim, avaliar a possibilidade de reciclagem de FS catiónicos imobilizados em nanopartículas magnéticas.

Para estudar as modificações oxidativas nos fosfolípidos membranares foi utilizada uma abordagem lipidómica que combinou técnicas de cromatografia e espetrometria de massa. O ensaio de FOX2 foi utilizado para determinar a concentração de hidroperóxidos lipídicos gerados após tratamento. As modificações oxidativas nas proteínas totais foram avaliadas por eletroforese unidimensional em gel de poliacrilamida (SDS-PAGE). As alterações no conteúdo intracelular de ácidos nucleicos foram avaliadas por eletroforese em gel de agarose e a quantificação de DNA de cadeia dupla foi determinada por fluorimetria. As alterações oxidativas da IF a nível molecular foram avaliadas por espetroscopia de infravermelho. Nos ensaios laboratoriais, as bactérias ($10^8$ UFC $mL^{-1}$) foram irradiadas com luz branca (4.0 mW $cm^{-2}$), após incubação com o FS (Tri-$Py^+$-Me-PF ou Tetra-$Py^+$-Me) nas concentrações de 0.5 e 5.0 µM, para *S. warneri* e *E. coli*, respetivamente. As bactérias foram irradiadas com diferentes doses de luz (até 9.6 J $cm^{-2}$ para *S. warneri* e 64.8 J $cm^{-2}$ para *E. coli*) e as alterações foram determinadas ao longo do tempo de irradiação. No estudo dos fosfolípidos apenas foi testada a porfirina Tri-$Py^+$-Me-PF e uma dose de luz de 64.8 J $cm^{-2}$.

A eficiência da IF no contexto de aquacultura foi avaliada em duas condições diferentes: em solução tampão, variando a temperatura, pH, salinidade e concentração de oxigénio; e em amostras de água de aquacultura, para reproduzir as condições de fotoinativação *in situ*. Para monitorizar a cinética do processo em tempo real, registou-se o valor da bioluminescência de *V. fischeri* durante os ensaios. Foi usada uma concentração de 5.0 µM de Tri-$Py^+$-Me-PF nos estudos com solução tampão e 10 a 50 µM nos estudos com água de aquacultura. A luz branca artificial (4.0 mW $cm^{-2}$) e a irradiação solar (40 mW $cm^{-2}$) foram utilizadas como fontes de luz. A concentração bacteriana utilizada para todos os ensaios foi $10^7$ UFC $mL^{-1}$ (correspondente a um nível de bioluminescência de $10^5$ unidades relativas de luz).

A eficiência da IF de *V. fischeri* por híbridos nanomagnete-porfirina (porfirina Tri-$Py^+$-Me-PF imobilizada em nanopartículas de $Fe_3O_4$ e $CoFe_2O_4$) foi testada em ciclos de reciclagem e reutilização. A foto-estabilidade da porfirina Tri-$Py^+$-Me-PF não imobilizada foi avaliada por espetrofotometria de UV-visível, e a foto-oxidação dos núcleos magnéticos das nanopartículas por difração de raios X, após 24 h de irradiação em suspensão aquosa.

**resumo**

Os resultados deste trabalho mostraram que *E. coli* foi totalmente inativada com ambas as porfirinas, enquanto *S. warneri* foi completamente inativado apenas com a Tri-$Py^{+}$-Me-PF, ao fim do tempo de irradiação previamente estabelecido.

A IF induziu alterações no perfil fosfolipídico bacteriano, com aumento da abundância relativa de algumas das classes maioritárias de fosfolípidos, decréscimo de ácidos gordos insaturados, formação de espécies moleculares oxidadas a partir de ácidos gordos insaturados, nomeadamente nas cardiolipinas de *S. warneri* e nas fosfatidiletanolaminas de *E. coli*. Estas espécies oxidadas foram identificadas como derivados hidroxi e hidroperoxi (observados em *E. coli*) e também grupos carbonilo (em *S. warneri*). A formação de hidroperóxidos lipídicos confirmou os danos oxidativos nos fosfolípidos.

A IF causou redução do conteúdo intracelular dos ácidos nucleicos bacterianos. Em *E. coli* observou-se a seguinte hierarquia de modificações: rRNA 23S > rRNA 16S > DNA genómico. Os ácidos nucleicos de *S. warneri* foram extensivamente reduzidos com a Tri-$Py^{+}$-Me-PF após 5 min de irradiação, mas menos reduzidos com a Tetra-$Py^{+}$-Me, após 40 min de irradiação. Esta degradação dos ácidos nucleicos ocorreu paralelamente à inativação e quando as células já estavam inativadas mais do que 99.9%.

A IF induziu uma diminuição geral do conteúdo proteico de ambas as bactérias, sugerindo degradação em larga escala, ocorrendo as alterações de forma mais rápida e evidente com a porfirina Tri-$Py^{+}$-Me-PF. Observou-se o aumento da expressão de algumas proteínas, alterações no peso molecular, desaparecimento após tratamento e formação de novas proteínas. As alterações foram associadas a mecanismos de resposta ao stress oxidativo.

A espetroscopia de infravermelho mostrou ser um método rápido e económico de avaliar as alterações induzidas pela IF ao nível molecular. Evidenciou os resultados obtidos pelos métodos convencionais com maior detalhe, nomeadamente ao nível das ligações, grupos funcionais e conformações moleculares.

As variações de pH (6.5 - 8.5), temperatura (10 - 25 ºC), salinidade (20 - 40 g $L^{-1}$) e concentração de oxigénio não afetaram significativamente a IF de *V. fischeri*, uma vez que em todas as condições testadas o sinal bioluminescente diminuiu até ao limite de deteção do método (redução ≈ 7 $\log_{10}$). Os ensaios com água de aquacultura mostraram que a eficiência do processo é afetada pela presença de matéria em suspensão. A IF total de *V. fischeri* em água de aquacultura foi conseguida com luz solar na presença de 20 µM de Tri-$Py^{+}$-Me-PF.

Os híbridos nanomagnete-porfirina puderam ser reutilizados em 6 ciclos de IF e reciclados em 3 ciclos. Na reciclagem, houve perda de atividade de ciclo para ciclo, atribuída à perda de nanopartículas durante a recuperação. A acumulação de matéria orgânica causou uma redução da eficiência do processo durante a reutilização, contudo foi observada a eliminação de 38 a 42 $\log_{10}$ de bactérias ao fim de 21h30 a 27h de tratamento. O FS não foi foto-degradado e a magnetite das nanopartículas não foi afetada pela irradiação ou pela oxidação inerente ao processo fotodinâmico.

O presente trabalho demonstrou o caráter multi-alvo da inativação fotodinâmica, pela elucidação dos mecanismos oxidativos que ocorrem ao nível dos principais constituintes moleculares das bactérias. Também demonstrou que a inativação fotodinâmica é uma metodologia com potencial para ser implementada na desinfeção de águas de aquacultura utilizando fotossensibilizadores imobilizados, permitindo a sua reutilização e reciclagem, com a possibilidade de reduzir os custos associados a este tipo de tratamento.

**keywords**

*Escherichia coli*, *Staphylococcus warneri*, cationic porphyrins, reactive oxygen species, oxidative stress, lipid peroxidation, nucleic acids, protein oxidation, infrared spectroscopy, bioluminescence, *Vibrio fischeri*, aquaculture, magnetic nanoparticles

**abstract**

Photodynamic inactivation (PDI) is defined as the process of cell destruction by oxidative stress resulting from the interaction between light and a photosensitizer (PS), in the presence of molecular oxygen. PDI of bacteria has been extensively studied in recent years, proving to be a promising alternative to conventional antimicrobial agents for the treatment of superficial and localized infections. Moreover, the applicability of PDI goes far beyond the clinical field, as its potential use in water disinfection, using PS immobilized on solid supports, is currently under study.

The aim of the first part of this work was to study the oxidative modifications in phospholipids, nucleic acids and proteins of *Escherichia coli* and *Staphylococcus warneri*, subjected to photodynamic treatment with cationic porphyrins. The aims of the second part of the work were to study the efficiency of PDI in aquaculture water and the influence of different physical-chemical parameters in this process, using the Gram-negative bioluminescent bacterium *Vibrio fischeri*, and to evaluate the possibility of recycling cationic PS immobilized on magnetic nanoparticles.

To study the oxidative changes in membrane phospholipids, a lipidomic approach has been used, combining chromatographic techniques and mass spectrometry. The FOX2 assay was used to determine the concentration of lipid hydroperoxides generated after treatment. The oxidative modifications in the proteins were analyzed by one-dimensional polyacrylamide gel electrophoresis (SDS-PAGE). Changes in the intracellular nucleic acids were analyzed by agarose gel electrophoresis and the concentration of double-stranded DNA was determined by fluorimetry. The oxidative changes of bacterial PDI at the molecular level were analyzed by infrared spectroscopy. In laboratory tests, bacteria ($10^8$ CFU $mL^{-1}$) were irradiated with white light (4.0 mW $cm^{-2}$) after incubation with the PS (Tri-$Py^+$-Me-PF or Tetra-$Py^+$-Me) at concentrations of 0.5 and 5.0 µM for *S. warneri* and *E. coli*, respectively. Bacteria were irradiated with different light doses (up to 9.6 J $cm^{-2}$ for *S. warneri* and up to 64.8 J $cm^{-2}$ for *E. coli*) and the changes were evaluated throughout the irradiation time. In the study of phospholipids, only the porphyrin Tri-$Py^+$-Me-PF and a light dose of 64.8 J $cm^{-2}$ were tested.

The efficiency of PDI in aquaculture has been evaluated in two different conditions: in buffer solution, varying temperature, pH, salinity and oxygen concentration, and in aquaculture water samples, to reproduce the conditions of PDI *in situ*. The kinetics of the process was determined in real-time during the experiments by measuring the bioluminescence of *V. fischeri* ($10^7$ CFU $mL^{-1}$, corresponding to a level of bioluminescence of $10^5$ relative light units). A concentration of 5.0 µM of Tri-$Py^+$-Me-PF was used in the experiments with buffer solution, and 10 to 50 µM in the experiments with aquaculture water. Artificial white light (4.0 mW $cm^{-2}$) and solar irradiation (40 mW $cm^{-2}$) were used as light sources.

**abstract**

The efficiency of the PDI of *V. fischeri* with nanomagnet-porphyrin hybrids (porphyrin Tri-$Py^+$-Me-PF immobilized on $Fe_3O_4$ and $CoFe_2O_4$ nanoparticles) was assessed in recycling and reuse experiments. The photo-stability of the free porphyrin (Tri-$Py^+$-Me-PF) was assessed by UV-vis spectrometry and the photo-oxidation of the magnetic cores of the nanoparticles was assessed by X-ray diffraction, after 24 h of irradiation in aqueous suspension.

The results showed that *E. coli* was completely inactivated with both porphyrins and *S. warneri* was completely inactivated only with Tri-$Py^+$-Me-PF, after the pre-established irradiation time.

PDI induced changes in bacterial phospholipid profile, increasing the relative abundance of some of the major classes of phospholipids, decreasing unsaturated fatty acids, generating oxidized molecular species from unsaturated fatty acids, in particular in cardiolipins from *S. warneri* and phosphatidylethanolamines from *E. coli*. These oxidized species were identified as hydroxy and hydroperoxy derivatives (observed in *E. coli*) as well as bearing carbonyl groups (in *S. warneri*). The formation of lipid hydroperoxides confirmed oxidative damage in phospholipids.

PDI caused a reduction of intracellular nucleic acids. In *E. coli*, the following hierarchy of modifications was observed: 23S rRNA > 16S rRNA > genomic DNA. Nucleic acids of *S. warneri* were extensively reduced with Tri-$Py^+$-Me-PF after 5 min of irradiation, but less affected with Tetra-$Py^+$-Me after 40 min of irradiation. The degradation of nucleic acids was parallel to the inactivation and when more than 99.9 % of the cells were inactivated.

PDI induced a decrease in overall protein content of both bacteria, suggesting large-scale degradation, with more evident changes with Tri-$Py^+$-Me-PF. There was increased expression of certain proteins, changes in their molecular weight, disappearance after treatment, and formation of new proteins. These changes were associated with response mechanisms to oxidative stress.

Infrared spectroscopy proved to be a fast and economic tool to screen the modifications induced by PDI at the molecular level, supporting the results obtained by conventional methods in more detail, particularly in terms of bonding types, functional groups and molecular conformations.

Variations in pH (6.5 - 8.5), temperature (10 - 25 ºC), salinity (20 - 40 g $L^{-1}$) and oxygen concentration did not significantly affect the PDI of *V. fischeri*, since in all tested conditions the bioluminescent signal decreased to the limit of detection (≈ 7 $\log_{10}$ survival reduction). The experiments with aquaculture water showed that the process efficiency is affected by the presence of suspended matter. Total inactivation of *V. fischeri* in aquaculture water was achieved with sunlight in the presence of 20 µM of Tri-$Py^+$-Me-PF.

Nanomagnet-porphyrin hybrids could be reused in 6 cycles of PDI and recycled in 3 cycles. In recycling, there was loss of activity from cycle to cycle assigned to nanoparticle loss during recovery. The accumulation of organic matter caused a reduction in the efficiency of the process during reuse experiments; however, there was a reduction of 38 to 42 $\log_{10}$ of bacteria after 21h30 to 27 h of treatment. The PS was not photo-degraded and the magnetite from the nanoparticles was not affected by irradiation or by oxidation inherent to the photodynamic process.

This work demonstrated the multi-target nature of photodynamic inactivation, by elucidating the oxidative mechanisms that occur at the main molecular components of bacteria. It also shown that photodynamic inactivation is a methodology with potential to be implemented in the disinfection of aquaculture water, using immobilized photosensitizers, allowing their recycling and reuse, with the possibility of reducing the costs associated with this type of treatment.

# Table of Contents

## List of Abbreviations

| | |
|---|---|
| $^1O_2$ | singlet oxygen |
| AFM | atomic force microscopy |
| ALA | aminolevulinic acid |
| ANOVA | analysis of variance |
| aPDT | antimicrobial photodynamic therapy |
| ATP | adenosine triphosphate |
| BHT | butylated hydroxytoluene |
| CFU | colony forming unit |
| CL | cardiolipin |
| DC | dark control |
| DLS | dynamic light scattering |
| DMSO | dimethyl sulfoxide |
| dsDNA | double-stranded deoxyribonucleic acid |
| EDS | energy-dispersive X-ray spectroscopy |
| EDTA | ethylenediamine tetraacetic acid |
| ESI | electrospray ionization |
| FMN | flavin mononucleotide |
| GC-FID | gas chromatography with flame ionization detector |
| GC-MS | gas chromatography-mass spectrometry |
| HILIC | hydrophilic interaction liquid chromatography |
| Hpde | hematoporphyrin derivative dimethyl ether |
| HpIX | hematoporphyrin IX derivative |
| HPLC | high-performance liquid chromatography |
| HSP | heat shock protein |
| ICCD | intensified charge-coupled device |
| ISC | intersystem crossing |
| LC | light control |
| $LD_{50}$ | median lethal dose |
| LED | light emitting diode |
| LOOH | lipid hydroperoxide |
| LPG | lysyl-phosphatidylglycerol |
| LPS | lipopolysaccharide |
| lx | lux |
| MB | methylene blue |
| MIC | minimum inhibitory concentration |
| MRSA | methicillin-resistant *Staphylococcus aureus* |
| MS | mass spectrometry |
| NADH | nicotinamide adenine dinucleotide |
| NADPH | nicotinamide adenine dinucleotide phosphate |
| NMR | nuclear magnetic resonance |
| NP | nanoparticle |
| OD | optical density |
| OMP | outer membrane protein |
| PA | phosphatidic acid |

| | |
|---|---|
| PACT | photodynamic antimicrobial chemotherapy |
| PAGE | polyacrylamide gel electrophoresis |
| PBS | phosphate buffered saline |
| PCR | polymerase chain reaction |
| PDI | photodynamic inactivation |
| PDT | photodynamic therapy |
| PE | phosphatidylethanolamine |
| PG | phosphatidylglycerol |
| PI | phosphatidylinositol |
| PL | phospholipid |
| PPIX | protoporphyrin IX |
| PS | photosensitizer |
| RB | rose Bengal |
| RLU | relative light units |
| ROS | reactive oxygen species |
| RPM | revolutions per minute |
| rRNA | ribosomal ribonucleic acid |
| SDS | sodium dodecyl sulphate |
| SEM | scanning electron microscopy |
| TAE | Tris-acetate-EDTA |
| TBO | toluidine blue O |
| TEM | transmission electron microscopy |
| TLC | thin-layer chromatography |
| TSA | triptic soy agar |
| TSB | triptic soy broth |
| UV | ultraviolet |
| XO | xylenol orange |
| XRD | X-ray diffraction |

## Thesis outline

This thesis documents the research work carried out in the area of photodynamic inactivation of bacteria using cationic porphyrins as photosensitizers.

The study of this therapeutic modality acquires high importance and timeliness in so far as the current use of antimicrobial agents to combat infections faces serious problems of microbial resistance. On the other hand, the scarcity of water resources and the lack of proper treatment of effluents, calls for investment in new methods of water disinfection, for which the photodynamic inactivation may be an alternative.

This document is divided into two parts, with different general purposes.

Both parts begin with in-depth literature reviews (chapters 1, 7 and 8) serving as a basis for the following experimental work.

In the first part (chapters 2 to 6), the damages induced by photosensitization in key cellular components of bacteria (phospholipids, proteins and nucleic acids) were assessed using reference methods and a fast method, in order to get a better understanding of the underlying mode of action of the photodynamic process in these cells. In the experiments, two bacterial strains with clinical relevance were used: the Gram-positive bacterium *Staphylococcus warneri* and the Gram-negative bacterium *Escherichia coli*.

In the second part (chapters 9 and 10), the potential application of photodynamic inactivation was evaluated in the environmental context, as a method of disinfecting water and capable of being recyclable. In the experiments, the naturally bioluminescent Gram-negative marine bacterium *Vibrio fischeri* was used.

The two selected cationic porphyrins differ in the number of charges and in the meso substituents. The porphyrin 5,10,15-tris(1-methylpyridinium-4-yl)-20-(pentafluorophenyl)porphyrin triiodide (Tri-Py$^{+}$-Me-PF) is a promising and efficient derivative synthesized in the Department of Chemistry of University of Aveiro and was generally compared with the well-studied 5,10,15,20 tetrakis(1-methylpyridinium-4-yl)porphyrin (Tetra-Py$^{+}$-Me).

Chapter 1 intended to provide insight into the mechanism of action of photodynamic inactivation of bacteria with greater focus on specific cellular targets, reviewing the most recent literature on this subject.

Chapter 2 describes a preliminary study on the oxidative damage of *S. warneri* phospholipids through the photodynamic process with the porphyrin Tri-Py$^{+}$-Me-PF, using mass spectrometry-based analysis of lipids.

In chapter 3, the same methodological approach was employed in order to study the oxidative damage of *E. coli* phospholipids upon photosensitization with Tri-$Py^{+}$-Me-PF.

Chapter 4 presents the oxidative effects of photodynamic inactivation on the intracellular nucleic acids of *S. warneri* and *E. coli* photosensitized with both cationic porphyrins, by agarose gel electrophoresis and fluorimetry.

Chapter 5 intended to evaluate the oxidative effects induced by photosensitization in the protein profile of both bacteria with both cationic porphyrins, using one-dimensional sodium dodecyl sulfate-polyacrylamide gel electrophoresis.

Chapter 6 reports the study of the global biomolecular changes induced by the photodynamic process on both bacteria with both porphyrins, assessed by infrared spectroscopy.

Chapter 7 reviews the potential applications of photodynamic inactivation of microorganisms and organisms in non-clinical context, using porphyrins as photosensitizers.

Chapter 8 emphasizes the importance and usefulness of microbial bioluminescence as a fast, easy and efficient means to monitor the photoinactivation process, in clinical and environmental experiments, using bioluminescent strains of microorganisms.

Chapter 9 studied the efficiency of photodynamic inactivation in aquaculture water. The influence of various physical and chemical parameters of the artificial aqueous medium was assessed during photoinactivation of *V. fischeri*. Additionally, the efficiency of the photoinactivation of this bacterium was evaluated in aquaculture water samples.

Chapter 10 describes the synthesis and characterization of porphyrins immobilized in solid supports of magnetic character. Their recovery, reuse and recycling after photoinactivation of *V. fischeri* was also tested in several cycles on a small scale. In these studies, the bioluminescent method was used to monitor the kinetics of photoinactivation.

At last, chapter 11 presents the main conclusions of the thesis.

# Part I

# Chapter 1. An insight on bacterial cellular targets of photodynamic inactivation

The content of this chapter is currently under peer-review.
Alves E, Tomé JPC, Faustino MAF, Neves MGPMS, Cunha Â, Almeida A. An insight on bacterial cellular targets of photodynamic inactivation. Future Medicinal Chemistry. submitted.

# 1 An insight on bacterial cellular targets of photodynamic inactivation

## 1.1 Abstract

The emergence of microbial resistance is becoming a global problem in clinic and environmental areas. As such, the development of drugs with novel modes of action will be vital to meet the threats created by the rise in microbial resistance. Microbial photodynamic inactivation is receiving considerable attention for its potentialities as a new antimicrobial treatment. This review addresses the interactions between photosensitizers and bacterial cells (binding site and cellular localization), the ultrastructural, morphological and functional changes observed at initial stages and during the course of photodynamic inactivation, the oxidative alterations in specific molecular targets, and a possible development of resistance.

## 1.2 Background

Antimicrobial resistance is a global threat that is continually increasing. Scientific advances can no longer keep up with this increase. In Europe, it is estimated that every year there are about 25,000 deaths from hospital-acquired bacterial infections. (1) Among the multi-resistant bacteria with higher incidence are methicillin-resistant *Staphylococcus aureus* (MRSA), vancomycin-resistant *Enterococcus faecium*, third-generation cephalosporin-resistant *Escherichia coli*, third-generation cephalosporin-resistant *Klebsiella pneumoniae* and carbapenem-resistant *Pseudomonas aeruginosa*. (1)

As morbidity and mortality from bacterial infections assumes increasing economic and social impact, urgent action to reverse this situation is required. In addition to the need to promote an adequate and rationalized use of antimicrobials, it is imperative to develop innovative therapeutic approaches. (2)

The mode of action of an antibiotic is defined by the way it binds to a specific target, inhibiting cell function and, consequently, cell growth. (3) Its action spectrum is limited, resulting from the direct inhibition of cell-wall assembly, inhibition of cytoplasmic membrane function, inhibition of protein synthesis or DNA replication. (4) Because of this specificity, chemical or morphological changes on the target and also the overexpression of efflux pumps and the synthesis of drug-degrading enzymes can lead to a decreased efficacy of the drug (5, 6) and, therefore, to the development of resistance to a specific class of antibiotics used. (7) In this regard, a multi-target antimicrobial approach would be suitable to overcome the resistance problem.

The inactivation of microorganisms by oxidative stress can be induced by administering a photoactive compound (photosensitizer, PS) with subsequent activation by light. The outcome from the action between PS and visible light, in the presence of molecular oxygen, are irreversible damages at various molecular constituents of cells (lipids, proteins, enzymes, DNA). (8, 9) This approach is called photodynamic antimicrobial chemotherapy (PACT) (10) or antimicrobial photodynamic inactivation (PDI), which has emerged as a promising alternative for the treatment of localized infections. (11, 12)

In PDI, most studied PS are based on tetrapyrrolic macrocycles, with particular emphasis on porphyrins. (13) Many other compounds, including phenothiaziniums and xanthene dyes have been envisioned as potential candidates. (14) In Figure 1.1 are depicted the chemical structures of some families of PS used in PDI and the corresponding acronyms discussed in this review.

The photodynamic effect triggers electron transfer reactions or energy transfer from the light to the surroundings (Figure 1.2). In the presence of light (hv), the $^1$PS in the ground state ($S_0$) absorbs a photon and goes to $^1$PS*, an excited singlet state ($S_n$). Then, it can lose energy by fluorescence emission (F) returning to $S_0$ or by an intersystem crossing (ISC) process it can be converted to an excited triplet state $^3PS^*$ ($T_1$). In this state, the return to the ground state ($S_0$) can occur by phosphorescence emission (P) or by energy transfer to ground state molecular oxygen ($^3O_2$) (type II mechanism) or by electron transfer to the surrounding substrates (type I mechanism), leading to the formation of reactive oxygen species. (8) Both mechanisms may occur simultaneously but type II is described as the predominant for the PS used in photodynamic procedures. (15)

Singlet oxygen ($^1O_2$) is highly reactive and has an extremely short lifetime due to its unstable electronic configuration. Its lifetime in water is approximately 3 - 4 μs and its diffusion range is limited, depending on the surrounding medium (16, 17); in pure water it is about 1 μm (18) and is less than 50 nm in protein-rich lipid layers. (18-21)

One of the most important features of the PS is to have a high $^1O_2$ quantum yield ($\Phi_\Delta$) (16) as it is reported for rose Bengal, $\Phi_\Delta$ = 0.76 (22), methylene blue, $\Phi_\Delta$ = 0.39 (17) or 5,10,15,20 tetrakis(1-methylpyridinium-4-yl)porphyrin (Tetra-Py$^+$-Me), $\Phi_\Delta$ = 0.74. (8) Although a high generation of $^1O_2$ is considered an essential requirement, a PS should ideally have other characteristics such as: photostability; amphiphilicity; selectivity for the target cells; solubility; and absence of dark toxicity or mutagenicity. (23, 24)

Another important aspect for an efficient bacterial photoinactivation is the net charge of the PS that must be positive concerning the photoinactivation of Gram-negative bacteria, since there is lack of activity of anionic and neutral PS against this type of bacteria. This condition

relates to the structure of the bacterial wall (Figure 1.3). Gram-positive bacteria have a cell wall composed of lipoteichoic and teichoic acids organized in multiple layers of peptidoglycan (30 - 100 nm) (25), which confers a degree of porosity to bacteria that allows the penetration of the PS into the cell. In Gram-negative bacteria, the presence of an intricate outer membrane in the cell wall creates an impermeable barrier to antimicrobial agents. The outer membrane consists of glycolipids in the outer leaflet, mainly lipopolysaccharides, lipoproteins and β-barrel proteins, a phospholipid bilayer in the inner leaflet which anchors these constituents, and peptidoglycan (2 - 7 nm). (25, 26)

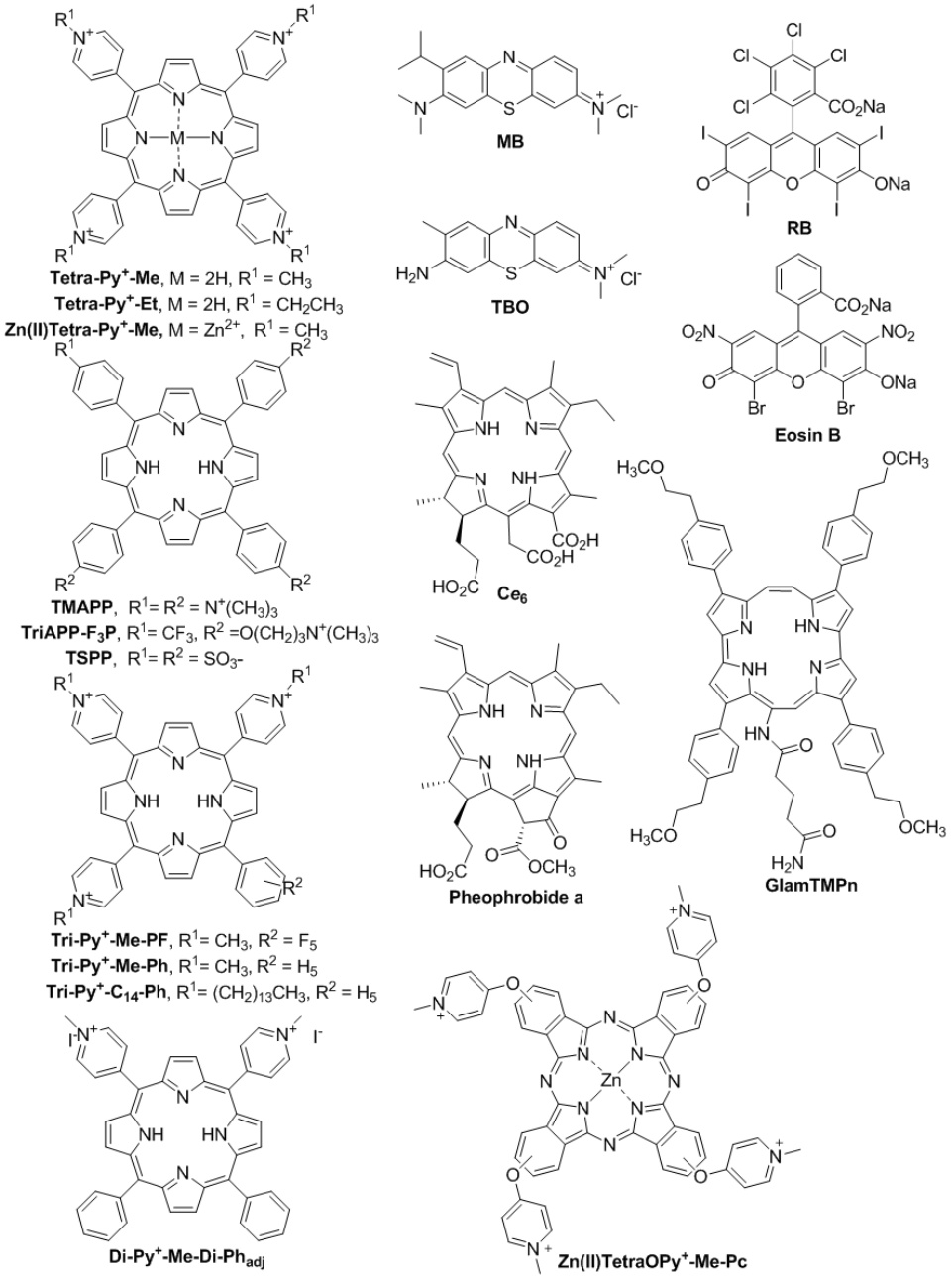


**Figure 1.1** Some of the photosensitizer structures and corresponding acronyms discussed in this review. MB, methylene blue; TBO, toluidine blue O; RB, rose Bengal; C*e*$_6$, chlorin $e_6$

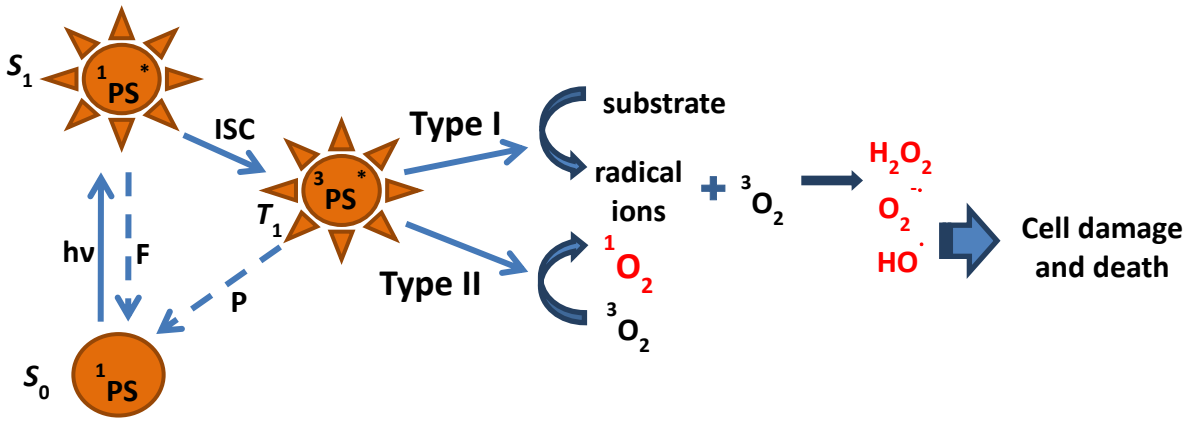


**Figure 1.2** Photoprocesses that occur during photodynamic inactivation.

Lipopolysaccharides (LPS) play a critical role in the cell defense against antimicrobial agents. They are composed by a hydrophobic component (lipid A), core polysaccharides, and *O*-antigen repeats at the cell's surface. (27) Molecules of LPS can avidly join, particularly if divalent cations such as $Mg^{2+}$ and $Ca^{2+}$ are present in the cell surface, stabilizing the negative charge of the phosphate groups in the molecules. Since the acyl chains are highly saturated, they promote a strong accommodation of LPS. (27) The electrostatic forces generated between the positively charged PS and the constituents of the Gram-negative cell wall promote the destabilization of the wall native organization (12, 28), allowing the binding and eventual penetration of the PS into the cell. For this reason, the cationic PS have broader spectrum of action.

Additionally to the ability to photoinactivate drug sensitive and multidrug-resistant bacterial strains, PDI has also been shown to be very effective in eliminating viruses, fungi and parasites with PS concentrations at micromolar range. (11-13, 29, 30) The multi-target nature of PDI minimizes the risk of resistance development which provides an advantage over conventional antibiotics.

In order to obtain new insights on the action mechanism of PDI in bacteria, several studies have been focused on: i) how a specific PS interacts with the cell, ii) the cellular region where it is located, iii) the ultra-structural, morphological and functional changes taking place at initial stages and during PDI; iv) oxidative alterations in specific molecular targets and; v) the possibility of developing resistance.

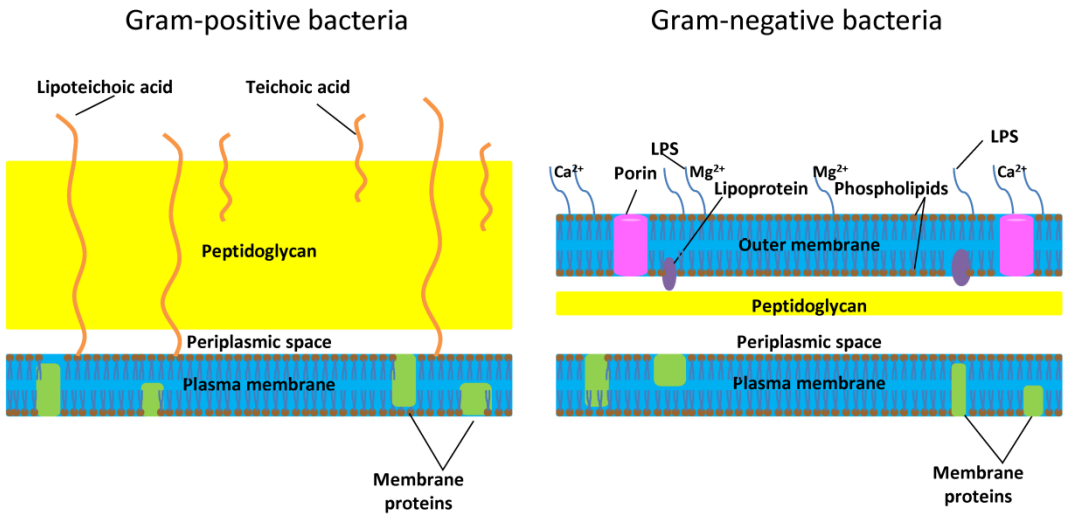


**Figure 1.3** Schematic illustration of the cellular envelope of Gram-positive and Gram-negative bacteria.

## 1.3 Interactions between photosensitizers and cellular constituents

PS molecules bounded to the outer membrane may interact with different cellular constituents based on their affinities for these components. In particular, cationic PS have high affinity for anionic biopolymers of the outer wall of Gram-negative bacteria, such as LPS, proteins and some classes of phospholipids.

The phenothiazinium dyes such as methylene blue (MB) and toluidine blue O (TBO) possess similar photophysical and photochemical properties (31) but their efficiency in bacterial photoinactivation is different, being higher in the case of TBO. (32) On the other hand, while the uptake of these two PS by bacteria is the same, the specific binding to individual constituents of outer membrane of Gram-negative bacteria is different. TBO has a higher affinity for LPS, and MB for proteins, in this case possibly due to primary binding to siderophores. (33) These small molecules (400 - 2000 Da), linked to receptor proteins, facilitate the transport of external molecules such as iron or antibiotics across the membrane. A complex formed between the PS and the siderophore-receptor protein would translocate the PS throughout the membrane. (33) Thus, the damage caused by these phenothiazinium dyes appears to rely on distinct mechanisms. Once TBO is more efficient than MB, the mechanism involving LPS appears to be more effective (34) than that involving proteins. Having in regard the multi-target nature of PDI, both mechanisms can coexist and also involve other anionic membrane polymers. (33)

The phospholipid membranes of Gram-negative bacteria are composed mainly by zwitterionic phosphatidylethanolamines (PEs, 70 - 75% of total phospholipids) and anionic phosphatidylglycerols (PGs, 20 - 25% of total phospholipids). (35) The affinity of cationic

peptides to PGs seems to be higher than for LPS due to the easier accessibility to the anionic phospholipid group compared to that of LPS. (36) On the other hand, in the Gram-positive bacteria, PGs represent the major phospholipid class. (37) The absence of an outer membrane and the porous structure of the peptidoglycan cell wall allow the entry of these PS molecules through the cell wall and the electrostatic binding with the phosphate groups of PGs. Not only the PS can bind to PGs but it can also cause defects or rearrangements in these molecules. (38) This observation may explain why the binding and the photoinactivation of this type of bacteria is more efficient in the presence of cationic PS.

The interaction of porphyrinic PS with membrane phospholipids of Gram-negative bacteria does not seem to be only of electrostatic nature. It should be considered the relative position (immersion depth) and the orientation of the PS on the membrane-water interface, which determine its degree of hydrophobicity and, consequently, the connection with the membrane. (39) Studies involving cationic porphyrins in Gram-negative membrane models showed that Tetra-$Py^{+}$-Me and 5,10,15-tris(1-methylpyridynium-4-yl)-20-phenylporphyrin chloride (Tri-$Py^{+}$-Me-Ph) (PS with four and three positive charges, respectively) stay almost flat relatively to the phospholipid bilayer, while 5,10-bis(1-methylpyridynium-4-yl)-15,20-diphenylporphyrin chloride (Di-$Py^{+}$-Me-Di-$Ph_{adj}$, a PS with two adjacent positive charges) has a large immersion depth. The phenyl groups attached to the porphyrinic ring enter the membrane but the charged substituents (pyridynium groups) do not go beyond the region of carbonylester group (polar head) of the phospholipid. (39) This spatial arrangement of the PS on the membrane prevents the complete neutralization of the charges because not all substituents are involved in electrostatic interactions. (40) Besides, the presence of a metal cation in the center of the macrocycle seems to contribute to a higher neutralization of the charges which is higher for the 5,10,15,20-tetrakis(1-methylpyridynium-4-yl)porphyrinato zinc(II) (Zn(II)Tetra-$Py^{+}$-Me) than for the corresponding free-base Tetra-$Py^{+}$-Me. (40) This higher neutralization increases significantly the electrostatic attraction between the porphyrin and phospholipids as a result of an effective metal-phosphate coordination. (41) In addition to the affinity of PS for different cellular components, also the number of positive charges, the degree of hydrophobicity and the spatial distribution of substituents seem to play an important role in these relationships.

It is well known that charged PS such as porphyrins or phthalocyanines are able to bind to and interact with DNA in different ways. These interactions occur via intercalation between guanine-cytosine base pairs, or externally by groove-binding at adenine-thymine sites or by PS self-stacking binding. (42-44) This interaction may be influenced by the number and position of the charges (45, 46) as well as by the peripheral substituents and metal ions present in the

macrocycle. (47) PDI-induced DNA damage may occur by three mechanisms: direct interaction between excited PS molecules with DNA; reactive oxygen species-mediated reactions; and reactions involving other secondary intermediates, as decomposition products of the excited molecules or lipid peroxidation products. (48) Guanine bases of DNA are particularly reactive being 8-oxo-7,8-dihydro-20-deoxyguanosine the main oxidation product by reaction with $^1O_2$. (49)

## 1.4 Cellular localization of the photosensitizer

The mechanism of binding of the PS to the cells and its specific cellular localization is not yet fully understood. The site of binding will be where the first damages of photodynamic effect will occur, due to the *in situ* generation of $^1O_2$ and free radicals. (50)

In theory, three situations may arise concerning the cellular localization of the PS: 1) it does not bind to the cells and remains outside, and so the damage is restricted to the cell wall; 2) it binds to the cells, in a loose or tight way, being located more externally or internally by diffusion, depending on the interaction mode with cellular components; or 3) it binds to the cells and is taken up (actively transported into the cell), or translocated through the wall to the plasma membrane.

The PS binding and its internalization into cells is affected by several factors: PS structure (51, 52), PS concentration (53-55), degree of hydrophobicity (54, 56, 57), PS solvent (58), cell density (59), bacterial strain and Gram-type. (56, 60, 61) It seems obvious that a greater PS accumulation on the cell will directly correlate with the PDI efficiency (52, 57, 62), but this may not always be true. (33, 56, 61)

An optimized PDI protocol (phototoxicity to bacteria with minimal damage to the host) includes a period of 5 to 10 min of incubation in the dark with PS prior to irradiation (28) once it is assumed that the binding takes place during this time interval and does not increase significantly at longer periods. (52, 63) During this contact time, the PS can interact with the cellular components of the bacterial wall.

Anionic PS can easily inactivate Gram-positive bacteria but much higher concentrations are required to indirectly inactivate Gram-negative bacteria. (60) For instance, rose Bengal (RB) does not need to be directly bound to Gram-negative bacteria in order to inactivate them. It is probably located in a relatively superficial layer of the bacteria and thus the $^1O_2$ generated externally is able to inactivate the cells without PS binding. (60)

Anionic PS can act on bacteria by electrostatic interactions with cell wall divalent cations ($Ca^{2+}$ and $Mg^{2+}$) and by protein transporters, and not by simple diffusion. (64) In this way, the

inactivation of Gram-negative bacteria by the photodynamic process with anionic PS can only be achieved alongside with additional agents such as EDTA (64) or the polycationic peptide polymyxin B (65) to increase the cell permeability and promote a better penetration of the PS. On the other hand, cationic PS can interact with bacteria also by electrostatic interactions and, in the case of Gram-negative bacteria, by self-promoted uptake pathways. (66)

For MB, a mono-cationic thiazine derivative, there is a competitive binding for divalent cations of the bacterial cell walls. If in Gram-negative bacteria these ions stabilize the normal structure of LPS by electrostatic bonds, in Gram-positive strains, the carboxylate groups of proteins and peptidoglycan cross-links, together with phosphate groups of teichoic and lipoteichoic acids, represent the major calcium binding sites. (67, 68) So, these PS-cation interactions cause displacement of ions with further PS uptake. (64) Moreover, the differences observed in PS binding between the Gram-negative *Proteus mirabilis* and *Escherichia coli* have been assigned to the diversity among enterobacteria regarding the composition of LPS, namely the structure of the lipid A and the core polysaccharides. (69, 70)

Different PDI efficiencies among MB, RB, and the cationic porphyrin Tetra-$Py^+$-Me in Gram-positive and Gram-negative bacteria have been reported. (60) These differences are associated with the overall charge of the PS and their $^1O_2$ quantum yield. The $^1O_2$ quantum yield of RB is similar to that of Tetra-$Py^+$-Me and higher than that of MB, but to inactivate *E. coli* a higher concentration of RB is needed. (60) On the other hand, if the $^1O_2$ quantum yield of several xanthenes dyes is the same and the cell rate inactivation is different, the difference may be related to the hydrophobicity of the PS. (57)

Several cationic *meso*-substituted porphyrins and phthalocyanines have higher affinity for Gram-negative bacteria due to their amphiphilic character provided by the hydrophobic planar aromatic core and the positively charged moieties in the *meso* positions of the tetrapyrrolic macrocycle. (28, 54) The amphiphilic character of the porphyrinic PS may be provided by the combination of different number of positive charges into different patterns with highly lipophilic groups, asymmetric distribution of charges at the peripheral position and the introduction of aromatic hydrocarbon side groups. (71-75) It has been suggested that porphyrins are located near the outer surface of the cytoplasmic membrane (62) or in the outer membrane (54) of Gram-negative bacteria. Time-resolved spectroscopic studies have indicated that the PS accumulates both inside and outside the cell, bound to nucleic acids and to the external structure of the cell wall, after a 18 h period of incubation of *E. coli* with Tetra-$Py^+$-Me. (76) However other studies in which *E. coli* was incubated with Tetra-$Py^+$-Me only up to 4 h, suggested an external location of the PS. (51) After shorter incubation times, when bound to the cells, PS molecules appear to be located in the outer membrane (in the case of

Gram-negative bacteria), somewhere between the outer surface and the periplasmic space (Table 1.1). According to these observations, conclusions about the precise location of these PS cannot be made at this point.

On the whole, it can be assumed that the amount of PS that binds to bacteria depends on, at least, two PS features: amphiphilic character and affinity for the cellular components. A recent study supports this premise. (56) The cationic porphyrins Tri-$Py^+$-Me-PF and Tetra-$Py^+$-Me efficiently photoinactivate *E. coli* and *Staphylococcus warneri*, but the inactivation rate is higher with Tri-$Py^+$-Me-PF. (77) Regardless of this fact, Tri-$Py^+$-Me-PF has a higher affinity for *E. coli* and Tetra-$Py^+$-Me for *S. warneri*. In *S. warneri*, Tri-$Py^+$-Me-PF binds to a lesser extent than Tetra-$Py^+$-Me but the amount of PS removed after washing is lower, therefore molecules remain more tightly bound to bacteria due to their amphiphilic character.

## 1.5 Photodynamic cellular damage

### 1.5.1 Ultrastructural changes

The ultrastructural changes on photosensitized bacterial cells have been assessed by transmission electron microscopy (TEM). In the Gram-negative bacterium *E. coli* treated with the cationic PS, 5,10,15-tris[4-(3-*N,N,N*-trimethylammoniumpropoxy)phenyl]-20-(4-trifluoromethylphenyl)porphyrin (TriAPP-$F_3$P), TMAPP (59) or with (2(3),9(10),16(17),23(24)-tetrakis[4-(*N*-methylpyridyloxy)]phthalocyaninato) zinc(II) (Zn(II)TetraO$Py^+$-Me-Pc (63), TEM revealed low density areas corresponding to aggregation of cytoplasmic macromolecules, alteration and irregularities in cell barriers, and multilamellar membrane structures directly connected to the cytoplasmic membrane. Photoinactivation by these PS seem to potentially interfere with membrane functions namely with membrane biosynthesis. (59) In *E. coli* treated with 5,10,15,20-tetrakis(1-ethylpyridinium-4-yl)porphyrin (Tetra-$Py^+$-Et), the first modifications were observed on the cell wall and assigned to pronounced loss of the outlining of the outer membrane. With a higher concentration of PS, plasma membrane damage with leakage of inner content was inferred from white spots and bubble formation. (54) Protochlorophyllide-treated *E. coli* showed deposition of electron-dense material on the cytoplasmic membrane and formation of large electron-lucent areas indicative of chromosomal location. (78) *Yersinia pseudotuberculosis* photosensitized with this PS revealed disruption of the outer membrane and cytoplasmic membrane with DNA release. (78)

**Table 1.1** Cellular localization of several photosensitizers in bacteria

| Reference | Photosensitizer | Dark incubation time with PS | Bacteria | Cellular localization | Detection method | Amount of PS bound to cells | Concentration of PS |
|---|---|---|---|---|---|---|---|
| **(33)** | MB and TBO | 15 min | *Pseudomonas aeruginosa* | Outer membrane through LPS (TBO) or through proteins (MB) | Spectrophotometry and Confocal laser scanning microscopy | MB: 58%, TBO: 57% | NM |
| **(51)** | Chlorin $e_6$ and Tetra-$Py^+$-Me | 1,3 5 and 24h | *Escherichia coli* | Outside associated with the cell | Confocal laser scanning microscopy | ND | 3 to 5 µM |
| **(53)** | Hematoporphyrin derivative | 30 min | *Staphylococcus aureus and Escherichia coli* | Membrane | Confocal laser scanning microscopy | ND | 25 µg $mL^{-1}$ (*S. aureus*) and 75 µg $mL^{-1}$ (*E.coli*) |
| **(54)** | Tetra-$Py^+$-Et | 30 min | *Escherichia coli* | Outer membrane[a)] | Spectrofluorimetry | 50% after 1 washing; 20% after 3 washings; 4.5 nmol PS $mg^{-1}$ protein (with 3.5 µM PS) | 0.1 to 3.5 µM |
| **(58)** | MB | NM | *Enterococcus faecalis* | Wall surface | Luminescence spectrometry | ND | 100 µM |
| **(60)** | Tetra-$Py^+$-Me, RB and MB | 10 min | *Enterococcus hirae and Escherichia coli* | Tetra-$Py^+$-Me and MB: inside the cells; RB: outside the cells[a)] | Spectrophotometry | ND | 0.73 to 3.65 µM |
| **(62)** | Tetra-$Py^+$-Me, TMAPP, TSPP | 5 min | *Staphylococcus aureus* | Cell envelope near to the outer surface of cytoplasmic membrane[a)] | Spectrophotometry | TMPyP: 35%, TTMAPP: 17%, TSPP: 1% | 1 µM |
| **(76)** | Tetra-$Py^+$-Me | 18h | *Escherichia coli* | Wall and nucleic acids | Spectrofluorimetry and time-resolved fluoresence spectroscopy | $5\times10^5$ molecules of PS $cell^{-1}$ (with 8 µM PS) | 0.5 to 16 µM |

ND, not determined; NM, not mentioned; a) suggested by the authors as the detection methods used are unspecific to precisely locate the PS

PDI of the Gram-positive bacteria *S. aureus* and *Listeria monocytogenes* treated with protochlorophyllide showed alterations on the cell's division area with spherical or curved cytoplasmic membrane. Partial loss of the cell wall with release of cytoplasmic contents was observed in *Bacillus subtilis*. (78) PDI of *Streptococcus mitis* with (2(3),9(10),16(17),23(24)-tetrakis[2-(*N,N,N*-trimethylammonium)ethoxy]phthalocyaninato) zinc (II) revealed multillamelar mesosome-like structures arising from the septa and cell wall, segregation patterns in the cytoplasm, irregularities in the cell wall and variability in cell wall thickness. (79)

### 1.5.2 Morphological changes

#### 1.5.2.1 Scanning electron microscopy

Independently of the photodynamic efficiency achieved with each PS, different morphological alterations on bacteria have been depicted by scanning electron microscopy (SEM). *E. coli* cells photosensitized with TriAPP-$F_3$P and TMAPP appeared shrunken, indicating indirectly an alteration in the membrane integrity, and constricted in the presence of TriAPP-$F_3$P but not of TMAPP. These differences were assigned as distinct capacities of these porphyrin derivatives in permeating bacterial membrane. (59) After Zn(II)TetraOPy$^+$-Me-Pc mediated PDI, *E. coli* cells appeared shrunken with small vesiculations on their surface attributed to release of outer membrane vesicles due to stress response. (63)

Fragmentary cell walls with several pits, gaps and large leakage indicate severe damage on *E. coli* treated with hypocrellin. (80) Irregular surfaces, wrinkled and shriveled cells, and pores on *E. coli*'s cell envelope were observed after PDI with hypericin. (55) In the Gram-positive *Streptococcus mitis*, presence of bubbles of various shapes appeared on cell surface upon mild PDI treatment with (2(3),9(10),16(17),23(24)-tetrakis[2-(*N,N,N*-trimethylammonium)ethoxy]phthalocyaninato) zinc (II) without bacterial lysis or complete inactivation. (79)

#### 1.5.2.2 Atomic force microscopy

In recent years, atomic force microscopy (AFM) has been used in addition to SEM to monitor the morphological changes of bacteria after photodynamic treatment, particularly in terms of surface, texture and shape, providing a deeper understanding of the action mechanism of different PS. This technique is more advantageous than TEM or SEM because sample preparation is much easier and less time consuming, minimizing additional damage that may occur during its preparation. (81, 82)

Photosensitization of *S. aureus* with TBO caused an increase in roughness, a decrease in extracellular slime, and bleb formation, suggesting damage to the cell wall. (83) AFM analysis of intact *S. aureus* showed smooth and homogeneous surfaces with small particles of about 120 nm. After treatment with hematoporphyrin monomethyl ether, there was a decrease in height and roughness (i.e., in the size of these particles) indicating changes in the chemical composition of the bacterial wall. (53)

In *E. coli* treated with TBO, several modifications on the cell surface were observed progressively with the light dose applied: increased roughness and rigidness with large depressions; reduction in the mean cell height; reduction in overall length; and distortion with deep grooves. The initial alterations, observed at a lower light dose, were associated with structural changes of the components of the outer membrane and with inner membrane damage, which is consistent with the interaction of the PS with the LPS of the bacteria (83), as previously discussed, also enhancing PS penetration into the membrane. With higher doses of light, deeper grooves (83), ruptures, indentations, decreased height and volume (84) suggested the complete destruction of the cell wall including the inner membrane with subsequent leakage of cytoplasmic contents. (83) With MB, the changes observed in *L. monocytogenes* (84) and *E. coli* (85) were similar to these. In the latter, the primary targets of PDI were the extracellular slime, as evidenced by the clearer environment around the treated cells and cell wall, although to a minor extent. In addition to the effects of light dose, cell density was found to be an important variable in the effectiveness of PDI as well, since in this condition there was no significant change in cell morphology. (85)

### 1.5.3 Integrity

#### 1.5.3.1 Cell wall

The assessment of the membrane integrity of the bacteria can be made by fluorescence microscopy with the LIVE/DEAD® viability assay. This test includes two fluorescent dyes: SYTO9 that penetrates in both viable and nonviable bacteria and propidium iodide that penetrates bacteria only with damaged membranes and quenches SYTO9 fluorescence. Viable cells emit green light and nonviable cells emit red light. (86) *Enterococcus faecalis* cells subjected to PDI with MB dissolved in a solvent system of glycerol:ethanol:water (MIX) stained red, while with MB dissolved in water they stained green, indicating the cell wall damage induced by MB in MIX. However, cell wall damage was also observed in the absence of irradiation indicating the damaging effect of components such as glycerol and ethanol in MIX

solvent. (58) Propidium iodide was also taken up by *E. coli* and *S. aureus* photosensitized with TBO. (83)

#### 1.5.3.2 Plasma membrane

The integrity of the cell membrane may be evaluated by spectroscopic measurement of intracellular components released with strong UV absorption at 260 nm. (87) The detection of the activity of various cytoplasmic enzymes (β-galactosidase and respiratory chain dehydrogenases), the quantification of total protein, and reducing sugars are also indicators of membrane permeabilization.

In general, there is a decrease of membrane integrity during PDI as a function of PS concentration and light dose, along with the inactivation rate and cell morphological changes. (54, 55, 83) The Zinc(II)TetraOPy$^{+}$-Me-Pc (2 μM) causes a 4 log reduction in *E. coli* viability upon 54 J cm$^{-2}$ but, even after 432 J cm$^{-2}$, the absorbance at 260 nm was almost unchanged. Instead, there was a progressive increase in β-galactosidase activity suggesting some membrane permeability enhancement. (63) With the cationic porphyrin Tetra-Py$^{+}$-Et (1 μM), there was severe damage to the membranes (inner and outer membrane) with a decrease in β-galactosidase activity and increased protein amount upon 20 J cm$^{-2}$. (54) With the TriAPP-$F_3$P and TMAPP (1 μM), the membrane damage was not sufficiently increased to release higher molecular weight species even after exposure to 1296 J cm$^{-2}$. (59) Xanthene PS showed distinct effects on the membrane of *S. aureus*: while 1 μM RB largely inactivates bacteria (4 logs) and 64% of the absorbing materials are released, phloxine B just begins the inactivation (1 log and 10% leakage). (57)

TBO-mediated PDI causing a 2 log reduction in *E. coli and S. aureus* survival, induced faster leakage of cytoplasmic constituents on the former than on the latter. (83) An explanation for this difference relies on the thickness of the cell wall and the lifetime of reactive oxygen species. That is, although a larger amount of PS is required to destroy the complex outer membrane of the Gram-negative bacteria cell wall, the thin layer of peptidoglycan enhances rapid leakage of the cell contents, while in Gram-positive bacteria, despite the low concentration of PS required to inactivate the cell, the thickness of the multi-layered peptidoglycan (20 - 80 nm) slows down the leakage of cellular contents. (83, 88) As TBO has high affinity to LPS (33), the interactions with this biopolymer may be the cause for greater photodynamic susceptibility of Gram-negative in comparison to Gram-positive bacteria.

### 1.5.4 Functional changes

#### 1.5.4.1 Plasma membrane

The membrane potential generated by the respiratory chain of bacteria is used by ATP synthase complex to drive ATP synthesis. (89) As a result, inhibition of membrane potential leads to inactivation of membrane transport systems and enzymes such as NADH dehydrogenase and ATPase (90), although ATPase appears to be less susceptible to PDI because its structure is partially protected by the hydrophobic layer of the inner membrane. (90) At lower PS concentrations, although there is inactivation of ATP synthesis due to cell wall disintegration, ATPase remains active. (88) The consequent increase in membrane permeability totally inactivates the energy producing system of bacteria. Cationic porphyrin PS appear to act directly on this system by inhibiting respiration soon after the onset of PDI in both Gram-positive (62) and Gram-negative bacteria. (54, 62) This rapid inhibition contrasts with the slower changes in membrane permeability (as a result of the increased efflux of $K^+$) (54, 62) and was identified as the main cause of *S. aureus* PDI in the early stages. (62) As these membrane functions are impaired early on, it would take longer for the PS to be able to diffuse into the cytoplasm and attack DNA. (62)

The cationic porphyrins Tetra-$Py^+$-Me and TMAPP decrease membrane potential and respiration efficiency early after irradiation in *S. aureus* but the second PS has a stronger effect. The anionic porphyrin 5,10,15,20-tetrakis(4-sulfonatophenyl)porphyrin (TSPP) has much weaker effect. (62) Moreover, the effect of RB on these electrochemical parameters is stronger than that of TMAPP, especially in impairing the $K^+$ pump. (91) Among other xanthene dyes, RB quickly induces an increase in $K^+$ permeability and inhibition of respiration. Thus, cationic porphyrin PS appear to inhibit membrane potential by inhibiting respiration and xanthene dyes by increasing membrane permeability. (57)

#### 1.5.4.2 Proteins

Membrane proteins are considered to be major targets of photodynamic oxidation, not only because they perform vital functions in bacteria (25) but also due to their abundance, their ability to bind to exogenous chromophores and quickly react with excited state species. (92, 93)

Singlet oxygen-mediated protein oxidation leads to formation of protein peroxides, carbonyls, side-chain products, cross-links and aggregates, protein unfolding and enzyme inactivation. (92, 93) These damages have been evidenced by enzymatic assays with the inactivation or loss of function of lactate dehydrogenase, NADH dehydrogenase, ATPase and

succinate dehydrogenase (80, 90, 94), quantification of total carbonyls (61, 95, 96), and by analysis of protein profile after PDI by sodium dodecyl sulfate-polyacrylamide gel electrophoresis (SDS-PAGE). (58, 84, 90, 94, 95, 97) However, this analysis is qualitative and unspecific, only detecting global changes at the protein levels. Possible altered functions may be deduced by analyzing the electrophoretic patterns, typically characterized by attenuation and/or disappearance of the bands and formation of cross-linked materials on the top of the gels. These modifications in outer membrane proteins and enzymes are time-dependent and occur simultaneously with the decrease of cell survival.

The first proteomic analysis of membrane proteins of *S. aureus* photosensitized by Tetra-$Py^{+}$-Me in sub-lethal doses showed that this oxidative damage is selective, affecting the expression of several functional classes of proteins, including those involved in metabolic activities, in response to the oxidative stress, in cell division, and in sugar uptake. For instance, DnaK, EfTS and RL10, which are involved in protein synthesis, decreased 5-fold, 3-fold and completely disappeared, respectively. KatA, involved in detoxification, increased 8-fold after treatment. On the other hand, D-lactacte dehydrogenase (LdHD) involved in energy metabolism was strongly depressed or almost disappeared. (95)

The increased expression of proteins involved in fermentative pathways [pyruvate formate-lyase (PflB), arginine deiminase (ArcA) and catabolic ornithine carbamoyltransferase (ArcB)] and the reduction of enzymes involved in the direct (chaperone protein DnaK) and indirect (ferritin, FtnA) response to oxidative stress implies a dual mechanism of action of PDI: oxygen consumption forces an exchange to the fermentative and glycolysis pathways, but the selective damage to various specific enzymes of this pathways does not allow the exchange. Additionally, there was fragmentation in some proteins (structural damage) and oxidation in others, with possible loss of function (functional damage). This suggests that the damages induced by PDI are specific and are likely to be dependent on the location of the PS in the bacteria. (95)

#### 1.5.4.3 Lipids

Although the bacterial membrane is likely to be the main target of PDI, information on phospholipids, essential structural components of membranes, is scarce because the identification and characterization of photodynamic damages on lipids is quite complex. Reactive oxygen species may cause direct oxidative modification of unsaturated lipids and indirect modification via reactive products of lipid peroxidation. (9, 98) Lipid hydroperoxides are significant non-radical long-lived intermediates of the peroxidative process and may be formed by interaction of lipids with $^{1}O_{2}$, which modifies the structure and the function of

target molecules and the damaging effects may extend to the surrounding milieu. (9, 98) Bacterial lipids are mostly monounsaturated and, consequently, not as prone to oxidation as polyunsaturated lipids. (99) Studies with bacterial lipids and phospholipids have sought to provide a deeper knowledge on the interaction between the PS and the cell membrane. (33, 40, 100) More recently, some efforts have been carried out to investigate lipid peroxidation in bacteria subjected to PDI. In UVB-resistant *Micrococcus sp.* and *Pseudomonas sp.*, lipid peroxidation by cationic galactoporphyrins was not significant in the early stages of PDI but occurred cumulatively, being greater with the most efficient PS. (61)

The first lipidomic studies on the phospholipid oxidation of Gram-positive and Gram-negative bacteria after PDI with a cationic *meso*-substituted porphyrin (Tri-$Py^{+}$-Me-PF) revealed formation of new oxidized molecular species, in addition to lipid hydroperoxides, and changes in the relative amounts of the different phospholipid classes. (101, 102) In the Gram-positive *Staphylococcus warneri*, there was an increase in the amount of phosphatidylglycerols (PGs), and a decrease of cardiolipins and other phospholipids. Also, oxidized molecular species were identified, including hydroxy and hydroperoxy derivatives from unsaturated fatty acyl chains of cardiolipins. The increase of PGs was ascribed as possible indirect oxidation reactions caused by reactive oxygen species or as a result of the interaction between these anionic phospholipids, which represent the major class in the membrane of these bacteria, and the cationic PS molecules. Possibly, PGs could be physically modified by rearrangements or separation of phospholipids, causing defects in the membrane and enhancing greater permeability to the PS. (101) In *E. coli*, hydroxy and hydroperoxy derivatives were also identified as oxidized molecular species from unsaturated fatty acyl chains of phosphatidylethanolamines, the major phospholipid component. The decrease in the amount of the unsaturated fatty acids C16: 1 and C18: 1 was assigned to oxidative modifications. (102)

#### 1.5.4.4 Nucleic acids

Although some PS can bind to DNA and form strong complexes, this may not be the main target of PDI considering that: a) PDI is a multi-target process mainly affecting the constituents of the cell wall and bacterial membrane; b) the chronological sequence of the harmful effects acquires some selectivity according to the binding site of the PS; and c) the lifespan and the site where $^{1}O_{2}$ is produced restrains its diffusion radius, and consequently, the spatial range of action. This observation acquires utmost importance considering the use of PDI to treat localized infections, where it is intended to completely eliminate microorganisms by selective accumulation of PS in these cells without inducing resistance and likewise prevent the PS to bind to eukaryotic cells, causing harmful effects.

Results from PDI experiments show that photocleavage of bacterial DNA occurs when cells are largely photoinactivated or are no longer viable, thus a decrease in the intracellular DNA content occurs in parallel to the decrease in cell survival. Time and light dose-dependent marked reductions in the nucleic acids extracted from photosensitized Gram-positive and Gram-negative bacteria indicate photocleavage, specifically single strand breaks, in genomic DNA (58, 59, 63, 84, 96, 103), in RNA (56, 103) and in plasmid DNA. (63, 103) In the case of plasmid DNA, there might be a conversion from supercoiled DNA (form I) to nicked circular DNA (form II). (59, 63)

Moreover, the extent of DNA damage may be influenced by the structure of the PS (56, 59) and by their features. As an example, TagFR-protein, a PS with intracellular expression, failed to induce visible damage to the genomic DNA of *E. coli* at maximum light dose (3200 J $cm^{-2}$) although a light-induced inner membrane damage was observed. (104)

It still cannot be categorically stated that PDI does not interfere with DNA, *in vivo*, without bacterial inactivation. Even so, PDI resistance mechanisms have not yet been identified, only some responses to oxidative stress by upregulation in the expression of enzymes and proteins (see below Bacterial resistance to PDI). Based on the knowledge presented so far, the mechanism of action of PDI in bacteria may be illustrated according to Scheme 1.1.

## 1.6 Biofilms

A biofilm may be defined as a cell community in the form of a polymeric matrix consisting of polysaccharides, proteins, lipids and extracellular DNA and sticking to an inert or living surface. (105) Biofilms may be constituted by single species or more, and their complexness hampers their elimination. (105) Several biofilm-forming bacterial species are important etiological agents of nosocomial infections mainly associated with medical implants or periodontal diseases, so PDI has been largely studied on biofilm-forming species as a way to improve the current therapeutic options. (30)

Biofilm visualization by SEM allows assessing adherence of bacteria to substrates, the biofilm structure, as well as distribution, type and viability of bacteria. (106) In PDI treated biofilms, SEM detects reduction of the biofilm namely by a decrease in the number of adherent bacteria and the extracellular matrix, followed by disruption in a light-dose dependent manner. Very few aggregated colonies (107-109), small clusters (109, 110), short chains and single cells can be seen (109) and, in some cases, with single large pores in the bacterial cell walls. (111)

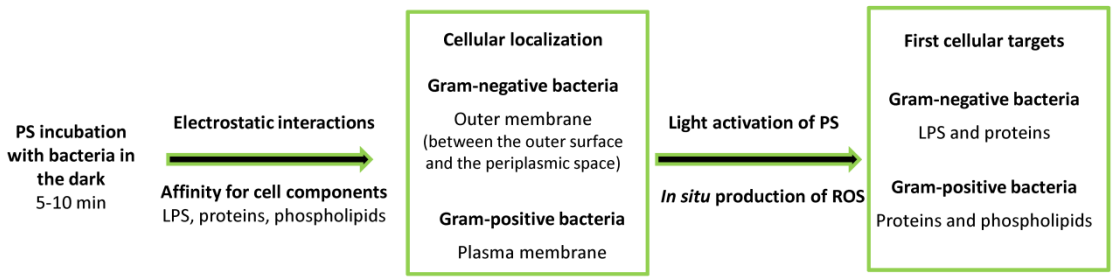


**Scheme 1.1.** Representation of the interactions between the photosensitizer and the bacteria before the onset of photosensitization to the most likely binding sites and major cellular targets.

Confocal laser scanning microscopy analysis of a biofilm assesses the distribution and thickness of cells in their structure. An increased permeability of bacterial cells after PDI is revealed by the fluorescent stains used to determine the viability of the bacteria (propidium iodide penetrates in nonviable bacteria which emit red fluorescence after PS uptake). The fact that the cell membrane becomes more permeable after PDI may indicate that this is an important target of photodamage. (46, 107, 109, 112) Moreover, in addition to detected nonviable cells at the outer layer of the biofilm, the reduced biofilm thickness observed after PDI is indicative of cell inactivation within the biofilms. (107, 108, 112-114) According to these observations, the PS diffusion and the penetration of light into the structure of the biofilm seems not to be a deterrent, since there are inactivated cells distributed throughout the biofilm structure. (108, 112) Also the larger number of dead cells found inside the biofilm (114) may be due to a reduction of cell-to-cell contact or cell-to-matrix interactions. (112) However, the reduction of susceptibility of multi-species biofilms to PDI with MB was attributed to a reduced penetration of the PS. (115) For merocyanine 540, for example, there was bleaching of the dye through the experiment. (109) On the other hand, the phenotypic and structural features of the biofilms also affect the susceptibility evidenced by a difference in major extracellular components among strains (110), biofilm formation ability between species (112) and strains (111, 114), and low efficiency of PDI on mature biofilms (older than 24 h) if the thickness and density of biofilm influences PS uptake. (110)

It was previously stated that the PDI efficiency for biofilm treatment is dependent mainly on PS penetration and light to the deeper layers (112) and also on the degree to which the PS binds to bacterial slime. (116) In this way, the efficiency is conditioned not only by microbial features and light parameters, but also by characteristics of the PS and their interaction modes with the cellular targets. Regarding the sign of the charge of PS, substantial differences in the efficiency of destruction of two-week old biofilms of *E. faecalis* were found between RB and MB (which is more efficient). (114) This was justified by the extracellular

polymeric substance associated with biofilms. The hindrance of the PS diffusion to more sensitive intracellular sites, the PS trapping by the polymeric substance outside of the cell, or the negative charges on the cell wall surface could promote repulsion of the anionic RB. (116) Also with regard to substituent groups in the PS structure, there was a preferential interaction of the PS with *S. aureus* cell wall between the porphyrins Tetra-$Py^{+}$-Me and Tri-$Py^{+}$-$C_{14}$-$Py^{+}$-Me. (108) The Tetra-$Py^{+}$-Me was less efficient on biofilm inactivation to PDI than Tri-$Py^{+}$-$C_{14}$-$Py^{+}$-Me, even with longer incubation times. The uptake experiments revealed that Tri-$Py^{+}$-$C_{14}$-$Py^{+}$-Me penetrates deeper into the bacterial membranes appearing homogeneously distributed, which may be justified by the more lipophilic character of Tri-$Py^{+}$-$C_{14}$-$Py^{+}$-Me due to its long tail. On the other hand, Tetra-$Py^{+}$-Me being highly hydrophobic preferably concentrates at membrane-water interfaces where less photosensitive targets are present. (108)

The structural, biochemical and metabolic features of microbial cells in biofilm greatly limit their efficient photoinactivation compared with their planktonic counterparts. (114) This fact would imply the use of higher concentrations of PS to eradicate the biofilm in infected eukaryotic cells, which should be avoided because of possible toxicity. On the other hand, the extrapolymeric matrix may be an obstacle to the penetration of PS, requiring application of higher light doses to achieve the desired effect. (105) The results of recent studies on the effect of PDI in several bacterial biofilms are shown in Table 1.2. Although PDI is more effective than antibiotics (115), the most recent strategies of inactivation of these bacterial communities seek a synergistic effect between different therapeutic approaches, such as PDI, antibiotics and biofilm-disrupting enzymes, for example. (105)

## 1.7 Bacterial resistance to PDI

Studies of bacterial resistance to PDI are generally based on sub-lethal treatments (i.e., partial inactivation of bacteria) followed by the growth of surviving colonies in repeated cycles under the same conditions. The photoinactivation profile of *Peptostreptococcus micros* and *Actinobacillus actinomycetemcomitans* treated with porphycenes 2,7,12,17-tetrakis(2-methoxyethyl)-9-glutaramidoporphycene (GlamTMPn) and 2,7,12,17-tetrakis(2-methoxyethyl)-9-*p*-carboxybenzyloxyporphycene in 10 cycles was unchanged. Also, the treatments did not interfere with the susceptibility of the bacteria to various classes of antibiotics. (117) Likewise, the PDI of *S. aureus* (susceptible and resistant strains to methicillin), and *E. coli* (susceptible strain) by MB in 25 and 11 cycles, respectively, did not induce

**Table 1.2** Photodynamic inactivation studies in bacterial biofilms

| Reference | Strains (Age of biofilm) | PS | Light source (wavelength, power density) | Survival reduction (amount, PS concentration, light dose or irradiation time) | Observations |
|---|---|---|---|---|---|
| (107) | Methicillin-resistant *Staphylococcus aureus* and methicillin-resistant *Staphylococcus epidermidis* (24h) | 5-ALA | Semicondutor laser (635 nm, 0 - 300 J $cm^{-2}$) | > 80%, 40 mM, 300 J $cm^{-2}$ | |
| (108) | *Staphylococcus epidermidis* (24h) | Tetra-$Py^{+}$-Me, Tri-$Py^{+}$-$C_{14}$-$Py^{+}$-Me | Tungsten lamp (400 - 800 nm, 166 mW $cm^{-2}$) | Tri-$Py^{+}$-$C_{14}$-$Py^{+}$-Me: 3 log, 0.8 µM, 300 J $cm^{-2}$; Tetra-$Py^{+}$-Me: 3 log, 10 µM (after 1h incubation), 300 J $cm^{-2}$ | Tri-$Py^{+}$-$C_{14}$-$Py^{+}$-Me exhibited dark toxicity at concentrations higher than 2 µM |
| (109) | *Staphylococcus epidermidis* (16h) | merocyanine 540 | Diode laser (Nd:YAG) (532 nm, 0.33 W $cm^{-2}$) | c.a. 3 log, 20 µg $mL^{-1}$, 600 J $cm^{-2}$ | |
| (110) | *Staphylococcus epidermidis* (24h) | Tetra-$Py^{+}$-Me | Tungsten lamp (400 - 800 nm, 166 mW $cm^{-2}$) | c.a. 1.5 - 2 log, 10 µM, 200 J $cm^{-2}$ | Synergistic action of PDI with other therapeutic strategies (antibiotic or phagocytosis) |
| (111) | *Porphyromonas gingivalis, Aggregatibacter actimomycetemcomitans* and a multi-species biofilm (4-day-old) | TBO | LED (625 - 635 nm, 2 W $cm^{-2}$) | *P. gingivalis*: 2 - 7 log, *A. actinomycetemcomitans*: 2 - 5 log, Multi-species: 1 log, 0.1 mg $mL^{-1}$, 60s | Synergistic action of PDI with $H_2O_2$ |
| (112) | *Staphylococcus aureus* and *Staphylococcus epidermidis* (16h) | TBO | Laser (640 nm, 42 mW $cm^{-2}$) | c.a. 5 - 6 log, 40 µM, 200 J $cm^{-2}$ | EDTA pre-treatment improved PDI in *S. epidermidis* but not in *S. aureus* |
| (113) | *Pseudomonas aeruginosa* (24h) | Tetra-$Py^{+}$-Me | 100-Watt mercury vapor lamp (> 400 nm, 220 - 240 J $cm^{-2}$) | 4.1 log in wild-type biofilms and 3.9 log in pqsA mutant biofilms, 225 µM, 10 min | Tetra-*p*-tosylate altered biofilm structure in the dark and promoted the action of tobramycin |
| (114) | *Enterococcus faecalis* (4-day-old) | MB and RB | Optical fiber (540 ±15 nm for RB and 660 ±15 nm for MB, 300 - 600 mW) | > 5 log, 100 µM, 25 - 30 J $cm^{-2}$ | MB combined with efflux pump inhibitor verapamil enhanced PDI |
| (115) | Multispecies biofilms (7-day-old) | MB | Diode laser (665 nm, 100 mW $cm^{-2}$) | c.a. 33%, 25 - 50 µg $mL^{-1}$, 30 J $cm^{-2}$ | |

resistance in the bacteria. (118) Similarly, the photodynamic process with the porphyrin Tri-Py-$Me^{+}$-PF did not triggered resistance neither in *E. coli* nor in *Vibrio fischeri* in 10 cell generations partially inactivated, and viability was not recovered after lethal treatment, i.e., total inactivation of colony forming units. (119) Similar results were obtained after 20 cycles of treatment of *S. aureus* and *P. aeruginosa* with the cationic phthalocyaninato zinc(II) RLP068/Cl. However, in the absence of light, there was an increase in the minimum inhibitory concentration (MIC) of RLP068/Cl for *S. aureus*, which was not increased by 10 repeated cycles. Although this MIC is higher than that required to cause lethal damage using PDI, there was bacterial inactivation after exposure to light, which on one hand eliminates the effect on the MIC increased in the dark, but does not rule out the possible development of resistance. (120)

PDI does not seem to induce the development of mutants or be constrained by the resistance pattern of bacteria to antibiotics (96, 121), to ionizing radiation (122) and to UV-B radiation (61). However, there seems to be a strain-dependent phenomenon concerning PDI efficiency, as MRSA strains have revealed higher resistance to PDI than their methicillin-sensitive counterparts, probably assigned to slime production by the MRSA strains. (123)

On the other hand, oxidative stress responses can be set off by up-regulation of the expression of enzymes and proteins. An increase in the activity of superoxide dismutases (SodA and SodM) and in the transcript level of these enzymes, involved in the response to oxidative stress, was observed in *S. aureus* in a strain-dependent manner (only on those more PDI susceptible strains), so this increase does not seem to directly affect the vulnerability of these bacteria to PDI. (124) In addition, $^{1}O_2$ is able to inactivate these and other antioxidant enzymes, such as catalase (125), and inhibit the expression of virulence factors, as observed in light-activated MB on staphylococcal V8 protease, α-haemolysin and sphingomyelinase. (126)

Upregulation of heat-shock protein (HSP) GroEL, which stabilizes lipid membranes and refolds denatured proteins during stress, was detected in *Streptococcus mutans* after PDI with RB, without DNA degradation. (127) Increased GroEL expression was also observed in *E. coli* with TBO, as well as upregulation of the highly conserved chaperone DnaK. (128) Thus, induction of HSP has been suggested as a possible mechanism of development of resistance.

In contrast, Tetra-$Py^{+}$-Me mediated PDI of *S. aureus* showed down-regulation in DnaK biosynthesis. (95) This decrease, preventing a response to the detoxification by reactive oxygen species, suggests that there may be an accumulation of proteins and the formation of cross-linked complexes in the cells. Therefore, it was suggested that the induced damage in proteins is specific and other factors related with the PS localization in the cell may play a

major role. (95) More recently, a gene regulation dependent on Agr, a global transcription regulator, was shown by chlorin $e_6$ mediated-PDI in *S. aureus*. Agr regulator was also shown to be required for *S. aureus* survival to PDI. (129)

Furthermore, it is known that some PS are substrates for multidrug efflux pumps in both Gram-positive and Gram-negative bacteria (96, 130) but this does not affect the efficiency of PDI. (96) In this way, the combination of PDI with efflux pump inhibitors (facilitator of the pump NorA) has been suggested to promote the therapeutic effect in *P. aeruginosa* and *S. aureus* with phenothiazinium PS (MB and dimethyl methylene blue) but the process cannot be extended to RB or benzoporphyrin derivative. (131)

Given this evidence is still too early to say that there is development of resistance because the PDI-induced responses also vary with the PS tested.

## 1.8 Future perspective

The photodynamic inactivation (PDI) of bacteria seems to be a promising strategy to answer the development of resistance to antibiotics. Although the approach is not a recent discovery, it was temporarily pushed aside due to the appearance of antibiotics and the initial efficiency associated to this type of drugs. However, with the appearance of bacterial resistance, many efforts were developed to rescue and to boost the approach in order to obtain an efficient eradication of a wide spectrum of microorganisms.

As the research of the enormous potential of PDI increases worldwide, we are at a stage where the studies are directed towards the potential development of resistance mechanisms, the possible specificity of the mechanism of action, and the effective strategies to eradicate complex structures such as biofilms, through the synergistic use of distinct therapeutic approaches. The detailed study of these aspects will help to optimize the structure of photosensitizers. Moreover, several strategies of drug targeting and drug delivery vehicles continue to be widely studied.

Treatment of infections by photodynamic therapy is a localized process, and thus is limited to superficial areas of the body such as the skin or the oral cavity. Progress is required in light delivery systems and on the definition of light parameters, in order to extend the application of PDI to generalized infections. In this case, the stimulation of the immune system by PDI opens a long way of research in the infection field.

At the present time, PDI is considered to be a young discipline, given that there are few *in vivo* studies with animal models and a limited number of clinical trials for different clinical conditions. However, the existing evidence is promising and further work will dictate the progress in this area.

# Chapter 2. Photodynamic oxidation of *Staphylococcus warneri* membrane phospholipids: new insights based on lipidomics

The content of this chapter has been published as:
Alves E, Melo T, Simões C, Faustino MAF, Tomé JPC, Neves MGPMS, et al. Photodynamic oxidation of *Staphylococcus warneri* membrane phospholipids: new insights based on lipidomics. Rapid Commun Mass Spectrom. 2013;27(14):1607-18.

# 2 Photodynamic oxidation of *Staphylococcus warneri* membrane phospholipids: new insights based on lipidomics

## 2.1 Abstract

The photodynamic process involves the combined use of light and a photosensitizer, which, in the presence of oxygen, originates cytotoxic species capable of oxidizing biological molecules, such as lipids. However, the effect of the photodynamic process in the bacterial phospholipid profile by a photosensitizer has never been reported. A lipidomic approach was used to study the photodynamic oxidation of membrane phospholipids of *Staphylococcus warneri* by a tricationic porphyrin [5,10,15-tris(1-methylpyridinium-4-yl)-20-(pentafluorophenyl)porphyrin triiodide, Tri-Py$^{+}$-Me-PF].

*S. warneri* ($10^8$ colony forming units $mL^{-1}$) was irradiated with white light (4 mW $cm^{-2}$, 21.6 J $cm^{-2}$) in the presence of Tri-Py$^{+}$-Me-PF (5.0 μM). Non-photosensitized bacteria were used as control (irradiated without porphyrin).

After irradiation, total lipids were extracted and separated by thin-layer chromatography (TLC). Isolated fractions of lipid classes were quantified by phosphorus assay and analyzed by mass spectrometry (MS): off-line TLC/ESI-MS, hydrophilic interaction (HILIC)-LC/MS and MS/MS.

The most representative classes of *S. warneri* phospholipids were identified as phosphatidylglycerols (PGs) and cardiolipins (CLs). Lysyl-phosphatidylglycerols (LPGs), phosphatidylethanolamines (PEs), phosphatidylcholines (PCs) and phosphatidic acids (PAs) were also identified. After photodynamic treatment, an overall increase in the relative abundance of PGs was observed as well as the appearance of new oxidized species from CLs, including hydroxy and hydroperoxy derivatives. Formation of high amounts of lipid hydroperoxides was confirmed by FOX2 assay. Photodynamic oxidation of phospholipid standards revealed the formation of hydroperoxy and dihydroperoxy derivatives, confirming the observed CL oxidized species in *S. warneri*.

Membrane phospholipids of *S. warneri* are molecular targets of the photoinactivation process induced by Tri-Py$^{+}$-Me-PF. The overall modification in the relative amount of phospholipids and the formation of lipid hydroxides and hydroperoxides indicate the lethal damage caused to photosensitized bacterial cells.

## 2.2 Introduction

The photodynamic inactivation (PDI) of microorganisms has gained increasing importance due to its ability to eliminate a broad spectrum of pathogenic microorganisms, and to its application in different fields (clinical, environment and public health). (13) In the clinical area, given the concern with multidrug-resistant strains, it has acquired greater impact as a potential alternative to common antimicrobial agents.

The photodynamic process involves the combined action of a light source, molecular oxygen and a photosensitive compound, called a photosensitizer. (132) This interaction gives rise to reactive oxygen species such as singlet oxygen and/or free radicals which are capable of oxidizing many biological molecules (enzymes, proteins, lipids and nucleic acids) and lead to cell death. (98, 133) This process is not apparently reversible and resistance mechanisms have not yet been observed. (119, 120, 134, 135)

There is general consensus on the importance of using cationic porphyrins as photosensitizers (with two or more charges) for efficient PDI of both Gram-positive and Gram-negative bacteria. (77, 136, 137) The amphiphilic character conferred by the different substituents on the phenyl ring does not significantly affect their photophysical properties. (137) The structural differences in the cell walls of these microorganisms were proven to be dependent on the use of cationic photosensitizers which were the most promising ones for their efficient inactivation. (136) Due to the constitution of their walls, seemingly simple, Gram-positive bacteria are more easily photoinactivated than Gram-negative bacteria.

The various layers of peptidoglycan of the cell wall associated with lipoteichoic and teicuronic acids confer a high degree of porosity for this type of bacteria, allowing the entry of several macromolecules with a molecular weight of 30,000 to 60,000 Da. (138) Thus, after the diffusion of the photosensitizer across the cell wall, it binds to the cytoplasmic membrane, which represents a critical target for bacterial cell photoinactivation. (139)

With a molecular weight of 1132.97 Da, 5,10,15-tris(1-methylpyridinium-4-yl)-20-(pentafluorophenyl)porphyrin triiodide (Tri-Py$^{+}$-Me-PF, Figure 2.1) has been demonstrated to be a promising broad-spectrum antimicrobial agent. (77, 140-144) However, although several studies have shown different damage caused by PDI of microorganisms at a morphological and/or functional level (63, 78, 103, 145), the mechanism of the photodynamic process in bacteria, with respect to membrane components, in particular phospholipids, is not fully known. These membrane components are essential in cell structure maintenance (35) and interact with other biomolecules based on their distinct chemical nature. (146) Therefore, since phospholipids are the main components of cytoplasmic membranes, where

photosensitizers seem to be preferentially located, it is important to study the action of PDI on them. (147) Although bacterial lipids include mainly monounsaturated fatty acids, and thus are not as prone to oxidation as polyunsaturated fatty acids (99, 148), they can also be oxidized. It is therefore important to clarify if lipid peroxidation is essential in the mechanism of bacterial destruction. In the PDI of bacteria, in addition to the lipid peroxidation caused by reactive oxygen species, there may be a disruption or rearrangement of the membrane phospholipids to allow cell binding of the photosensitizer. Furthermore, it is important to know the differences in the oxidation/rearrangement of membrane phospholipids in bacteria.

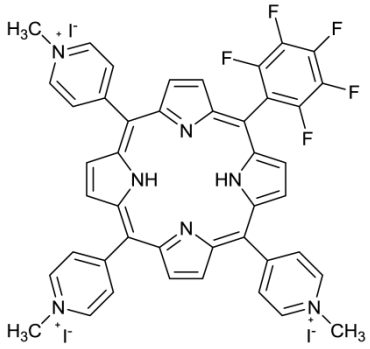


**Figure 2.1** Structure of 5,10,15-tris(1-methylpyridinium-4-yl)-20-(pentafluorophenyl)porphyrin triiodide (Tri-$Py^{+}$-Me-PF).

*Staphylococcus aureus* have been widely used as a model of Gram-positive bacteria, including in antimicrobial photodynamic inactivation. (149-151) However, coagulase-negative staphylococci are gaining clinical relevance, especially because of their virulence factors, involving adhesion, aggregation and biofilm formation. (152) They are responsible for opportunistic and healthcare-associated infections (153-155) and have also shown an increasing resistance to multiple antimicrobial agents. (152, 156)

*Staphylococcus warneri* is a coagulase-negative species generally found in normal microbial skin flora. (157) Although it is a rare cause of human disease, it has been implicated in several infection conditions: urinary tract infections (158), vertebral osteomyelitis (159), bacteremia (160), meningitis (161), septic arthritis (162), sepsis (163), and endocarditis in patients with implanted medical devices. (164-166) Its pathogenicity in neonatal intensive care units (167), its predominance as a species of coagulase-negative staphylococci cultured from the hands (167, 168), and its decreased antimicrobial agent susceptibility (168, 169) have also been reported. The reported clinical cases have highlighted the importance of *S. warneri* as a potentially opportunistic etiological agent.

The membrane phospholipid compositions among *Staphylococcus* species are qualitatively and quantitatively dissimilar (170) and, therefore, these species do not always

respond similarly to the action of antimicrobial agents. Lipidomics studies have shown that the major phospholipid classes in coagulase-negative species of *Staphylococcus* (171) are the anionic phosphatidylglycerols (PGs) and cardiolipins (CLs). Minor or trace amounts of the cationic lysylphosphatidylglycerols (LPGs) (which abound in *S. aureus*), phosphatidic acid, phosphatidyl diglycosyldiglyceride and unidentified phospholipids were also found in these strains. (171) In a recent study with several strains of *S. aureus*, the determined ranges of their main phospholipid classes were: PGs (57 - 83%), LPGs (7 - 25%) and CLs (3 - 15%). (37) However, for coagulase-negative strains there is no reported data on the phospholipidic pattern.

The aim of this study, after identification of the phospholipidic pattern of the *S. warneri* strain, was to evaluate the effect of the photodynamic process on its phospholipid profile using the cationic photosensitizer Tri-$Py^{+}$-Me-PF. The changes in the membrane phospholipid composition of cells irradiated in the presence and absence of Tri-$Py^{+}$-Me-PF were analyzed using a lipidomic approach, combining thin-layer chromatography (TLC) with mass spectrometry techniques, and are intended to give some insight on the mechanism(s) of membrane damage of Gram-positive bacteria by PDI.

## 2.3 Material and Methods

### 2.3.1 Photosensitizer

The cationic porphyrin Tri-$Py^{+}$-Me-PF (Figure 2.1) was prepared according to reported procedures. (172, 173) The purity of the compound was confirmed by thin-layer chromatography (TLC) and by $^{1}H$ NMR spectroscopy. Stock solutions were prepared in dimethyl sulfoxide (500 µM work solution) and sonicated for 30 min at room temperature before use.

### 2.3.2 Reagents

Phospholipid standards were purchased from Avanti Polar Lipids, Inc. (Alabaster, AL, USA) and used without further purification. The PG standard was a mixture of PG molecular species (Egg PG, ref. 841138C). HPLC grade chloroform and methanol were purchased from Fisher Scientific Ltd. (Loughborough, UK). All other reagents were purchased from major commercial sources. Milli-Q water (Synergy®, Millipore Corporation, Billerica, MA, USA) was used. TLC silica gel 60 glass plates (20 x 20 cm) with concentrating zone were purchased from Merck (Darmstadt, Germany).

### 2.3.3 Isolation and identification of bacteria and growth conditions

*S. warneri* from hand skin was isolated in our laboratory and cultured in tryptic soy broth (TSB, Merck), aerobically, for 24 h at 37 °C. The cells were coagulase-negative, Gram-positive cocci. The organism was identified on the basis of its *dnaJ* gene sequence. (174)

Genomic DNA was extracted from overnight grown bacteria (14 h at 37 °C, 100 rpm), as described previously. (175) Polymerase chain reaction (PCR) amplification and DNA sequencing were performed with the following pair of *dnaJ* degenerate primers: SA-(F) 5'-GCCAAAAGAGACTATTATGA-3' and SA-(R) 5'-ATTGYTTACCYGTTTGTGTACC-3'. (174)

The 25 µL PCR mixture contained approximately 1 µL of template, 0.5 µM of each primer and 12.5 µL of 2x Fermentas DreamTaq PCR Master Mix (Thermo Scientific, Vilnius, Lithuania).

The reaction mixture was first incubated at 95 °C for 10 min, followed by five cycles of 94 °C for 30 s, 45 °C for 30 s and 72 °C for 60 s, then subjected to 30 cycles of 94 °C for 30 s, 50 °C for 30 s and 72 °C for 60 s, and completed with a final extension at 72 °C for 3 min in a TProfessional Trio thermocycler (Biometra, Goettingen, Germany).

The PCR products were analyzed by electrophoresis (BioRad, Munich, Germany) in 1% agarose gel (Fluka, Munich, Germany), with GreenSafe, at 60 V for 90 min in 1x TAE buffer (0.04 M Tris-acetate, Sigma; 0.001 M EDTA, Sigma-Aldrich (Munich, Germany); pH 8.0), and purified and sequenced at external facilities (StabVida, Caparica, Portugal). The sequences were compared with sequences available in the GenBank® database (National Center for Biotechnology Information, Bethesda, MD, USA) by using the BLAST (Basic Local Alignment Search Tool) service to determine their closest relative. The analysis of the sequence in BLAST showed a maximum identity of 99% with *Staphylococcus warneri* (Accession No. AB234328).

For the experiments, *S. warneri* cells from a freshly cultured plate were inoculated in TSB and grown overnight aerobically at 37 °C, at 100 rpm. An aliquot was then transferred into fresh TSB under the same growth conditions to reach the early stationary phase (optical density at 600 nm: 1.9 ± 0.1), corresponding to ≈ $10^8$ colony forming units (CFU) $mL^{-1}$. Bacterial cells were used in two different ways: sample (cells irradiated with photosensitizer) and control (cells irradiated without photosensitizer). The cells were harvested by centrifugation (10 min, 13,000 x *g*, 4 °C) (Avanti® J-25, Beckman Coulter, Inc., Brea, CA, USA), washed three times with sterile phosphate-buffered saline (PBS: 8.0 g NaCl, 0.2 g KCl, 1.44 g $Na_2HPO_4$ and 0.24 g $KH_2PO_4$ per liter; pH 7.4) and resuspended in PBS to achieve a final concentration of $10^8$ CFU $mL^{-1}$.

### 2.3.4 Photosensitization protocol

The sample consisted of a bacterial suspension (49.5 mL in a 600 mL sterilized glass beaker) containing 500 µL of Tri-$Py^{+}$-Me-PF stock solution (5.0 µM). In the control, the porphyrin solution was replaced by PBS. The sample was incubated in the dark for 10 min under stirring (100 rpm) at 25 °C, in order to promote the PS binding to the cells. The control and sample then underwent a 90 min period of irradiation (total light dose 21.6 J $cm^{-2}$) with artificial white light (PAR radiation, 380 - 700 nm, 13 OSRAM 21 lamps (Munich, Germany) of 18 W each) with a irradiance of 4 mW $cm^{-2}$ (measured with a model LI-250 radiometer, Li-Cor Inc., Lincoln, NE, USA), and stirred at 100 rpm. After irradiation, the cells were harvested by centrifugation (10 min, 13,000 x *g*, 4 °C), washed three times with Milli-Q water at 4 °C, and the pellet was then kept on ice until lipid extraction.

### 2.3.5 Lipid extraction

The total lipids from bacteria were extracted following the modified Bligh and Dyer method. (176) A volume of 7.5 mL of chloroform/methanol (2:1, v/v) was added to bacterial cells (previously resuspended in 2 mL of water), in Pyrex glass centrifuge tubes. The mixture was well homogenized by inverting vigorously the tubes several times and incubated on ice for 210 min. The samples were centrifuged at 2000 rpm for 10 min (Mixtasel, JP Selecta S.A., Barcelona, Spain) at room temperature to resolve a two-phase system: an aqueous upper phase and an organic lower phase from which lipids were obtained. After transferring the organic phase to a clean tube, the extraction was repeated twice. The extracts were dried under nitrogen flow, dissolved in 300 µL of chloroform, and stored at –20 °C in 2 mL amber glass vials.

### 2.3.6 Quantification of phospholipids by phosphorus assay

Quantification of phospholipids in the total lipid extract and in the spots separated by TLC was performed according to Bartlett and Lewis. (177) Concentrated perchloric acid (0.65 mL, 70% m/v) was added to the samples in acid-washed glass tubes and the mixture was incubated for 60 min at 180 °C in a heating block (Block Heater SBH200D/3, Stuart®, Bibby Scientific Ltd., Stone, UK). After incubation, 3.3 mL of water, 0.5 mL of 2.5% of ammonium molybdate and 10% of ascorbic acid were added. The reaction mixture was well homogenized in a vortex mixer after each addition and incubated for 10 min at 100 °C in a water bath (Precisterm, JP Selecta S.A.). Standards from 0.2 to 1.5 µg of phosphate (standard solution of

$NaH_2PO_4.2H_2O$, 439 mg $L^{-1}$ of water, i.e. 100 µg of phosphorus $mL^{-1}$) underwent the same treatment as the samples.

Finally, the absorbances of the standards and samples were measured at 800 nm, at room temperature, in a microplate UV-Vis spectrophotometer (Multiskan GO, Thermo Scientific, Hudson, NH, USA). The relative abundance of each phospholipid class was calculated by relating the amount of phosphorus in each spot or in the total extract to the total amount of phosphorus in the sample.

### 2.3.7 Thin-layer chromatography

Phospholipids from the total lipid extract were separated by TLC using silica gel plates. Prior to separation, the plates were washed with chloroform/methanol (1:1, v/v) and activated (sprayed or impregnated) with 2.3% boric acid in ethanol and placed in an oven at 100 °C for 15 min. Plates with spots containing 20 µg of lipids were developed in a solvent mixture of chloroform/ethanol/water/triethylamine (30:35:7:35, v/v/v/v). Separated lipid spots were revealed by exposing the plates to primuline (50 µg/100 mL acetone/water, 80:20, v/v) and visualized with a UV lamp (254 and 366 nm; Camag, Berlin, Germany). (178) The spots were then scraped off the plates and extracted from silica with chloroform/methanol (2:1, v/v), quantified, and analyzed by mass spectrometry.

### 2.3.8 Quantification of hydroperoxides by FOX2 assay

The FOX2 assay is based on the direct measurement of hydroperoxides, which react with an excess of ferrous ions at low pH in the presence of the ferric ion indicator dye xylenol orange (XO). The amount of ferric ion generated is measured as the Fe-XO complex in the visible region. The lipid hydroperoxides were quantified in the total lipid extracts obtained from the control and samples (after irradiation). Aliquots (50 µL) of the total lipid extracts from *S. warneri* controls and samples were added to FOX2 reagent (950 µL) in microtubes, homogenized in a vortex mixer and incubated for 30 min at room temperature, in the dark. After incubation, the absorbance of the samples was read at 560 nm against $H_2O_2$ standards with concentrations ranging from 0.0 to 0.4 mM ($H_2O_2$ 1 mM, FOX2 reagent and water). The reagent (100 mL) was prepared as follows: 250 µM $(NH_4)_2Fe(SO_4).6H_2O$ (9.8 mg) and 25 mM $H_2SO_4$ (139 µL) were dissolved in 5 mL of water, mixed with 4 mM 2,6-di-*tert*-butyl-*p*-hydroxytoluene (BHT) (88.2 mg), 100 µM xylenol orange (7.2 mg) and 45 mL of methanol; another 45 mL of methanol and 5 mL of water were then added. (179)

### 2.3.9 Phospholipid separation and quantification by hydrophilic interaction (HILIC) liquid chromatography mass spectrometry

Total lipid extracts were also analyzed by HILIC-LC/MS. PL classes were separated on an Waters Alliance 2690 HPLC system (Waters Corp., Milford, MA, USA) coupled to a Finnigan LXQ electrospray linear ion trap mass spectrometer (Thermo Fisher, San Jose, CA, USA). Mobile phase A consisted of 10% water, 55% acetonitrile and 35% methanol, with 10 mM ammonium acetate, and mobile phase B consisted of 60% acetonitrile and 40% methanol with 10 mM ammonium acetate. The total lipid extracts were diluted in mobile phase A and 15 µL of the reaction mixture was introduced into an Ascentis Si HPLC Pore column (15 cm x 1.0 mm, 3 µm; Sigma-Aldrich). The solvent gradient was programmed as follows: gradient started with 0% of A and 100% B, linearly increased to 100% of A in 20 min, and isothermally held for 35 min, returning to the initial conditions in 5 min. The flow rate through the column was 16 µL/min obtained using a pre-column split (Accurate, LC Packings, San Francisco, CA, USA). (180)

### 2.3.10 Mass spectrometry

Phospholipid analysis was carried out by negative-ion electrospray ionization mass spectrometry (ESI-MS) on a Finnigan LXQ linear ion trap mass spectrometer (Thermo Fisher). The ESI-MS conditions were: electrospray voltage 4.7 kV; capillary temperature 275 °C, and the sheath gas (He) flow rate 25 units. A precursor ion isolation width of 0.5 *m/z* units was used, with a 30 ms activation time for MS/MS experiments. Full scan MS spectra and MS/MS spectra were acquired with a maximum ionization time of 50 ms and 200 ms, respectively. The normalized collision energy (CE) varied between 17 and 20 (arbitrary units) for MS/MS. Data acquisition and treatment of results were carried out with the Xcalibur® Data System 2.0 (Thermo Scientific, San Jose, CA, USA).

### 2.3.11 Photodynamic treatment of phospholipid standards

Phospholipid standards (PG and CL) were dissolved in 1 mL of chloroform (1 mg $mL^{-1}$). Aliquots of 250 µL (250 µg) were transferred to 50 mL glass beakers, dried with nitrogen, and resuspended with sonication in 2 mL of 5 mM $NH_4HCO_3$, pH 7.4, with formation of liposomes. This procedure was carried out in duplicate for each standard: one of the beakers was exposed to light (control standard) and the second beaker was exposed to light in the presence of 5.0 µM of Tri-$Py^+$-Me-PF (treated standard). The irradiation conditions were the same as described for *S. warneri* (see *2.3.4. Photosensitization protocol*). After 90 min of light irradiation, the control and treated standards were processed to obtain only the phospholipids for further TLC

and MS analysis. A mixture of chloroform/methanol/water (8:4:3, v/v/v) was added to the samples, followed by homogenization with a vortex, centrifugation at 2000 rpm for 10 min at room temperature, removal of the organic phase, drying with nitrogen, dissolution in 250 µL of chloroform and storage at –20 °C.

### 2.3.12 Statistical analysis

Quantification of phospholipids and quantification of hydroperoxides were carried out independently, three times ($n$ = 3), both for the control and for the sample. The results were analyzed using one-way analysis of variance (ANOVA) with the Bonferroni post-hoc test (for quantification of phospholipids) and Student's $t$-test (for the quantification of hydroperoxides), and are presented as means ± standard deviation. Statistics were carried out using PRISM® GraphPad Software, Inc. (La Jolla, CA, USA). A value of $p < 0.05$ was considered significant.

## 2.4 Results

### 2.4.1 Chromatographic analysis and quantification of phospholipids

Analysis and quantification of *S. warneri* phospholipids were carried out after TLC separation of the total lipid extracts. Chromatographic separation showed seven different spots for the non-photosensitized cells (control) and seven different spots for the photosensitized ones (sample) (Figure 2.2a).

The amount of phospholipids in each spot was determined by the phosphorus assay and the results presented in Figure 2.2b show that the highest concentrations corresponded to spot 4 of the control, and to spot 4' of the sample. These spots migrated at the level of the PG standard.

Identification of the different phospholipid classes separated by TLC was carried out by ESI-MS and MS/MS analysis in negative- and positive-ion modes, after extraction of the lipid content from each separated spot (see below). Phospholipidomic analysis was also performed by HILIC-LC/MS of the total lipid extract of non-photosensitized *S. warneri* (Figure 2.2c).

### 2.4.2 Determination of the concentration of lipid hydroperoxides

In order to confirm that the observed changes in the phospholipid profile implied by the TLC results could be associated with oxidative modification of the bacterial lipids, the formation of hydroperoxides was assessed using the FOX2 assay.

The results obtained after quantification of lipid hydroperoxides, in the total lipid extract from the bacteria after irradiation, are presented in Figure 2.3a, and show that the concentration of lipid hydroperoxides in the sample after photosensitization (0.0015 µg OOH / µg of pohspholipid) was 97.5% higher than that found in the control ($p < 0.05$, Student's *t*-test).

These results confirm that photo-oxidation of lipids occurs after irradiation in the presence of the photosensitizer.

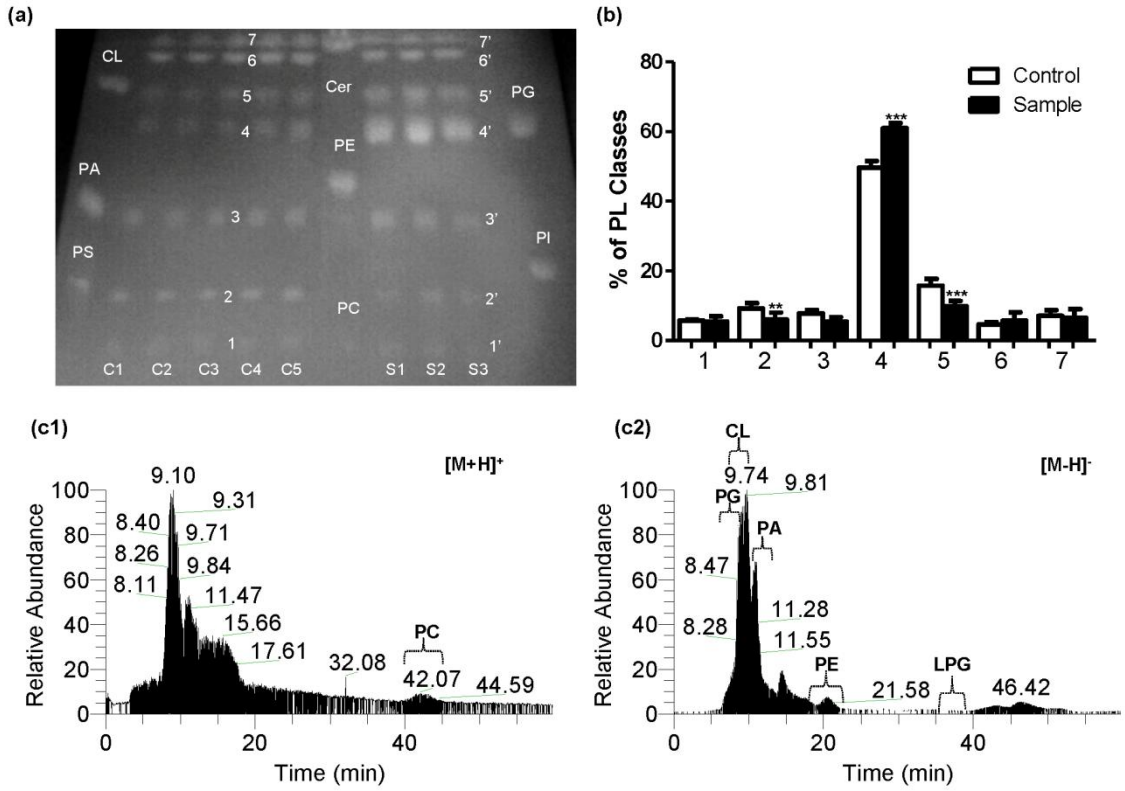


**Figure 2.2 (a)** Thin-layer chromatogram of fractioned *S. warneri* total lipids. Lanes C1-C5 represent the different fractions of the non-photosensitized cells (controls) and lane S1-S3 the different fractions of photosensitized cells (samples). The migration of known standards is shown for comparison (CL, cardiolipin; PA, phosphatidic acid; PS, phosphatidylserine; Cer, ceramide; PE, phosphatidylethanolamine; PC, phosphatidylcholine; PG, phosphatidylglycerol; PI, phosphatidylinositol); **(b)** Percentage of the different fractions of phospholipids (PL) separated by TLC of non-photosensitized (control) and photosensitized (sample) *S. warneri*. Error bars represent standard deviation of three independent experiments; **(c)** HILIC-HPLC-MS chromatograms of total lipid extracts of non-photosensitized *S. warneri* (**c1**, positive mode and **c2**, negative mode). The retention time of each phospholipid class is also represented.

### 2.4.3 Determination of membrane phospholipid composition

In order to identify each lipid class that underwent oxidation, MS analysis of the major phospholipid classes was performed after TLC separation. ESI-MS analysis in negative-ion mode, with formation of $[M–H]^-$ ions, allowed the identification of PGs in spot 4 of the control. Figure 2.4a2 shows the ESI mass spectrum of spot 4 of the control between *m/z* 650 and 800

where PGs were detected, with the most abundant ions at *m/z* 707.6, 735.6 and 763.6, and *m/z* 735.6 being the most prominent one. CLs were identified in spot 5 of the control and the mass spectrum where this class is detected (region *m/z* 1370 - 1600) shows three prominent peaks at *m/z* 1443.4, 1471.4 and 1499.4 (Figure 2.4b2).

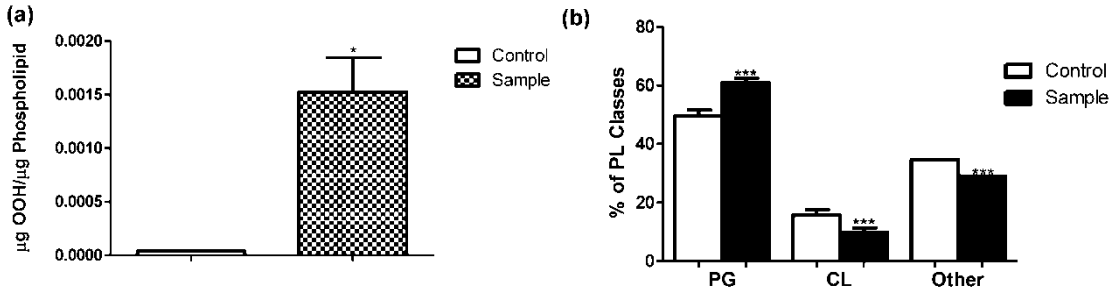


**Figure 2.3 (a)** Comparison of the concentration of hydroperoxides determined by FOX2 assay between non-photosensitized (control) and photosensitized (sample) *S. warneri*. Error bars represent standard deviation of three independent experiments and * the significant difference from control ($p < 0.05$); **(b)** Percentage of the main phospholipid classes identified in *S. warneri*. After separation by TLC and analysis by ESI-MS, it was found that the most abundant classes in this strain were PGs and CLs, both in the non-photosensitized (control) and in the photosensitized (sample) cells. The effect of photo-treatment is visible by the change in percentages of these two classes. Error bars represent standard deviation of three independent experiments and * the significant difference from control ($p < 0.05$).

HILIC-LC/MS analysis in negative-ion mode, with the formation of $[M–H]^-$ ions (Figure 2.2c2), allowed the identification of PGs and CLs, and also phosphatidic acids (PAs), phosphatidylethanolamines (PEs) and lysylphosphatidylglycerols (LPGs). The results for PGs and CLs were consistent with those obtained by direct analysis.The mass spectra of the PAs, PEs and LPGs were similar for the control and the sample, and the phospholipid profiles of each class are shown in Figures 2.5a, 2.5b and 2.5c, respectively.

The PAs had retention times in the range of 11 to 13 min, with the most intense peaks at *m/z* 633.4, 661.4 and 689.4. The PEs had retention times in the range of 18 to 22 min, with most intense peaks at *m/z* at 714.5, 738.4 and 766.5. The LPGs were identified in the range 36 to 39 min with the most intense peaks at *m/z* 821.4, 835.4 and 863.5.

In positive-ion mode, with formation of $[M+H]^+$ ions, HILIC-LC/MS analysis (Figure 2.2c1) allowed the identification of phosphatidylcholines (PCs). These species were identified in the range of 40 - 45 min, with most abundant ions at *m/z* 758.6, 760.6 and 786.6 (Figure 2.5d).

All ions identified as being derived from PGs, CLs, PAs, PEs, LPGs and PCs in the MS spectra were analyzed by ESI-MS/MS in order to confirm their structural features. This approach generated a huge amount of data that was analyzed and interpreted individually,

since no databases are available to obtain the information automatically. This analysis allowed the identification of the head group of each phospholipid and the confirmation of their fatty acyl chain composition according to previously identified fragmentation pathways. (181)

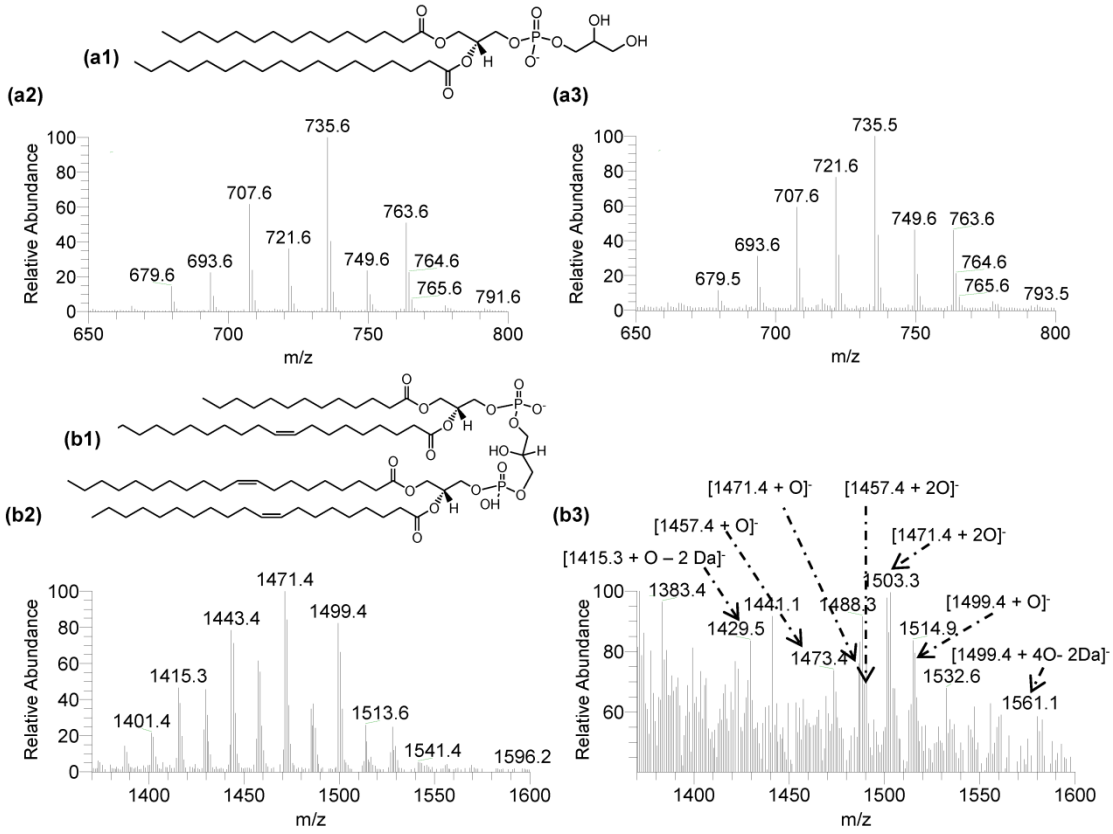


**Figure 2.4 (a1)** General structures of phosphatidylglycerol (PG); **(a2)** Negative-ion ESI-MS spectrum of PGs extracted from *S. warneri* irradiated without photosensitizer (control); **(a3)** Negative-ion ESI-MS spectrum of PGs extracted from *S. warneri* irradiated in the presence of photosensitizer (5.0 µM of Tri-$Py^{+}$-Me-PF) (sample); **(b1)** General structures of cardiolipin (CL); **(b2)** Negative-ion ESI-MS spectrum of CLs extracted from *S. warneri* irradiated without photosensitizer (control); **(b3)** Negative-ion ESI-MS spectrum of CLs extracted from *S. warneri* irradiated in the presence of photosensitizer (5.0 µM of Tri-$Py^{+}$-Me-PF) (sample). Irradiation conditions: artificial white light (4 mW $cm^{-2}$) for 90 min (21.6 J $cm^{-2}$).

As an example of the analysis performed for all classes, Figure 2.6 shows the MS/MS spectrum of the ion at *m/z* 821.2 corresponding to LPG (16:0/14:0), where ions formed by loss of 146 and 128 Da correspond to loss of the lysine moiety. In the MS/MS spectrum it can be seen the carboxylate anion, $RCOO^{-}$ at *m/z* 255.3, corresponding to fatty acid 16:0, and the ion at *m/z* 391.1 to the loss of 202 Da from the head, plus 228 Da from loss of the fatty acid 14:0 (-RCOOH). The ion at *m/z* 611.6 is due to the loss of the keto form (-RC=O) (821-(228-18)) of the fatty acid 14:0.

In addition, the most complex phospholipids, CLs, constituted by two phosphatidylglycerols linked by a glycerol unit and four fatty acyl chains, were also analyzed by MS/MS, using previously defined fragmentation pathways. (182)

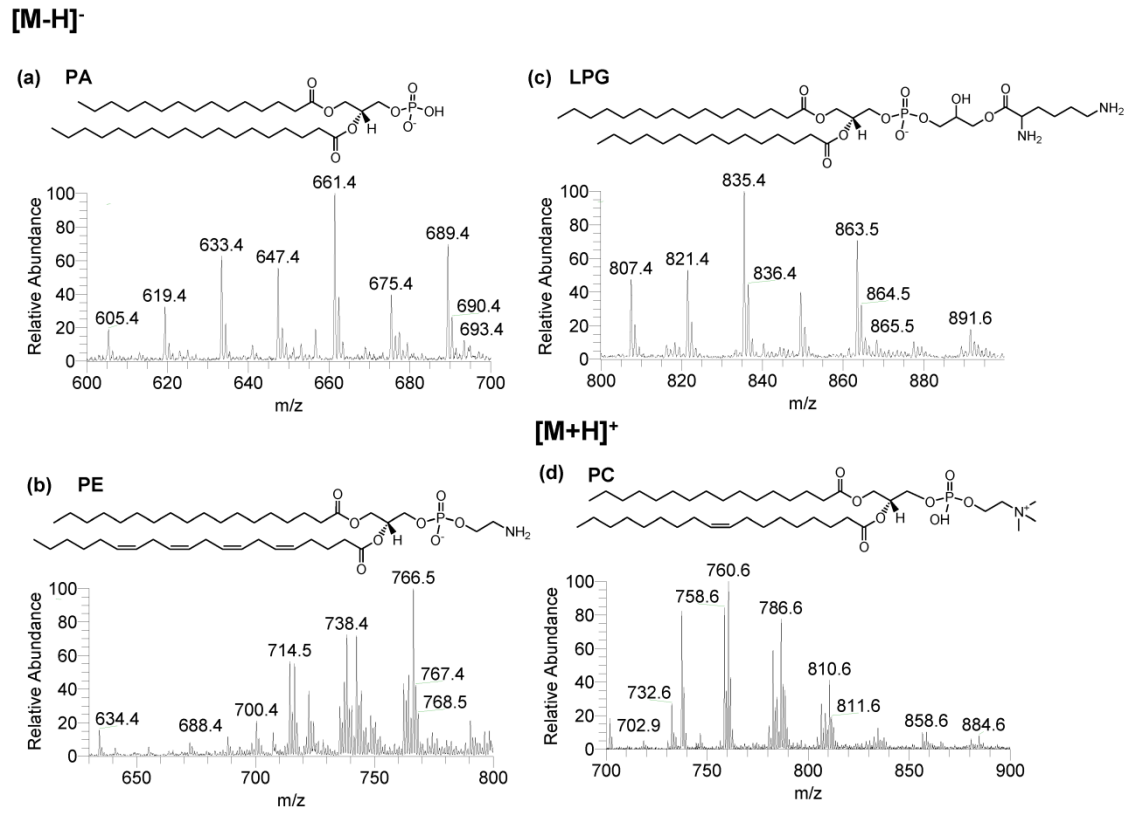


**Figure 2.5** General structures and ESI-MS spectra of other phospholipid classes identified by HPLC-MS in *S. warneri*. In negative-ion mode: **(a)** phosphatidic acids; **(b)** phosphatidylethanolamines; **(c)** lysyl-phosphatidylglycerols; and in positive-ion mode: **(d)** phosphatidylcholines.

The molecular species of the phospholipid classes from *S. warneri* characterized by ESI-MS/MS are presented in Tables 2.1 - 2.6 (at the end of this Chapter). Several $[M–H]^-$ ions were identified, as a mixture of isobaric forms. Most of the PGs and PAs were composed mainly of saturated fatty acyl chains. The other classes were composed of saturated and unsaturated fatty acyl chains, with a large variety of fatty acyl residues.

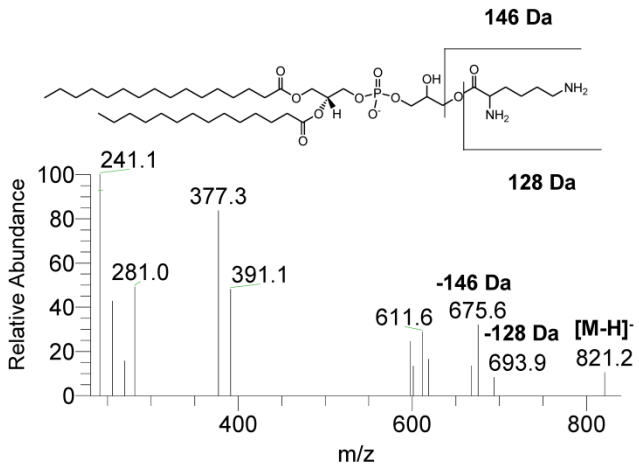


**Figure 2.6** MS/MS spectrum of $[M-H]^-$ ions at *m/z* 821.2 corresponding to LPG (16:0/14:0). The proposed structure for the product ions observed in the MS/MS spectrum is also represented.

### 2.4.4 Evaluation of the photodynamic effect in major phospholipid classes

Comparison between control and sample MS spectra of PGs (Figure 2.4a2 *vs.* Figure 2.4a3) shows that some alterations occurred during the photodynamic process. There is an overall increase in the relative abundance of some ions, namely those at *m/z* 721.6 and 749.6. An increase in the intensity of the ion at *m/z* 693.6 was also observed; however, no new ions suggesting the presence of oxidized species were detected.

In contrast, the photodynamic process induced more severe alterations on the profile of CLs. The mass spectrum of CLs obtained from photosensitized cells (sample) (Figure 2.4b3), when compared with the control (Figure 2.4b2), shows some new ions suggesting the formation of oxidized species. These new ions have mass increments of 32 *m/z* units (addition of two oxygen atoms with formation of a hydroperoxy group), 16 *m/z* units (formation of hydroxy or epoxy groups) and 14 *m/z* units (formation of a carbonyl group), formed by decomposition of CL hydroperoxides (summarized in Table 2.7, at the end of this Chapter). These results are evidence for the presence of oxidation products of CLs as hydroperoxide derivatives (CL+2O) and are in agreement with the results obtained with the FOX2 assay.

Confirmation of oxidative modification of CL was accomplished by MS/MS analysis of the oxidized species. As an example, the MS/MS fragmentation of the $[M–H]^-$ ion of the oxidation product CL at *m/z* 1449.9 [CL-(C16:0)(C18:2+OO)/(C17:0)(C18:0] (Figure 2.7a1) will be explained. The MS/MS spectrum shows product ions identified as phosphatidic acids (PAs) at *m/z* 689.5 [(C17:0)(C18:0)] and 703.4 [(C16:0)(C18:2+OO)]. Phosphatidic acid (PA) ions plus 136 *m/z* units were also identified at *m/z* 825.6 [(C17:0)(C18:0)+136] and 839.6 [(C16:0)(C18:2+OO)+136] while the ion corresponding to monophosphatidic acid (PA–RCOOH) was detected at *m/z* 447.3 [(C18:2+OO)+ 136] (Figure 2.7a1). MS3 of the product ion at *m/z* 703.5 (Figure 2.7a2) allows the presence of the CL oxidation product to be confirmed. Figure 2.7b presents the proposed structures for the product ions observed from the MS/MS spectrum of the CL oxidized ion at *m/z* 1449.9.

Quantification of phospholipids by phosphorus assay of the control and sample spots, corroborated by the characterization of molecular species by ESI-MS/MS, showed that the major phospholipid fraction of this *S. warneri* strain corresponds to PGs (49.6% of the total amount of phosphorus determined in the isolated spot of silica from TLC). The amount of CLs determined was 15.8% (Figure 2.3b). After photodynamic treatment, there was a significant increase ($p < 0.05$, one-way ANOVA) in PGs (from 49.6% to 61.0%) and a decrease in CLs (from 15.8% to 9.9%) and other phospholipids (34.6% to 29.1%).

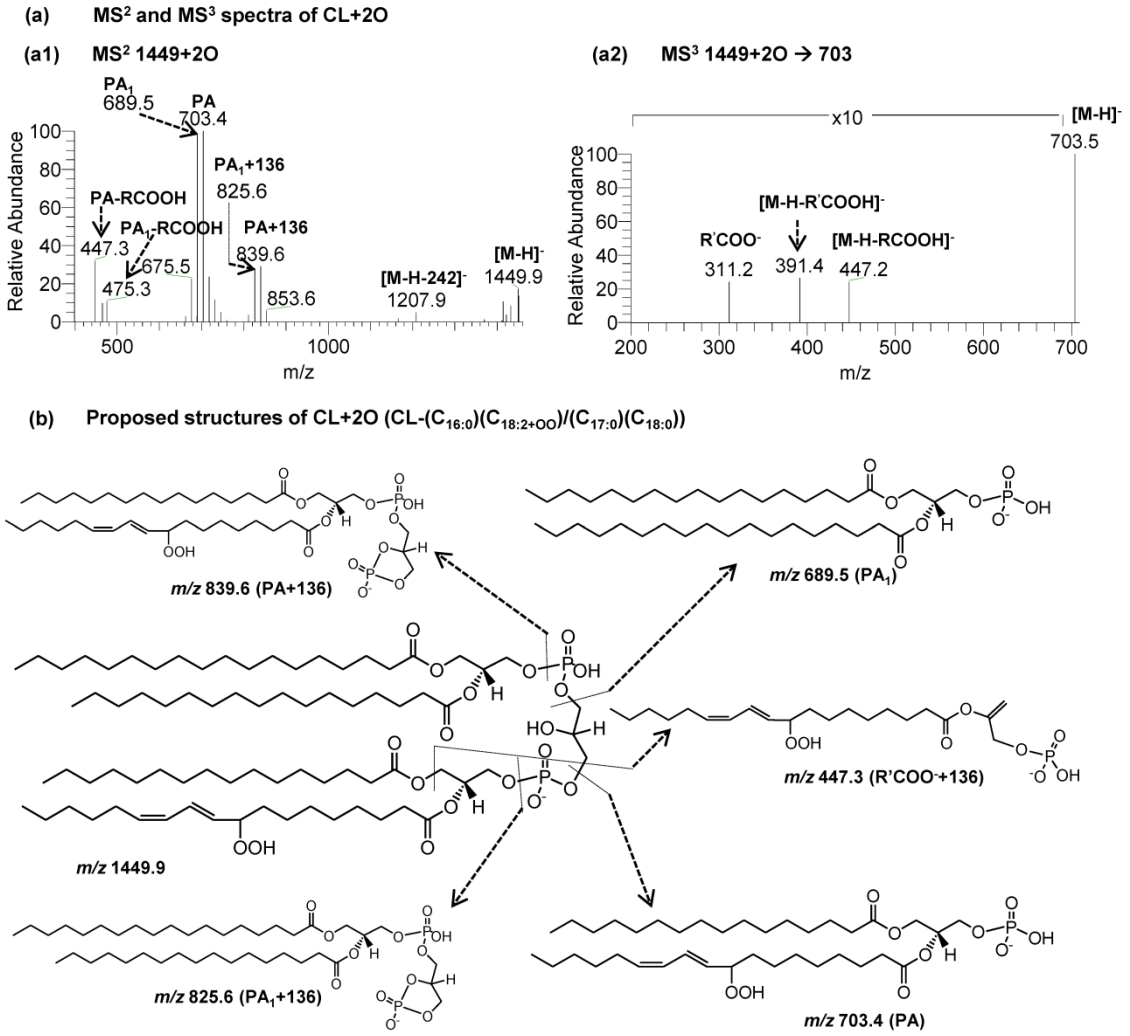


**Figure 2.7 (a1)** MS/MS spectrum of the $[M-H]^-$ ions at *m/z* 1449.9 of CL(69:2)+2O; **(a2)** MS3 of $[M-H]^-$ ions at *m/z* 703.5 of CL(69:2)+2O; **(b)** Proposed structures derived from fragmentation of CL-(C16:0)(C18:2+OO)/(C17:0)(C18:0) oxidation product.

### 2.4.5 Photodynamic oxidation of phospholipid standards

Photo-oxidation of the phospholipid standards (PG and CL) was compared with the results obtained for the photosensitized cells. For the PG standard mixture, the mass spectrum of the control revealed the presence of major $[M–H]^–$ ions at *m/z* 747.6 and 773.5, corresponding to PG (16:0/18:1) and PG (18:1/18:1), respectively (Figure 2.8(a)). The ESI-MS spectrum of the PG standard after irradiation in the presence of Tri-$Py^+$-Me-PF (Figure 2.8(b)) shows new ions at *m/z* 779.5 and 805.5 corresponding, respectively, to PG hydroperoxides: PG(16:0/18:1)+2O and PG (18:1/18:1)+2O with the hydroperoxy units located in the unsaturated fatty acyl chains. The ion at *m/z* 837.5 corresponds to PG (18:1/18:1)+4O, identified as a derivative bearing two hydroperoxy units. No other products suggesting oxidative changes in the polar head were identified. As the PG fatty acyl chains identified in

photosensitized bacteria are mainly saturated ones (Table 2.1), they did not undergo oxidation (Figure 2.4(a3)), only showing changes in their relative abundance.

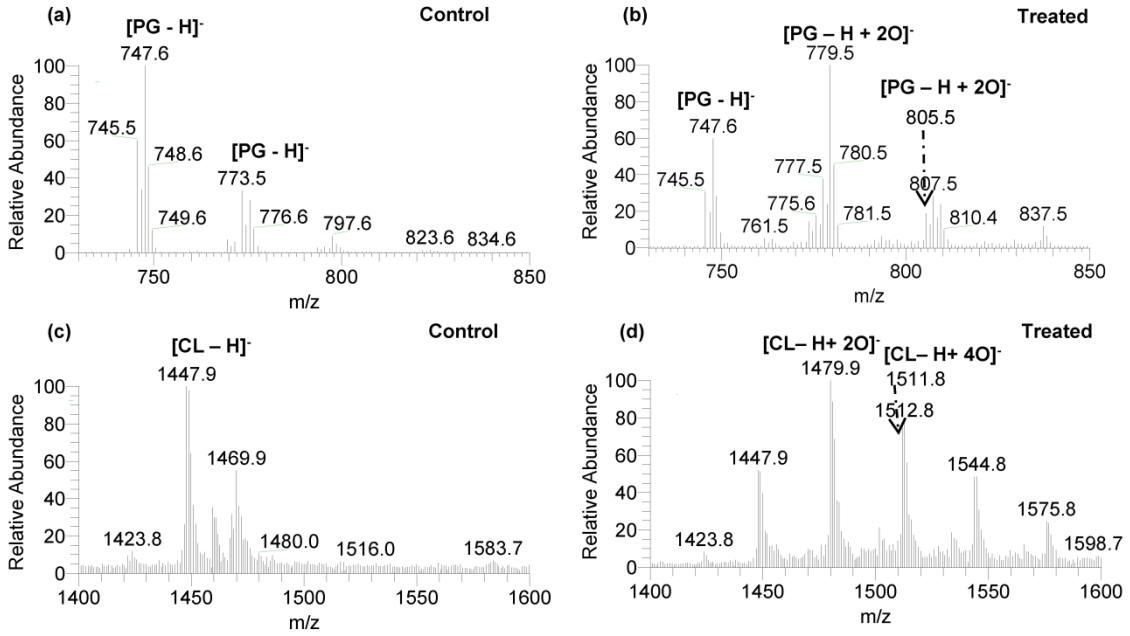


**Figure 2.8** Negative-ion ESI-MS spectra of phospholipid standards. Control standards (**a** and **c**) were irradiated without Tri-Py$^{+}$-Me-PF. Treated standards (**b** and **d**) were irradiated (with artificial white light, 4 mW cm$^{-2}$) for 90 min (21.6 J cm$^{-2}$) in the presence of 5.0 μM of Tri-Py$^{+}$-Me-PF. PG, phosphatidylglycerol; CL, cardiolipin.

For the CL standard, the mass spectrum of the control (Figure 2.8(c)) shows an abundant ion at *m/z* 1447.9 corresponding to the $[M–H]^{–}$ ion of CL bearing four acyl chains with two double bonds $[18:2]_4$. The mass spectrum of the corresponding photosensitized standard (Figure 2.8(d)) shows, in addition to the ion at *m/z* 1447.9, ions at *m/z* 1479.9 and 1511.8 due, respectively, to the addition of two and four oxygen atoms in the unsaturated fatty acyl chains of CL $(18:2)_4$. These ions correspond to the formation of the oxidation products hydroperoxy-CL (CL+2O) and dihydroperoxy-CL (CL+4O), respectively. The ion at *m/z* 1544.8 corresponds to the oxidation product of CL resulting from the insertion of six oxygen atoms (1447 + 96), and the ion at *m/z* 1575.8 corresponds to the insertion of eight oxygen atoms (1447 + 128). These ions were previously identified in our laboratory during the oxidation of CL induced by the hydroxyl radical. (182)

## 2.5 Discussion

The photodynamic effect in the predominant classes of membrane phospholipids of *S. warneri* was studied, using a cationic amphiphilic porphyrin (Tri-Py$^{+}$-Me-PF). This porphyrin has been recognized as an efficient photosensitizer in the photoinactivation of bacteriophages

(143), Gram-positive and Gram-negative bacteria (77) and bacterial endospores. (144) It was also shown that the viability of the microorganisms is not affected by the irradiation conditions, nor does the porphyrin exhibit toxicity in the absence of light with the concentrations used. The route by which reactive oxygen species are produced by this photosensitizer was also studied in a Gram-negative bacterium (183), with a type II mechanism (183) being the predominant pathway (generation of singlet oxygen). This highly reactive excited state of molecular oxygen is involved in the process of lipid peroxidation (type II process), responsible for changing the structure and function of the target as well as of surrounding molecules. (9, 98)

It is known that the membrane phospholipids of coagulase-negative *S. warneri* cells are mostly PGs and CLs. (171) In control cells, ESI-MS, HILIC-LC/MS and MS/MS were used to identify PGs, CLs and other minor classes of phospholipids, such as PAs, PEs, LPGs and PCs in this strain of *S. warneri*. PGs represent the major class (49.6%), followed by CLs (15.8%) (Figure 2.3b). The intense ions observed at *m/z* 707.5 and *m/z* 735.5 (Figure 2.4a2), are consistent with the presence of the phospholipid PG(31:0) and PG(33:0), which have already been observed as major species for *S. epidermidis*. (170) Another major ion was found at *m/z* 763.6, consistent with PG(35:0). This phospholipid was also observed in other species of *Staphylococcus*, but in lower concentrations than in this strain, which shows the quantitative differences among strains. (170) As the fatty acid composition of PGs is mainly saturated acyl chains, oxidation did not occur in this phospholipid class in photosensitized cells. However, an overall increase (from 49.6% to 61.0%) could be observed (Figure 2.3b) in the relative abundance of ions of this class, after the photodynamic treatment. A major increase was observed for the ions at *m/z* 693.6, 721.6 and 749.6, assigned as PG(30:0), PG(32:0) and PG(34:0). The ion at *m/z* 749.6 is one of the most abundant in the coagulase-negative *S. epidermidis*, *S. haemolyticus* and *S. hominis.* (170)

ESI-MS and MS/MS analysis of CLs in control cells showed a prevalence of unsaturated fatty acyl chains which are more susceptible to suffer oxidation than the saturated ones. The ions identified by ESI-MS/MS in photosensitized cells revealed mass increments of 32, 16 and 14 *m/z* units, indicating formation of oxidized species of CL (Figure 2.4b3). These increments can be explained by the addition of oxygen, affording the hydroperoxy-CL which can decompose to hydroxy and keto species. It was shown previously that photodynamic oxidation of CL in the presence of a phthalocyanine yielded mainly hydroperoxy species (184) that can decompose and dehydrate with the formation of hydroxy and keto derivatives. The presence of these species was also confirmed from the results of the ESI-MS/MS analysis, using the methodology previously proposed by our group. (182) The high percentage of lipid

hydroperoxides determined by FOX2 assay after photodynamic treatment (97.5% higher in the sample than in the control) (Figure 2.3a) confirmed that the oxidative modification of lipids involves the formation of hydroperoxides and this is in agreement with the oxidative process described recently in CLs. (182) The effects of photodynamic treatment in selected phospholipid standards also confirm the formation of hydroperoxy derivatives, and also dihydroperoxy derivatives in the photosensitization conditions used for these bacteria. Photo-oxidation of phospholipid standards in the presence of the photosensitizers yields mainly hydroperoxides accompanied by minor amounts of hydroxy derivatives. The higher proportion of CL hydroxy derivatives in bacteria lipid extracts may be due to the decomposition of lipid hydroperoxides into the corresponding hydroxyl derivatives elicited by metal cations that exist *in vivo.* (185, 186)

The decrease in the CLs fraction (from 15.8% to 9.9%) and the increase in the PGs fraction (from 49.6% to 61.0%) in photosensitized cells (sample) suggest that photo-oxidation of CLs (constituted by four acyl chains) might induce oxidative cleavage, yielding diacyl species with similar polarity to PGs, or even generate new PG species that co-elute in the PGs fraction. Oxidative cleavage of CLs has already been observed during oxidation induced by gamma irradiation. (187) The decrease in the abundance of CLs due to the oxidation could be caused by the diminishing of PA precursors. (35)

In addition to the lipid peroxidation that occurs in the unsaturated fatty acyl chains of CLs upon photodynamic treatment by reactive oxygen species formed during the process, an interaction between the photosensitizer and the membrane lipids also occurs. A recently suggested mechanism of membrane damage involving antimicrobial cationic agents and anionic lipids (188-190) might justify the increase of PGs and decrease of CLs; however, this hypothesis will have to be further studied. It has been reported that the agent (with multiple cationic groups, conformational flexibility and sufficient hydrophobicity) can induce the separation of lipid components, as it binds to anionic lipids, causing rearrangements and leaving defects in the membrane that will lower the permeability barrier between the cell and its surroundings. (188-190) Anionic lipids are then recruited from other locations in the membrane where they are required for specific functions. (188-190) These segregated phases or domains do not lead to toxicity and are a cell defense mechanism. This subject has not yet been studied in photodynamic therapy, but it might explain the behavior of the photosensitizer at the membrane level, and the alterations that occur in the lipids and phospholipids.

The lipid profile of *S. warneri* is affected by the photodynamic process using the cationic porphyrin Tri-Py$^{+}$-Me-PF at 5.0 μM and visible light (21.6 J cm$^{-2}$), as demonstrated by

lipidomics. ESI-MS, HILIC-LC/MS and MS/MS experiments showed that there are modifications in the relative abundance of some phospholipids, the phosphatidylglycerols (PGs), and that the reactive oxygen species generated during the photodynamic process lead to the oxidation of unsaturated molecular species, present in high abundance in cardiolipins (CLs), through the formation of hydroperoxy, hydroxy and carbonyl groups.

This study highlights the lipid peroxidation of bacterial membrane as cellular damage occurring in the photodynamic process. The observed photo-oxidative changes in *S. warneri* phospholipids provide some insights into the mechanistic inactivation of this type of bacteria.

**Table 2.1** Major molecular species of phosphatidylglycerols identified in *S. warneri*

| $[M-H]^-$ *m/z* (C:N) | Fatty Acyl Chains | $[M-H]^-$ *m/z* (C:N) | Fatty Acyl Chains | $[M-H]^-$ *m/z* (C:N) | Fatty Acyl Chains |
|---|---|---|---|---|---|
| 651.6 (27:0) | 13:0/14:0 | 735.6 (33:0) | 19:0/14:0 | 771.6 (36:3) | 14:0/22:3 |
| 665.6 (28:0) | 12:0/16:0 | 735.6 (33:0) | 20:0/13:0 | 773.6 (36:2) | 18:1/18:1 |
| 665.6 (28:0) | 13:0/15:0 | 745.6 (34:2) | 16:0/18:2 | 773.6 (36:2) | 18:0/18:2 |
| 665.6 (28:0) | 14:0/14:0 | 745.6 (34:2) | 16:1/18:1 | 773.6 (36:2) | 16:1/20:1 |
| 679.6 (29:0) | 14:0/15:0 | 745.6 (34:2) | 14:0/20:2 | 773.6 (36:2) | 16:0/20:2 |
| 679.6 (29:0) | 13:0/16:0 | 747.6 (34:1) | 14:0/20:1 | 775.6 (36:1) | 18:0/18:1 |
| 693.6 (30:0) | 15:0/15:0 | 747.6 (34:1) | 14:1/20:0 | 775.6 (36:1) | 20:0/16:1 |
| 693.6 (30:0) | 16:0/14:0 | 747.6 (34:1) | 16:0/18:1 | 775.6 (36:1) | 16:0/20:1 |
| 693.6 (30:0) | 17:0/13:0 | 747.6 (34:1) | 18:0/16:1 | 775.6 (36:1) | 17:0/19:1 |
| 693.6 (30:0) | 18:0/12:0 | 747.6 (34:1) | 15:0/19:1 | 775.6 (36:1) | 17:0/cy19:0 |
| 705.6 (31:1) | 13:0/18:1 | 747.6 (34:1) | 15:0/cy19:0 | 775.6 (36:1) | 14:0/22:1 |
| 705.6 (31:1) | 15:0/16:1 | 749.6 (34:0) | 19:0/15:0 | 777.6 (36:0) | 18:0/18:0 |
| 707.6 (31:0) | 16:0/15:0 | 749.6 (34:0) | 17:0/17:0 | 777.6 (36:0) | 19:0/17:0 |
| 707.6 (31:0) | 17:0/14:0 | 749.6 (34:0) | 18:0/16:0 | 777.6 (36:0) | 20:0/16:0 |
| 707.6 (31:0) | 18:0/13:0 | 749.6 (34:0) | 20:0/14:0 | 777.6 (36:0) | 21:0/15:0 |
| 721.6 (32:0) | 16:0/16:0 | 749.6 (34:0) | 21:0/13:0 | 777.6 (36:0) | 22:0/14:0 |
| 721.6 (32:0) | 17:0/15:0 | 761.6 (35:1) | 15:0/20:1 | 791.6 (37:0) | 15:0/22:0 |
| 721.6 (32:0) | 18:0/14:0 | 761.6 (35:1) | 17:0/18:1 | 791.6 (37:0) | 17:0/20:0 |
| 721.6 (32:0) | 19:0/13:0 | 761.6 (35:1) | 20:0/15:1 | 791.6 (37:0) | 18:0/19:0 |
| 731.6 (33:2) | 15:0/18:2 | 761.6 (35:1) | 20:0/cy15:0 | 791.6 (37:0) | 16:0/21:0 |
| 731.6 (33:2) | 16:1/17:1 | 761.6 (35:1) | 13:0/22:1 | 797.6 (38:4) | 18:1/20:3 |
| 731.6 (33:2) | 16:1/cy17:0 | 763.6 (35:0) | 18:0/17:0 | 797.6 (38:4) | 18:2/20:2 |
| 731.6 (33:2) | 16:0/17:2 | 763.6 (35:0) | 20:0/15:0 | 797.6 (38:4) | 16:1/22:3 |
| 733.6 (33:1) | 14:0/19:1 | 763.6 (35:0) | 21:0/14:0 | 797.6 (38:4) | 18:0/20:4 |
| 733.6 (33:1) | 14:0/cy19:0 | 763.6 (35:0) | 16:0/19:0 | 797.6 (38:4) | 16:0/22:4 |
| 733.6 (33:1) | 15:0/18:1 | 763.6 (35:0) | 13:0/22:0 | 799.6 (38:3) | 18:1/20:2 |
| 733.6 (33:1) | 16:0/17:1 | 771.6 (36:3) | 18:1/18:2 | 799.6 (38:3) | 18:2/20:1 |
| 733.6 (33:1) | 16:0/cy17:0 | 771.6 (36:3) | 16:1/20:2 | 799.6 (38:3) | 18:0/20:3 |
| 735.6 (33:0) | 17:0/16:0 | 771.6 (36:3) | 16:0/20:3 | 799.6 (38:3) | 16:0/22:3 |
| 735.6 (33:0) | 18:0/15:0 | 771.6 (36:3) | 18:0/18:3 | 799.6 (38:3) | 16:1/22:2 |

$[M-H]^-$ ions of phosphatidylglycerol observed in the ESI-MS spectra, with the attribution of the fatty acyl composition of each phospholipid molecular species, accordingly to the interpretation of the correspondent MS/MS spectra. Numbers in parenthesis (C:N) indicate the number of carbon atoms (C) and double bonds (N) in the fatty acid side chains.

**Table 2.2** Major molecular species of cardiolipins identified in *S. warneri*

| $[M-H]^-$ *m/z* (C:N) | Fatty Acyl Chains |
|---|---|
| 1387.4 (67:3) | 14:1/18:0/13:0/22:2; 14:1/17:0/14:0/22:2; 15:0/22:2/14:1/16:0; 22:2/18:1/13:0/14:0 |
| 1387.4 (67:3) | (18:1)3/13:0; (18:1)2/14:1/17:0; (20:1)2/14:1/13:0; 14:1/17:0/22:0/14:2 |
| 1387.4 (67:3) | 18:1/13:0/22:0/14:2; 18:1/17:0/18:0/14:2; 20:1/18:0/15:0/14:2; 20:1/16:0/17:0/14:2 |
| 1387.4 (67:3) | 14:1/18:1/20:1/15:0 |
| 1401.4 (68:3) | (16:1)2/19:1/17:0; (16:1)2/20:1/16:0; (17:1)3/17:0; 16:0/(17:1)2/18:1; 14:0/(17:1)2/20:1 |
| 1401.4 (68:3) | 14:0/(18:1)3; 16:0/16:1/(18:1)2; (19:1)2/16:1/14:0; 16:0/16:1/17:1/19:1 |
| 1401.4 (68:3) | 16:1/17:1/18:1/17:0; 16:1/18:1/20:1/14:0; 17:1/18:1/19:1/14:0; (16:0)2/18:1/18:2 |
| 1401.4 (68:3) | (17:0)2/16:1/18:2; 18:2/17:1/16:0/17:0; 18:2/19:1/14:0/17:0; 18:2/20:1/14:0/16:0; |
| 1401.4 (68:3) | (16:1)2/cy19:0/17:0; (cy17:0)3/17:0; 16:0/(cy17:0)2/18:1; 14:0/(cy17:0)2/20:1; |
| 1401.4 (68:3) | (cy19:0)2/16:1/14:0; 16:0/16:1/cy17:0/cy19:0; 16:1/cy17:0/18:1/17:0; |
| 1401.4 (68:3) | cy17:0/18:1/cy19:0/14:0; 18:2/cy17:0/16:0/17:0; 18:2/cy19:0/14:0/17:0 |
| 1415.3 (69:3) | (16:1)2/18:1/19:0; (16:1)2/19:1/18:0; (16:1)2/20:1/17:0; (18:1)3/15:0; (18:1)2/16:1/17:0 |
| 1415.3 (69:3) | (18:1)2/19:1/14:0;(18:1)2/13:0/20:1; 16:1/(19:1)2/14:0; 18:1/(19:1)2/13:0 |
| 1415.3 (69:3) | (20:1)2/16:1/13:0; 17:0/19:2/15:0/18:1; 16:0/19:2/16:0/18:1; 19:0/19:2/13:0/18:1 |
| 1415.3 (69:3) | 18:0/19:2/14:0/18:1; 17:0/19:2/13:0/20:1; 14:0/19:2/16:0/20:1; (15:0)2/19:2/20:1 |
| 1415.3 (69:3) | 14:0/19:2/17:0/19:1; 16:0/19:2/15:0/19:1; 18:0/19:2/13:0/19:1; 19:2/16:1/20:0/14:0 |
| 1415.3 (69:3) | 19:2/16:1/19:0/15:0; 19:2/16:1/(17:0)2; 19:2/16:1/18:0/16:0; 16:0/17:2/17:0/19:1 |
| 1415.3 (69:3) | 20:0/17:2/13:0/19:1; 19:0/17:2/14:0/19:1; 18:0/17:2/15:0/19:1; 19:0/17:2/13:0/20:1 |
| 1415.3 (69:3) | (16:0)2/17:2/20:1; 18:0/17:2/14:0/20:1; 17:0/17:2/15:0/20:1; 14:0/17:2/20:0/18:1 |
| 1415.3 (69:3) | 19:0/17:2/15:0/18:1; 16:0/17:2/18:0/18:1; (17:0)2/17:2/18:1; 17:2/16:1/19:0/17:0 |
| 1415.3 (69:3) | 17:2/16:1/(18:0)2; 17:2/16:1/20:0/16:0; 18:1/16:1/19:1/16:0; 18:1/16:1/20:1/15:0 |
| 1415.3 (69:3) | 20:1/16:1/19:1/14:0; (16:1)2/cy19:0/18:0; (18:1)2/cy19:0/14:0; 16:1/(cy19:0)2/14:0 |
| 1415.3 (69:3) | 18:1/(cy19:0)2/13:0; 14:0/19:2/17:0/cy19:0; 16:0/19:2/15:0/cy19:0; 18:0/19:2/13:0/cy19:0 |
| 1415.3 (69:3) | 16:0/17:2/17:0/cy19:0; 20:0/17:2/13:0/cy19:0; 19:0/17:2/14:0/cy19:0 |
| 1415.3 (69:3) | 18:0/17:2/15:0/cy19:0; 18:1/16:1/cy19:0/16:0; 20:1/16:1/cy19:0/14:0 |
| 1417.4 (69:2) | 13:0/(18:0)2/20:2; 14:0/17:0/18:0/20:2; 15:0/16:0/18:0/20:2; 15:0/(17:0)2/20:2; |
| 1417.4 (69:2) | (16:0)2/17:0/20:2 ; 16:0/17:0/18:0/18:2 |
| 1419.4 (69:1) | 14:0/16:0/17:0/22:1; 15:0/(16:0)2/22:1; 13:0/16:0/18:0/22:1; 13:0/(17:0)2/22:1; |
| 1419.4 (69:1) | 14:0/15:0/18:0/22:1; 14:0/16:0/17:0/22:1; (15:0)2/17:0/22:1 |
| 1443.4 (71:3) | 16:0/20:3/13:0/22:0; 16:0/20:3/14:0/21:0; 16:0/20:3/16:0/19:0; 16:0/20:3/18:0/17:0 |
| 1443.4 (71:3) | 16:0/20:3/20:0/15:0; 13:0/20:0/18:0/20:3; 13:0/(19:0)2/20:3 ; 15:0/17:0/19:0/20:3; |
| 1443.4 (71:3) | 15:0/(18:0)2/20:3; 14:0/17:0/20:0/20:3; 14:0/18:0/19:0/20:3; 13:0/18:0/20:0/20:3 |
| 1443.4 (71:3) | 13:0/17:0/21:0/20:3; 22:0/14:0/15:0/20:3; (19:0)2/13:0/20:3; (18:0)2/15:0/20:3 |
| 1443.4 (71:3) | (15:0)2/21:0/20:3; (17:0)3/20:3 (16:1)2/22:1/17:0; (16:1)2/18:1/21:0; (16:1)2/22:0/17:1; |
| 1443.4 (71:3) | (18:1)3/17:0; (18:1)2/18:0/17:1; (18:1)2/19:0/16:1; (18:1)2/21:0/14:1; 22:1/(18:1)2/13:0 |
| 1443.4 (71:3) | (22:1)2/14:1/13:0; (14:1)2/22:1/21:0; (17:1)3/20:0; (17:1)2/15:0/22:1; (17:1)2/21:0/16:1 |
| 1443.4 (71:3) | (17:1)2/19:0/18:1; 16:1/14:1/22:1/19:0; 14:1/17:1/18:1/22:0; 14:1/17:1/22:1/18:0 |

**Table 2.2** Major molecular species of cardiolipins identified in *S. warneri* (cont.)

| $[M-H]^-$ *m/z* (C:N) | Fatty Acyl Chains |
|---|---|
| 1443.4 (71:3) | 14:1/18:1/22:1/17:0; 16:1/17:1/18:1/20:0; 16:1/17:1/22:1/16:0; 14:1/18:1/22:1/15:0 |
| 1443.4 (71:3) | 18:1/17:1/22:1/14:0; (16:1)2/22:0/cy17:0; (18:1)2/18:0/cy17:0; (cy17:0)3/20:0; |
| 1443.4 (71:3) | (cy17:0)2/15:0/22:1; (cy17:0)2/21:0/16:1; (cy17:0)2/19: 0/18:1; 14:1/cy17:0/18:1/22:0; |
| 1443.4 (71:3) | 14:1/cy17:0/22:1/18:0; 16:1/cy17:0/18:1/20:0; 16:1/cy17:0/22:1/16:0; |
| 1443.4 (71:3) | 18:1/cy17:0/22:1/14:0 |
| 1445.4 (71:2) | 17:1/14:1/(20:0)2; (17:1)2/20:0/17:0; (17:1)2/19:0/18:0; 19:0/20:0/14:1/18:1 |
| 1445.4 (71:2) | 17:1/18:1/20:0/16:0; 17:1/18:1/19:0/17:0; 17:1/18:1/(18:0)2; (18:1)2/16:0/19:0 |
| 1445.4 (71:2) | (18:1)2/17:0/18:0; (18:1)2/15:0/20:0; (18:0)3/18:2; (16:0)2/19:0/18:2 |
| 1445.4 (71:2) | 17:0/19:0/18:0/18:2; 14:0/20:0/19:0/18:2; 15:0(19:0)2/18:2; (17:0)2/18:0/18:2 |
| 1445.4 (71:2) | 13:0/20:0/20:0/18:2; 15:0/20:0/18:0/18:2; 16:0/20:0/17:0/18:2; 16:0/18:0/19:0/18:2 |
| 1445.4 (71:2) | cy17:0/14:1/(20:0)2; (cy17:0)2/20:0/17:0; (cy17:0)2/19:0/18:0 |
| 1445.4 (71:2) | cy17:0/18:1/20:0/16:0; cy17:0/18:1/19:0/17:0; cy17:0/18:1/(16:0)2 |
| 1457.4 (72:3) | (17:1)2/18:0/20:1; 17:1/19:1/18:0/18:1; 17:1/(19:1)2/17:0; 17:1/19:1/16:0/20:1 |
| 1457.4 (72:3) | 17:1/18:1/17:0/20:1; 17:0/18:0/17:1/20:2; (18:1)3/18:0; (18:1)2/17:0/19:1; |
| 1457.4 (72:3) | (18:1)2/16:0/20:1; (19:1)2/18:1/16:0; 16:1/18:1/18:0/20:1; (17:0)2/18:1/20:2 |
| 1457.4 (72:3) | 16:0/20:2/18:0/18:1; (19:1)2/18:0/16:1; 17:0/19:1/16:1/20:1; 16:0/20:2/17:0/19:1 |
| 1457.4 (72:3) | 16:0/16:1/(20:1)2; (16:0)2/20:2/20:1; 20:2/16:1/(18:0)2; (17:0)2/18:0/20:3 |
| 1457.4 (72:3) | 16:0/(18:0)2/20:3; 18:0/18:2/16:0/20:1; (17:0)2/20:1/18:2; (18:0)2/18:2/18:1 |
| 1457.4 (72:3) | 18:0/18:2/17:0/19:1; (cy17:0)2/18:0/20:1; cy17:o/cy19:0/18:0/18:1; cy17:0/(cy19:0)2/17:0; |
| 1457.4 (72:3) | cy17:0/cy19:0/16:0/20:1; cy17:0/18:1/17:0/20:1; 17:0/18:0/cy17:0/20:2 |
| 1457.4 (72:3) | (18:1)2/17:0/cy19:0; (cy19:0)2/18:1/16:0; (cy19:0)2/18:0/16:1 |
| 1457.4 (72:3) | 17:0/cy19:0/16:1/20:1; 16:0/20:2/17:0/cy19:0; 18:0/18:2/17:0/cy19:0 |
| 1471.4 (73:3) | 13:0/20:0/20:1/20:2; 14:0/19:0/20:1/20:2; 15:0/18:0/20:1/20:2; 16:0/17:0/20:1/20:2 |
| 1471.4 (73:3) | 13:0/(20:1)3; 22:0/17:0/14:2/20:1; 21:0/18:0/14:2/20:1; 20:0/19:0/14:2/20:1 |
| 1471.4 (73:3) | 22:0/14:0/17:2/20:1; 21:0/15:0/17:2/20:1; 20:0/16:0/17:2/20:1; 19:0/17:0/17:2/20:1; |
| 1471.4 (73:3) | (18:0)2/17:2/20:1; (20:1)2; 18:1/15:0; 20:2/18:1/22:0/13:0; 22:0/19:0/14:2/18:1 |
| 1471.4 (73:3) | 21:0/20:0/14:2/18:1; 22:0/16:0/17:2/18:1; 21:0/17:0/17:2/18:1; 20:0/18:0/17:2/18:1 |
| 1471.4 (73:3) | (19:0)2/17:2/18:1 |
| 1499.4 (75:3) | 13:0/20:0/22:1/20:2; 14:0/19:0/22:1/20:2; 18:0/15:0/22:1/20:2; 17:0/16:0/22:1/20:2; |
| 1499.4 (75:3) | 13:0/22:0/20:1/20:2; 15:0/20:0/20:1/20:2; 19:0/16:0/20:1/20:2; 17:0/18:0/20:1/20:2; |
| 1499.4 (75:3) | 19:0/22:0/14:1/20:2; 16:0/22:0/17:1/20:2; 18:0/20:0/17:1/20:2; (19:0)2/17:1/20:2; |
| 1499.4 (75:3) | 15:0/22:0/18:1/20:2; 17:0/20:0/18:1/20:2; 19:0/18:0/18:1/20:2; (22:2)2/14:1/17:2; |
| 1499.4 (75:3) | 17:2/17:1/22:0/19:0; 17:2/18:1/22:0/18:0; 17:2/18:1/(20:0)2; 17:2/20:1/22:0/16:0; |
| 1499.4 (75:3) | 17:2/20:1/20:0/18:0; 17:2/17:1/(19:0)2; 17:2/22:1/22:0/15:0; 17:2/22:1/20:0/17:0; |
| 1499.4 (75:3) | 17:2/22:1/18:0/19:0; 14:1/17:1/22:1/22:0; 14:1/19:0/22:1/22:0; 17:1/18:1/20:1/20:0; |
| 1499.4 (75:3) | 17:1/18:1/22:1/18:0; 16:0/17:0/22:1/20:2; 22:1/18:1/20:1/15:0; 18:2/20:1/15:0/22:0; |
| 1499.4 (75:3) | 18:2/20:1/17:0/20:0;18:2/20:1/19:0/18:0; 18:2/22:1/22:0/14:0; 18:2/22:1/20:0/16:0; |
| 1499.4 (75:3) | 18:2/22:1/(18:0)2; 18:2/22:1/19:0/17:0; 18:2/18:1/22:0/17:0; 18:2/18:1/20:0/19:0; |
| 1499.4 (75:3) | 18:2/17:1/22:0/18:0; 18:2/17:1/(20:0)2; 17:0/14:2/22:0/22:1; 19:0/14:2/20:0/22:1; |
| 1499.4 (75:3) | 22:0/14:2/19:0/20:1; 14:2/17:1/(22:0)2; (17:2)2/22:1/19:0; 19:0/20:1/(18:1)2 |

**Table 2.2** Major molecular species of cardiolipins identified in *S. warneri* (cont.)

| $[M-H]^-$ *m/z* (C:N) | Fatty Acyl Chains |
|---|---|
| 1499.4 (75:3) | (18:1)2/17:1/22:0; 17:0/22:1/(18:1)2; (20:1)3/15:0; (20:1)2/17:1/18:0; (20:1)2/18:1/17:0; |
| 1499.4 (75:3) | (20:1)2/22:1/13:0; 13:0/18:1/(22:1)2 14:1/17:0/(22:1)2 ; 17:1/14:0/(22:1)2 |
| 1499.4 (75:3) | 16:0/22:0/cy17:0/20:2; 18:0/20:0/cy17:0/20:2; (19:0)2/cy17:0/20:2; |
| 1499.4 (75:3) | 17:2/cy17:0/22:0/19:0; 17:2/cy17:0/(19:0)2; cy17:0/18:1/20:1/20:0 |
| 1499.4 (75:3) | cy17:0/18:1/22:1/18:0; 18:2/cy17:0/22:0/18:0; 18:2/cy17:0/(20:0)2; |
| 1499.4 (75:3) | 14:2/cy17:0/(22:0)2; 18:1)2/cy17:0/22:0; 20:1)2/cy17:0/18:0; cy17:0/14:0/(22:1)2 |
| 1501.4 (75:2) | 18:2/20:0/19:0/18:0; 18:2/(19:0)3; (19:1)2/18:0/19:0; 16:1/19:1/(20:0)2 |
| 1501.4 (75:2) | 17:2/(20:0)2/18:0; 17:2/(19:0)2/20:0; 15:0/20:0/18:1/22:1; 16:0/19:0/18:1/22:1; |
| 1501.4 (75:2) | 18:1/19:1/20:0/18:0; 18:1/19:1/(19:0)2; 15:0/16:0/(22:1)2; 19:0/20:0/(18:1)2 |
| 1501.4 (75:2) | 19:1/22:1/20:0/14:0; 19:1/22:1/19:0/15:0; 19:1/22:1/18:0/16:0; |
| 1501.4 (75:2) | (cy19:0)2/18:0/19:0; 16:1/cy19:0/(20:0)2; 18:1/cy19:0/20:0/18:0; 18:1/cy19:0/(19:0)2; |
| 1501.4 (75:2) | cy19:0/22:0/20:0/14:0; cy19:0/22:1/19:0/15:0; cy19:0/22:1/18:0/16:0 |

$[M-H]^-$ ions of cardiolipin observed in the ESI-MS spectra, with the attribution of the fatty acyl composition of each phospholipid molecular species, accordingly to the interpretation of the correspondent MS/MS spectra. Numbers in parenthesis (C:N) indicate the number of carbon atoms (C) and double bonds (N) in the fatty acid side chains.

**Table 2.3** Major molecular species of phosphatidic acids identified in *S. warneri*

| $[M-H]^-$ *m/z* (C:N) | Fatty Acyl Chains | $[M-H]^-$ *m/z* (C:N) | Fatty Acyl Chains |
|---|---|---|---|
| 605.4 (29:0) | 13:0/16:0 | 661.4 (33:0) | 14:0/19:0 |
| 605.4 (29:0) | 14:0/15:0 | 665.4 (34:5) | 14:0/20:5 |
| 619.4 (30:0) | 14:0/16:0 | 669.4 (34:3) | 16:0/18:3 |
| 619.4 (30:0) | 15:0/15:0 | 673.4 (34:1) | 14:0/20:3 |
| 627.4 (31:3) | 13:0/18:3 | 673.4 (34:1) | 20:0/14:1 |
| 633.4 (31:0) | 15:0/16:0 | 673.4 (34:1) | 21:0/13:1 |
| 633.4 (31:0) | 14:0/17:0 | 673.4 (34:1) | 24:0/12:1 |
| 633.4 (31:0) | 13:0/18:0 | 675.4 (34:0) | 14:0/20:0 |
| 647.4 (32:0) | 14:0/18:0 | 675.4 (34:0) | 15:0/19:0 |
| 647.4 (32:0) | 15:0/17:0 | 675.4 (34:0) | 16:0/18:0 |
| 647.4 (32:0) | 16:0/16:0 | 675.4 (34:0) | 17:0/17:0 |
| 647.4 (32:0) | 13:0/19:0 | 689.4 (35:0) | 15:0/20:0 |
| 655.4 (33:3) | 15:0/18:3 | 689.4 (35:0) | 16:0/19:0 |
| 661.4 (33:0) | 15:0/18:0 | 689.4 (35:0) | 17:0/18:0 |
| 661.4 (33:0) | 16:0/17:0 | 699.4 (36:2) | 18:1/18:1 |
| 661.4 (33:0) | 13:0/20:0 | | |

$[M-H]^-$ ions of phosphatidic acid observed in the ESI-MS spectra, with the attribution of the fatty acyl composition of each phospholipid molecular species, accordingly to the interpretation of the correspondent MS/MS spectra. Numbers in parenthesis (C:N) indicate the number of carbon atoms (C) and double bonds (N) in the fatty acid side chains.

**Table 2.4** Major molecular species of phosphatidylethanolamines identified in *S. warneri*

| $[M-H]^-$ *m/z* (C:N) | Fatty Acyl Chains | $[M-H]^-$ *m/z* (C:N) | Fatty Acyl Chains | $[M-H]^-$ *m/z* (C:N) | Fatty Acyl Chains |
|---|---|---|---|---|---|
| 634.4 (28:0) | 14:0/14:0 | 724.5 (35:4) | 17:2/18:2 | 744.5 (36:1) | 14:0/22:1 |
| 662.4 (30:0) | 14:0/16:0 | 724.5 (35:4) | 17:1/18:3 | 746.4 (36:0) | 18:0/18:0 |
| 676.4 (31:0) | 15:0/16:0 | 724.5 (35:4) | cy17:0/18:3 | 762.4 (38:6) | 16:0/22:6 |
| 676.4 (31:0) | 14:0/17:0 | 724.5 (35:4) | 15:0/20:4 | 762.4 (38:6) | 18:1/20:5 |
| 676.4 (31:0) | 13:0/18:0 | 726.5 (35:3) | 18:1/17:2 | 762.4 (38:6) | 18:2/20:4 |
| 688.4 ( 32:1) | 16:0/16:1 | 726.5 (35:3) | 17:1/18:2 | 762.4 (38:6) | 16:1/22:5 |
| 688.4 (32:1) | 14:0/18:1 | 726.5 (35:3) | cy17:0/18:2 | 764.4 (38:5) | 18:1/20:4 |
| 688.4 (32:1) | 18:0/14:1 | 726.5 (35:3) | 17:0/18:3 | 764.4 (38:5) | 18:0/20:5 |
| 688.4 (32:1) | 13:0/19:1 | 726.5 (35:3) | 15:1/20:2 | 764.4 (38:5) | 18:2/20:3 |
| 688.4 (32:1) | 13:0/cy19:0 | 726.5 (35:3) | cy15:0/20:2 | 764.4 (38:5) | 16:0/22:5 |
| 688.4 (32:1) | 15:0/17:1 | 726.5 (35:3) | 15:0/20:3 | 764.4 (38:5) | 16:1/22:4 |
| 688.4 (32:1) | 15:0/cy17:0 | 728.5 (35:2) | 18:1/17:1 | 766.5 (38:4) | 18:0/20:4 |
| 700.4 (33:2) | 15:1/18:1 | 728.5 (35:2) | 18:1/cy17:0 | 766.5 (38:4) | 18:1/20:3 |
| 700.4 (33:2) | cy15:0/18:1 | 728.5 (35:2) | 18:2/17:0 | 766.5 (38:4) | 18:2/20:2 |
| 700.4 (33:2) | 16:1/17:1 | 728.5 (35:2) | 16:1/19:1 | 766.5 (38:4) | 18:3/20:1 |
| 700.4 (33:2) | 16:1/cy17:0 | 728.5 (35:2) | 16:1/cy19:0 | 766.5 (38:4) | 16:0/22:4 |
| 700.4 (33:2) | 16:0/17:2 | 728.5 (35:2) | 15:0/20:2 | 766.5 (38:4) | 16:1/22:3 |
| 700.4 (33:2) | 15:0/18:2 | 728.5 (35:2) | 15:1/20:1 | 768.5 (38:3) | 18:0/20:3 |
| 712.5 (34:3) | 16:0/18:3 | 728.5 (35:2) | cy15:0/20:1 | 768.5 (38:3) | 18:1/20:2 |
| 712.5 (34:3) | 16:1/18:2 | 740.4 (36:3) | 18:0/18:3 | 768.5 (38:3) | 18:2/20:1 |
| 714.5 (34:2) | 16:1/18:1 | 740.4 (36:3) | 16:0/20:3 | 768.5 (38:3) | 16:0/22:3 |
| 714.5 (34:2) | 16:0/18:2 | 740.4 (36:3) | 16:1/20:2 | 768.5 (38:3) | 16:1/22:2 |
| 714.5 (34:2) | 14:1/20:1 | 740.4 (36:3) | 19:1/17:2 | 770.5 (38:2) | 18:2/20:0 |
| 714.5 (34:2) | 17:1/17:1 | 740.4 (36:3) | cy19:0/17:2 | 770.5 (38:2) | 18:0/20:2 |
| 714.5 (34:2) | cy17:0/cy17:0 | 742.5 (36:2) | 16:0/20:2 | 770.5 (38:2) | 18:1/20:1 |
| 714.5 (34:2) | 15:1/19:1 | 742.5 (36:2) | 18:0/18:2 | 770.5 (38:2) | 16:1/22:1 |
| 714.5 (34:2) | cy15:0/cy19:0 | 742.5 (36:2) | 18:1/18:1 | 772.4 (38:1) | 18:0/20:1 |
| 716.5 (34:1) | 16:0/18:1 | 742.5 (36:2) | 16:1/20:1 | 774.4 (38:0) | 18:0/20:0 |
| 716.5 (34:1) | 18:0/16:1 | 742.5 (36:2) | 17:1/19:1 | 790.4 (40:6) | 18:0/22:6 |
| 716.5 (34:1) | 17:0/17:1 | 742.5 (36:2) | cy17:0/cy19:0 | 790.4 (40:6) | 20:2/20:4 |
| 716.5 (34:1) | 17:0/cy17:0 | 742.5 (36:2) | 14:1/22:1 | 790.4 (40:6) | 18:1/22:5 |
| 716.5 (34:1) | 19:0/15:1 | 744.5 (36:1) | 18:0/18:1 | 790.4 (40:6) | 20:3/20:3 |
| 716.5 (34:1) | 19:0/cy15:0 | 744.5 (36:1) | 20:0/16:1 | 796.4 (40:3) | 18:0/22:3 |
| 722.4 (36:4) | 15:1/20:4 | 744.5 (36:1) | 16:0/20:1 | 796.4 (40:3) | 18:1/22:2 |
| 722.4 (36:4) | cy15:0/20:4 | 744.5 (36:1) | 19:0/17:1 | 798.4 (40:2) | 18:1/22:1 |
| 722.4 (35:5) | 15:0/20:5 | 744.5 (36:1) | 19:0/cy17:0 | 798.4 (40:2) | 18:0/22:2 |
| 722.4 (35:5) | 17:2/18:3 | 744.5 (36:1) | 17:0/19:1 | | |
| 724.5 (35:4) | cy15:0/20:3 | 744.5 (36:1) | 17:0/cy19:0 | | |

$[M-H]^-$ ions of phosphatidylethanolamine observed in the ESI-MS spectra, with the attribution of the fatty acyl composition of each phospholipid molecular species, accordingly to the interpretation of the correspondent MS/MS spectra. Numbers in parenthesis (C:N) indicate the number of carbon atoms (C) and double bonds (N) in the fatty acid side chains.

**Table 2.5** Major molecular species of lysyl-phosphatidylglycerols identified in *S. warneri*

| $[M-H]^-$ *m/z* (C:N) | Fatty Acyl Chains |
|---|---|
| 807.4 (29:0) | 14:0/15:0 |
| 807.4 (29:0) | 16:0/13:0 |
| 821.4 (30:0) | 15:0/15:0 |
| 821.4 (30:0) | 16:0/14:0 |
| 821.4 (30:0) | 17:0/13:0 |
| 835.4 (31:0) | 16:0/15:0 |
| 835.4 (31:0) | 18:0/13:0 |
| 835.4 (31:0) | 17:0/14:0 |
| 849.4 (32:0) | 16:0/16:0 |
| 849.4 (32:0) | 18:0/14:0 |
| 861.4 (33:1) | 15:0/18:1 |
| 861.4 (33:1) | 16:0/17:1 |
| 861.4 (33:1) | 16:0/ cy17:0 |
| 863.4 (33:0) | 18:0/15:0 |
| 863.4 (33:0) | 17:0/16:0 |

$[M-H]^-$ ions of lysyl-phosphatidylglycerol observed in the ESI-MS spectra, with the attribution of the fatty acyl composition of each phospholipid molecular species, accordingly to the interpretation of the correspondent MS/MS spectra. Numbers in parenthesis (C:N) indicate the number of carbon atoms (C) and double bonds (N) in the fatty acid side chains.

**Table 2.6** Major molecular species of phosphatidylcholines identified in *S. warneri*

| $[M+H]^+$ *m/z* (C:N) | Fatty Acyl Chains | $[M+H]^+$ *m/z* (C:N) | Fatty Acyl Chains |
|---|---|---|---|
| 706.5 (30:1) | 14:0/16:1 | 784.6 (36:4) | 18:1/18:3 |
| 706.5 (30:1) | 16:0/14:1 | 784.6 (36:4) | 14:0/22:4 |
| 708.4 (30:0) | 15:0/15:0 | 784.6 (36:4) | 16:1/20:3 |
| 708.4 (30:0) | 12:0/18:0 | 786.6 (36:3) | 18:1/18:2 |
| 722.6 (31:0) | 15:0/16:0 | 786.6 (36:3) | 18:0/18:3 |
| 732.6 (32:2) | 16:1/16:1 | 786.6 (36:3) | 16:0/20:3 |
| 732.6 (32:2) | 14:1/18:1 | 788.6 (36:2) | 18:0/18:2 |
| 732.6 (32:2) | 14:0/18:2 | 788.6 (36:2) | 18:1/18:1 |
| 734.6 (32:1) | 16:0/16:1 | 788.6 (36:2) | 16:1/20:1 |
| 734.6 (32:1) | 14:0/18:1 | 790.6 (36:1) | 18:0/18:1 |
| 736.6 (32:0) | 16:0/16:0 | 790.6 (36:1) | 16:0/20:1 |
| 754.6 (34:5) | 12:0/22:5 | 790.6 (36:1) | 16:1/20:0 |
| 754.6 (34:5) | 14:1/20:4 | 792.6 (36:0) | 18:0/18:0 |
| 758.6 (34:3) | 16:0/18:3 | 792.6 (36:0) | 16:0/20:0 |
| 758.6 (34:3) | 16:1/18:2 | 808.6 (38:6) | 18:3/20:3 |
| 758.6 (34:3) | 14:0/20:3 | 810.6 (38:5) | 18:1/20:4 |
| 760.6 (32:2) | 16:1/18:1 | 810.6 (38:5) | 18:0/20:5 |
| 760.6 (32:2) | 16:0/18:2 | 812.4 (38:4) | 18:0/20:4 |
| 760.6 (32:2) | 14:2/20:0 | 812.4 (38:4) | 18:1/20:3 |
| 762.6 (32:1) | 16:0/18:1 | 812.4 (38:4) | 18:3/20:1 |

| | | | |
|---|---|---|---|
| 762.6 (32:1) | 18:0/16:1 | 814.6 (38:3) | 18:0/20:3 |
| 764.6 (34:0) | 16:0/18:0 | 816.4 (38:2) | 16:0/22:2 |
| 780.6 (36:6) | 18:3/18:3 | 816.4 (38:2) | 18:1/20:1 |
| 782.6 (36:5) | 16:1/20:4 | 818.4 (38:1) | 18:1/20:0 |
| 784.6 (36:4) | 16:0/20:4 | 818.4 (38:1) | 16:0/22:1 |
| 784.6 (36:4) | 18:2/18:2 | 820.4 (38:0) | 16:0/22:0 |

$[M-H]^+$ ions of phosphatidylcholine observed in the ESI-MS spectra, with the attribution of the fatty acyl composition of each phospholipid molecular species, accordingly to the interpretation of the correspondent MS/MS spectra. Numbers in parenthesis (C:N) indicate the number of carbon atoms (C) and double bonds (N) in the fatty acid side chains.

**Table 2.7** Oxidized molecular species of cardiolipins identified in *S. warneri* after photodynamic treatment

| **$[M-H]^-$ *m/z* (C:N)** | **Sample (oxidized cardiolipins)** |
|---|---|
| 1429.5 (69:3) | $[1415 - H + O - 2\ Da]^-$ |
| 1449.4 (69:3) | $[1417 - H + 2O]^-$ |
| 1473.4 (72:3) | $[1457 - H + O]^-$ |
| 1487.3 (73:3) | $[1471 - H + O]^-$ |
| 1489.5 (72:3) | $[1457 - H + 2O]^-$ |
| 1503.3 (73:3) | $[1471 - H + 2O]^-$ |
| 1515.1 (75:3) | $[1499 - H + O]^-$ |
| 1532.6 (75:3) | $[1499 - H + 2O]^-$ |
| 1561.1 (75:3) | $[1499 - H + 4O - 2\ Da]^-$ |

$[M-H]^-$ ions of cardiolipins in photosensitized cells (sample) observed in negative ESI-MS/MS. Numbers in parenthesis (C:N) indicate the number of carbon atoms (C) and double bonds (N) in the fatty acid side chains.

# Chapter 3. Photodynamic oxidation of *Escherichia coli* membrane phospholipids: new insights based on lipidomics

The content of this chapter is currently in press as:
Alves E, Santos N, Melo T, Maciel E, Dória L, Faustino MAF, et al. Photodynamic oxidation of *Escherichia coli* membrane phospholipids: new insights based on lipidomics. Rapid Commun Mass Spectrom. DOI: 10.1002/rcm.6739.

# 3 Photodynamic oxidation of *Escherichia coli* membrane phospholipids: new insights based on lipidomics

**Abstract**

The irreversible oxidation of biological molecules, such as lipids, can be achieved with a photosensitizing agent and subsequent exposure to light, in the presence of molecular oxygen. Although lipid peroxidation is an important toxicity mechanism in bacteria, the alterations caused by the photodynamic therapy on bacterial phospholipids are still unknown. In this work, the photodynamic oxidation of *Escherichia coli* membrane phospholipids was studied using a lipidomic approach.

*E. coli* ATCC 25922 were irradiated 90 min with white light (4 mW $cm^{-2}$, 21.6 J $cm^{-2}$) in the presence of a tricationic porphyrin [(5,10,15-tris(1-methylpyridinium-4-yl)-20-(pentafluorophenyl)porphyrin tri-iodide, Tri-$Py^{+}$-Me-PF]. Lipids were extracted and separated by thin-layer chromatography. Phospholipid classes were quantified by phosphorus assay and analyzed by electrospray ionization-tandem mass spectrometry. Fatty acids were analyzed by gas chromatography. Quantification of lipid hydroperoxides was performed by FOX2 assay. Analysis of the photodynamic oxidation of a phospholipid standard was also performed.

The approach used allowed to see that the photodynamic treatment induced the formation of a high amount of lipid hydroperoxides in an *E. coli* lipid extract. Quantification of fatty acids revealed a decrease in the unsaturated C16:1 and C18:1 species suggesting that oxidative modifications were responsible for their variation. It was also observed that photosensitization induced the oxidation of phosphatidylethanolamines with C16:1, C18:1 and C18:2 fatty acyl chains, with formation of hydroxy and hydroperoxy derivatives.

Membrane phospholipids of *E. coli* are molecular targets of the photodynamic effect induced by Tri-$Py^{+}$-Me-PF. The overall change in the relative amount of unsaturated fatty acids and the formation of PE hydroxides and hydroperoxides evidence the damages in bacterial phospholipids caused by this lethal treatment.

## 3.2 Introduction

Research on the photodynamic inactivation (PDI) of microorganisms has increased intensively during the last decade due to its potential applications in medical, environmental or public health areas. (13, 30, 191) The photodynamic process refers to the combined use of light and a photosensitizer in the presence of oxygen. (132) This treatment leads to the formation of reactive oxygen species (ROS) which are cytotoxic and capable of oxidizing many biological molecules (enzymes, proteins, lipids and nucleic acids). (98, 133) The process does not seem to be reversible or elicit resistance in exposed microorganisms. (119, 120, 134, 135)

The formation of ROS by PDI may involve the interaction between the light-excited photosensitizer with a substrate (type I mechanism) or with molecular oxygen ($^3O_2$) (type II mechanism). (8) In the former, hydrogen peroxide ($H_2O_2$) as well as free radicals such as superoxide anion radicals ($O_2^{-\bullet}$) and hydroxyl radical ($HO^\bullet$) are produced, and, in the latter, singlet oxygen ($^1O_2$) is produced. (8) ROS cause direct oxidative modification of cellular constituents, namely in unsaturated lipids. Lipids and proteins can be modified by oxidative reactions leading to changes in their structure and loss of function. (9, 98) It is unclear, however, whether lipid peroxidation is an important toxicity mechanism in bacteria because bacterial lipids are mainly monounsaturated, thus not so prone to oxidation. (99) ROS also cause indirect modification, via reactive products of lipid peroxidation. (98) This means that, besides the damages originated in lipids, following reactions derived from lipid peroxidation could disseminate to surrounding molecules, eventually more vitally important such as proteins or nucleic acids, altering their structure and function. (98) Lipid hydroperoxides (LOOHs) are important non-radical long-lived intermediates of the peroxidative process and can also be formed by two routes: type I chemistry with $HO^\cdot$ as the proximal lipid oxidant, generated by Fenton chemistry; or by type II chemistry with $^1O_2$ as the proximal oxidant, generated by the combined action of a photosensitizer and light. (9, 98)

Several studies have shown different damages caused in bacteria by PDI at a morphological and/or functional level (54, 59, 78, 103, 145) and existing research on photodynamic oxidation of membrane lipids is mostly directed toward photodynamic therapy of cancer. (184, 192, 193) Although the essential roles of phospholipids in bacterial cells are widely acknowledged (35, 194, 195), there is only one study concerning the photodynamic oxidation of bacterial membrane phospholipids of a Gram-positive bacterium, *Staphylococcus warneri*. (101) The results showed that the photosensitization affected *S. warneri* membrane phospholipids, leading to changes in their relative amount and to the formation of lipid hydroperoxides and hydroxides, evidencing the damages at the lipid level. (101)

*Escherichia coli* is commonly chosen as a representative biological model for Gram-negative bacteria. This type of bacteria present a cell wall structurally far more complex than Gram-positive bacteria (195) which makes the inactivation by photodynamic treatment difficult. This problem is circumvented by the use of cationic photosensitizers (136), capable of crossing the outer membrane of Gram-negative bacteria and reaching the cytoplasmic membrane. In addition to the phospholipid bilayer of the plasma membrane of both Gram types, only Gram-negative bacteria have an outer membrane in their cell wall comprising, besides other non-lipid components, another phospholipid bilayer, lipoproteins and lipopolysaccharides. (38) *E. coli* membrane phospholipids comprise mainly three classes: the

zwitterionic phosphatidylethanolamines (PEs), and the anionic phosphatidylglycerols (PGs) and cardiolipins (CLs). (35, 194, 196)

The exposure of these anionic lipids, along with lipopolysaccharides (in Gram-negative bacteria) and lipoteichoic acids (in Gram-positive bacteria) or peptidoglycan, provides the selectivity of cationic antimicrobial agents for toxicity against bacteria. (38) In the case of Gram-negative bacteria, the molecules of a cationic photosensitizer lead to displacement and removal of the $Mg^{2+}$ and the $Ca^{2+}$ ions which neutralize the superficial negative charges, promoting electrostatic repulsion with destabilization of the native organization of the wall, inducing the release of lipopolysaccharides into the medium. (197) Furthermore, the number of positive charges along with the amphiphilic character and conformational flexibility of the photosensitizer are factors that would facilitate its preferential interaction with anionic lipids, thus breaching the permeability barrier of bacterial membranes. (38)

The aim of this study was to evaluate the effect of the photodynamic process in the phospholipid profile of an *E. coli* strain using the cationic photosensitizer 5,10,15-tris(1-methylpyridinium-4-yl)-20-(pentafluorophenyl)porphyrin tri-iodide (Tri-$Py^{+}$-Me-PF, Figure 3.1). This porphyrin was chosen due to the promising results demonstrated on the PDI of a broad range of microorganisms. (77, 140-144, 198, 199) The changes in the membrane phospholipid composition of cells irradiated in the presence and in the absence of porphyrin were analyzed using a lipidomic approach, combining thin-layer chromatography with mass spectrometry and gas chromatography techniques, and are intended to give an insight into the mechanism(s) of membrane damage of Gram-negative bacteria induced by PDI.

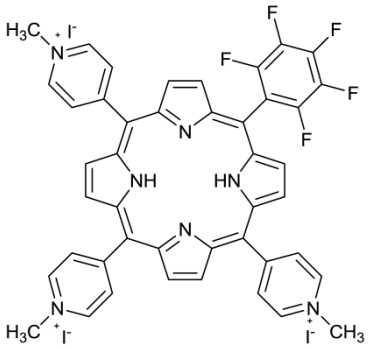


**Figure 3.1** Structure of the 5,10,15-tris(1-methylpyridinium-4-yl)-20-(pentafluorophenyl)porphyrin tri-iodide.

## 3.3 Material and Methods

### 3.3.1 Photosensitizer

The porphyrin Tri-Py$^{+}$-Me-PF was prepared according to the literature. (142, 198) The purity of the compound was confirmed by thin-layer chromatography (TLC) and by $^{1}$H NMR spectroscopy. Stock solutions were prepared in dimethyl sulfoxide (500 µM work solution) and sonicated for 30 min at room temperature before use.

### 3.3.2 Reagents

Phospholipid standards: 1-palmitoyl-2-oleoyl-*sn*-glycero-3-phosphatidylethanolamine (POPE, ref. 850757C); PE (16:0/18:1, ref. 850757C); PG (Egg PG, ref. 841138C); and CL (Heart, Bovine - Sodium Salt, ref. 840012C) were purchased from Avanti® Polar Lipids, Inc. (Alabaster, AL, USA) and used without further purification.

HPLC grade chloroform and methanol were purchased from Fisher Scientific Ltd. (Loughborough, UK). Ammonium iron(II) sulfate hexahydrate [$(NH_4)_2Fe(SO_4).6H_2O$], 2,6-di-tertbutyl-4-methylphenol (BHT), and xylenol orange disodium salt were purchased from Sigma Aldrich (Steinheim, Germany). $H_2SO_4$ was purchased from Carlo Erba Reagents (Milan, Italy). All other reagents were purchased from major commercial sources. Milli-Q water (Synergy®, Millipore Corporation, Billerica, MA, USA) was used. TLC silica gel 60 glass plates (20 x 20 cm) with concentrating zone were purchased from Merck (Darmstadt, Germany).

### 3.3.3 Bacteria and growth conditions

*E. coli* ATCC® 25922™ (VA, USA) from a fresh cultured plate was inoculated in tryptic soy broth (TSB, Merck) and grown overnight aerobically at 37 °C. Then an aliquot was transferred into fresh TSB medium at the same growth conditions to reach the early stationary phase (optical density at 600 nm ≈ 1.6), corresponding to ≈ $10^9$ colony forming units (CFU) $mL^{-1}$. *E. coli* cells were used in two different ways: sample (cells irradiated with photosensitizer) and control (cells irradiated without photosensitizer). Cells were harvested by centrifugation (10 min, 13,000 x *g*, 4 °C) (Avanti® J-25, Beckman Coulter, Inc., Brea, CA, USA), washed three times with sterile phosphate buffered saline (PBS: 8 g NaCl, 0.2 g KCl, 1.44 g $Na_2HPO_4$ and 0.24 g $KH_2PO_4$ per liter; pH 7.4) and resuspended in PBS to achieve a final concentration of $10^8$ CFU $mL^{-1}$.

### 3.3.4 Photosensitization protocol

The sample consisted of a bacterial suspension (49.5 mL in a 600 mL sterilized glass beaker) containing 500 µL of Tri-$Py^{+}$-Me-PF stock solution (5.0 µM). In the control, the porphyrin solution was replaced by PBS. The sample was incubated in the dark for 10 min under stirring (100 rpm) at 25 °C, in order to promote the photosensitizer binding to the cells. The control and sample then underwent a 90 min period of irradiation (total light dose 21.6 J $cm^{-2}$) with artificial white light (PAR radiation, 380 - 700 nm, 13 OSRAM 21 lamps (Munich, Germany) of 18 W each) with an irradiance of 4 mW $cm^{-2}$ measured with a model LI-250 radiometer (Li-Cor Inc., Lincoln, NE, USA), stirred at 100 rpm. After irradiation, the cells were harvested by centrifugation (10 min, 13,000 x *g*, 4 °C), washed three times with Milli-Q water at 4 °C, and the pellet was then kept on ice until lipid extraction.

### 3.3.5 Lipid extraction

The total lipids from bacteria were extracted immediately after photosensitization, following the modified Bligh and Dyer method. (176) A volume of 7.5 mL of chloroform:methanol (2:1, v/v) was added to bacterial cells (previously resuspended in 2 mL of water), in Pyrex glass centrifuge tubes. The mixture was well homogenized by inverting vigorously the tubes several times and incubated on ice for 210 min. The samples were centrifuged at 2000 rpm for 10 min (Mixtasel, JP Selecta S.A., Barcelona, Spain) at room temperature to resolve a two-phase system: an aqueous upper phase and an organic lower phase from which lipids were obtained. After transferring the organic phase to a clean tube, the extraction was repeated twice. The extracts were dried under nitrogen flow, dissolved in 300 µL of chloroform, and stored at -20 °C in 2 mL amber glass vials.

### 3.3.6 Quantification of phospholipids by phosphorus assay

Quantification of phospholipids in the total lipid extract and in the spots separated by TLC was performed according to Bartlett and Lewis. (177) Concentrated perchloric acid (0.65 mL, 70% m/v) was added to the samples in acid-washed glass tubes and the mixture was incubated for 60 min at 180 °C in a heating block (Block Heater SBH200D/3, Stuart®, Bibby Scientific Ltd., Stone, UK). After incubation, 3.3 mL of water, 0.5 mL of 2.5% of ammonium molybdate and 10% of ascorbic acid were added. The reaction mixture was well homogenized in a vortex mixer after each addition and incubated for 10 min at 100 °C in a water bath (Precisterm, JP Selecta S.A.). Standards from 0.2 to 1.5 µg of phosphate from a phosphate solution (standard solution of $NaH_2PO_4.2H_2O$, 439 mg $L^{-1}$ of water, i.e. 100 µg of phosphorus

$mL^{-1}$) underwent the same treatment as the samples. The absorbance of standards and samples was measured at 800 nm, at room temperature, in a microplate UV-Vis spectrophotometer (Multiskan GO, Thermo Scientific, Hudson, NH, USA). The relative abundance of each phospholipid class was calculated by the relation of the amount of phosphorus in each spot to the phosphorous amount of the total lipid extract in the sample applied in the TLC spot.

### 3.3.7 Separation by TLC

Phospholipids from the total lipid extract were separated by TLC using silica gel plates. Prior to separation, the plates were washed with chloroform:methanol (1:1, v/v) and activated (sprayed or impregnated) with 2.3% of boric acid in ethanol and placed in an oven at 100 °C for 15 min. Plates with spots containing 20 µg of lipids were developed in a solvent mixture of chloroform:ethanol:water:triethylamine (30:35:7:35, v/v/v/v). Separated lipid spots were revealed by exposing the plates to primuline (50 µg/100 mL acetone:water, 80:20, v/v) and visualized with a UV lamp (254 and 366 nm) (Camag, Berlin, Germany). (178) The spots were then scraped off from the plates and extracted from the silica with chloroform:methanol (2:1, v/v), quantified as described above, and analyzed by mass spectrometry.

### 3.3.8 Quantification of hydroperoxides by FOX2 assay

The lipid hydroperoxides were quantified in the total lipid extracts obtained from control and samples (after irradiation). Aliquots (50 µL) of the total lipid extracts from *E. coli* controls and samples were added to FOX2 reagent (950 µL) in microtubes, homogenized in a vortex mixer and incubated for 30 min at room temperature, in the dark. After incubation, the absorbance of the samples was read at 560 nm against $H_2O_2$ standards with concentrations ranging from 0.0 - 0.4 mM ($H_2O_2$ 1 mM, FOX2 reagent and water). The reagent (100 mL) was prepared as follows: 250 µM $(NH_4)_2Fe(SO_4).6H_2O$ (9.8 mg) and 25 mM $H_2SO_4$ (139 µL) were dissolved in 5 mL of water, mixed with 4 mM 2,6-di-tertbutyl-*p*-hydroxytoluene (BHT) (88.2 mg), 100 µM xylenol orange (7.2 mg) and 45 mL of methanol; another 45 mL of methanol and 5 mL of water were then added. (179)

### 3.3.9 Analysis by mass spectrometry

Phospholipid analysis was carried out by electrospray ionization mass spectrometry (ESI-MS) and tandem mass spectrometry analysis (MS/MS) in negative-ion mode in a Finnigan LXQ linear ion trap mass spectrometer (ThermoFisher, San Jose, CA, USA). ESI-MS conditions

were: electrospray voltage 4.7 kV; capillary temperature 275 °C and the sheath gas (He) flow rate 25 units. A precursor ion isolation width of 0.5 *m/z* was used, with a 30 ms activation time for MS/MS experiments. Full scan MS spectra and MS/MS spectra were acquired with maximum ionization time of 50 ms and 200 ms, respectively. The normalized collision energy (CE) varied between 17 and 20 (arbitrary units) for MS/MS. Data acquisition and treatment of results were carried out with the Xcalibur® Data System 2.0 (Thermo Scientific, San Jose, CA, USA).

### 3.3.10 Fatty acid analysis by gas chromatography with flame ionization detection (GC-FID)

The total fatty acyl substituents were measured by GC after transesterification of lipid bacterial extracts (approximately 30 μg of total phospholipid). The fatty acids were prepared using a methanolic solution of potassium hydroxide (2.0 M) according to the previously described method. (200) Volumes of 2 μL of the hexane solution containing methylated fatty acids were submitted to GC analysis. The GC injection port was programmed at 523.15 K and the detector at 543.15 K. The oven temperature was programmed as follows: initially stayed 3 min at 323.15 K, raised to 453.15 K (25 K $min^{-1}$), isothermally held for 6 min, with a subsequent increase to 533.15 K (40 K $min^{-1}$) and maintained there for 3 min, performing 19 min totally. The carrier gas was hydrogen flowing at 1.7 mL $min^{-1}$. The gas chromatograph (Clarus 400, PerkinElmer, Inc., MA, USA) was equipped with DB-1 column with 30 m length, 0.25 mm internal diameter and 0.15 μm film thickness (J&W Scientific, Agilent Technologies, Folsom, CA, USA) and a flame ionization detector. The relative concentrations of fatty acids were calculated by the percent area method with proper normalization considering the sum of all areas of the identified fatty acids.

### 3.3.11 Statistical analysis

Quantification of phospholipids and quantification of hydroperoxides were carried out independently, three times ($n$ = 3), both for the control and for the sample. The results were analyzed using one-way analysis of variance (ANOVA) with the Bonferroni post-hoc test (for quantification of phospholipids) and Student's *t*-test (for the quantification of hydroperoxides), and are presented as means ± standard deviation. Statistics were carried out using PRISM® GraphPad Software, Inc. (La Jolla, CA, USA). A value of $p < 0.05$ was considered significant.

## 3.4 Results

### 3.4.1 Quantification of lipid hydroperoxides

The quantification of lipid hydroperoxides generated after the photodynamic treatment of *E. coli* was performed by FOX2 assay in the total lipid extracts from control and sample (Figure 3.2). There was a significant increase in the concentration of lipid hydroperoxides in the sample after photosensitization (0.063±0.012 µg OOH / µg of phospholipid), which is 93.6% higher than the one found in the control ($p < 0.05$, Student's *t*-test). These results confirm that phospholipid photo-oxidation occurs after irradiation in the presence of the photosensitizer.

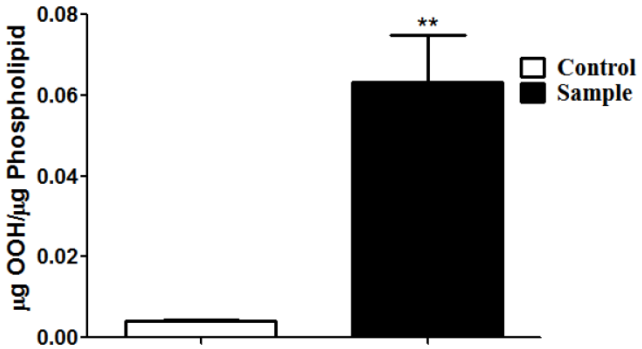


**Figure 3.2** Comparison of the concentration of hydroperoxides in the total lipid extract determined by FOX2 assay between non-photosensitized (control) and photosensitized (sample) *E. coli*. Error bars represent standard deviation of three independent experiments and * the significant difference from control ($p < 0.05$).

### 3.4.2 Variation in the fatty acyl composition after photodynamic treatment

The quantification of the relative fatty acyl composition obtained from the total lipid extracts of control and sample after photosensitization was carried out by GC-FID (Figure 3.3). The fatty acids C16:0, C16:1, cyC17:0, C18:1 (C18:1n9 and C18:1n11), C18:0 and cyC19:0 were identified. There was coelution of the C18:1n11 and C18:0 fatty acids. Significant differences were noticed in the relative amount of some fatty acids after photodynamic treatment. C18:1n11 and C18:0 were not differentiated under the experimental conditions. However, they could be differentiated by GC/MS, using another GC column or other derivatization procedure. (201) There was a significant increase in the relative content of the C16:0 ($p < 0.001$) species and a decrease in the relative amounts of the monounsaturated fatty acids C16:1 and C18:1n9 ($p < 0.05$ in this last case).

### 3.4.3 Analysis of phospholipids by off-line TLC and MS

The analysis and quantification of *E. coli* phospholipids was carried out after separation of the total lipid extracts by TLC. During lipid extraction from TLC spots, some lipids are lost but the lipid profiling remains constant and lipids with different polar heads and fatty acyl composition are extracted to a similar extent. (202) The chromatographic separation showed three different spots for the non-photosensitized (control) and photosensitized cells (sample) (Figure 3.4A, lanes 2 and 3 respectively). The identification of the phospholipid spots was accomplished by comparison with phospholipid standards (PE, PG and CL) applied on the TLC plate and further analysis of each spot by ESI-MS and MS/MS. The three identified spots corresponded to PEs, PGs and CLs. The amount of phospholipids in each spot was determined by phosphorus assay (Figure 3.4B), as follows: PEs, 53%; PGs, 40%; and CLs, 7%. However, no significant differences were observed between the relative abundance of each class of phospholipids in the control and in the sample.

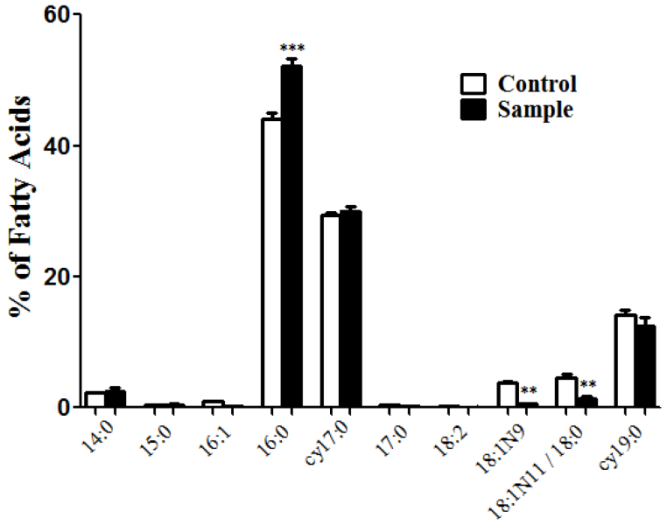


**Figure 3.3** Fatty acyl profile of total lipid extracts from control and sample analyzed by GC-FID and relative content of the major fatty acids from *E. coli*. Values are means ± standard deviation, $^{**}p < 0.05$ and $^{***}p < 0.001$.

To find out if any phospholipid molecular species was modified by oxidation, the spots obtained after TLC were analyzed by ESI-MS in negative-ion mode (Figure 3.5). PEs and PGs were identified in the ESI-MS spectra as $[M-H]^-$ ions (Figure 3.5A and 3.5B, respectively) while CLs were identified by the formation of the $[M-H]^-$ ions and their correspondent doubly charged $[M-2H]^{2-}$ ions (Figure 3.5D and 3.5C, respectively). The molecular species identified in each class are resumed in Tables 3.1-3.3, at the end of this Chapter.

### 3.4.4 Evaluation of the photodynamic effect in *E. coli* major phospholipid classes

A comparison between the ESI-MS spectra of the control cells and the sample cells demonstrates changes in molecular profile in the PEs class (Figure 3.5A). In the ESI-MS spectrum of the sample (Figure 3.5A2) it is possible to see an increase in the relative abundance of ions at *m/*z 746.5, 758.5 and 774.5, suggesting that oxidation of PE molecular species most probably occurred due to photosensitization.

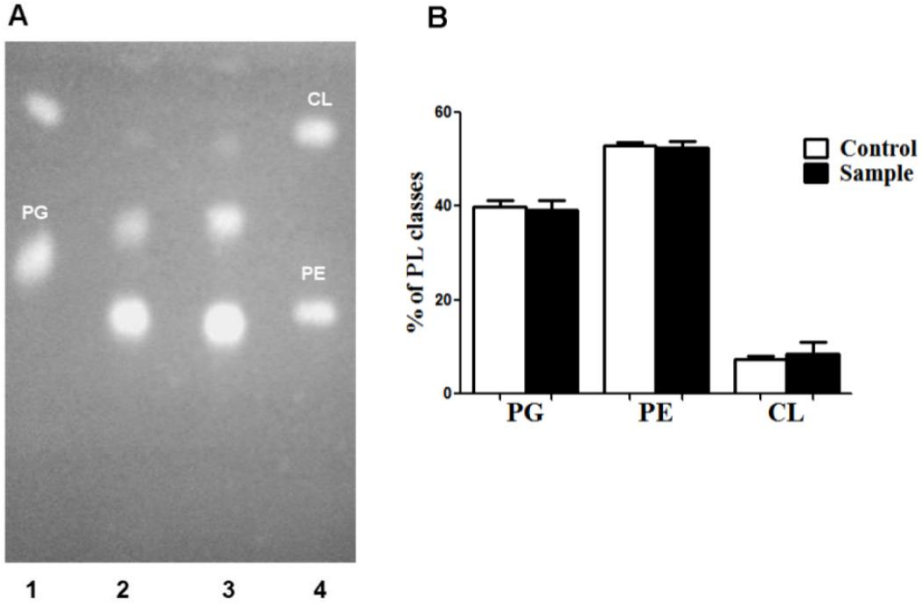


**Figure 3.4 (A)** Thin-layer chromatogram of fractioned *E. coli* total lipids. Lanes 1 and 4 correspond to pure phospholipid standards: phosphatidylglycerol (PG, lane 1), phosphatidylethanolamine (PE, lane 4) and cardiolipin (CL, lanes 1 and 4). Lane 2 represents the different fractions of the non-photosensitized cells (control) and lane 3 the different fractions of photosensitized cells (sample). **(B)** Percentage of the different fractions of phospholipids separated by TLC of non-photosensitized (control) and photosensitized (sample) *E. coli* (5.0 µM of Tri-Py$^{+}$-Me-PF). Irradiation conditions: artificial white light (4 mW cm$^{-2}$) for 90 min (21.6 J cm$^{-2}$). Error bars represent standard deviation of three independent experiments ($p > 0.001$).

The PE oxidation products at *m*/z 746.5 (*m/z* 714.6+32 Da) were identified as the hydroperoxy derivatives of PE 16:1/18:1 and PE 16:0/18:2. The PE oxidation products at *m/z* 758.5 (*m/z* 742.5+16 Da) and 774.5 (*m/*z 742.5+32 Da) were identified, respectively, as the hydroxy and hydroperoxy derivatives of PEs 18:1/18:1 and 16:1/20:1. According to MS/MS analysis of PE molecular species (Table 3.1), the majority are composed of saturated and cyclic fatty acyl chains, thus not prone to oxidation. For the other PE molecular species with one monounsaturated fatty acyl chain, any oxidation species were identified although their formation, in very low abundance, cannot be excluded. Furthermore, the observed oxidized PE species have two unsaturated acyl chains (16:1 and 18:1) or have a polyunsaturated fatty acid (PUFA), namely C18:2, thus a higher probability of being oxidized.

The analysis of the photodynamic effect on PGs revealed that no oxidation products were observed, due to the predominant occurrence of saturated fatty acyl chains in their constitution (Figure 3.5B). A similar situation was observed in the case of CLs where no oxidation species were identified, although their formation in very low abundance cannot be excluded.

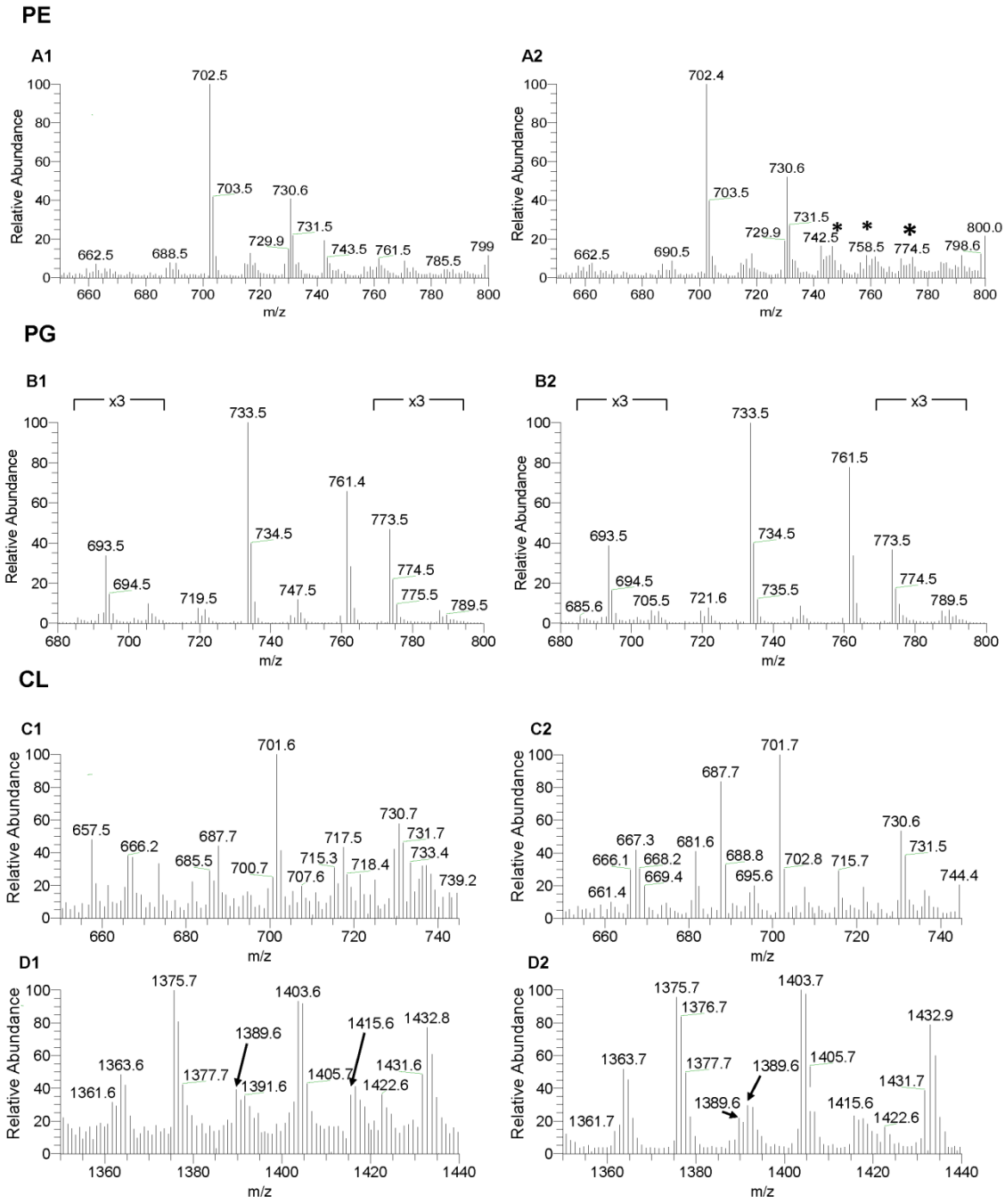


**Figure 3.5** Comparison of ESI-MS spectra of phosphatidylethanolamine (PE), phosphatidylglycerol (PG) and cardiolipin (CL) extracted from *E. coli* irradiated without photosensitizer (control) (**A1**, **B1**, **C1** and **D1**, respectively) and irradiated in the presence of photosensitizer (5.0 µM of Tri-Py$^{+}$-Me-PF) (sample) (**A2**, **B2**, **C2** and **D2**, respectively). PE oxidation products at *m/z* 746.5 and 774.5 are indicated with * (A2). Irradiation conditions: artificial white light (4 mW cm$^{-2}$) for 90 min (21.6 J cm$^{-2}$).

### 3.4.5 Photodynamic oxidation of a PE by MS

The analysis by MS/MS using model systems allows the identification of the typical fragmentation pathways of phospholipids modified by photodynamic treatment. As *E. coli* cells have a high abundance of monounsaturated fatty acids in their membranes, the modifications induced by Tri-Py$^{+}$-Me-PF were also studied, using the same irradiation conditions, in POPE, a PE standard with a monounsaturated fatty acyl chain (16:0/18:1), by ESI-MS and MS/MS. Figure 3.6 (A and B) show the MS spectra of POPE under non-photosensitized and photosensitized conditions, respectively. As it can be seen in Figure 3.6B, the major oxidation product at *m/z* 748.4 corresponds to a POPE hydroperoxide derivative (*m/*z 716.4 + 32 Da). The MS/MS spectrum of this species (Figure 3.6C) shows a low abundance ion attributed to the carboxylate anion [RCOO+2O]$^{-}$ at *m/z* 313.2 and a major product ion formed by loss of water from this oxidized fatty acyl anion [RCOO + 2O - $H_2O$]$^{-}$ at *m/z* 295.2. An unmodified saturated acyl chain (C16:0) was observed at *m/z* 255.2. Ions due to the loss of the *sn*-1 fatty acyl chain as an acid derivative and the *sn*-2 modified fatty acyl chain as a keto derivative were also found at *m/z* 492.3 and 452.3, respectively.

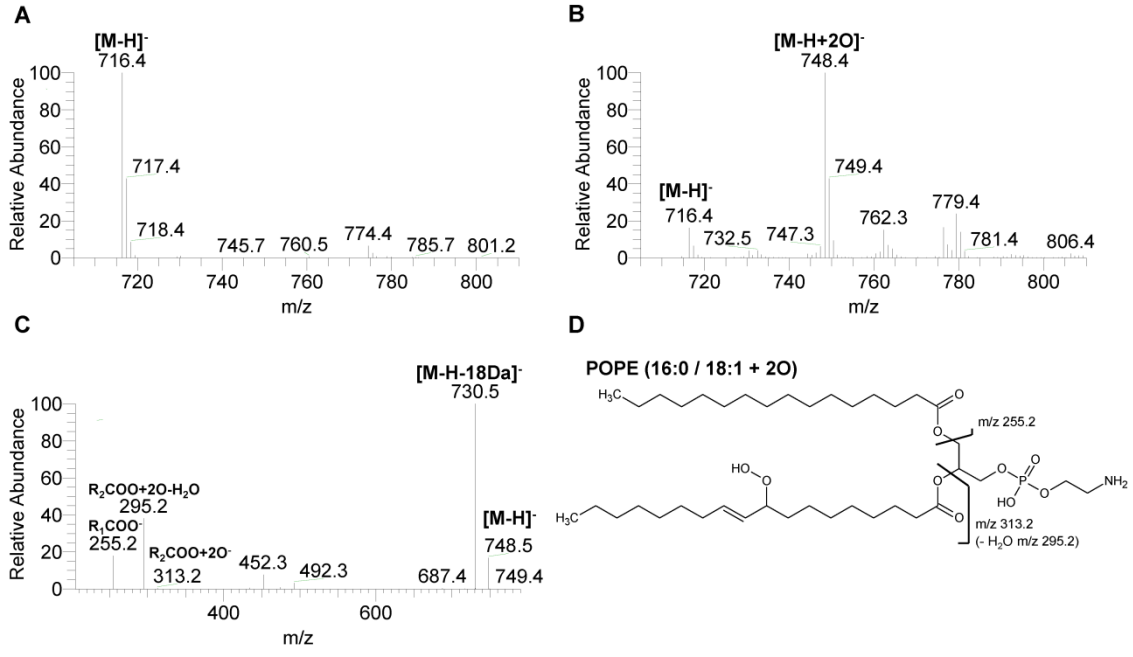


**Figure 3.6** ESI-MS spectra of 1-palmitoyl-2-oleoyl-*sn*-glycero-3-phosphatidylethanolamine (POPE) irradiated without photosensitizer **(A)** and irradiated in the presence of photosensitizer (5.0 µM of Tri-Py$^{+}$-Me-PF) **(B)**. MS/MS spectrum of the [M-H]$^{-}$ ion of POPE+2O at *m/z* 748.5 **(C)**. Structure of POPE+2O **(D)**. In this structure the hydroperoxide is located at C9 but other possible locations cannot be excluded. Irradiation conditions: artificial white light (4 mW cm$^{-2}$) for 90 min (21.6 J cm$^{-2}$).

The analysis by ESI-MS/MS (Figure 3.7 and 3.8) of the new ions at *m/z* 746.5 and 774.4 identified in *E. coli* (Figure 3.5A2) as corresponding to PE hydroperoxides allowed their

confirmation as hydroperoxides species. It was not possible to confirm the formation of the hydroxy derivative (*m/z* 758.5) based on the MS/MS analysis due to the overlapping of unmodified PE with the same *m/z* value. In the ESI-MS/MS spectrum of the ion at *m/z* 746.5 (Figure 3.7) there is a major product ion at *m/z* 267.2 that was attributed to the ion [RCOO (C16:1) + 2O - $H_2O$]$^-$, formed by the loss of water from the C16:1+2O carboxylate anion (Figure 3.7C). This product ion indicates the presence of the oxidized PE species with an oxidized C16:1 fatty acyl chain, identified as PE (16:1+2O/18:1). In the same ESI-MS/MS spectrum there is a minor product ion at *m/z* 311.3 that was identified as the carboxylate anion of hydroperoxide linoleic acid [RCOO (C18:2) + 2O]$^-$ and a product ion at *m/z* 255.2 corresponding to the C16:0 carboxylate chain (Figure 3.7B). These ions confirm the presence of the oxidized PE (16:0/18:2+2O).

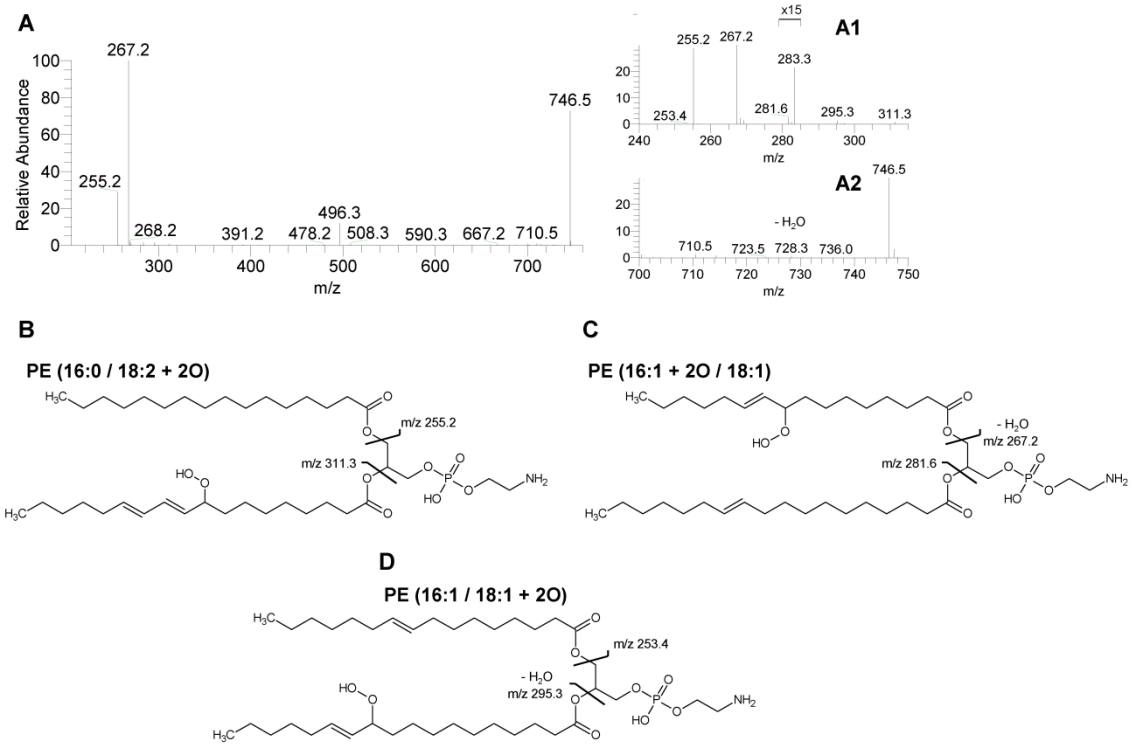


**Figure 3.7** MS/MS spectrum of the ion at *m/z* 746.6 (PE 714+2O) **(A)** with insets showing an expanded view of the spectrum at *m/z* 240 - 315 **(A1)** and at *m/z* 700 - 750 **(A2)**; and the proposed structures for the hydroperoxy derivatives PE16:0/18:2+2O **(B)**, PE16:1+2O/18:1 **(C)** and PE16:1+/18:1+2O **(D)**.

The formation of another isomer but with the hydroperoxy group attached to a C18:1 chain is confirmed by the presence of the product ion at *m/z* 295.3 (Figure 3.7D) and this isomer was identified as PE (16:1/18:1+2O).

The oxidation product identified at *m/z* 774.4 was also attributed as being due to two possible isomers, namely PE (18:1/18:1+2O) and PE (16:1+2O/20:0). The ions at *m/z* 295.3 and 281.2 correspond, respectively, to the modified and unmodified C18:1 chain (Figure 3.8B)

while the small ion peak at *m/z* 267.2 suggests the presence of the other isomer (16:1+2O/20:0) (Figure 3.8C). The position of the hydroperoxy group was tentatively assigned in the structures based on one probable position. However, other locations of the hydroxy and hydroperoxy groups cannot be excluded.

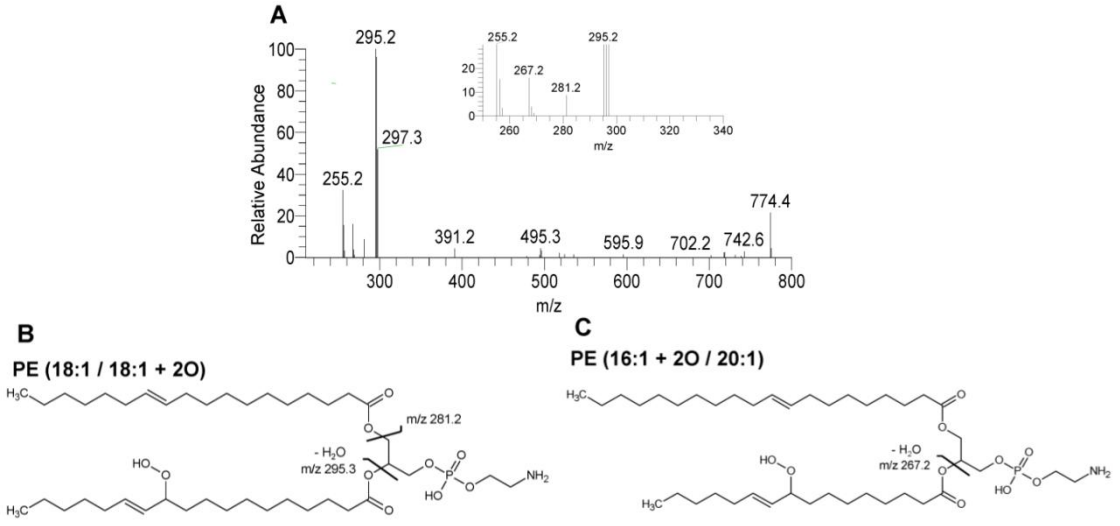


**Figure 3.8** MS/MS spectrum of the ion at *m/z* 774.6 (PE 742+2O) **(A)** with an inset showing an expanded view of the spectrum at *m/z* 250 - 340, and the proposed structures: PE18:1/18:1+2O **(B)** and PE16:1+2O/20:1 **(C)**.

## 3.5 Discussion

This study focuses on the photodynamic oxidation of the predominant classes of *E. coli* membrane phospholipids by a tricationic amphiphilic porphyrin (Tri-Py$^{+}$-Me-PF) and white light. The Tri-Py$^{+}$-Me-PF is recognized as an efficient photosensitizer in the photoinactivation of bacteriophages (143, 199), bacteria (77, 140-142), and bacterial endospores. (144, 203) In these studies, it was reported that the microorganisms are not affected by the irradiation conditions and that Tri-Py$^{+}$-Me-PF does not exhibit toxicity in the absence of light. In particular, the reduction of *ca.* 6 $\log_{10}$ CFU mL$^{-1}$ of *E. coli* ATCC 25922 was achieved with a concentration of 5.0 μM of this porphyrin after 90 min of irradiation with an irradiance of 4 mW cm$^{-2}$ (21.6 J cm$^{-2}$) and an initial bacterial concentration of 1 x 10$^{8}$ CFU mL$^{-1}$. (56) The mechanism of PDI for this photosensitizer was also studied in a Gram-negative bacterium, being the type II mechanism the predominant pathway (generation of $^{1}O_{2}$). (183) Singlet oxygen is involved in the process of lipid peroxidation (type II process), responsible for changing the structure and function of the target as well as of surrounding molecules. (9, 98)

It is known that the membrane phospholipids of *E. coli* are mostly PEs, PGs and CLs. (35) These data were obtained by various authors from cells collected in exponential (log) phase (196, 204) and in the stationary phase. (176) It is also known that variables such as strain,

growth medium, temperature and time of incubation of the bacteria affect the results, therefore comparison of results require that standardized conditions are strictly verified. In this study, the bacterial cells were harvested and tested in the early stationary phase. The results obtained after analysis by ESI-MS of the TLC spots isolated from fractionation of the total lipid extract allowed the detection of PEs, PGs, and in minor proportion CLs. Considering these classes, it was possible to quantify and to identify by phosphorus assay, accompanied by negative-ion ESI-MS analysis, PEs as the major phospholipid class (53%), followed by PGs (40%) and CLs (7%). These findings are in agreement with the scientific literature on this topic where PEs are usually identified as the major class (70 - 75%), followed by PGs (20 - 25%) and CLs (5 - 10%), composing approximately 95% of glycerol phosphate-based phospholipids. (35, 194, 196)

The fatty acyl profile identified is in accordance with previous published results and with the identification by MS/MS of the phospholipid profile. The fatty acids C16:0, C16:1, cyC17:0, cyC19:0 were identified, as well as two isomers of C18:1 (one at C9 and another at C11), both already identified in *E. coli*. (176, 201, 205, 206) The decrease in the monounsaturated fatty acids is most probably due to modifications caused by oxidation of the unsaturated fatty acids linked to the phospholipids, which validates the occurrence of lipid peroxidation after photosensitization**.**

Among the three phospholipid classes studied, the PE class is the most prone to oxidation due to the presence of unsaturated fatty acyl chains, identified by ESI-MS/MS. Furthermore, the observed modified PE species have two unsaturated acyl chains (16:1 and 18:1) or have a polyunsaturated fatty acid, namely C18:2, thus a higher probability of being oxidized. Interestingly, although linoleic acid is not considered a major fatty acid in *E. coli*, it was already identified by GC-MS. (201)

The formation of hydroperoxides was already observed during the photo-oxidation of CLs in the presence of a photosensitizer. (184, 193) The hydroxy derivative results from the decomposition of the hydoperoxy derivative. (207)

The high percentage of lipid hydroperoxides determined by FOX2 assay after photodynamic treatment of *E. coli* (93.6% higher in the sample when compared with control), confirms that the oxidative modifications of lipids involve the formation of hydroperoxides and is in agreement with the oxidative process described recently in CLs. (182) The detection by ESI-MS/MS of molecular species with *m/z* values corresponding to the addition of two oxygen atoms (mass increments of +32 Da) in unsaturated fatty acyl chains of PEs from photosensitized *E. coli* is in accordance with the presence of hydroperoxy derivatives.

The comparison of the effects of photo-oxidation between the photosensitized PEs extracted from *E. coli* and the selected PE standard (POPE) corroborates the formation of hydroperoxy derivatives as a major modification by photosensitization. The use of phospholipid standards to study the photosensitization-induced changes demonstrated the damages that are caused in phospholipids under the considered conditions, thus further work will be carried out in detail in the near future.

Very recently, the photodynamic oxidation of membrane phospholipids of the Gram-positive bacterium *Staphylococcus warneri* by Tri-Py$^{+}$-Me-PF was studied, using lipidomics, to gain some insight into the action mechanism of bacterial photodynamic inactivation and PGs and CLs were identified as the main phospholipid classes. (101) After photosensitization there was a significant increase in the relative abundance of some molecular species of PGs and oxidation of unsaturated molecular species present in high abundance in CLs, through the formation of hydroperoxy, hydroxy and carbonyl groups. Besides the lipid peroxidation observed in CLs upon photodynamic treatment, it was speculated that an interaction between the photosensitizer and the membrane lipids could also occur, in a recently suggested mechanism of membrane damage involving the interaction between antimicrobial cationic agents and anionic lipids, with the formation of lipid domains (38), to justify the increase in PGs and the decrease in CLs. Due to its features of having multiple cationic groups, conformational flexibility and sufficient hydrophobicity, the antimicrobial agent could induce the separation of lipid components, as it binds to anionic lipids (as PGs and CLs), causing rearrangements and leaving defects in the membrane that would lower the permeability barrier between the cell and its surroundings. (38) This theory, along with photo-oxidation, could help to justify or to understand the effects of the photosensitization of Gram-positive bacteria at the membrane level, namely in phospholipids.

In this work, *E. coli*, a well-studied Gram-negative bacterium, was used and as it is known the differences between the cell wall structures of the two Gram types determine the efficiency of the photodynamic treatment. (197) Not only is their cell wall composition very different but also their cytoplasmic membrane. At least 15% of anionic lipids (PGs or CLs or both) are present in all bacteria, independently of the Gram type. (38) The exposure of these anionic lipids along with lipopolysaccharides (in Gram-negative bacteria) or lipoteichoic acids (in Gram-positive bacteria) or peptidoglycan is what provides the selectivity of cationic antimicrobial agents for toxicity against bacteria. (38) However, the segregated phases or domains of lipids mentioned above do not lead to toxicity and are a cell defense mechanism. (38)

In the case of photodynamic inactivation, where the photosensitizer should not be toxic to the cells, their destruction is led by the irreversible oxidation of their major constituents through ROS formed during the process. It is acknowledged that unsaturated membrane lipids are determinant targets of ROS action in photodynamic reactions. (9) On the other hand, as lipid hydroperoxides are much longer-lived than free radical precursors or products, they are possibly more dangerous to the organisms because they may be able to disseminate in a wider way through the cellular membranes (9) and so there is no chance to overcome lipid oxidation.

As lipid phase segregation may occur in the cytoplasmic membrane of Gram-positive bacteria as a result of the interaction of the photosensitizer with lipids, the same may not be true or determinant in Gram-negative bacteria, as a consequence of the nature of the phospholipid/lipid composition (38), in the cytoplasmic membrane and in the external membrane of the cell wall, and other molecules can be involved.

In summary, the lipid profile of *E. coli* ATCC 25922 in the stationary phase of growth is affected by the photodynamic process using the tricationic porphyrin Tri-Py$^{+}$-Me-PF at 5.0 μM and visible light (21.6 J cm$^{-2}$), as demonstrated by lipidomics. ESI-MS and ESI-MS/MS evidenced that there are modifications in the relative abundance of some molecular species of phospholipids, namely in PEs, and that the reactive oxygen species generated during the photodynamic process lead to the oxidation of unsaturated molecular species, present in high abundance in PEs, through the formation of hydroxy and hydroperoxy groups.

This study highlights lipid peroxidation of bacterial membranes as a cellular damage involved in the photodynamic process. The observed photo-oxidative changes in *E. coli* ATCC 25922 phospholipids with the photosensitization conditions used provide some insights on the mechanistic inactivation of this microorganism.

**Table 3.1** Major molecular species of phosphatidylethanolamines identified in *E. coli*

| $[M-H]^{-}$ *m/z* | Fatty Acyl Chains |
|---|---|
| (C:N) | Control |
| 662.5 (30:0) | 14:0/16:0[a] |
| 688.5 (32:1) | 16:0/16:1[a,b]; 14:0/18:1 |
| 688.5 (32:0 cy) | 15:0/cy17:0[b] |
| 690.5 (32:0) | 16:0/16:0[a,b]; 14:0/18:0 |
| 702.5 (33:0 cy) | 16:0/cy17:0[a,b]; 14:0/cy19:0; 15:0/18:1 |
| 714.6 (34:2) | 16:1/18:1[a,b]; 16:0/18:2 |
| 714.6 (34:0 cy/cy) | cy17:0/cy17:0[a,b] |
| 716.5 (34:1) | 16:0/18:1[a,b]; 16:1/18:0 |
| 716.5 (34:0 cy) | 17:0/cy17:0; 15:0/cy19:0 |

| | |
|---|---|
| 728.5 (35:1 cy) | cy17:0/18:1; 16:1/cy19:0 |
| 730.6 (35:1) | 17:0/18:1[a,b]; 16:1/19:0 |
| 730.6 (35:0 cy) | 16:0/cy19:0[b]; cy17:0/18:0[a,b] |
| 742.5 (36:2) | 18:1/18:1[a,b]; 16:1/20:1; 16:0/20:2 |
| 742.5 (36:0 cy/cy) | cy17:0/cy19:0[b] |
| 744.5 (36:1) | 16:0/20:1; 18:0/18:1[a]; 16:1/20:0; 14:0/22:1 |
| 744.5 (36:0 cy) | cy17:0/19:0; 17:0/cy19:0 |
| 758.5 (37:1) | 16:0/21:1; 18:1/19:0; 17:0/20:1 |
| 758.5 (37:0 cy) | 18:0/cy19:0; cy17:0/20:0 |
| 760.7 (37:0) | 18:0/19:0; 16:0/21:0 |
| 770.5 (38:2) | 18:1/20:1; 16:0/22:2 |
| 770.5 (38:1 cy) | cy17:0/21:1 |
| 770.5 (38:0 cy/cy) | cy19:0/cy19:0 |
| 772.5(38:1) | 16:0/22:1; 18:1/20:0; 18:0/20:1; 17:0/21:1; 16:1/22:0 |
| 772.5 (38:0 cy) | 19:0/cy19:0; cy17:0/21:0 |
| 774.5 (38:0) | 19:0/19:0; 16:0/22:0 |

$[M-H]^-$ ions of phosphatidylethanolamine observed in the ESI-MS spectra, with the attribution of the fatty acyl composition of each phospholipid molecular species, accordingly to the interpretation of the correspondent MS/MS spectra. Numbers in parenthesis (C:N) indicate the number of carbon atoms (C) and double bonds (N) in the fatty acid side chains. [a]Also identified by Kol et al. (206); and [b]by Oursel et al. (176)

**Table 3.2** Major molecular species of phosphatidylglycerols identified in *E. coli*

| **$[M-H]^-$ *m/z*** | **Fatty Acyl Chains** |
|---|---|
| **(C:N)** | **Control** |
| 691.5 (30:1) | 14:1/16:0; 14:0/16:1 |
| 693.5 (30:0) | 14:0/16:0[a] |
| 705.6 (31:1) | 15:0/16:1[a] |
| 705.6 (31:0 cy) | 14:0/cy17:0 |
| 719.5 (32:1) | 16:0/16:1[a]; 14:0/18:1[a] |
| 719.5 (32:0 cy) | 15:0/cy17:0[a] |
| 721.5 (32:0) | 16:0/16:0[a]; 14:0/18:0 |
| 733.5 (33:1) | 15:0/18:1 |
| 733.5 (33:0 cy) | 16:0/cy17:0[a]; 14:0/cy19:0 |
| 747.5 (34:1) | 16:0/18:1[a]; 18:0/16:1 |
| 747.5 (34:0 cy) | 17:0/cy17:0; 15:0/cy19:0 |
| 761.5 (35:1) | 17:0/18:1 |
| 761.5 (35:0 cy) | 16:0/cy19:0[a]; 18:0/cy17:0 |
| 773.5 (36:2) | 18:1/18:1 |
| 773.5 (36:0 cy/cy) | cy17:0/cy19:0 |
| 787.5 (37:1 cy) | 18:1/cy19:0; cy17:0/20:1 |
| 801.5 (38:0 cy/cy) | cy19:0/cy19:0 |

$[M-H]^-$ ions of phosphatidylglycerol observed in the ESI-MS spectra, with the attribution of the fatty acyl composition of each phospholipid molecular species, accordingly to the interpretation of the correspondent MS/MS spectra. Numbers in parenthesis (C:N) indicate the number of carbon atoms (C) and double bonds (N) in the fatty acid side chains. [a]Also identified by Oursel et al. (176)

**Table 3.3** Major molecular species of cardiolipins identified in *E. coli*

| **$[M-H]^-$ *m/z*** | **Fatty Acyl Chains** |
|---|---|
| **(C:N)** | **Control** |
| 1363.6 (65:0 cy) | 14:0/14:0/18:0/cy19:0 |
| 1363.6 (65:0 cy) | 14:0/16:0/cy17:0/18:0 |
| 1363.6 (65:0 cy) | 14:0/16:0/16:0/cy19:0 |
| 1375.7 (66:2) | 14:0/16:0/18:1/18:1 |
| 1375.7 (66:2) | 16:0/16:0/16:1/18:1[a] |
| 1375.7 (66:0 cy/cy) | 14:0/16:0/cy17:0/cy19:0 |
| 1375.7 (66:0 cy/cy) | 16:0/16:0/cy17:0/cy17:0[a] |
| 1375.7 (66:0 cy/cy) | 14:0/14:0/cy19:0/cy19:0[a] |
| 1389.6 (67:1 cy) | 16:0/16:0/cy17:0/18:1[a] |
| 1389.6 (67:1 cy) | 14:0/16:0/18:1/cy19:0 |
| 1391.6 (67:1) | 16:0/16:1/17:0/18:0 |
| 1391.6 (67:1) | 14:0/17:0/18:0/18:1 |
| 1391.6 (67:1) | 16:0/16:0/17:0/18:1 |
| 1391.6 (67:0 cy) | 14:0/14:0/cy19:0/20:0 |
| 1391.6 (67:0 cy) | 14:0/16:0/cy17:0/20:0 |
| 1391.6 (67:0 cy) | 14:0/cy17:0/18:0/18:0 |
| 1391.6 (67:0 cy) | 14:0/16:0/18:0/cy19:0 |
| 1391.6 (67:0 cy) | 14:0/17:0/17:0/cy19:0 |
| 1391.6 (67:0 cy) | 16:0/16:0/16:0/cy19:0 |
| 1403.6 (68:2) | 16:1/16:1/18:0/18:0 |
| 1403.6 (68:2) | 16:0/16:1/18:0/18:1 |
| 1403.6 (68:2) | 16:0/16:0/18:1/18:1[a] |
| 1403.6 (68:1 cy) | 16:0/16:1/cy17:0/19:0 |
| 1403.6 (68:0 cy/cy) | 16:0/16:0/cy17:0/cy19:0 |
| 1403.6 (68:0 cy/cy) | 16:0/cy17:0/cy17:0/18:0 |
| 1415.6 (69:2 cy) | 16:0/cy17:0/18:1/18:1 |
| 1415.6 (69:2 cy) | 18:1/16:1/16:0/cy19:0[a] |
| 1431.6 (70:0 cy/cy) | 16:0/16:0/cy19:0/cy19:0 |

$[M-H]^-$ ions of cardiolipin observed in the ESI-MS spectra, with the attribution of the fatty acyl composition of each phospholipid molecular species, accordingly to the interpretation of the correspondent MS/MS spectra. Numbers in parenthesis (C:N) indicate the number of carbon atoms (C) and double bonds (N) in the fatty acid side chains. [a]Also identified by Hsu and Turk. (205)

# Chapter 4. Nucleic acid changes during photodynamic inactivation of bacteria by cationic porphyrins

The content of this chapter has been published as:
Alves E, Faustino MAF, Tomé JPC, Neves MGPMS, Tomé AC, Cavaleiro JAS, et al. Nucleic acid changes during photodynamic inactivation of bacteria by cationic porphyrins. Bioorg Med Chem. 2013;21(14):4311–8.

# 4 Nucleic acid changes during photodynamic inactivation of bacteria by cationic porphyrins

## 4.1 Abstract

Light activation of photosensitizing dyes in presence of molecular oxygen generates highly cytotoxic reactive oxygen species leading to cell inactivation. Nucleic acids are molecular targets of this photodynamic action but not considered the main cause of cell death. The *in vivo* effect of the photodynamic process on the intracellular nucleic acid content of *Escherichia coli* and *Staphylococcus warneri* was evaluated herein.

Two cationic porphyrins (Tetra-$Py^+$-Me and Tri-$Py^+$-Me-PF) were used to photoinactivate *E. coli* (5.0 μM; $10^8$ cells $mL^{-1}$) and *S. warneri* (0.5 μM; $10^8$ cells $mL^{-1}$) upon white light irradiation at 4.0 mW $cm^{-2}$ for 270 min and 40 min, respectively. Total nucleic acids were extracted from photosensitized bacteria after different times of irradiation and analyzed by agarose gel electrophoresis. The double-stranded DNA was quantified by fluorimetry and the porphyrin binding to bacteria was determined by spectrofluorimetry.

*E. coli* was completely photoinactivated with both porphyrins (5.0 μM), whereas *S. warneri* was only completely inactivated by Tri-$Py^+$-Me-PF (0.5 μM). The hierarchy of nucleic acid changes in *E. coli* was in the order: 23S rRNA > 16S rRNA > genomic DNA. The nucleic acids of *S. warneri* were extensively reduced after 5 min with Tri-$Py^+$-Me-PF but almost unchanged with Tetra-$Py^+$-Me after 40 min of irradiation. The amount of Tri-$Py^+$-Me-PF bound to *E. coli* after washing the cells is higher than Tetra-$Py^+$-Me and the opposite was observed for *S. warneri*. The binding capacity of the photosensitizers is not directly related to the PDI efficiency or nucleic acid reduction and this reduction occurs in parallel with the decrease of surviving cells.

## 4.2 Introduction

The photodynamic inactivation (PDI) of bacteria refers to the destruction of these microorganisms by the concerted action of light, molecular oxygen and a photosensitizer (PS). The interaction among these agents can occur via two comptitive mechanisms: interaction between the light-excited PS with a substrate (type I mechanism) or with molecular oxygen (type II mechanism). Type I mechanism produces hydrogen peroxide and free radicals and type II mechanism originates singlet oxygen. (30, 208, 209) The reactive oxygen species originated (free radicals and singlet oxygen) are highly cytotoxic and cause structural and molecular damage to cells. (98)

A direct and efficient inactivation of Gram-negative bacteria is accomplished with the use of cationic PS. (136, 142, 210-212) These can interact electrostatically with the negatively charged constituents of the outer wall (lipoproteins, lipopolysaccharides) which facilitates their binding and entry. (213) On the other side, inactivation of Gram-positive bacteria is achieved with neutral, anionic and cationic PS which readily cross the relatively porous layers of peptidoglycan that constitute these cells. (213) However, the cascade of damages involved in the bacterial PDI is not yet fully elucidated.

It is generally accepted that damages occur mainly at the level of cytoplasmic membrane and cell wall constituents (multi-targeted photodamage) and that the nucleic acids are not the main or determining target of PDI (90, 121, 122, 214-216) because DNA photocleavage is observed when cells are already largely photoinactivated or no longer viable. (59, 121) Such statement is based on studies with easily photoinactivated bacterial strains that are defective for DNA repair mechanisms (90) or have very efficient DNA repair systems. (122, 216, 217) Furthermore, the cells can undergo extensive photosensitization without mutagenic effects. (10, 218)

As stated before, PDI can induce DNA damage through: direct reactions of the excited PS molecules with DNA; reactions mediated by reactive oxygen species; and reactions involving other secondary intermediates, as decomposition products of the excited molecules or lipid peroxidation products. (48) Guanine bases have been shown to be particularly reactive and their oxidation by singlet oxygen generates 8-oxo-7,8-dihydro-20-deoxyguanosine as a major product. (49) Besides DNA, it has also been detected damage in RNA extracted from *Escherichia coli* after treatment with hydrogen peroxide. (219, 220)

Usually, agarose gel electrophoresis show time-dependent marked reductions in the nucleic acids from photosensitized Gram-positive and Gram-negative bacteria. These reductions indicate nucleic acid photocleavage, specifically single strand breaks, depicted by smearings in genomic DNA (59, 103, 214), in total RNA (103) and in plasmid DNA. (90, 103, 214, 221) In this last case, conversion of supercoiled DNA (form I) to nicked circular DNA (form II) can occur. (42, 59, 221) However, there are exceptions to be highlighted, namely in the extent of damage observed on the same bacterium with different porphyrins (59, 221); between bacterial strains of the same species (214); and on isolated bacterial plasmid DNA with different PS (42), including cationic porphyrins with different charge number. (222) Furthermore, contrasting effects were observed in the photosensitized Gram-negative *E. coli*: intact chromosomal DNA (121) *versus* drastic reduction in DNA and RNA (103), along with maximal bacterial killing. Therefore, it is difficult from the available data to make conclusions about the effect of PDI on bacterial DNA.

Moreover, it is known that, in bacteria, the porphyrins can penetrate the cell wall to the periplasmic space and bind to the cytoplasmic membrane (62, 223, 224); bind to and interact with DNA in different ways (46, 222, 225-230); have a dual location (bound to the cell wall and to the nucleic acids) (76); or do not have to penetrate (51, 231) or even come into contact with the cells. (232) These various interaction modes cause different cellular damages and the damage spectrum of the photosensitization process is also different depending on the structural characteristics of the PS. (10, 46, 59, 228)

Some of these studies also determined the percentage or concentration of PS bound to the cells prior to irradiation. Similar PS binding capacity with dissimilar levels of photosensitivity was reported for two strains of Gram-positive methicillin-resistant *Staphylococcus aureus* with a non cationic porphyrin (214), while for *E. coli*, a binding capacity related with the PS molecular structure and with similar levels of photosensitivity was observed for different positively-charged porphyrins. (73)

Hence, the main described factors which may interfere with the photodynamic action on the bacterial nucleic acids by porphyrin derivatives are (28): (a) PS structure; (b) PS mechanisms of action (type I and/or type II); (c) PS cellular localization; (d) PS binding to bacterial cells; (e) PS concentration; (f) light dose; and (g) bacterial strain.

The aim of this study was to investigate, *in vivo*, the effect of the tetra- and tri-cationic PS, 5,10,15,20-tetrakis(1-methylpyridinium-4-yl)porphyrin tetra-iodide (Tetra-$Py^+$-Me) and 5,10,15-tris(1-methylpyridinium-4-yl)-20-(pentafluorophenyl) porphyrin tri-iodide (Tri-$Py^+$-Me-PF) on the concentration of intracellular nucleic acids of *E. coli* and *Staphylococcus warneri*. These two PS were selected based on previous studies where the Tri-$Py^+$-Me-PF proved to be more effective for microbial photoinactivation (e.g., bacteria, bacterial endospores) than Tetra-$Py^+$-Me (77, 140, 141, 144, 183, 203), a well-known standard PS. So it is important to clarify if the DNA is affected and if there are differences in the DNA modifications caused by both PS in Gram-positive (*S. warneri*) and Gram-negative (*E. coli*) bacteria. *Staphylococcus warneri* is a coagulase-negative bacterium normally found in normal microbial skin flora. (157) Although its clinical importance cannot be compared to that of *S. aureus*, it has gained clinical relevance as a potentially opportunistic etiological agent (158, 160, 161, 163, 164, 168) and its susceptibility to photodynamic treatment has never been tested.

## 4.3 Material and Methods

### 4.3.1 Photosensitizers

The cationic derivatives 5,10,15,20-tetrakis(1-methylpyridinium-4-yl)porphyrin tetra-iodide (Tetra-$Py^+$-Me) and 5,10,15-tris(1-methylpyridinium-4-yl)-20-(pentafluorophenyl)porphyrin tri-iodide (Tri-$Py^+$-Me-PF) were synthesized and characterized according to the literature. (142, 198, 233) Porphyrins purity was confirmed by thin layer chromatography and by $^1$H NMR spectroscopy. Stock solutions (500 μM) of each porphyrin derivative were prepared in dimethyl sulfoxide and sonicated for 30 min before use. The molecular structures of the PS are illustrated in Figure 4.1. Tetra-$Py^+$-Me in DMSO: $\lambda_{max}$ (log $\varepsilon$) 425 (5.46), 516 (4.30), 550 (3.78), 588 (3.86), 644 (3.34) nm; Tri-$Py^+$-Me-PF in DMSO: $\lambda_{max}$ (log $\varepsilon$) 422 (5.48), 485 (3.85), 513 (4.30), 545 (3.70), 640 (3.14) nm.

### 4.3.2 Bacterial strains and growth conditions

*E. coli* ATCC 25922 and *S. warneri*, isolated in our laboratory (234), from fresh cultured plates were inoculated in tryptic soy (TS) broth and grew overnight aerobically at 37 °C under 100 rpm. Then, an aliquot was transferred into fresh TS broth at the same growth conditions to reach the early stationary phase. For *E. coli*, an optical density at 600 nm ($OD_{600}$) of 1.6 ± 0.1 corresponded to ≈ $10^8$ colony forming units (CFU) $mL^{-1}$. For *S. warneri*, an $OD_{600}$ of 1.9 ± 0.1 corresponded to ≈ $10^8$ CFU $mL^{-1}$.

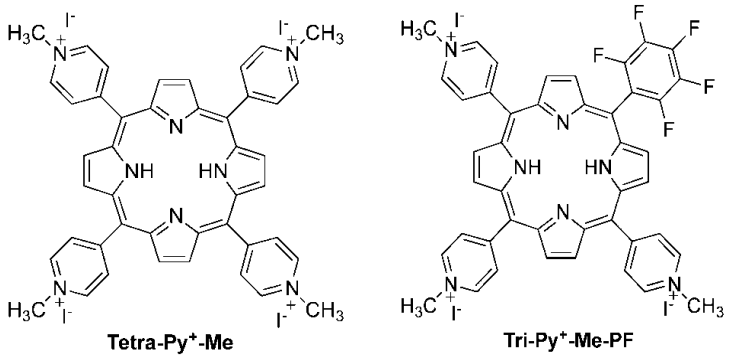


**Figure 4.1** Structure of the cationic porphyrins used in this study as photosensitizers.

### 4.3.3 Porphyrin binding to bacterial cells

The described procedure was based on the literature. (73) Briefly, bacteria from a stationary phase liquid culture (1.5 mL) were washed twice to remove cellular debris and resuspended in phosphate buffered saline (PBS 1x: 8.0 g NaCl, 0.2 g KCl, 1.44 g $Na_2HPO_4$ and

0.24 g $KH_2PO_4$ per liter; pH 7.4). They were incubated with each PS in the same concentrations as for the photoinactivation experiments, for 10 min, at room temperature, protected from light. The suspensions were centrifuged (17,000 x *g* for 15 min), the cell pellets were washed once with PBS to remove unbound porphyrin and resuspended in 2% aqueous SDS (1 mL). Then, they were incubated overnight at 4 °C and sonicated for 30 min. The fluorescence of the extracts was measured on a spectrofluorimeter (FluoroMax3, Horiba Jobin-Yvon, Edison, NJ, USA) with a slit of 2 nm. The excitation wavelength for Tri-$Py^+$-Me-PF was 422 nm and 425 nm for Tetra-$Py^+$-Me. The emission range was 600 - 800 nm. The measured fluorescence intensity allowed the determination of the corresponding PS concentration by interpolation with a calibration plot built with known concentrations of each PS, using the digestion solution as solvent. Simultaneously, aliquots from the bacterial suspensions were serially diluted and pour plated in tryptic soy agar for colony counting after overnight incubation at 37 °C. The binding value (PS molecules per cell) was calculated according to the literature. (235) Three independent assays were performed for each combination of bacterial strain–photosensitizer washed and non-washed.

#### 4.3.4 General photosensitization procedure and cell viability assays

Bacterial suspensions (≈ $10^8$ CFU $mL^{-1}$) were prepared, in PBS, from the early stationary phase cultures, distributed in 100 mL beakers (final volume of 10 mL per beaker), incubated in the dark with porphyrin for 10 min at 25 °C under 100 rpm stirring to promote the porphyrin binding to cells, and then irradiated by a light system, formed by 13 parallel OSRAM 18 W/21 - 840 lamps with an irradiance of 4.0 mW $cm^{-2}$, emitting in the range of 380 - 700 nm. Bacterial suspensions of *E. coli* were irradiated up to 270 min with 5.0 µM of each PS (total light dose of 64.8 J $cm^{-2}$) and sub-samples of 1.0 mL were collected before irradiation and after 15, 30, 60, 90, 180 and 270 min of light exposure. Bacterial suspensions of *S. warneri* were irradiated up to 40 min with 0.5 µM of each PS (total light dose of 9.6 J $cm^{-2}$) and sub-samples of 1.0 mL were collected before irradiation and after 5, 10, 15, 20, 30 and 40 min of light exposure. After each photosensitization period, the cells were serially diluted in PBS, plated in TS agar and incubated at 37 °C for 24 - 36 h for viability monitoring. The cell viability after each irradiation period was determined by counting the CFU on the most appropriate dilution on the agar plates. Control samples were carried out simultaneously with the PDI procedure: light control (LC) comprised a bacterial suspension exposed to light; and dark control (DC) comprised a bacterial suspension incubated with PS at the studied concentrations but protected from light. Three independent experiments were done and for each, two replicates were plated.

### 4.3.5 Extraction of nucleic acids, electrophoresis and quantification

For nucleic acids experiments, the photosensitization procedure was the same to that used in the cell viability assays but bacteria were concentrated by centrifugation previously to photosensitization to obtain an adequate amount of nucleic acids to be extracted. In this way, bacteria from the early stationary phase cultures (aliquots of 3 mL) were centrifuged for 10 min at 13,000 x *g*, in microtubes, at room temperature using a Heraeus® Pico™ 17 microcentrifuge (Thermo Scientific). The pellet was washed twice and resuspended in PBS in glass beakers (final volume of 10 mL). After the different photosensitization periods (0 - 270 min for *E. coli* and 0 - 40 min for *S. warneri*), each bacterial pellet was obtained by centrifugation at maximum velocity for 5 min in a microcentrifuge tube. They were resuspended in 100 µL of TE buffer 1x (10 mM Tris, 1 mM EDTA, pH 8.0) by repeated pipetting and 20 µL of lysozyme solution (30 mg $mL^{-1}$) were added. The mixture was lightly resuspended with a micropipette and incubated 1 h at 37 °C. After incubation, 50 µL of lysis solution were added and incubated 10 min at 65 °C. Then, 40 µL of an SDS 25% solution were added, mixed and incubated 10 min at 68 °C. Following, 50 µL of 5.0 M NaCl were added, mixed and incubated again 10 min at 68 °C. After vortexing for 10 min, DNA was extracted with 200 µL of chloroform, mixing well by inversion. After centrifugation for 5 min, the aqueous supernatant was removed to a new microcentrifuge tube. An equal volume of isopropanol was added to precipitate the nucleic acids and incubated 10 min at 4 °C. The extract was spun for 5 min and the supernatant discarded. Absolute ethanol (100 µL) was added, well mixed by inversion and incubated 15 min at 4 °C. After centrifugation for 5 min and very careful discarding of supernatant, the precipitate was washed with 100 µL of 70% ethanol. The supernatant was carefully removed and the pellet was dried and redissolved in 20 µL of TE buffer. Samples were gently mixed with 3 µL of loading buffer 6x: 0.09% (w/v) bromophenol blue, 0.09% xylene cyanol FF (w/v), 60% glycerol (v/v), 60 mM EDTA. DNA was analyzed by electrophoresis in 0.8% agarose gel in TAE buffer (TAE 1x: 0.04 M Tris–acetate, 0.001 M EDTA, pH 8.0), 2 h, at 120 V, 500 mA. GelRed™ (10,000x in water, Biotium) was the nucleic acid gel dye used to incorporate into the gel. The molecular weight marker used was the DNA Marker II (0.2 µg $µL^{-1}$, #SM0351, Fermentas) with DNA fragments in the range from 702 to 29,946 bp. The gel images were acquired with the Image Lab™ software (Bio-Rad).

The concentration of double-stranded DNA (dsDNA) in the samples extracted following photodynamic treatment was measured using the Qubit™ dsDNA HS Assay Kit Q32851 (Invitrogen) and the Qubit® fluorometer (Invitrogen), according to the manufacturer's instructions.

Light (LC) and dark control (DC) samples were carried out simultaneously. Three independent experiments were done and for each, two replicates were read.

### 4.3.6 Statistical analysis

The effect of the two PS on cell viability (number of CFU $mL^{-1}$ at each irradiation time, $n$ = 6) was analyzed by two-way univariate analysis of variance (ANOVA) model with the Bonferroni post-hoc test. The PS binding to bacteria ($n$ = 6) was analyzed by Student's $t$-test (IBM SPSS Statistics 20). Normal distributions were assessed by the Shapiro–Wilk test and homogeneity of variances by the Levene's test. A value of $p < 0.05$ was considered significant.

## 4.4 Results

### 4.4.1 Photodynamic inactivation

The survival curves of *E. coli* (≈ 8 log CFU $mL^{-1}$) upon phototreatment with 5.0 µM of PS (Figure 4.2a) show reductions close to the detection limit (7.7 log CFU $mL^{-1}$ with Tri-$Py^{+}$-Me-PF and 6.2 log CFU $mL^{-1}$ with Tetra-$Py^{+}$-Me). However, the kinetics of cell photoinactivation was very different between the two PS ($p$ <0.005, ANOVA). After 15 min of irradiation (3.6 J $cm^{-2}$), there was a reduction of 3.1 log CFU $mL^{-1}$ with Tri-$Py^{+}$-Me-PF and 0.2 log CFU $mL^{-1}$ with Tetra-$Py^{+}$-Me, and after 30 min (7.2 J $cm^{-2}$), a log reduction of 5.2 *versus* 2.9, respectively.

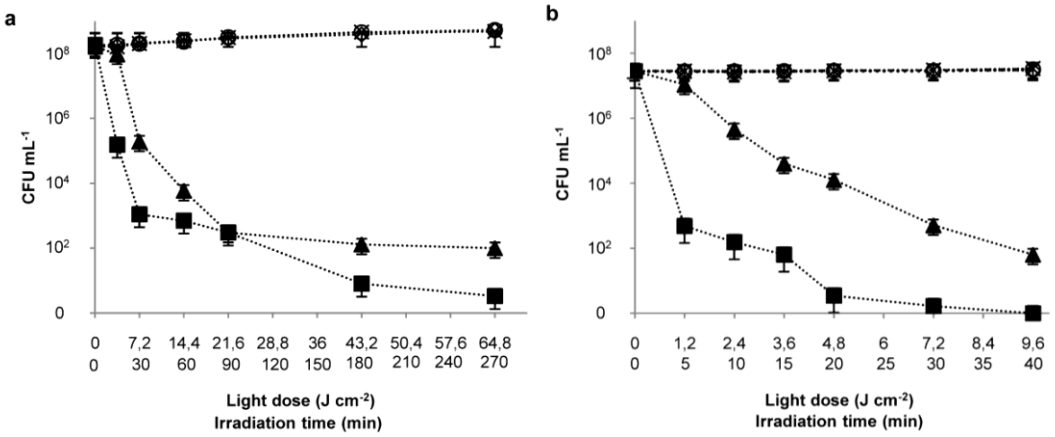


**Figure 4.2** Survival curves of **(a)** *E. coli* incubated with 5.0 µM of Tri-$Py^{+}$-Me-PF (filled square) and 5.0 µM of Tetra-$Py^{+}$-Me (filled triangle) and **(b)** *S. warneri* incubated with 0.5 µM of Tri-$Py^{+}$-Me-PF (filled square) and 0.5 µM of Tetra-$Py^{+}$-Me (filled triangle), exposed to white light (4.0 mW $cm^{-2}$) with different light doses. Light control (cross), dark control of Tri-$Py^{+}$-Me-PF (empty circle) and dark control of Tetra-$Py^{+}$-Me (filled circle). Values represent the mean of three independent experiments with two replicates each; error bars indicate the standard deviation.

The survival curves of *S. warneri* (≈ 8 log CFU $mL^{-1}$) upon phototreatment with 0.5 µM of porphyrin (Figure 4.2b) show different inactivation profiles for both PS. With Tri-$Py^{+}$-Me-PF there was a drastic reduction (4.8 log CFU $mL^{-1}$) after 5 min of irradiation (1.2 J $cm^{-2}$) contrasting with a negligible reduction (0.4 log CFU $mL^{-1}$) with Tetra-$Py^{+}$-Me. The photoinactivation kinetics was much faster ($p < 0.005$, ANOVA) with Tri-$Py^{+}$-Me-PF than with Tetra-$Py^{+}$-Me, reaching the detection limit after 40 min of irradiation (9.6 J $cm^{-2}$). Photoinactivation till the detection limit could not be seen for Tetra-$Py^{+}$-Me after 40 min, even though a reduction of 5.6 log CFU $mL^{-1}$ was achieved.

The results of control samples showed that the viability of both bacteria is neither affected by irradiation itself (light control) nor by the PS in the dark (dark control).

### 4.4.2 Porphyrin binding to bacteria

The results of porphyrin binding to the cells are represented in Figure 4.3 as the average number of molecules of PS per cell, for each bacterium and for each PS, without washing and with one washing step.

The binding of Tri-$Py^{+}$-Me-PF to *E. coli* was significantly higher than with Tetra-$Py^{+}$-Me (Figure 4.3a), without washing ($p = 0.000$) and with washing ($p = 0.000$). On the other side, the binding of Tetra-$Py^{+}$-Me to *S. warneri* was significantly higher than with Tri-$Py^{+}$-Me-PF (Figure 4.3b), without washing ($p = 0.000$) and with washing ($p = 0.000$).

Significant differences were also observed between the unwashed and the washed cells with the same PS. After washing with PBS, 35% of Tetra-$Py^{+}$-Me ($p = 0.002$) and 47% of Tri-$Py^{+}$-Me-PF ($p = 0.000$) remained bound to *E. coli* (Figure 4.3a).

In *S. warneri*, 47% of Tetra-$Py^{+}$-Me ($p = 0.000$) and 74% of Tri-$Py^{+}$-Me-PF ($p = 0.003$) remained bound to cells after washing (Figure 4.3b).

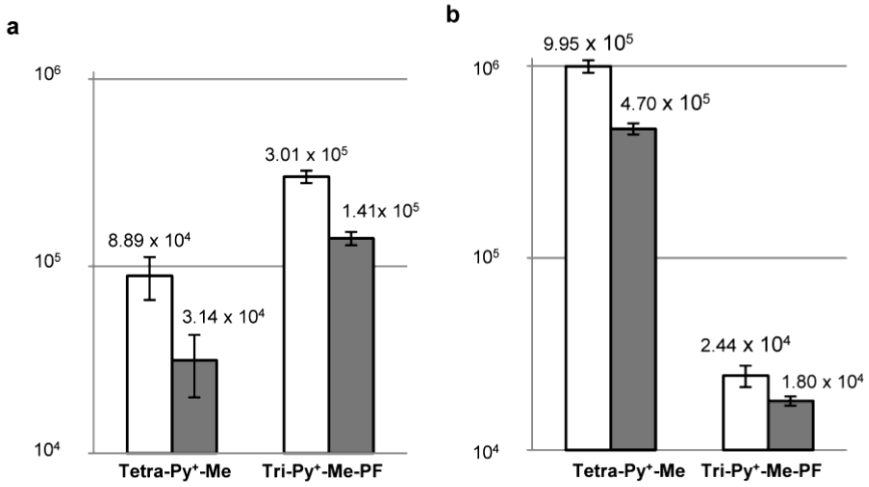

**Figure 4.3** Binding of Tetra-Py$^+$-Me and Tri-Py$^+$-Me-PF to **(a)** *E. coli* (5.0 µM of porphyrin) and to **(b)** *S. warneri* (0.5 µM of porphyrin) after 10 min of incubation in the dark at room temperature with none (white bars) and one (grey bars) washing steps represented by the number of photosensitizer molecules per cell. Values represent the mean of three independent experiments with two replicates each; error bars indicate the standard deviation.

### 4.4.3 Nucleic acids electrophoresis and quantification

The electrophoretic profiles of total nucleic acids extracted from *E. coli* cells that were irradiated up to 270 min (64.8 J cm$^{-2}$) with 5.0 µM of PS are shown in Figure 4.4. Photosensitization led to marked reductions in nucleic acids over time. With Tri-Py$^+$-Me-PF (right image), after 15 min of irradiation, there was a marked reduction of genomic DNA and rRNA. After 30 min, there was also a reduction of other nucleic acids (possibly degraded DNA and mRNA), and after 60 min no bands were detected. With Tetra-Py$^+$-Me (left image) progressive and drastic changes were also observed in the electrophoretic profiles, although slower than with Tri-Py$^+$-Me-PF. Hence, after 15 min of irradiation, all fractions were still visible (DNA and rRNA). After 30 min there was a greater reduction in 23S rRNA than in 16S rRNA, and after 60 min only faint bands of genomic DNA were observed. After this period, no more bands could be seen.

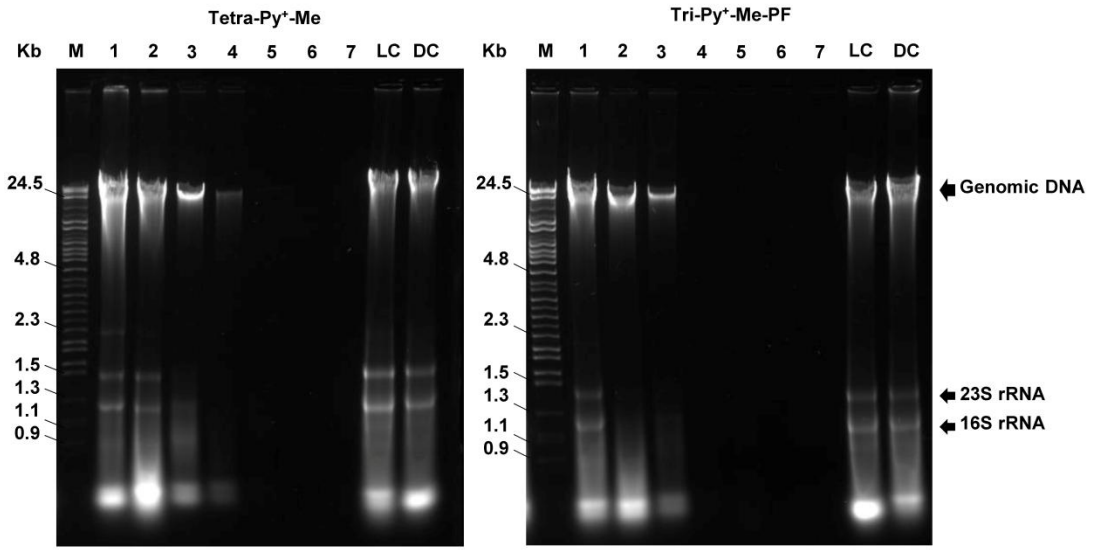


**Figure 4.4** Electrophoretic profiles of total nucleic acid samples extracted from *E. coli*. Cells were incubated for 10 min in the dark with 5.0 µM of Tetra-Py$^+$-Me and Tri-Py$^+$-Me-PF and irradiated with visible light (4.0 mW cm$^{-2}$) for 0, 15, 30, 60, 90, 180 and 270 min (lanes 1 - 7, respectively). M: molecular weight marker; LC: light control (*E. coli* suspension irradiated 270 min); DC: dark control (*E. coli* suspension with 5.0 µM of the studied photosensitizer incubated 270 min in the dark).

The electrophoretic profiles of total nucleic acids extracted from *S. warneri* irradiated up to 40 min (9.6 J cm$^{-2}$) with 0.5 µM of PS are shown in Figure 4.5. Photosensitization with Tri-Py$^+$-Me-PF led to drastic reductions in genomic DNA after the first irradiation periods (5, 10

and 15 min), where very faint bands could be seen (lanes 2 - 4, right image) and no bands in the further irradiation periods. On the other side, even though there was a DNA decrease with Tetra-Py$^+$-Me, it was not as drastic as with Tri-Py$^+$-Me-PF and a DNA band is still visible after 40 min of irradiation.

In the samples at 0 min (lane 1) and in control samples (lanes LC and DC) the profiles remained unchanged. In these cases, the genomic DNA and the RNA fractions (in the case of *E. coli*) can be seen.

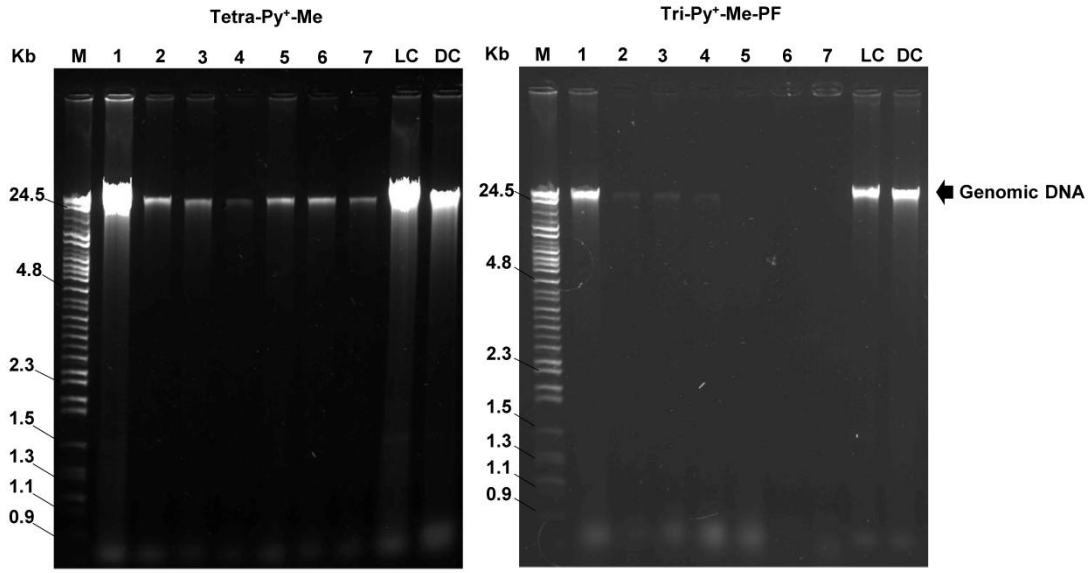


**Figure 4.5** Electrophoretic profiles of total nucleic acid samples extracted from *S. warneri*. Cells were incubated in the dark with 0.5 µM of photosensitizer and irradiated with visible light (4.0 mW cm$^{-2}$) for 0, 5, 10, 15, 20, 30 and 40 min (lanes 1 - 7, respectively). M: molecular weight marker; LC: light control (*S. warneri* suspension irradiated 40 min); DC: dark control (*S. warneri* suspension with 0.5 µM of photosensitizer incubated 40 min in the dark).

### 4.4.4 dsDNA concentration and cell survival

The effects of the photodynamic treatment of bacterial cells with the two PS on the concentration of intracellular dsDNA and on the survival of bacteria are shown in Tables 4.1 and 4.2. The amount of dsDNA after photodynamic treatment was calculated in relation to the amount of dsDNA obtained at time 0 min and was converted into percentage.

For *E. coli* (Table 4.1), the reduction of intracellular dsDNA concentration was time-dependent and simultaneous to survival reduction but the kinetics of photoinactivation and DNA damage is faster with Tri-Py$^+$-Me-PF than with Tetra-Py$^+$-Me. On average, there was a decrease in dsDNA of 23.1% *versus* 14.3% after 15 min, 55.1% *versus* 42.8% after 30 min, and 98.4% and 81.2% after 60 min of irradiation with Tri-Py$^+$-Me-PF and Tetra-Py$^+$-Me, respectively.

For *S. warneri* (Table 4.2), the reduction of intracellular dsDNA concentration after photosensitization with Tri-Py$^{+}$-Me-PF was also time-dependent and simultaneous to survival reduction. However, the same is not true for Tetra-Py$^{+}$-Me. Even though there is a linear decrease in cell survival during the experiment, the DNA content was not affected the same extent, remaining on average ca. 58.2% of intact DNA in the cells.

**Table 4.1** Comparison of dsDNA concentration with survival of *E. coli* after photodynamic treatment with 5.0 µM of Tetra-Py$^{+}$-Me and Tri-Py$^{+}$-Me-PF

| | | **Tetra-Py$^{+}$-Me (5.0 µM)** | | **Tri-Py$^{+}$-Me-PF (5.0 µM)** | |
|---|---|---|---|---|---|
| Irradiation time (min) | Light dose (J cm$^{-2}$) | [DNA] decrease | Cell inactivation | [DNA] decrease | Cell inactivation |
| | | % | log CFU mL$^{-1}$ | % | log CFU mL$^{-1}$ |
| 0 | 0 | 0 | 0 | 0 | 0 |
| 15 | 3.6 | 14.3 | 0.2 | 23.1 | 3.1 |
| 30 | 7.2 | 42.8 | 2.9 | 55.1 | 5.2 |
| 60 | 14.4 | 81.2 | 4.4 | 98.4 | 5.4 |
| 90 | 21.6 | 99.8 | 5.7 | 98.3 | 5.8 |
| 180 | 43.2 | 99.8 | 6.1 | 99.1 | 7.2 |
| 270 | 64.8 | 99.8 | 6.2 | 99.6 | 7.7 |

The decreases corresponding to each irradiation time were calculated in relation to the initial value just before the photosensitization (0 min). The values presented are the average of three independent experiments for each case.

## 4.5 Discussion

This study sought to assess the PDI effects caused by two cationic porphyrins (Tri-Py$^{+}$-Me-PF and Tetra-Py$^{+}$-Me) on the nucleic acids of *E. coli* and *S. warneri* during the inactivation of cell suspensions. The selected experimental conditions (bacterial concentration, PS concentration and light dose) were based on a previous work, where the physicochemical properties and the ability of bacterial PDI of seven cationic porphyrins with different charge numbers (1 - 4) and *meso* groups was studied. (77) The most efficient PS was Tri-Py$^{+}$-Me-PF. Tetra-Py$^{+}$-Me is a porphyrin widely used in the effective PDI of bacteria and viruses and was compared herein with Tri-Py$^{+}$-Me-PF. The results showed that these compounds are effective PS in the PDI of both bacteria, leading to a decrease in cell survival over 99.9% with very low light doses (lower than 5.0 J cm$^{-2}$ for *S. warneri* and lower than 8.0 J cm$^{-2}$ for *E. coli*).

In *E. coli*, marked reductions were observed in the nucleic acids over time with both porphyrins. These differences coincided with the inactivation profile represented in the cell survival curves and are in agreement with earlier findings. (103) The two cationic PS cause the same effect in cells (DNA reduction and survival decrease) but with Tri-Py$^{+}$-Me-PF the changes

occur faster. Under the experimental conditions used, the hierarchy of changes to nucleic acids of *E. coli* was: 23S rRNA > 16S rRNA > genomic DNA as it could be established from the electrophoretic profiles. Although it has been reported that during the PDI the change in genomic DNA occurs first than in total RNA (103), a different hierarchy was established from the gradual reduction detected in the different RNA bands. In fact, it is generally accepted that RNA is more labile than DNA and more susceptible to degradation by deleterious treatments (236) as it is the case. As suggested before, the direct effect of singlet oxygen on DNA or the indirect effect on the transcription machinery proteins bound to DNA may cause a marked decrease in the RNA pool. (236)

**Table 4.2** Comparison of dsDNA concentration with survival of *S. warneri* after photodynamic treatment with 0.5 µM of Tetra-$Py^+$-Me and Tri-$Py^+$-Me-PF

| | | **Tetra-$Py^+$-Me (0.5 µM)** | | **Tri-$Py^+$-Me-PF (0.5 µM)** | |
|---|---|---|---|---|---|
| Irradiation time (min) | Light dose ($J\ cm^{-2}$) | [DNA] decrease % | Cell inactivation log CFU $mL^{-1}$ | [DNA] decrease % | Cell inactivation log CFU $mL^{-1}$ |
| 0 | 0 | 0 | 0 | 0 | 0 |
| 5 | 1.2 | 19.6 | 0.4 | 66.2 | 4.8 |
| 10 | 2.4 | 37.9 | 1.8 | 69.9 | 5.3 |
| 15 | 3.6 | 38.1 | 2.8 | 78.0 | 5.6 |
| 20 | 4.8 | 38.3 | 3.3 | 82.8 | 6.9 |
| 30 | 7.2 | 45.3 | 4.7 | 91.9 | 7.2 |
| 40 | 9.6 | 58.2 | 5.6 | 92.2 | 7.5 |

The decreases corresponding to each irradiation time were calculated in relation to the initial value just before the photosensitization (0 min). The values presented are the average of three independent experiments for each case.

In the case of *S. warneri*, photosensitization with Tri-$Py^+$-Me-PF led to a marked reduction in genomic DNA concentration (66%) after the shorter irradiation period (5 min), where there was the greater decrease of cell survival (4.8 log CFU $mL^{-1}$). On the other hand, with Tetra-$Py^+$-Me, the same survival decrease was observed after 30 min with a 45% reduction of DNA. Since the detection limit of cell survival was not reached, it is probable that a greater or total DNA reduction can be achieved with a prolonged irradiation time.

Information on the effects of photodynamic action of porphyrins on bacterial nucleic acids is still contradictory and scarce in scientific literature. It was reported that the photodynamic action of deuteroporphyrin in *E. coli* pre-treated with polymyxin B nonapeptide, which increases the membrane permeability, is responsible by changes in the chromosomal DNA. (221) Also, photodynamic treatment of *Acinetobacter baumannii* and *E. coli* by Tetra-$Py^+$-Me induces DNA damage after a long period of illumination and total bacterial eradication.

However, when the total bacterial photoinactivation is carried out with an intense light (140 - 150 mW $cm^{-2}$) for very short periods (2 - 5 min) the chromosomal DNA remains intact. (121) So, the study of the effect of Tetra-$Py^{+}$-Me on *E. coli* nucleic acids has provided divergent conclusions. (103, 121) The authors used different bacterial strains, porphyrin concentrations, irradiances and light doses. Therefore, these variables seem to be important in the obtained effects.

The photosensitization of *E. coli* cells by the tetracationic porphyrin Tetra-$Py^{+}$-Me and visible light is considered to be highly influenced by the amount of bound PS. (90) Contrarily, no obvious correlation between cell photosensitivity and the amount of this porphyrin bound to the cells has been observed. (136) In this study, it was shown that the amount of bound porphyrin depends on the bacterial strain and on the PS structure. In the case of *E. coli*, the amount of bound Tri-$Py^{+}$-Me-PF is higher than that of Tetra-$Py^{+}$-Me and this may justify their differences in the survival profile and intracellular nucleic acid content during the photodynamic treatment. However, a different situation is observed for *S. warneri* where the amount of bound Tetra-$Py^{+}$-Me is higher than that of the more effective Tri-$Py^{+}$-Me-PF. Studies performed with *Enterococcus hirae* revealed that this Gram-positive bacterium accumulates higher amounts of PS than *E. coli* but this fact does not make the former more sensitive to PDI than the later. (237)

On the other side, despite the higher amount of Tetra-$Py^{+}$-Me molecules bound to *S. warneri* relatively to Tri-$Py^{+}$-Me-PF molecules, it turns out that, in percentage, the amount of Tri-$Py^{+}$-Me-PF which is bound to *E. coli* and to *S. warneri* is higher than Tetra-$Py^{+}$-Me, that is, even after washing, the molecules of Tri-$Py^{+}$-Me-PF remain tightly attached to bacteria (specially to *S. warneri*), probably due to its structure. Thus, the type and the cellular localization of the PS are probably as important in the final outcome of the sensitization process as the total amount of bound PS. (237) The particular efficiency of Tri-$Py^{+}$-Me-PF may not only be associated with a higher production of singlet oxygen, but also with its localization and amphiphilic character. (77) In fact, the singlet oxygen production by Tetra-$Py^{+}$-Me and Tri-$Py^{+}$-Me-PF previously evaluated showed that the 1,3-diphenylisobenzofuran (DPBF) photodegradation was higher in the presence of Tri-$Py^{+}$-Me-PF than in the presence of Tetra-$Py^{+}$-Me considered a good singlet oxygen generator. (77) Also, the partition coefficients of these porphyrins determined in a butan-1-ol/water system (log $P_{B/W}$) indicated that the most hydrophilic photosensitizer was Tetra-$Py^{+}$-Me (-1.97) and the most amphiphilic one was Tri-$Py^{+}$-Me-PF (-0.17). In this way, the particular efficiency of Tri-$Py^{+}$-Me-PF can be associated with its high production of singlet oxygen and also with its amphiphilic character. (77) Related to

this, some hydrophobic-type factors have been suggested to contribute to the binding process of amphiphilic porphyrins to bacteria. (238)

As demonstrated herein, Tri-Py$^{+}$-Me-PF is highly efficient (more than Tetra-Py$^{+}$-Me) on reduction of bacteria viability and of total nucleic acid of the two bacterial groups used. These same effects were observed on *E. coli* photosensitized with Tetra-Py$^{+}$-Me. (103) Additionally, it still cannot be assured to what extent the PS binding to DNA is critical to photodynamic inactivation. (42, 222, 239)

As has been highlighted, the antimicrobial photodynamic action is a multi-targeted cascade of events and not a 'one drug—one site of action' possibility. (10) The design of a PS should be thought considering its optimal characteristics (13) and systematic *in vivo* and *in vitro* studies should be comparable.

In this study, under the irradiation conditions used (irradiance of 4.0 mW cm$^{-2}$ and 270 min for *E. coli* and 40 min for *S. warneri*) nucleic acid changes occur simultaneously to cell survival decrease of *E. coli* and *S. warneri*. The binding capacity of the photosensitizers is different between both bacteria (Tri-Py$^{+}$-Me-PF has higher affinity for *E. coli* and Tetra-Py$^{+}$-Me for *S. warneri*) and is not directly related neither to the extent of cell inactivation nor to the reduction in nucleic acid content.

Different irradiation conditions (irradiance and exposure time to light) may be responsible for different DNA reduction profiles after photosensitization and they should always be considered when establishing an antimicrobial protocol.

# Chapter 5. Modifications in the protein profile of *Escherichia coli* and *Staphylococcus warneri* induced by photosensitization with cationic porphyrins

# 5 Modifications in the protein profile of *Escherichia coli* and *Staphylococcus warneri* induced by photosensitization with cationic porphyrins

## 5.1 Abstract

Oxidative stress induced by photodynamic treatment of microbial cells causes irreversible damages on vital cellular components such as proteins. Photodynamic inactivation (PDI) of bacteria is achieved by exciting a photosensitizer with visible light in an oxygenated environment, and can be used in the treatment of superficial and localized infections. The oxidative alterations of PDI in specific molecular targets are currently under study and, herein, the modifications induced by two cationic porphyrinic photosensitizers on the proteins of Gram-positive and Gram-negative bacteria were evaluated.

The cationic porphyrins 5,10,15-tris(1-methylpyridinium-4-yl)-20-(pentafluorophenyl)porphyrin tri-iodide (Tri-$Py^+$-Me-PF) and 5,10,15,20-tetrakis(1-methylpyridinium-4-yl)porphyrin tetra-iodide (Tetra-$Py^+$-Me) were used to photosensitize *Escherichia coli* and *Staphylococcus warneri* upon white light irradiation at an irradiance of 4.0 mW $cm^{-2}$. After different photosensitization periods, proteins were extracted from bacteria and analyzed by one-dimensional SDS-PAGE. Apparent molecular weights and band intensities were determined after an irradiation period corresponding to a reduction of 50% in cell viability.

After photodynamic treatment there was a general loss of bacterial proteins, assigned to large scale protein degradation. Protein loss was more pronounced after PDI with Tri-$Py^+$-Me-PF in both bacteria. There was an increase in the concentration of some proteins as well as an increase in the molecular weight. Most of the observed protein modifications may be associated to induction of responses to oxidative damage.

Proteins of *E. coli* and *S. warneri* are important PDI targets and, apparently, even though the attempt to respond to cell injury by upregulation or synthesis of new proteins of response to stress, the damage is lethal and can inhibit cellular response both during and after treatment.

## 5.2 Introduction

Reactive oxygen species (ROS) cause oxidative damage to biological molecules, namely lipids, nucleic acids, carbohydrates and proteins. (240) These ROS (singlet oxygen, $^1O_2$, and free radicals) have a very short lifespan in biological systems (nano to milliseconds) and, therefore,

a limited diffusion radius (some micrometers). (20, 92) ROS can be produced by photodynamic action (132), *i.e.*, through the concerted action of molecular oxygen, a photosensitizer (PS) and a light source of a wavelength corresponding to the maximum absorption peak of the PS. (8)

Although it is widely accepted that most of the PS can generate both $^1O_2$ and free radicals, due to its energetic and chemical features (241), $^1O_2$ is considered the main damaging species in photodynamic inactivation (PDI). PS with an overall cationic charge, such as porphyrin derivatives, can permeabilize the cell wall and bind preferably to the bacterial cytoplasmic membrane. This originates an efficient elimination of Gram-positive and Gram-negative bacteria. (65, 223) However, the effect of porphyrins depends not only on their physicochemical properties but also on the particular site where they bind and act. (242)

In bacteria, the cytoplasmic membrane consists of a phospholipid bilayer, some minor lipids and proteins. Since bacteria are devoid of intracellular organelles, inner membrane proteins play vital functions, such as energy production, lipid biosynthesis, protein secretion and transport. (25)

Proteins are considered major cellular targets of photodynamic oxidation not only because of their essential functions but also because they are highly abundant, may have endogenous chromophores, can bind to exogenous chromophoric materials and can rapidly react with other excited state species. (92, 93)

The outer membrane of Gram-negative bacteria is a lipid bilayer composed of glycolipids, mainly lipopolysaccharides, and two classes of proteins, lipoproteins and β-barrel proteins, also named outer membrane proteins (OMPs). (25)

In Gram-positive bacteria, surface proteins recognize components of the host cellular matrix (fibronectin, fibrinogen, elastin) (243), and are attached to peptidoglycan, to teichoic acids (adhesins) or to stem peptides within the peptidoglycan layers. (244) There are other proteins involved in immune system evasion, internalization and phage binding. (25)

Protein oxidation is, by definition, its covalent modification induced by ROS or by reaction with by-products of oxidative stress. (240) The processes involving oxidation by $^1O_2$ can induce deep changes in the proteins' structure and function. (241) Those $^1O_2$-mediated damages start, in general, at electron rich side-chains of amino acid residues (due to double bonds or sulfur moieties) such as cysteine, cystin, histidine, tyrosine, methionine and tryptophan residues. (245) Reaction with these residues origins new reactive species that damage other targets, leading to a cascade of deleterious events. (241) These new targets can be other proteins (241), lipids or DNA. (246, 247) The major consequences of $^1O_2$-mediated protein oxidation are enzyme inactivation, protein peroxides and carbonyls formation, side-

chain product formation, backbone fragmentation, formation of cross-links and aggregates, and protein unfolding. (92, 93)

Several *in vitro* studies have reported the photodynamic effect of PS in human proteins such as serum albumin (248, 249), or have identified the major protein damages in bacteria under oxidative stress. (250) *In vivo* studies of bacterial PDI using porphyrins are few and use sodium dodecyl sulphate-polyacrylamide gel electrophoresis (SDS-PAGE), enzymatic assays, and quantification of total carbonyls, to characterise protein damage. SDS-PAGE of membrane proteins normally reveals modifications on the electrophoretic pattern of the irradiated samples, namely the attenuation or disappearance of some proteins and the increased concentration of high molecular weight products, correspondent to cross-linked material. (90, 95, 97) Inactivation or loss of enzyme function has been reported for lactate dehydrogenase, NADH dehydrogenase, ATPase and also for succinate dehydrogenase. (90) These modifications in outer membrane proteins and enzymes are time-dependent and concomitant to a decrease of cell survival. The amount of protein carbonyls also increases with irradiation time. (61)

Oxidative damage to membrane proteins and bacterial enzymes have also been demonstrated using other PS such as phthalocyanines (94) and phenothiazinium dyes, as methylene blue (58, 84) or toluidine blue O. (251-253)

A single report describing the molecular targets of bacterial PDI by proteomics has shown that most of the altered proteins of *Staphylococcus aureus* by porphyrin treatment are involved in metabolic activities such as the response to oxidative stress, cell division and sugar uptake. (95) It has also been suggested that the damages induced by PDI are specific and are likely to be dependent on the location of the PS in the bacteria. (95)

Despite these contributions of proteomics on the study of the PDI of Gram-positive bacteria, there are, as far as it is known, no reports comparing the photo-oxidative effects of structurally different porphyrin derivatives on the protein profiles of the two types of bacteria.

The aim of this study was to evaluate and to compare the photo-oxidative effect of two efficient cationic porphyrins with different photoinactivation profiles on the proteins of Gram-positive and Gram-negative bacteria.

## 5.3 Material and Methods

### 5.3.1 Photosensitizers

The two cationic porphyrin derivatives selected for this study, 5,10,15-tris(1-methylpyridinium-4-yl)-20-(pentafluorophenyl)porphyrin tri-iodide (Tri-Py$^{+}$-Me-PF) and

5,10,15,20-tetrakis(1-methylpyridinium-4-yl)porphyrin tetra-iodide (Tetra-$Py^{+}$-Me) have already been described in the previous chapters (see subchapter 4.3.1).

### 5.3.2 Bacterial strains and growth conditions

The growth conditions of *Escherichia coli* ATCC 25922 and *Staphylococcus warneri* were the same as previously described (see subchapter 4.3.2).

### 5.3.3 Photosensitization procedure

The photosensitization procedure was the same to that used in the cell viability assays (Chapter 4, subchapter 4.3.4) with slight modifications.

Before irradiation, bacterial pellets were obtained by centrifugation (18 mL of early stationary phase cell culture), washed twice with PBS and re-suspended in glass beakers (final volume of 60 mL). The centrifugation conditions were 10 min at 13,000 x *g*, 20 °C, in 50 mL tubes for Avanti® J-25 (Beckman Coulter, Inc.). After photosensitization (0 - 270 min for *E. coli* and 0 - 40 min for *S. warneri*), bacterial pellets were obtained by centrifugation at the same conditions mentioned above.

### 5.3.4 Protein extraction and quantification

Cells pellets were carefully suspended in an urea solution [8 M urea, 100 mM Tris, 100 mM Bicine, and 2% SDS (w/v)] and disrupted with a sonicator (U200S control, JK IKA Labortechnik, Germany) at 50% maximum output. Cells were sonicated with bursts (2 seconds each) alternating with cooling in an ice bath (3 seconds), for a total of 120 seconds. Cell debris were pelleted by centrifugation at 17,000 x *g* for 10 min and supernatants were kept at -80°C until analysis.

Protein concentrations were determined by the BCA protein assay kit (Pierce, Rockford, USA) according to the manufacturer's instructions, with slight modifications. Each sample was quantified in triplicate and compared to a bovine serum albumin calibration curve prepared in the same urea solution.

### 5.3.5 Protein electrophoresis (SDS-PAGE)

Twenty five µg of *E. coli* and 5 µg of *S. warneri* proteins were reduced (2% β-mercaptoethanol), denaturated (5 min at 100 °C) and separated by SDS–PAGE. (254) The separation was performed in the Mini-PROTEAN 3 (Bio-Rad) with lab casted SDS polyacrylamide gels (15%). Gels ran for 2 h, at 120 V and at 4 °C. The apparent molecular

weight of the proteins was determined using a molecular weight calibration kit as marker, consisting of a mixture of proteins with 250, 150, 100, 75, 50, 37, 25, 20, 15 and 10 kDa (Precision Plus Protein Standards All Blue, Bio-Rad). Proteins were visualized by silver staining (255) or by colloidal Coomassie staining. (256) Each gel image was acquired using the GS-800 calibrated imaging densitometer (Bio-Rad).

Apparent molecular weights and band intensities were determined using the Quantity One v4.1 software (Bio-Rad). Band optical density (OD) was determined, subtracted for background and corrected for OD differences between gels, as described earlier. (257) All samples were analyzed in triplicate.

### 5.3.6 Protein assignment

The assignment of proteins was based on the previously determined molecular weights of protein bands, according to specific literature for each bacterial strain. (258, 259) The search considered representative protein bands after PDI: new, increased or disappearing. The molecular weights found (within a range of ± 0.4 kDa) were assigned to possible proteins and to their respective accession number, and afterwards this information was confronted with the information of UniProt database.

## 5.4 Results

The reduction in cell viability as well as the kinetics of photoinactivation of *E. coli* and *S. warneri* with Tri-$Py^{+}$-Me-PF and Tetra-$Py^{+}$-Me (see subchapter 4.4.1) depended on the porphyrin and on the light dose used.

The protein profile of the photosensitized bacteria was also affected by the porphyrin and the light dose, as revealed by SDS-PAGE shown in Figures 5.1 and 5.2 for *E. coli* and *S. warneri*, respectively.

In the light and dark controls (non-photosensitized bacteria), there were no changes in the protein profile (lanes LC in Figures 5.1 and 5.2, DC not shown), nor at 0 min of irradiation (bacteria incubated 10 min in the dark with porphyrin but not irradiated, lanes 0' in Figures 5.1 and 5.2). With irradiation and in the presence of porphyrin, a general disappearance of bacterial proteins was seen, assigned to large scale protein degradation. However, for the same light doses, the porphyrins acted differently: protein's degradation was more pronounced in the case of photo-treatment with Tri-$Py^{+}$-Me-PF (Figures 5.1 and 5.2).

In order to point out possible differences in the effects of the two porphyrins on the protein profile of each bacterium, gel analysis was based on the reduction of cell viability to

about half after PDI; this means that the analysis was performed at the irradiation time corresponding to a reduction of about 4 $\log_{10}$ survival, considering an initial bacterial concentration of 8 $\log_{10}$ (see previous results in subchapter 4.4.1).

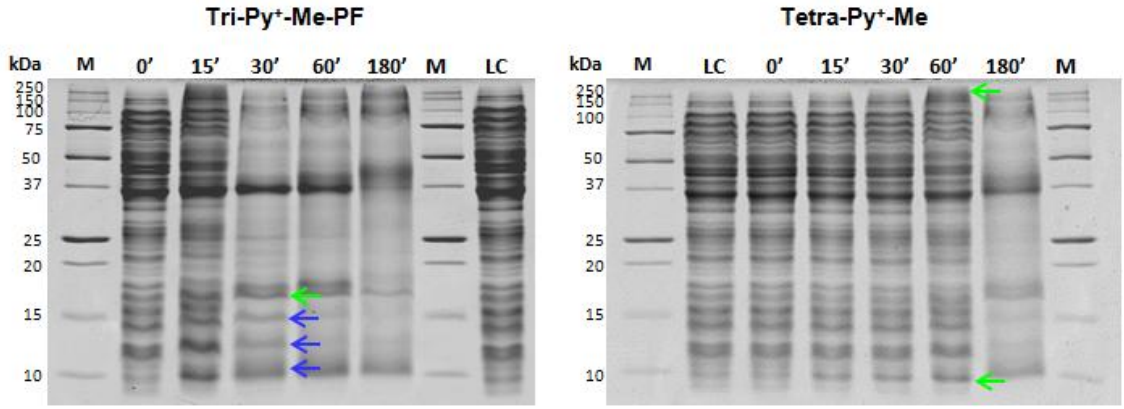


**Figure 5.1** SDS-PAGE of *Escherichia coli* proteins after photosensitization. Cells were incubated for 10 min in the dark with 5.0 µM of photosensitizer and irradiated with visible light (4.0 mW $cm^{-2}$) for different irradiation times. M: molecular weight marker; LC: light control (irradiated cell suspension); dark controls were carried out simultaneously but were omitted in the images. Blue arrows represent new protein bands. Green arrows indicate representative protein bands with increased intensity after treatment.

In *E. coli*, this reduction was observed after 30 min with Tri-$Py^+$-Me-PF and after 60 min with Tetra-$Py^+$-Me. In *S. warneri*, the ca. 50% reduction in survival was observed after 5 min with Tri-$Py^+$-Me-PF and after 20 min with Tetra-$Py^+$-Me.

By comparison with the controls, there was a clear alteration on the protein profile of *E. coli* after 30 min of irradiation with Tri-$Py^+$-Me-PF (Figure 5.1). There was an increase in the density of the band with 16.8 kDa and new bands with 14.9 kDa and 10.7 kDa (Figures 5.1 and 5.3).

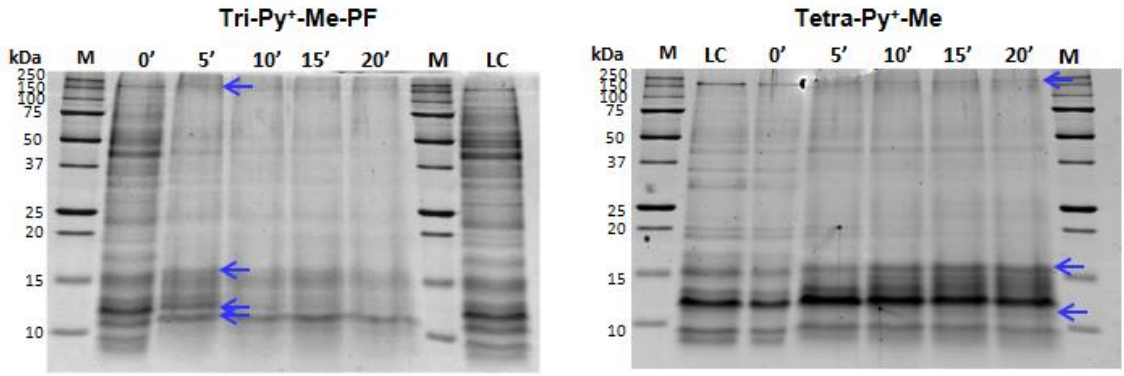


**Figure 5.2** SDS-PAGE of *Staphylococcus warneri* proteins after photosensitization. Cells were incubated in the dark with 0.5 µM of photosensitizer and irradiated with visible light (4.0 mW $cm^{-2}$) for different irradiation times. M: molecular weight marker; LC: light control (irradiated cell suspension); dark controls were carried out simultaneously but were omitted in the images. Blue arrows represent new protein bands that appear after treatment.

On the other hand, the protein profile of *E. coli* after 60 min of irradiation with 5.0 µM of Tetra-Py$^{+}$-Me was quite different and not as dramatically modified as with Tri-Py$^{+}$-Me-PF (Figure 5.1). There was an increase in the protein bands with 263.2 kDa, 201.8 kDa and 9.8 kDa (Figure 5.4). Also, some proteins disappeared after 60 min of treatment (with 94.6 kDa, 87.3 kDa, 60.6 kDa, 59 kDa and 12 kDa, Figure 5.4).

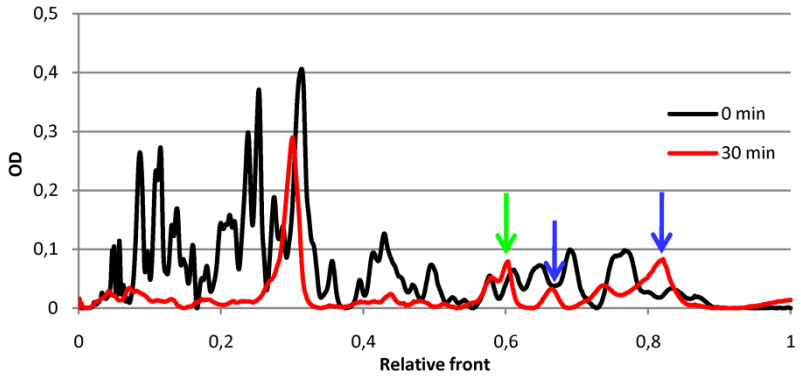


**Figure 5.3** Lane optical density (OD) of *Escherichia coli* proteins after photosensitization with Tri-Py$^{+}$-Me-PF (black line, 0 min and red line, 30 min of irradiation). Blue arrows represent new protein bands. Green arrow indicates a representative protein band with increased intensity after treatment.

The photosensitization of *S. warneri* with both porphyrinic photosensitizers induced changes in the protein profile after the first irradiation times (Figure 5.2). However, the induced changes were much more pronounced with Tri-Py$^{+}$-Me-PF than Tetra-Py$^{+}$-Me as it was observed for *E. coli*. In the presence of Tetra-Py$^{+}$-Me, after 20 min of irradiation, protein bands with 15.7 kDa and 12.4 kDa showed increased intensity. New proteins with 200.2 kDa, 14.6 kDa and 14.0 kDa were detected (Figures 5.2 and 5.5). Also, an increase in the molecular weight of some proteins could be observed (orange arrows in Figure 5.5).

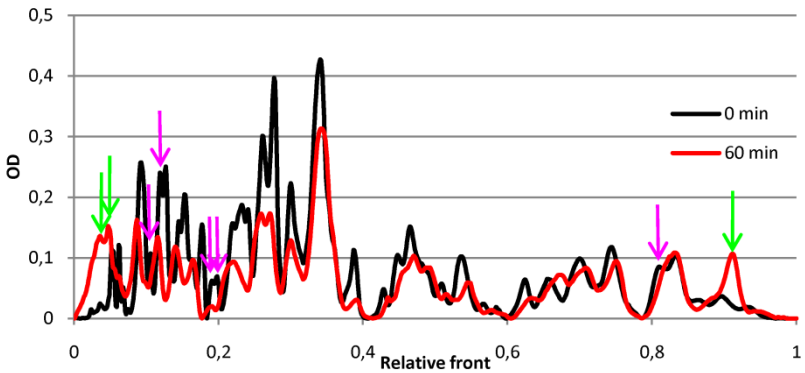


**Figure 5.4** Lane optical density (OD) of *Escherichia coli* proteins after photosensitization with Tetra-Py$^{+}$-Me (black line, 0 min and red line, 60 min of irradiation). Pink arrows represent protein bands that disappear after treatment. Green arrows indicate representative protein bands with increased intensity after treatment.

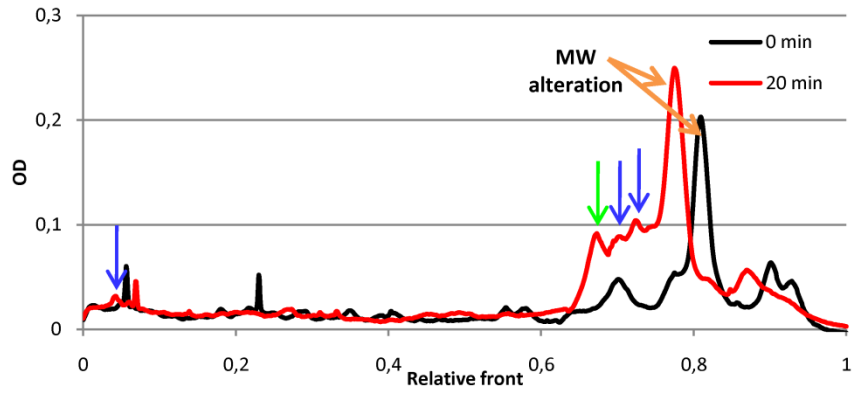


**Figure 5.5** Lane optical density (OD) of *Staphylococcus warneri* proteins after photosensitization with Tetra-Py$^{+}$-Me (black line, 0 min and red line, 20 min of irradiation). Blue arrows represent new protein bands and green arrows, representative proteins bands with increased intensity after treatment. Orange arrows indicate protein bands with increased molecular weight.

The protein pattern of *S. warneri* was drastically changed after 5 min of irradiation with Tri-Py$^{+}$-Me-PF, with a marked decrease of almost all bands (Figure 5.2) and the formation of some proteins, with molecular weights of 196.3 kDa, 15.9 kDa, 12.4 kDa and 11.3 kDa (Figure 5.6).

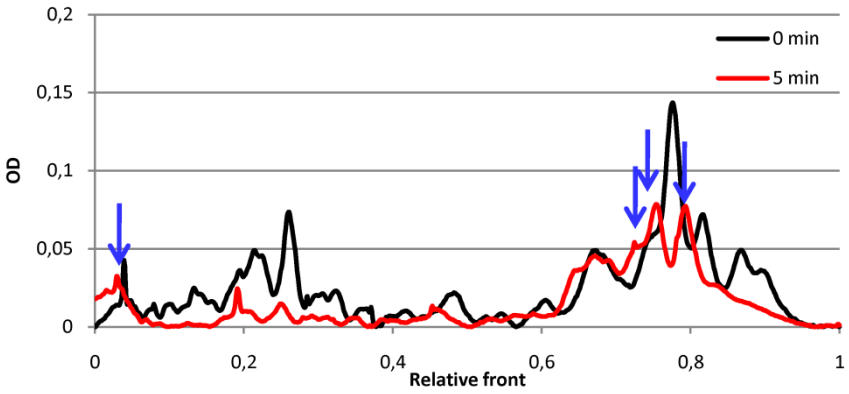


**Figure 5.6** Lane optical density (OD) of *Staphylococcus warneri* proteins after photosensitization with Tri-Py$^{+}$-Me-PF (black line, 0 min and red line, 5 min of irradiation). Blue arrows represent new protein bands.

## 5.5 Discussion

This study aimed to provide insight into the photo-oxidative effect of two cationic porphyrin derivatives on the protein profile of Gram-negative and Gram-positive bacteria by SDS-PAGE. (92, 93)

In general, the widespread disappearance of protein bands over time suggests degradation in large scale. In some cases, there is an increase in the intensity of some protein bands, possibly caused by increased expression of these proteins, indicating a probable

specificity in the response to the damage induced by PDI. On the other hand, there is a slight increase in the molecular weight of some proteins (1 - 5 kDa) which may be indicative of changes, and also the appearance of aggregates of high molecular weight (>100 kDa), probably related with formation of cross-linked complexes found in the top of the gels. These evidences agree with the literature about the effects of photoinactivation on bacterial proteins. (90, 95, 97)

Once the method used in this study does not allow the identification of proteins without complementary methods, the protein assignment of differentially expressed proteins after PDI, was based on their molecular weights. (258, 259) The gathered information concerning presumable proteins from *E. coli* is summarized in Table 5.1 and from *S. warneri* in Table 5.2.

The protein profile of *E. coli* after photosensitization with the two selected porphyrins is different. Apart from the degradation of most proteins over time, it was found that, after 30 min of photosensitization with Tri-Py$^{+}$-Me-PF, there was an increase in the intensity of a protein (16.8 kDa) putatively corresponding to Dps, a protein responsible for DNA protection during protein starvation (see Table 5.1). This protein binds nonspecifically to DNA, protecting cells from toxicity, as shown by *E. coli* exposure to hydrogen peroxide. (260) New protein bands (10.7 and 14.9 kDa) assigned to stress response proteins (YggX, UspG, OsmC, see Table 5.1) were also identified by gel analysis.

With Tetra-Py$^{+}$-Me, the process of *E. coli* protein degradation is slower, which is in agreement with the slowest photoinactivation rate of these bacteria with this porphyrin. (56) There was an increase in the intensity of a band (with 9.8 kDa) corresponding presumably to stress response proteins (YgiN or GrcA). At the same time, several other bands disappeared (87.3 and 60.6 kDa). These bands may be assigned to proteins involved in metabolic or biosynthetic processes (MdoG or PpsA) as well as in cellular response to stress (e.g., DnaK or GroL). GroL has been reported to be overexpressed in *Streptococcus mutans* photosensitized with rose Bengal, without DNA degradation. (127) In *E. coli* photosensitized with toluidine blue O, there is also upregulation of GroL and DnaK. (128) According to these evidences, the induction of heat shock proteins has been suggested as a possible mechanism of development of resistance. (128) However, PDI of *S. aureus* by Tetra-Py$^{+}$-Me leads to a decrease of enzymes involved in direct and indirect response to ROS (95), as also suggested by the observations from this study. These contradictory conclusions might be due to the use of different PS type (porphyrin *vs* phenothiazinium derivatives) and PDI protocols (e.g., irradiation conditions).

In the case of *S. warneri*, there was also a large degradation of the majority of proteins, being more evident the difference caused by porphyrin Tri-Py$^{+}$-Me-PF in the beginning of the

**Table 5.1** Presumable proteins of *Escherichia coli* modified after photodynamic treatment with Tri-Py$^{+}$-Me-PF and Tetra-Py$^{+}$-Me. Possible assignments were based on the literature (ref. 259) and on UniProt database.

| | | Determined molecular weight (kDa) | Possible assignments Ref. (259) | Access no. | Gene id. | Protein name | Biological process |
|---|---|---|---|---|---|---|---|
| *E. coli* treated with Tri-Py$^{+}$-Me-PF | Upregulated | **16.8** | 16.8 | P0ABT2 | Dps | DNA protection during starvation protein | DNA condensation; Iron storage |
| | New | **14.9** | 15.0 | P0C0L2 | OsmC | Peroxiredoxin OsmC | Response to oxidative stress |
| | | | 15.0 | P02413 | RplO | 50S ribosomal protein L15 | Translation |
| | | | 15.1 | P0A6E6 | AtpC | ATP synthase epsilon chain | Plasma membrane ATP synthesis coupled proton transport |
| | | **10.7** | 11.0 | P0A8P3 | YggX | Probable $Fe^{2+}$-trafficking protein | Response to oxidative stress |
| | | | 10.6 | P39177 | UspG | Universal stress protein G | Response to stress |
| | | | 10.7 | P0AES9 | HdeA | Acid stress chaperone HdeA | Cellular response to acidity |
| *E. coli* treated with Tetra-Py$^{+}$-Me | Upregulated | **9.8** | 9.9 | P0ADU2 | YgiN | Probable quinol monooxygenase YgiN | Response to oxidative stress |
| | | | 9.8 | P68066 | GrcA | Autonomous glycyl radical cofactor | Response to stress |
| | Undetectable after PDI | **94.6** | 94.0 | P0A9M0 | Lon | Lon protease | Cellular response to stress; misfolded or incompletely synthesized protein catabolic process; response to heat |
| | | **87.3** | 87.4 | P33136 | MdoG | Glucans biosynthesis protein G | Glucan biosynthetic process; oligosaccharide biosynthetic process; response to osmotic stress |
| | | | 87.4 | P07395 | PheT | Phenylalanine-tRNA ligase beta subunit | Phenylalanyl-tRNA aminoacylation; tRNA processing |
| | | | 87.4 | P23538 | PpsA | Phosphoenolpyruvate synthase | Gluconeogenesis; pyruvate metabolic process |
| | | **60.6** | 60.7 | P77306 | YqiK | Inner membrane protein YqiK | Unknown |
| | | | 60.4 | P11875 | ArgS | Arginine-tRNA ligase | Protein biosynthesis |
| | | | 60.6 | P0A6Y8 | DnaK | Chaperone protein DnaK | DNA replication; Stress response |
| | | | 60.8 | P0A6F5 | GroL | 60 kDa chaperonin | Cell cycle; cell division; protein folding; protein refolding; response to heat |
| | | **59.0** | 59.4 | P02942 | Tsr | Methyl-accepting chemotaxis protein I | Chemotaxis |
| | | **12.0** | 12.2 | P0A8Q6 | ClpS | ATP-dependent Clp protease adapter protein ClpS | Proteolysis involved in cellular protein catabolic process |
| | | | 12.3 | P0A7K2 | RplL | 50S ribosomal protein L7/L12 | Translation |

treatment. The formation of new proteins was detected, namely some of high molecular weight, probably associated with the formation of cross-linked complexes. Other proteins,

detected after treatment, but not in the controls, may be associated with specific functions of response to PDI, such as teichoic acid biosynthesis (e.g., glycerol-3-phosphate cytidyltransferase, see Table 5.2).

**Table 5.2** Presumable proteins of *Staphylococcus warneri* modified after photodynamic treatment with Tri-Py$^+$-Me-PF and Tetra-Py$^+$-Me. Possible assignments were based on the literature (ref. 258) and on UniProt database.

| | | Determined molecular weight (kDa) | Possible assignments Ref. (258) | Access no. | Gene id. | Protein name | Biological process |
|---|---|---|---|---|---|---|---|
| ***S. warneri* treated with Tri-Py$^+$-Me-PF** | **New** | **196.3** | Cross-links | | | | |
| | | **15.9** | 15.7 | L7WVR6 | | Putative Holliday junction resolvase | DNA recombination; DNA repair; nucleic acid phosphodiester bond hydrolysis |
| | | | 15.8 | L7WY50 | | Glycerol-3-phosphate cytidylyltransferase | Teichoic acid biosynthetic process |
| | | **11.3** | 11.2 | L7WYE7 | GatC | Aspartyl/glutamyl-tRNA(Asn/Gln) amidotransferase subunit C | Translation |
| ***S. warneri* treated with Tetra-Py$^+$-Me** | **Upregulated** | **15.7** | 15.8 | L7WY50 | | Glycerol-3-phosphate cytidylyltransferase | Teichoic acid biosynthetic process |
| | | | 15.6 | L7WXX9 | RplO | 50S ribosomal protein L15 | Translation |
| | | | 15.6 | L7WUN7 | LacA | Galactose-6-phosphate isomerase subunit lacA | Lactose catabolic process |
| | | | 15.7 | L7WVR6 | | Putative Holliday junction resolvase | DNA recombination; DNA repair; nucleic acid phosphodiester bond hydrolysis |
| | **New** | **200.2** | Cross-links | | | | |
| | | **14.6** | 14.6 | L7WUN1 | RpsI | 30S ribosomal protein S9 | Translation |
| | | **14.0** | 14.0 | L7WXY2 | RpsM | 30S ribosomal protein S13 | Translation |

The results suggest that most protein modifications triggered by PDI with Tri-Py$^+$-Me-PF and Tetra-Py$^+$-Me may be associated with induction of oxidative damage responses. Also, these responses appear to be very short-lived, since possible defense mechanisms triggered by bacteria are destroyed, as can be inferred by the case of *E. coli* photosensitized with Tetra-Py$^+$-Me, where several undetected protein bands after PDI can be associated to these mechanisms. This may explain the effectiveness of antimicrobial PDI, evidenced by the supposed degradation of stress response proteins, reducing the likelihood of developing resistance mechanisms, which otherwise have not yet been identified. (117-119)

The data from this study reveal that, using the cationic porphyrins Tri-Py$^{+}$-Me-PF and Tetra-Py$^{+}$-Me, the proteins of *E. coli* and *S. warneri* are important PDI targets and, apparently, even though the attempt to respond to cell injury by overexpression of proteins or synthesis of new protein in response to stress, the damage is lethal.

# Chapter 6. Biomolecular changes in photosensitized bacteria studied by infrared spectroscopy

# 6 Biomolecular changes in photosensitized bacteria studied by infrared spectroscopy

## 6.1 Abstract

The photodynamic inactivation (PDI) of microorganisms lies in their elimination by oxidative stress generated by combining oxygen, light and a photosensitizer. Knowing the mode of action of microbial PDI can help to optimize the inactivation protocol, as well as to understand the mechanisms of response to such stress.

In this study, the molecular changes induced by photosensitization in the presence of the cationic porphyrins (5,10,15-tris(1-methylpyridinium-4-yl)-20-pentafluorophenylporphyrin, Tri-$Py^+$-Me-PF and 5,10,15,20-tetrakis(1-methylpyridinium-4-yl)porphyrin, Tetra-$Py^+$-Me) plus white light (4.0 mW $cm^{-2}$) on proteins, lipids, nucleic acids and polysaccharides of the Gram-negative bacterium *Escherichia coli* and of the Gram-positive bacterium *Staphylococcus warneri* were evaluated by infrared spectroscopy.

Differences between the two porphyrins were identified both on *E. coli* and on *S. warneri* related with PDI kinetics but not with the cellular targets. Tri-$Py^+$-Me-PF induces cellular modifications faster than Tetra-$Py^+$-Me. Photodynamic treatment caused an increase in methyl groups associated with lipids and in carbonyls associated with lipid oxidation. Additionally, the effects of PDI on proteins were also revealed by changes in their conformation and composition as well as changes in the glycosylation status of the bacterial proteins. Evidences of oxidative damage to nucleic acids were also found. Most of the changes observed in *E. coli* occur at the level of proteins, lipids and nucleic acids. In *S. warneri*, the main changes were detected in proteins but alterations in nucleic acids and polysaccharides were also observed.

The obtained results are in accordance with those previously reported using conventional methodologies (electrophoresis, chromatography and mass spectrometry) highlighting that infrared spectroscopy is a fast and reliable tool to monitor biochemical changes in bacterial cells induced by photosensitization.

## 6.2 Introduction

Efficient inactivation of microorganisms can be achieved through oxidative stress induced by the interaction of a light-excited molecule (photosensitizer, PS) in the presence of molecular oxygen, in a process named photodynamic inactivation (PDI). As PDI emerges as an alternative therapeutic option to treat localized infections towards conventional antimicrobial

compounds (11, 12), scientific research has been focusing on a possible specificity of the mode of action and on the cellular and molecular targets of microbial PDI, namely bacterial PDI. (54, 59, 63, 79, 95, 103).

The study of ultra-structural, morphological and functional changes taking place at initial stages and during PDI of bacteria have been carried out so far, through conventional methods such as microscopy (54, 55, 79), spectrophotometry (54, 57) or electrophoresis. (58, 94, 97). In the last few years, more specific methods have come up, including electrochemical sensors (62, 91), atomic force microscopy (53, 83, 85), and proteomic (95) and lipidomic (101, 102) approaches using mass spectrometry techniques. In this way, as the research on antimicrobial PDI acquires more impact, fast-screening, sensitive, precise, cost-effective and reliable tools are required to monitor the major damages induced by PDI on different microorganisms with distinct photosensitizers.

Infrared (IR) spectroscopy allows the identification and classification of microbial cells with regard to their overall chemical composition. (261) IR spectroscopy is a form of vibrational spectroscopy and IR spectra reflect both the molecular structure and the molecular environment. (262) The IR spectrum of an intact cell is a highly specific fingerprint and thus, changes occurring in cell components (water, lipids, proteins, nucleic acids and polysaccharides) are easily detected. (263)

The generation of high-quality data in a short period of time, coupled with the fact of being a specific and a non-destructive technique, requiring minimal sample manipulation (261), makes IR spectroscopy very appealing in the screening of the major cellular damages on photosensitized microorganisms. As far as it is known, there is only one study using IR spectroscopy to assess the damage caused by PDI on bacteriophage proteins (264), while the evaluation of the oxidative damage effects in bacterial components induced by $TiO_2$ photocatalysis (265, 266) or UV radiation (267) by this method, have already been reported.

In this work, the goal was to study the global modifications on the different functional groups of the biological molecules of Gram-negative and Gram-positive bacteria induced by photosensitization with two efficient cationic porphyrins, using IR spectroscopy.

## 6.3 Material and Methods

### 6.3.1 Photosensitizers

The two cationic porphyrins Tri-$Py^{+}$-Me-PF and Tetra-$Py^{+}$-Me used in this study have been already mentioned and described in the previous chapters (Chapters 4 and 5).

### 6.3.2 Bacterial strains and growth conditions

The growth conditions of *Escherichia coli* ATCC 25922 and *Staphylococcus warneri* were the same as previously described (Chapters 4 and 5).

### 6.3.3 Photosensitization procedure

For IR spectroscopy experiments, the photosensitization procedure was the same to that used in the cell viability assays already described in Chapter 4 (subchapter 4.3.4) but, as for nucleic acid and protein extraction, bacteria were concentrated by centrifugation previously to photosensitization to obtain an adequate pellet to be analyzed by the spectrometer.

After the different photosensitization periods (0 to 270 min for *E. coli* and 0 to 40 min for *S. warneri*), each bacterial pellet was obtained by centrifugation at maximum velocity for 5 min in a microcentrifuge tube. The pellets were washed twice with PBS solution to remove residual DMSO, the porphyrins' solvent, to avoid interference with the interpretation of the spectra. The acquisition of spectra was obtained immediately after bacterial photosensitization. Light and dark controls were also included and treated simultaneously (as already described in Chapters 4 and 5).

### 6.3.4 Acquisition and analysis of spectra

Each bacterial pellet was spread over the horizontal diamond crystal of a Perkin-Elmer Spectrum BX System 2000 (Perkin-Elmer Corp., Norwalk, CT, USA) equipped with a GoldenGate single-reflection attenuated total reflectance (ATR) system with a deuterated triglycine sulfate (DTGS) detector, and completely dried under a gentle cold airflow. Measurements were recorded over the wavelength range 4000 - 600 $cm^{-1}$ with a spectral resolution of 8 $cm^{-1}$. The final spectra of the samples were achieved by averaging 32 scans. At least, three spectra of each sample were acquired, yielding nine replicates for each irradiation time in each strain. Spectra were normalized and baseline-corrected. The three most similar spectra were identified and used for subsequent chemometric analysis.

For principal component analysis (PCA), the original spectra were transferred via JCAMP.DX format into the data analysis software package described by Barros. (268)

## 6.4 Results

The original infrared spectra of the photosensitized and non-photosensitized bacteria are shown in Figure 6.1. The spectra of T0, consisting in a sample incubated 10 min in the dark

with porphyrin but not irradiated, and mentioned in the figures as “control”, were compared with the ones of irradiated samples. As the analysis of the spectra of irradiated samples showed no differences between the mode of action of both porphyrins, but only in terms of the photoinactivation kinetics, in the interpretation of the spectra it was only considered the major changes observed after irradiation in comparison with control and not between porphyrins.

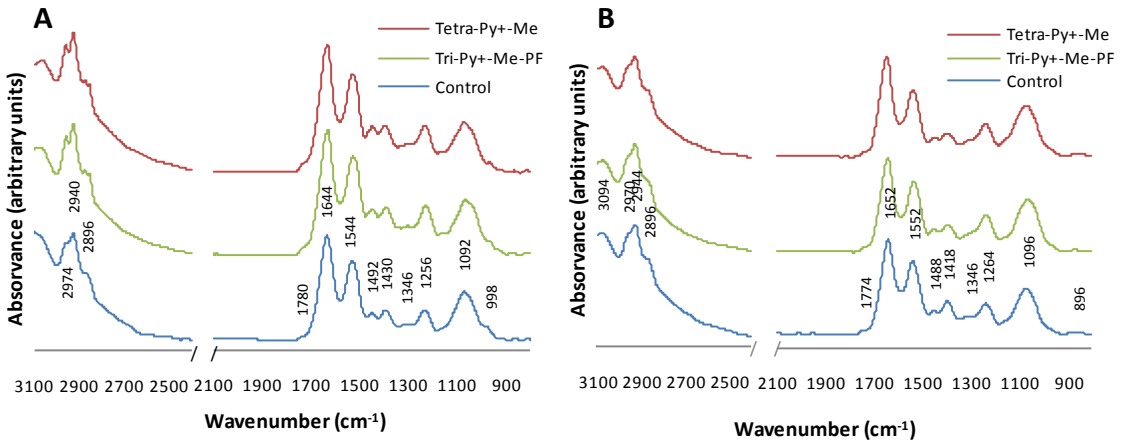


**Figure 6.1** Original spectra of bacteria photosensitized with Tri-Py$^{+}$-Me-PF and Tetra-Py$^{+}$-Me compared with T0 which was used as control. **A**) *Escherichia coli* and **B**) *Staphylococcus warneri*. Main bands are identified. The spectra were normalized, baseline-corrected and a 10-point smooth was applied. The presented spectra correspond to the average of 3 spectra. The region between 2400 and 2200 cm$^{-1}$ corresponding to the $CO_2$ region was removed from the spectra.

PCA scores and loadings plots from *E. coli* photosensitized with both porphyrins are presented in Figure 6.2.

In the PCA scores plot of *E. coli* treated with Tri-Py$^{+}$-Me-PF (Figure 6.2A), the controls (LC and DC) and the samples T0, T15 and T30 (positive PC1) were separated from irradiated samples from T60 to T270 (negative PC1), by the higher intensity of the bands at 1652 cm$^{-1}$ and 1556 cm$^{-1}$ (assigned to amide I and amide II of proteins) (269), 1622 cm$^{-1}$ (assigned to amide I of pleated sheet structures of proteins) (270), and 1719 cm$^{-1}$ (assigned to carbonyls from phospholipids) (271), as shown in Figure 6.2B.

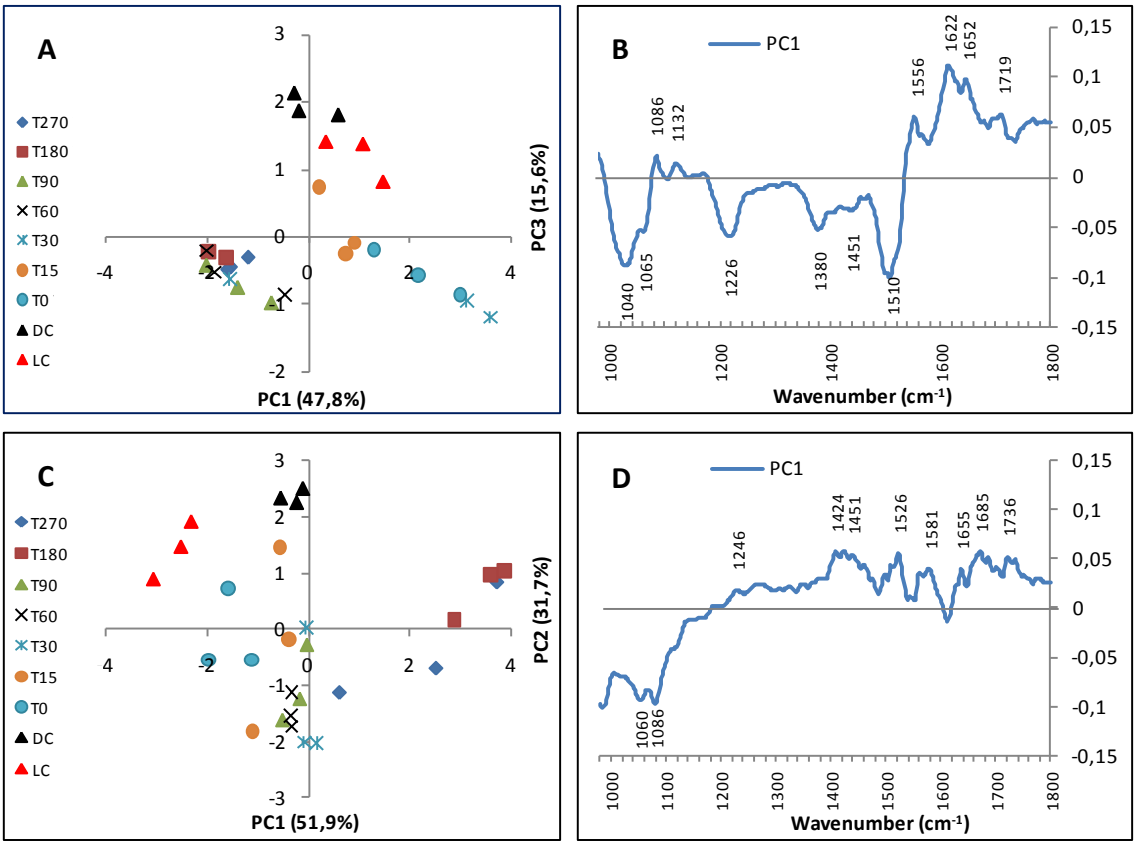


**Figure 6.2** Scores and loading plots for PCA analysis of photosensitized *Escherichia coli* with Tri-Py$^{+}$-Me-PF (**A**, **B**) and with Tetra-Py$^{+}$-Me (**C**, **D**), respectively, for different irradiation times. Number on the axis labels of scores plot indicate the percentage of the total variation in the data that was explained by the first, second and third principal components (PC1, PC2 and PC3).

The samples irradiated from 60 to 270 min (negative PC1) displayed enhanced intensities of bands at 1510 cm$^{-1}$ (assigned to the in-plane C-H bending vibrations from the phenyl rings) (272), 1451 cm$^{-1}$ (assigned to asymmetric $CH_3$ bending modes of the methyl groups of proteins) (273), and 1380 cm$^{-1}$ assigned to methyl groups of proteins (274, 275), or stretching in C-O bonds or deformation of C-H or N-H bonds of proteins. (276) Increased bands associated to nucleic acid structures were also identified: 1226 cm$^{-1}$ assigned to asymmetric $PO_2^-$ vibration (276), 1065 cm$^{-1}$ assigned to C-O stretching of the phosphodiester and the ribose (277) and 1040 cm$^{-1}$ assigned to stretching of the C-O bonds from ribose. (276)

In the PCA scores plot of *E. coli* irradiated with Tetra-Py$^{+}$-Me (Figure 6.2C), the samples irradiated for 180 and 270 min (positive PC1) were separated from all other samples and from controls (negative PC1). The contributions from the negative PC1 are the bands assigned to symmetric stretching of phosphodiester groups of nucleic acids at 1086 cm$^{-1}$ (278, 279), and stretching vibrations of C-O from deoxyribose at 1060 cm$^{-1}$. (271) Samples treated for longer irradiation times (positive PC1) showed higher intensities of several bands assigned to C=O stretching in lipids (1736 cm$^{-1}$) (280), C=O stretching and N–H wagging of amide I associated

with a disordered structure (non-hydrogen bonded) at 1685 $cm^{-1}$ (281), proteins in the α-helix conformation (1655 $cm^{-1}$) (274, 282), amide II of proteins (1526 $cm^{-1}$) (283), CC stretching vibration of the phenyl ring (1581 $cm^{-1}$) (272), asymmetric $CH_3$ bending modes of the methyl groups of proteins (1451 $cm^{-1}$) (273); flexible vibration of C-H of proteins (1424 $cm^{-1}$) (284) and asymmetric $PO_2^-$ stretching from nucleic acids (1246 $cm^{-1}$). (285, 286)

Further evidence of molecular modifications on photosensitized *E. coli* were obtained from the analysis of different spectral regions, where increases and alterations in the intensity of several bands were observed (Figure 6.3).

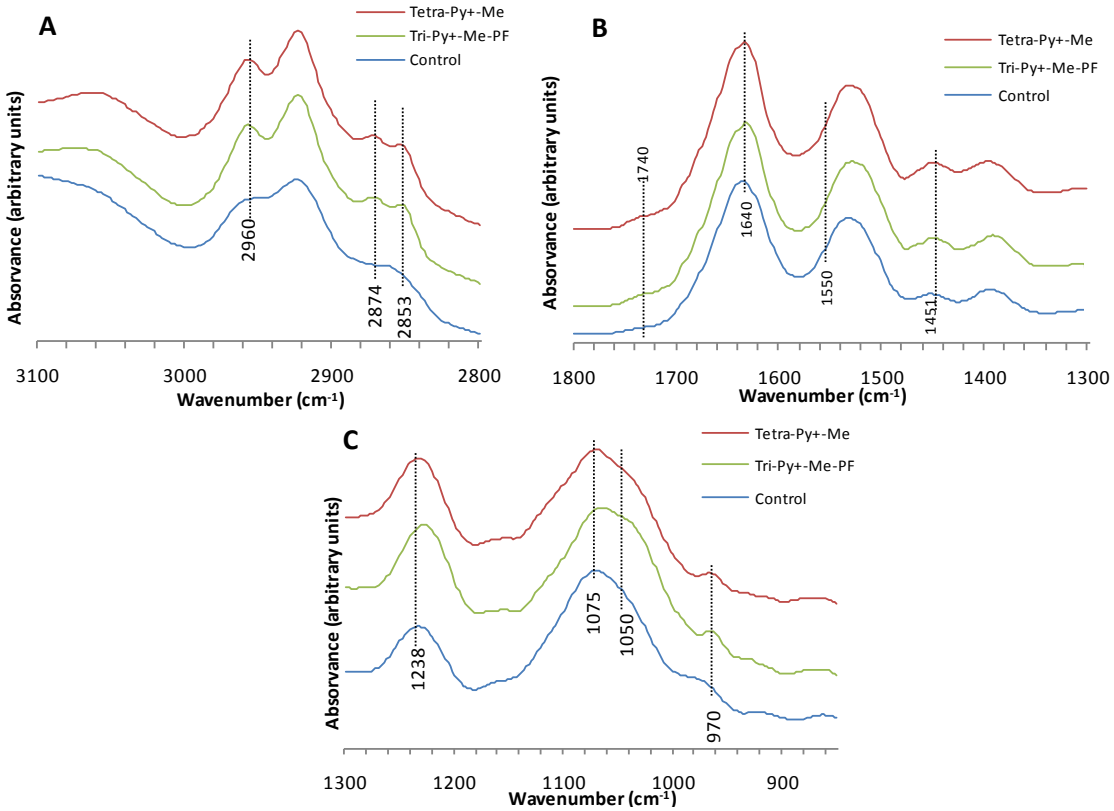


**Figure 6.3** Infrared spectra of control (T0) and photosensitized *Escherichia coli* in the spectral regions of 3100-2800 $cm^{-1}$ (**A**), 1800-1300 $cm^{-1}$ (**B**) and 1300-850 $cm^{-1}$ (**C**).

In the region between 3100 - 2800 $cm^{-1}$ (Figure 6.3A), corresponding to the lipid region (280, 287), there was an increase in the bands comprising asymmetric vibrations of $CH_3$ groups (2960 $cm^{-1}$) (288), symmetric stretching vibration of $CH_3$ of acyl chains (2874 $cm^{-1}$) (280) and symmetric vibrations of $CH_2$ (2853 $cm^{-1}$). (289)

In the region between 1800 - 1300 $cm^{-1}$ (Figure6.3B), comprising the amide region (290), an alteration in the shape of the bands at 1640 $cm^{-1}$ and 1550 $cm^{-1}$ could be seen, assigned to amide I (291) and amide II (285, 292) of proteins, and an increase in the band at 1451 $cm^{-1}$ corresponding to asymmetric $CH_3$ bending modes of the methyl groups of proteins.

(273) There was also an increase in the band associated with ester C=O stretching vibration in phospholipids (1740 $cm^{-1}$). (280)

In the region between 1300 - 850 $cm^{-1}$ (Figure 6.3C), corresponding to the phosphodiester region (286), irradiated samples of *E. coli* were characterized by higher intensity in the band at 1238 $cm^{-1}$ assigned to asymmetric stretching of $PO_2^-$ from nucleic acids (phosphate I). (271, 276) The band at 1075 $cm^{-1}$ assigned to symmetric $PO_2^-$ stretching vibrations of phosphodiesters (273) from nucleic acids shifted to 1065 $cm^{-1}$. The increase in the absorption shoulder at 1050 $cm^{-1}$ can be assigned to C-O-C stretching of DNA and RNA. (287) There was also an increase in the intensity of the band at 970 $cm^{-1}$ assigned to vibration of $PO_2^-$ from nucleic acids. (293)

PCA scores and loadings plots from spectra of *S. warneri* photosensitized with both porphyrins are presented in Figure 6.4.

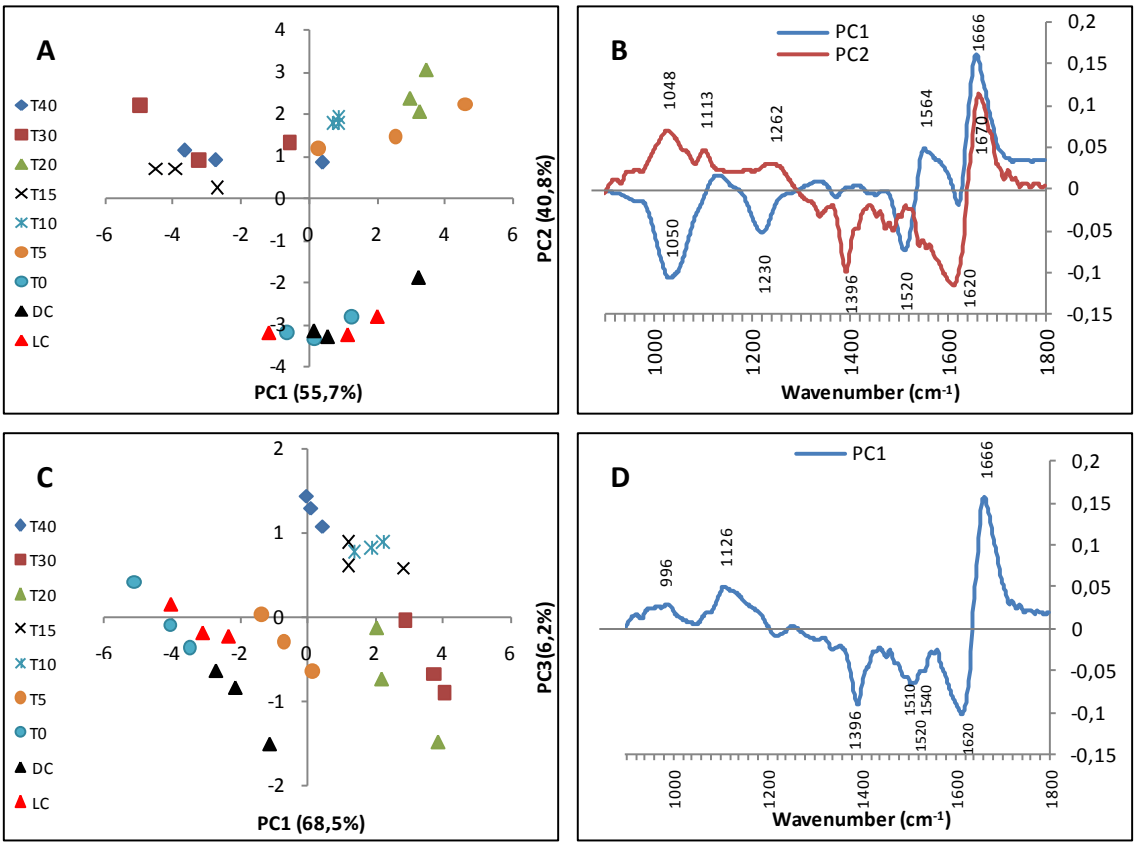


**Figure 6.4** Scores and loading plots for PCA analysis of photosensitized *Staphylococcus warneri* with Tri-$Py^+$-Me-PF (**A**, **B**) and with Tetra-$Py^+$-Me (**C**, **D**) for different irradiation times. Number on the axis labels of scores plot indicate the percentage of the total variation in the data that was explained by the first, second and third principal components (PC1, PC2 and PC3).

In the PCA scores plot of *S. warneri* treated with Tri-$Py^+$-Me-PF (Figure 6.4A), samples irradiated for 15, 30 and 40 min (negative PC1) were separated from controls and other irradiated samples (positive PC1), by the higher intensity of the bands assigned to N-

H bending and C-N stretching in amide II (1520 $cm^{-1}$) (294), C-O bands of the carbohydrates (1050 $cm^{-1}$) (288), and to asymmetric stretching of $PO_2^-$ (1230 $cm^{-1}$) (276, 277) (Figure 6.4B). Controls, T0 and samples irradiated for 5, 10 and 20 min (positive PC1) displayed enhanced intensities of the bands at 1666 $cm^{-1}$ (assigned to anti-parallel β-sheet of amide I) (281), and 1564 $cm^{-1}$ (assigned to amide II band, arising from N-H deformation and -C-N stretching in -CO-NH). (295) However, there was not a clear separation among irradiated samples, as T20 was located in positive PC1 along with controls. On the contrary, the modifications during PDI of *S. warneri* with Tri-$Py^+$-Me-PF were greatly discriminated by PC2 (Figure 6.4B). Negative PC2 clearly separated controls and T0 from irradiated samples (T5 to T40), by the higher intensities of the bands at 1620 $cm^{-1}$ (assigned to C=O stretching vibrations of amides linked to proteins) (296) and 1396 $cm^{-1}$ (assigned to symmetric $CH_3$ bending of the methyl groups of proteins). (297) Positive PC2, where irradiated samples were located, displayed higher intensities of the bands at 1670 $cm^{-1}$ (assigned to anti-parallel β-sheet of amide I of proteins) (281), 1048 $cm^{-1}$ (assigned to glycosylated protein bands) (267), 1113 $cm^{-1}$ (assigned to symmetric stretching of P-O-C of organic phosphates from nucleic acids) (271), and 1262 $cm^{-1}$ (assigned to symmetric stretching vibrations of $PO_2^-$ from nucleic acids). (271)

In the PCA scores plot of *S. warneri* treated with Tetra-$Py^+$-Me (Figure 6.4C), controls, T0 and T5 (negative PC1) were separated from samples irradiated from T10 to T40 (positive PC1). The negative PC1 (Figure 6.4D) shows enhanced intensities of the bands at 1620 $cm^{-1}$ (assigned to C=O stretching vibrations of amides linked to proteins) (296), 1540 $cm^{-1}$ (primarily to N–H bending with contributions from the C–N stretching vibrations of the peptide group) (266), 1510 $cm^{-1}$ (assigned to in-plane C-H bending vibration from the phenyl rings) (272), and 1396 $cm^{-1}$ (assigned to symmetric $CH_3$ bending of the methyl groups of proteins). (297) Samples irradiated from 10 min (positive PC1, Figure 6.4D) displayed increased intensities of the bands at 1666 $cm^{-1}$ (assigned to anti-parallel β-sheet of amide I) (281), 1126 $cm^{-1}$ (DNA and RNA backbones) (298) and 996 $cm^{-1}$ (assigned to C-O from ribose and C-C bonds, from nucleic acids). (271)

From the analysis of the spectra of photosensitized *S. warneri*, in the region between 1800 - 1300 $cm^{-1}$ (Figure 6.5A), comprising the amide region (290), a decreased intensity of the band of treated samples could be seen at 1396 $cm^{-1}$, assigned to symmetric $CH_3$ bending of the methyl groups of proteins (297). Also, in the region between 1300 - 850 $cm^{-1}$ (Figure 6.5B), there was an increase on the absorption shoulder at 1110 $cm^{-1}$ (assigned to C-O and C-C ring stretching from polysaccharides) (281), and the band at 1075 $cm^{-1}$ (assigned to symmetric $PO_2^-$ stretching vibrations of phosphodiesters from nucleic acids) (273) shifted to 1065 $cm^{-1}$.

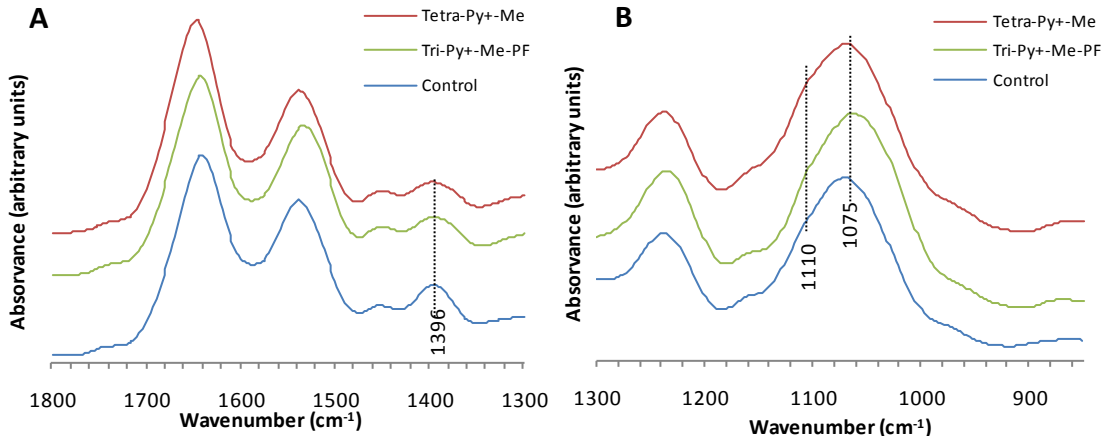


**Figure 6.5** Infrared spectra of control (T0) and photosensitized *Staphylococcus warneri* in the regions of 1800-1300 $cm^{-1}$ (**A**) and 1300-850 $cm^{-1}$ (**B**).

## 6.5 Discussion

The main aim of this study was to use IR spectroscopy to monitor the alterations on *E. coli* and *S. warneri* cellular components induced during photoinactivation with Tri-$Py^{+}$-Me-PF and Tetra-$Py^{+}$-Me.

The results from the principal component analysis (PCA) during photosensitization of *E. coli* with both porphyrins evidenced modifications on different cellular components.

The porphyrin Tri-$Py^{+}$-Me-PF originates, up to 30 min irradiation (revealed by positive PC1), formation of carbonyls (1719 $cm^{-1}$) resulting from lipid oxidation (299), and protein oxidation (1556, 1622 and 1652 $cm^{-1}$). After 60 min of irradiation, the effects in nucleic acids are clear (1040, 1065 and 1226 $cm^{-1}$) and important changes in the structure of proteins (1380, 1451, 1510 $cm^{-1}$) also occur.

With the porphyrin Tetra-$Py^{+}$-Me, although oxidative damage occurs more slowly, notable changes are detected on the various cellular components. Up to 90 min of irradiation (revealed by negative PC1), changes in the nucleic acids are observed (1060 and 1086 $cm^{-1}$). The PC1 separated the samples irradiated for 180 and 270 min from the remaining samples, essentially through the bands ascribed to proteins (1424, 1451, 1526 and 1655 $cm^{-1}$), where changes induced by oxidative stress can be observed (1581 and 1685 $cm^{-1}$). Bands corresponding to alterations on lipids (1736 $cm^{-1}$) and on nucleic acids (1246 $cm^{-1}$) are also detected. The PC2, although has not clearly separated the different samples, contributed with 31.7% to separate the samples irradiated for 30 - 90 min from samples irradiated for 180 - 270 min, showing that the changes in the bands assigned to proteins occur in those earliest times (1384 and 1510 $cm^{-1}$, data not shown).

The bands at 1510 and 1581 $cm^{-1}$ assigned to vibrations from phenyl rings that appear after treatment with both porphyrins, suggest a possible exposure of aromatic amino acids due to changes in the conformation of the native structure of the proteins. Singlet oxygen-mediated damages on proteins generally start at electron-rich side chains of amino acid residues (due to double bonds or sulfur moieties), such as the aromatic amino acids tyrosine and tryptophan. (245) Accordingly, the appearance of these bands can be attributed to oxidative modifications on amino acid side chains. (300, 301) Furthermore, the band at 1685 $cm^{-1}$ (disordered structure non-hydrogen-bonded of amide I) indicates changes in the conformation of proteins. These changes in proteins are corroborated by the results obtained by sodium dodecyl sulfate-polyacrylamide gel electrophoresis (SDS-PAGE) (Chapter 5). Alterations in protein conformation can be associated with stress response regulation mechanisms and repairing strategies (302), as it was already suggested in the discussion of Chapter 5.

The analysis of the spectra in the specific spectral regions has highlighted some molecular changes. The photosensitization resulted in an increased intensity of methyl bands (2960, 2974 and 2853 $cm^{-1}$) from phospholipids. Modifications in the phospholipid composition of *E. coli*, consistent with the observed changes in the band at 1740 $cm^{-1}$ assigned to esters of fatty acids (280), could explain the increase in methyl bands in the irradiated samples. Changes in the phospholipid fatty acid composition of *E. coli* photosensitized with Tri-$Py^{+}$-Me-PF determined by gas chromatography were previously observed (Chapter 3, subchapter 3.4.2).

Alterations in bands related to phosphate groups (increased band at 1238 $cm^{-1}$ and the shift in the band at 1075 $cm^{-1}$), and C-O-C stretching of DNA and RNA, and C-O from ribose (1050 and 986 $cm^{-1}$, respectively) of nucleic acids are indicative of oxidative damage caused by ROS in these molecules. As previously shown, there is degradation of nucleic acids of *E. coli* with both porphyrins over irradiation time, simultaneously to a reduction in the cell survival (Chapter 4, subchapter 4.4.4), which ocurr faster with Tri-$Py^{+}$-Me-PF.

In *S. warneri* photosensitized with both porphyrins, PCA analysis showed essentially changes at protein level but also in nucleic acids and polysaccharides.

With porphyrin Tri-$Py^{+}$-Me-PF, there are fundamental damages in proteins as early as 5 min of treatment represented by the bands at 1396, 1564, 1620 and 1666 $cm^{-1}$. Similarly, after 10 min of irradiation, various changes on proteins are triggered by Tetra-$Py^{+}$-Me (peaks at 1396, 1510, 1540 and 1620 $cm^{-1}$). These modifications include the β-sheet conformation of proteins (1666 to 1540 $cm^{-1}$), resulting from ROS-induced damage on protein native α-helix conformation to an abnormal β-sheet conformation. This conformational modification can expose hydrophobic amino acid residues and promote protein aggregation. (303)

On the other hand, the spectra of irradiated samples in the region 1800 - 1300 $cm^{-1}$ show that with both porphyrins there is a decrease in the band at 1396 $cm^{-1}$ (assigned to symmetric $CH_3$ bending of the methyl groups of proteins) (297), which may account for degradation of *S. warneri* proteins after photosensitization. With increasing irradiation exposure, changes are still observed in the protein content of the bacteria by formation of β-sheets from amide I with Tri-$Py^+$-Me-PF and Tetra-$Py^+$-Me (at 1666 $cm^{-1}$, and 1520 and 1670 $cm^{-1}$, respectively). These results agree with those obtained in Chapter 5 that evidenced the degradation of *S. warneri* proteins in large scale after photosensitization, with appearance of proteins of high molecular weight, presumably associated with the formation of cross-linked complexes.

The peak at 1048 $cm^{-1}$ was assigned to glycosylated proteins. (267) Protein glycosylation is an important post-translational modification that improves the functional diversity of proteins and influences their biological activity. (304) Glycosylation is also important in avoiding incorrect protein folding. (305) These post-translational modifications induced by photosensitization in bacterial proteins suggest a cellular response to injuries caused by ROS. Although not yet described for photosensitized bacteria, post-translational modifications in the response to photodynamic treatment have been reported in human and animal cell lines. (306, 307)

The bands at 1113, 1230, 1262 and 996 $cm^{-1}$ were assigned to phosphates from nucleic acids. The spectrum of irradiated samples in the region 1300 - 850 $cm^{-1}$ displays the shift of the band at 1075 $cm^{-1}$ to 1065 $cm^{-1}$, indicative of nucleic acid degradation. These results agree with those described in Chapter 4, where nucleic acid content was reduced during photosensitization of *S. warneri* simultaneously to cell inactivation.

Furthermore, some bands were displayed in the polysaccharide region (C-O bands between 1165 and 1030 $cm^{-1}$) (288), namely at 1126 $cm^{-1}$ (Figure 6.4D). The increase in the absorption shoulder at 1110 $cm^{-1}$ (Figure 6.5B) was also assigned to C-O and C-C ring stretching from polysaccharides. (281) These polysaccharides may be capsular polysaccharides which are often covalently linked to the peptidoglycan of Gram-positive bacteria. (308) Even though carbohydrates are relatively insensitive to singlet oxygen oxidation, especially when more reactive species such as hydroxyl radicals are present, secondary products and radical species formed from singlet oxygen activity could further react with carbohydrates. (309) In this way, the modifications assigned to polysaccharides only seem to occur after longer exposure to irradiation when major alterations have already occurred.

IR spectroscopy proved to be a fast and reliable tool to demonstrate the profound changes induced by photosensitization. Not only revealed changes in the structure of the

various molecular components of bacterial cells, but also suggested oxidative damages. The results obtained by conventional techniques used to identify biomolecules helped in validating the results from this study.

In the photosensitization conditions used herein, all major cellular biomolecules were affected, evidencing the multi-target nature of this process. (208) However, the greatest changes were observed on the proteins of both Gram-negative and Gram-positive bacteria. These studies also demonstrated that polysaccharides are afected by PDI but in a later stage.

Infrared spectroscopy, supported by complementary approaches such as mass spectrometry-based lipidomics and proteomics analyses, will help to provide further insight into the response mechanism to this type of oxidative stress as well as in optimizing the treatment protocol, by evaluating the effects on specific strains, the efficiency of different photosensitizers, and irradiation conditions.

# Part II

# Chapter 7. Potential applications of porphyrins in photodynamic inactivation beyond the medical scope

# 7 Potential applications of porphyrins in photodynamic inactivation beyond the medical scope

## 7.1 Abstract

Although the discovery of light-activated antimicrobial agents was reported in the 1900s, only more recently research work has been developed towards the use of photodynamic process as an alternative to more conventional methods of inactivation of micro(organisms). The photoprocess causes cell death through irreversible oxidative damage by reactive oxygen species produced by the interaction between a photosensitizing compound and a light source.

With great emphasis on the environmental area, photodynamic inactivation (PDI) has been tested in insect eradication and in water disinfection. Lately, other studies have been carried out concerning its possible use in aquaculture waters or to the control of food-borne pathogens. Other potential applications of PDI in household, industrial and hospital settings have been considered.

In the last decade, scientific research in this area has gained importance due to great developments in the field of materials chemistry but also because of the serious problem of the increasing number of bacterial species resistant to common antibiotics. In fact, the design of antimicrobial surfaces or self-cleaning materials is a very appealing idea from the economic, social and public health standpoints. Thus, PDI of micro(organisms) represents a promising alternative.

In this review, the efforts made in the last decade in the investigation of PDI of (micro)organisms with potential applications beyond the medical field will be discussed, focusing on porphyrins, immobilized or not on solid supports, as photosensitizing agents.

## 7.2 Introduction

Photodynamic therapy refers to the use of a light source (visible light of an appropriate wavelength), an oxidizing agent (molecular oxygen, $O_2$) and an intermediary agent (named photosensitizer, PS) able to absorb and transfer the energy of the light source to molecular oxygen leading to the formation of highly cytotoxic species (singlet oxygen [$^1O_2$], hydrogen peroxide [$H_2O_2$], and/or free radicals, such as superoxide [$O_2^{-\bullet}$] and hydroxyl radical [$HO^\bullet$]), causing a multi-targeted damage and destruction of living tissues. (218, 310) The generation of these reactive oxygen species (ROS) can occur *via* two mechanisms or pathways, known as type I and type II, which require the presence of $O_2$ (Figure 7.1). In the presence of light (**hv**),

the photosensitizer ($^1$**PS**) in the singlet ground state ($S_0$) absorbs a photon, affording the excited singlet state ($^1$**PS**$^*$). Then, it can lose energy by returning to $S_0$ with fluorescence emission (**F**) or, by an intersystem crossing (**ISC**) process, it can be converted in the long-lived triplet state ($T_1$). This excited triplet-state PS ($^3$**PS**$^*$) can decay to ground state by phosphorescence emission (**P**) or can react with a substrate, namely an electron donor molecule. In this case, the formation of radical ions can occur giving rise to radical ions which react with ground state oxygen ($^3$**O$_2$**), originating ROS (type I mechanism). Alternatively, $^3$**PS**$^*$ can transfer energy directly to $^3$**O$_2$** affording the excited singlet state ($^1$**O$_2$**) (type II mechanism). Both photoprocesses may occur simultaneously but type II is, in general, the predominant one. The cytotoxic species can cause irreversible damage to proteins, nucleic acids and lipids. (8, 9)

The advantage of being a process without a specific cell target renders photodynamic inactivation (PDI) effective in the oxidation of different biomolecules with the consequent destruction of several cell types. In fact, this methodology has a broad spectrum of activity and, using the same PS, is able to destroy human cells (310), viruses (311), bacteria (312), molds (313), yeasts (314), protozoa (315), helminths (316) and insects (317).

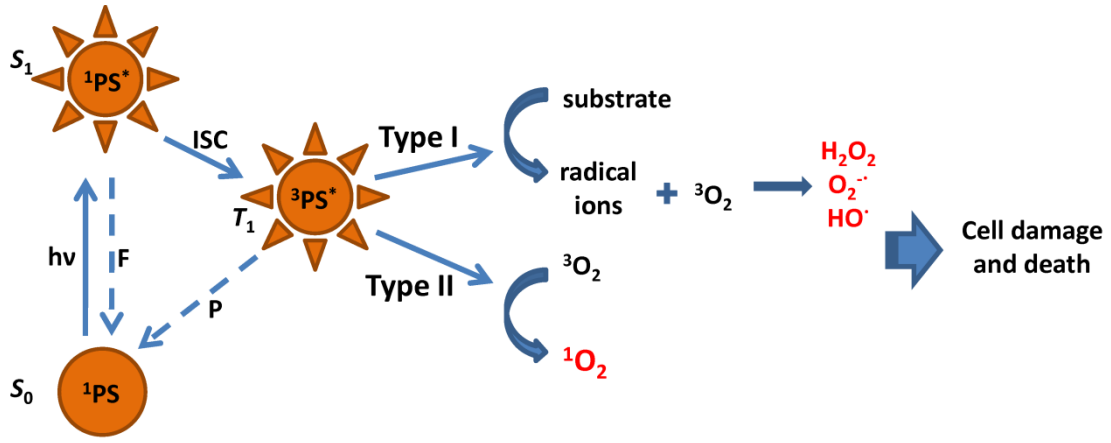


**Figure 7.1** Schematic representation of the photoprocesses that can occur during photodynamic inactivation.

Moreover, the ability to structurally tailor the PS as well as to successfully link it to other molecules, with a high degree of specificity (e.g., antibodies, enzymes, nucleic acids), or to solid supports gives this therapy a multiplicity of clinical and non-clinical applications.

The discovery that positively charged PS could effectively inactivate Gram-negative bacteria without the addition of permeabilizing agents (136, 211) brought a new impetus to the investigation on the PDI of microorganisms as a new therapeutic modality. The difference in susceptibility between the two types of bacteria, Gram-negative and Gram-positive, is explained on the basis of the structural features of their cell wall (Figure 7.2).

Gram-positive bacteria have a cell wall composed of lipoteichoic and teichoic acids organized in multiple layers of peptidoglycan, which confers a degree of porosity to bacteria so as to facilitate the anchoring and entry of PS into the cell. (12, 197) In Gram-negative bacteria, the presence of a complex outer membrane in the cell wall, consisting of phospholipids, lipids, lipopolysaccharides and lipoproteins, creates a permeability barrier to antimicrobial agents. (12, 197) The interaction between the cationic PS and the constituents of the Gram-negative cell wall generates electrostatic interactions that promote destabilization of the native organization of the wall, allowing the binding and eventual entry of the PS molecules into the cell. (12, 197) In the case of fungi, the cell wall contains chitin, glucans and lipoproteins that represent a barrier with intermediate permeability in comparison to Gram-positive and Gram-negative bacteria. (318) With regard to viruses, enveloped viruses are more easily inactivated than non-enveloped ones, but some studies show that non-enveloped viruses can also be efficiently inactivated by the phototoxic action of cationic PS (143), being the efficiency of their inactivation similar to that of Gram-negative bacteria. (77)

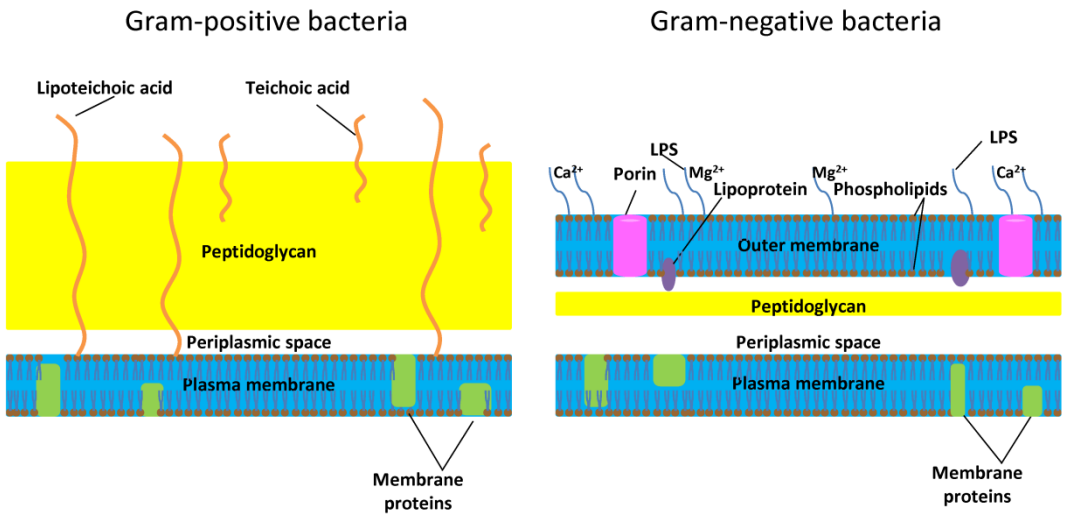


**Figure 7.2** Schematic illustration of the structure of cell wall and plasma membrane of Gram-positive and Gram-negative bacteria.

In recent years, the synthesis of new compounds for PDI has grown dramatically, many of them with very good inactivation results. Several classes of PS, such as phenothiazinium dyes (methylene blue, toluidine blue O), naturally occurring PS (chlorophyllin, psoralens, perylenequinonoid pigments), tetrapyrroles (porphyrins, phthalocyanines, chlorins, bacteriochlorins) and fullerenes have been successfully tested. (10, 30, 319)

The group of porphyrin derivatives has been prominent, not only because it includes the first formulation approved for photodynamic therapy of cancer (320) but also in the perspective of environmental applications, considering that the use of naturally occurring

porphyrins or synthetic related analogues arises as an economical, eco-friendly and human/animal safe option. (321)

Porphyrins are a class of heterocyclic aromatic compounds constituted by four subunits of pyrrole type linked by methynic bridges. The presence of these compounds is ubiquitous in nature as part of vital biochemical processes such as oxygen transport (heme group) and photosynthesis (chlorophylls). (322)

If photodynamic therapy is now an established procedure for the treatment of certain non-oncological and oncological diseases (320, 323, 324), it is still not used for infection treatment. (12, 209) In addition, the potential application of PDI to destroy (micro)organisms goes beyond the medical field, with particular focus on the environmental area. (191, 325-328)

In PDI studies related with non-clinical applications, artificial white light (halogen or xenon lamps) and sunlight have been used in order to achieve organisms' destruction. The light fluence (or fluence rate) can be given in W $m^{-2}$, in lux (lx) or in µE $m^{-2}$ $s^{-1}$ (with E standing for Einsteins in the former terminology, which has been replaced in the new terminology by M, meaning "mole of light"). These light units can be interconverted in the following way: 1 lx ≈ 9.5 x $10^{-3}$ mW $cm^{-2}$ ≈ 1.8 x $10^{-3}$ µM $m^{-2}$ $s^{-1}$. (329) For example, 100 - 150 lx may represent a shady room in natural light, 30,000 - 40,000 lx an overcast summer's day and 100,000 lx a very bright summer's day. (330) Since the experimental conditions described in literature reports are quite different, sometimes the results cannot be directly compared. The same light dose (J $cm^{-2}$) can be achieved by varying the light fluence rate, the irradiation time or both. (10) However, the effectiveness of the results may be different when using a high fluence rate over a short time period or a low fluence rate over a longer time, even though the light dose is the same in each case. (10, 199) In general, the PDI of microorganisms is more extensive when higher light fluence and longer treatment duration are used. (331) Increasing the duration of irradiation will improve the yield of treatment, compensating a low concentration of PS or a less efficient PS type. (332)

Due to its multi-target nature, and therefore low probability of triggering the development of resistance in (micro)organisms (117-119, 134), this therapy has been tested in various research areas as an alternative approach to actual methods to control insect pests, water quality, microbiological food quality; and also in the disinfection and sterilization of materials and surfaces in different contexts (industrial, household and hospital). Furthermore, the use of this form of eradicating microbes or noxious organisms becomes increasingly achievable in practice if one thinks that, for certain purposes, the PS may be immobilized on inhert solid supports allowing their reuse and recycling, making this technology of broad-spectrum activity, economic, sustainable, durable, and environmentally friendly. To this extent,

with the great development of nanotechnology and materials chemistry, several different supports have been created to immobilize a series of PS designed for photoinduced oxygenation reactions. (333)

The aim of this review is to present the efforts made in the last decade in the investigation of PDI of (micro)organisms beyond the medical field, using porphyrins as PS, either free or immobilized in solid supports. All the organisms used on PDI experiments mentioned in this review are listed in Table 7.1. The porphyrinic PS reported in these studies are listed in Table 7.2.

**Table 7.1** List of organisms used in non-clinical photodynamic inactivation experiments

| Organism | Organism type | Reference |
|---|---|---|
| *Acinetobacter baumannii* | Bacterium (Gn) | (334) |
| *Acremonium spp.* | Fungus (mold) | (335) |
| *Acremonium strictum* | Fungus (mold) | (336) |
| *Aedes aegypti* | Mosquito (dengue vector) | (337, 338) |
| *Aedes caspius* | Mosquito | (339) |
| *Aeromonas salmonicida* | Bacterium (Gn) | (141) |
| *Alternaria alternata* | Fungus (mold) | (336) |
| *Alternaria spp.* | Fungus (mold) | (335) |
| *Anopheles arabiensis* | Mosquito (malaria vector) | (340) |
| *Anopheles gambiae* | Mosquito (malaria vector) | (340) |
| *Anopheles sp.* | Mosquito (malaria vector) | (341) |
| *Artemia franciscana* | Crustacea (Branchiopoda) | (342) |
| *Ascaris lumbricoides* | Helminth | (331) |
| *Aspergillus flavus* | Fungus (mold) | (313) |
| *Aspergillus spp.* | Fungus (mold) | (335) |
| *Bacillus cereus* | Bacterium (Gp) | (343-348) |
| *Bactrocera oleae* | Fly (olive fly) | (349) |
| *Baculovirus* | Enveloped DNA virus | (350) |
| *Candida albicans* | Fungus (yeast) | (111, 351, 352) |
| *Ceratitis capitata* | Fly (Mediterranean fluit fly) | (349, 353) |
| *Chaoborus crystallinus* | Insect larvae (Diptera) | (321, 354) |
| *Chaoborus sp.* | Insect larvae (Diptera) | (355) |
| *Colpoda inflata* | Protozoan (Ciliophora) | (342) |
| *Culex pipiens* | Mosquito | (356, 357) |
| *Culex quinquefasciatus* | Mosquito | (337) |
| *Culex sp.* | Mosquito | (355) |
| Cultivable bacteria from aquaculture water | Bacteria | (141) |
| *Daphnia sp., Daphnia magna* | Crustacea (Branchiopoda) | (342, 355) |
| *Edwardsiella ictaluri* | Bacterium (Gn) | (358) |
| *Enterococcus faecalis* | Bacterium (Gp) | (77, 141, 198) |
| *Escherichia coli* | Bacterium (Gn) | (77, 119, 141, 198, 352, 359-377) |

**Table 7.2** List of organisms used in non-clinical photodynamic inactivation experiments *(cont.)*

| | | |
|---|---|---|
| Faecal coliforms | Bacterium (Gn) | (142, 332) |
| Faecal enterococci | Bacterium (Gp) | (142, 332) |
| *Flavobacterium columnare* | Bacterium (Gn) | (358) |
| *Fusarium avenaceum* | Fungus (mold) | (313, 336) |
| *Fusarium culmorum* | Fungus (mold) | (378) |
| *Fusarium poae* | Fungus (mold) | (378) |
| *Fusarium spp.* | Fungus (mold) | (335) |
| *Ichthyophthirius mulftifiliis* | Protozoan | (354, 379) |
| Influenza virus strain X-31, A/Aichi/2/68 (H3N2) | Virus | (380) |
| *Liriomyza bryoniae* | Fly (leafminer fly) | (381) |
| *Listeria monocytogenes* | Bacterium (Gp) | (343, 347, 368, 382-385) |
| *Mucor spp.* | Fungus (mold) | (335) |
| *Musca domestica* | Fly (house fly) | (357) |
| *Mycelia sterilia* | Fungus (mold) | (335) |
| *Mycobacterium smegmatis* | Bacterium (Acid-fast) | (363) |
| *Parasarcophaga argyrostoma* | Fly (flesh fly) | (386) |
| *Penicillium chrysogenum* | Fungus (mold) | (233) |
| *Penicillium spp.* | Fungus (mold) | (335) |
| *Photobacterium damselae subsp. damselae* | Bacterium (Gn) | (141) |
| *Photobacterium damselae subsp. piscicida* | Bacterium (Gn) | (141) |
| *Planktothrix perornata* | Cyanobacterium | (358) |
| *Polyomavirus* | Virus (Non-enveloped DNA virus) | (350) |
| *Pseudomonas aeruginosa* | Bacterium (Gn) | (334, 371) |
| *Pseudomonas sp.* | Bacterium (Gn) | (141) |
| *Rhizopus oryzae* | Fungus (mold) | (313, 336) |
| *Rhizopus spp.* | Fungus (mold) | (335) |
| *Saccharomyces cerevisiae* | Fungus (yeast) | (314) |
| *Salmonella enterica* | Bacterium (Gn) | (384, 387) |
| *Salmonella sp.* | Bacterium (Gn) | (368) |
| *Saprolegnia spp.* | Fungus (mold) | (369) |
| *Selenastrum capricornutum* | Green alga | (358) |
| *Staphylococcus aureus* | Bacterium (Gp) | (141, 334, 358, 361-363, 365-371, 374, 375, 388, 389) |
| *Stomoxis calcitrans* | Fly (house fly) | (390) |
| T4-like phage | Bacteriophage | (134, 143, 198) |
| *Taenia* sp. | Helminth | (331) |
| *Tetrahymena thermophila* | Protozoan (Ciliophora) | (342) |
| *Trichothecium roseum* | Fungus (mold) | (313) |
| *Ulocladium oudemansii* | Fungus (mold) | (314) |
| *Vibrio anguillarum* | Bacterium (Gn) | (141) |
| *Vibrio fischeri* | Bacterium (Gn) | (140) |
| *Vibrio parahaemolyticus* | Bacterium (Gn) | (141) |

Gn, Gram-negative; Gp, Gram-positive

## 7.3 Environmental applications

### 7.3.1 Insect pest elimination

The idea of using PS as photopesticides (or photoinsecticides) is not new. (391, 392) However, the use of porphyrins for this purpose was only mentioned from the late 80s of the last century. (393-396) Since then, the use of natural or synthetic porphyrin derivatives has been increasingly exploited to control and eradicate various types of insects, including pest flies capable of inducing significant damage to agricultural crops, and mosquitoes vectors of pathogens responsible for malaria (*Anopheles*), yellow fever (*Culex*, *Aedes*) dengue fever (*Aedes*) and encephalitis (*Aedes*, *Culex*, *Anopheles*). (337-340, 355-357)

Alternative strategies of pest control are needed, not only to avoid the harmful chemical pesticides, but also because there is, nowadays, a global distribution of these organisms. In the case of *Aedes aegypti*, for example, its sporadic presence has been recognized in mid-latitudes such as in Britain, France, Italy, Spain, Malta, Portugal and other european countries. (397) Very recently, in Madeira island (Autonomous Region of Madeira), Portugal, there was a dengue outbreak starting in October 2012 with 2170 cases of dengue fever notified until early April 2013. In mainland Portugal, 11 cases have been reported and 71 cases in thirteen European countries, all in travelers returning from the island, and none of them lethal. (398) Current updates of first detection or confirmation of the presence of other disease vectors can be found at the European Mosquito Bulletin website. (399)

Typically, experimental designs of laboratory studies, or studies under semi-field conditions, use fly larvae or adult mosquitoes, laboratory-reared or collected in breeding sites, which are brought into contact with solutions containing free-base porphyrins or porphyrin incorporated into baits. An initial period of dark incubation, more or less extended to allow the uptake/ingestion of PS is followed by irradiation with natural or artificial sunlight and determination of the mortality percentage or the median lethal dose ($LD_{50}$, i.e., the dose at which death is produced in 50% of the experimental organisms). Many studies also inspect the amount of porphyrin taken up, the anatomical site where it binds and its clearance.

In the photosensitized insect eradication, PS which are already registered as food additives, such as chlorophylls, chlorophyllins and their copper complexes (400, 401), or phototherapeutic agents as hematoporphyrin IX derivative (HpIX) or 5-aminolevulinic acid (ALA), used as a precursor of protoporphyrin IX (320), have been especially successful. They have a low cost production, lack of mutagenic activity, high efficiency and high level of safety to humans and, in general, to other mammalian species. (320, 402)

HpIX has been tested on *Ceratitis capitata* (Mediterranean fruit fly) and *Bactrocera oleae* (olive fly). (349) A sugar/protein bait containing 8 μM HpIX led to 100% mortality of *C. capitata* and *B. oleae* flies within the first day after 1 h and 2 h of exposure to 2080 μE $s^{-1}$ $m^{-2}$, respectively. However, a milder fluence rate such as 760 μE $s^{-1}$ $m^{-2}$ was also found effective in decreasing the number of surviving flies when the irradiation time was prolonged to 2 h. The lower photosensitivity of *B. oleae flies* was possibly due to the smaller amount of ingested HpIX and/or to its darker pigmentation. HpIX was localized in the cuticle, the midgut, the Malpighian tubes and the adipose tissue of the flies. (349) The same PS was also tested on *Stomoxis calcitrans* (house fly). (390) Flies fed with a concentration range from 4.7 to 7.5 μM of HpIX and irradiated for 1 h at a fluence rate of 1220 μE $s^{-1}$ $m^{-2}$ underwent total mortality after 2 – 3 days. Only at the highest HpIX dose, a significant percentage of dead flies was observed, for the 1 h of light exposure. This insect has a more darkly pigmented body and larger size than *C. capitata* and *B. oleae*. Besides HpIX, other *meso*-substituted porphyrins, with two, three and four positive or negative charges have been used for insect photosensitization. (390, 403) The most efficient porphyrin was 5,10-bis(1-methylpyridinium-4-yl)-15,20-diphenylporphyin, a dicationic amphiphilic porphyrin which at the concentration of 0.85 mM caused 100% mortality on *C. capitata* within 1 h of irradiation at a fluence rate of 1220 μE $s^{-1}$ $m^{-2}$. The photoinsecticidal efficiency of porphyrins seems to increase with the increasing hydrophobicity of the molecule, either by the reduction in the overall number of positive or negative charges or by the replacement of the 1-methylpyridinium moiety with phenyl rings.

The factors that appear to affect the efficiency of insects' photosensitivity by porphyrins have been identified by Ben Amor et al. (349, 390, 403), serving as a starting point for designing new strategies for treatment optimization and specificity increase. Such factors are fluence rate of irradiation, total light dose, porphyrin chemical structure (higher photosensitivity associated with higher degree of hydrophobicity of the PS, particularly obvious with the amphiphilic ones), concentration of porphyrin in the bait, thickness and color of the insect integument, and clearance from the organism in a 24 - 48 h time interval after the porphyrin uptake. (404)

HpIX and three more porphyrin derivatives were used in the PDI of different mosquito larvae under field conditions. A HpIX $LD_{50}$ of 3.2 mg $L^{-1}$ was established for the fourth instar of *C. quinquefasciatus* and this porphyrin was the only effective one on *A. aegypti* larvae. (337)

The strong and fast photo-larvicide activity of HpIX against *C. capitata* immature larval stages has also been reported. (353) The $LD_{50}$ of HpIX in the food, when activated by light (47 photons μmol $s^{-1}$ $m^{-2}$), was 0.173 mM, determined in the period entailed from egg hatching to adult ecdysis. The corresponding HpIX $LD_{50}$ during the dispersal period alone was 0.536 mM.

HpIX elicited a mortality of 90.87%, which was mainly concentrated during prepupal and early pupal stages. Loci in the brain and in the gut were damaged by ROS. (353)

Awad et al. (356) demonstrated the efficiency of HpIX and of a formulation based on HpXI powder, sugar and other additives (HpF), as larvicidal substances on *Culex pipiens* Egyptian field strains, exposed to 3, 9 and 18 h of natural sunrise. A HpIX concentration of 10 µM and 100 µM decreased the larval survival by 94% and 99.3% at the end of 5 days, respectively. On the other hand, concentrations of 1 µM and 10 µM of HpF formulation caused a decrease in larval survival of 92.7% and 99.2%, respectively, after 5 days. It was proposed that a synergistic effect occurred due to the incorporation of sugar and other additives to the HpIX, which could reflect the suitability of using the sugar as HpIX carrier in the commercial formula. (356)

El-Tayeb et al. (386) studied the effect of HpIX on the flesh fly *Parasarcophaga argyrostoma* in adult stage. A concentration of $10^{-2}$ M $L^{-1}$ of HpIX caused a mortality of 83% and 96% of the treated flies after exposure to natural sunlight with a fluence rate of 236.5 and 1935 W $m^{-2}$, respectively. Histological studies showed the high ability of HpIX to accumulate in the insect organs and to cause high extent damage in the alimentary canal tissue. The increase in fluence rate and in irradiation time enhanced fly mortality. So, although the most efficient HpIX concentration to control *P. argyrostoma* was $10^{-2}$ M $L^{-1}$, concentrations of $10^{-3}$ M $L^{-1}$ and $10^{-5}$ M $L^{-1}$ were sufficient to control *Musca domestica* and *Culex pipiens*, respectively. (357) More recently, larvae of the mosquito *Aedes caspius* have been efficiently photoinactivated using $10^{-3}$ M $L^{-1}$ of HpF formulation. The larval mortality has improved by increasing light irradiance and exposure times. (339)

In order to be applied to endemic areas with scarce economic resources, PS must be inexpensive. Some researchers have used natural and modified PS centered on chlorophyll derivatives (chlorophyllin and pheophorbide) and sunlight. *Chaoborus* sp., *Daphnia* sp. and *Culex* sp. larvae were photosensitized with chlorophyllin (15 mg $L^{-1}$), incubated in darkness overnight and were then irradiated for 3 – 4 h with artificial sunlight (PAR: 149.66 W $m^{-2}$, UV-A 32.67 W $m^{-2}$, and UV-V 0.77 W $m^{-2}$). After incubation, chlorophyllin eliminated the different organisms at remarkably low concentrations. The $LD_{50}$ value in *Culex* sp. larvae was about 6.88 mg $L^{-1}$, in *Chaoborus* sp. larvae of about 24.18 mg $L^{-1}$, and in *Daphnia* 0.55 mg $L^{-1}$. It was found that during the puparium, mosquito larvae are relatively insensitive to chlorophyllin treatment and, during metamorphosis, the chrysalid is encapsulated and totally stops food uptake. Probably because of that, the accumulation of chlorophyllin inside the organism is limited and the photodynamic effect is reduced. As well as in other studies, some dark toxicity has also been observed. Other small animals, like *Daphnia* and fish (*Chaoborus*) larvae are also affected

by chlorophyllin. (355) On the other hand, unlike fish larvae, more mature fish are unharmed and survive chlorophyllin treatment at concentrations, where, for example, *Culex* larvae are severely affected. This has been shown in field tests in Nigeria in which chlorophyllin was used on *Anopheles* larvae and successfully destroyed the mosquito larvae in a treated pond, without harming any of the other aquatic organisms. (341) Moreover, in addition to the inactivation of mosquito larvae, Wohllebe et al. (354) demonstrated for the first time that the photodynamic treatment of *C. crystallinus* larvae with 24 mg $L^{-1}$ of chlorophyllin solution gives a $LC_{50}$ with 0.26 MJ (PAR + UV-A + UV-B) and induces necrosis and apoptosis in these organisms. Chlorophyllin was orally uptaken and accumulated in the intestine (a dose of 3.2 mg $L^{-1}$ chlorophyllin with 3 h irradiation induced apoptosis in the intestinal cells). (354)

Besides chlorophyllin, magnesium chlorophyllin, zinc chlorophyll and copper chlorophyll have been tested on *C. crystallinus* larvae. (321) After 6 h of dark incubation and 3 h of light exposure (360 W $m^{-2}$), the $LD_{50}$ value of magnesium chlorophyllin was about 22.25 mg $L^{-1}$ and for zinc chlorophyll 17.53 mg $L^{-1}$. Copper chlorophyll ($LD_{50}$ 0.1 mg $L^{-1}$) was shown to be toxic also without light. Chlorophyllin ($LD_{50}$ 14.88 mg $L^{-1}$) was lyophilized immediately after extraction, and its photodynamic efficiency remained constant over a 30-day period, representing an increase in photodynamic efficiency of 50% compared to magnesium chlorophyllin isolated with standard methods (no lyophilization) and 18% compared to zinc chlorophyllin. The results showed that about 30 W $m^{-2}$ of solar radiation, which is less than 10% of full sunlight is, was sufficient to induce lethal photodynamic effects in larvae (around 30% of the mosquito larvae). Depending on the attenuation in a water body, photodynamic action can also take place below the water surface. Temperature has also been shown to influence the active chlorophyllin uptake by the larvae. (321)

As well as HpIX and chlorophyllin, the Hp derivative dimethyl ether (HPde) has also been shown to be a high potential photopesticide against the larvae of the leafminer fly *Liriomyza bryoniae*. (381) The insects exposed to a sugar bait containing 25 mM of HPde and irradiated for 30 min with broad spectrum visible light at a fluence rate of 30 mW $cm^{-2}$ (54 J $cm^{-2}$ light dose), died (100% mortality) 1 day after irradiation (in the case of the females) and 4 days after the irradiation (in the case of the males). The observed differences in the mortality kinetics between female and male flies were possibly due to the body size and biological activity of females. (381) The treatment efficiency strong also strongly depended on the type of PS used, explaining the different attractiveness of the insects for the bait according to the specificity of the PS contained in it. (381) In line with this need, different baits containing porphyrin to inactivate disease-transmitting vectors, have recently been designed and tested.

Lucantoni et al. (338) prepared a formulation constituted by 5-(1-decilpyridinium-4-yl)-10,15,20-tris(1-methylpyridinium-4-yl)porphyrin ($C_{14}$ porphyrin) and powdered food pellet (PFP). First, the $LC_{50}$ of $C_{14}$ porphyrin in solution was tested on photosensitized 3$^{rd}$ – early 4$^{th}$ instar *A. aegypti* larvae. $LC_{50}$ values of 0.1 µM (0.15 mg $L^{-1}$) and 0.5 µM (0.77 mg $L^{-1}$) were obtained after irradiation intervals of 12 h and 1 h, with 4.0 mW $cm^{-2}$ artificial white light, respectively. $C_{14}$ porphyrin was shown to be active after ingestion by the larvae and caused irreversible lethal damage to their intestinal tissues (midgut and caecal epithelia). The porphyrin carrier formulation (25 mg of PFP in 500 mL of 50 µM $C_{14}$ porphyrin) and a 5 µM of $C_{14}$ porphyrin solution were both 100% effective up to two weeks, and the amount of $C_{14}$ porphyrin required to prepare the C14PF-50 was 10 times smaller than the $C_{14}$ porphyrin required to treat the incubation medium. In the same direction, Fabris et al. (340) associated 5-(1-dodecilpyridinium-4-yl)-10,15,20-tris(1-methylpyridinium-4-yl)porphyrin ($C_{12}$ porphyrin) with two distinct carriers: a model of a pharmaceutical oral vehicle (Eudragit® S100, EU) and a model of foodstuff carrier (cat food pellet Friskies®, CF). These phorphyrin-carrier formulates (50 µM $C_{12}$ porphyrin dose) were tested against overnight fed *Anopheles gambiae* and *Anopheles arabiensis* larvae, exposed to sunlight (30 - 110 mW $cm^{-2}$) for 0.5 - 3 h. These conditions led to high photoinactivation efficiency against laboratory reared *A. gambiae* and *A. arabiensis* larvae (almost complete mortality). On wild (field-collected) larvae, the formulation EU-$C_{12}$ caused 100% mortality on *A. gambiae* M and S forms but CF-$C_{12}$ showed variable results depending on the site where the larvae were collected. Not only the association of the PS with suitable carriers promoted a fast and selective internalization of formulates by the *Anopheles* larvae which guaranteed their death upon subsequent sunlight exposure, but also the nature of the carrier affected the overall efficacy of the porphyrin formulates. This was shown by the administration of a 1:1 mixture of CF-$C_{12}$ and laboratory food for larvae (TetraMin®) inducing an extensive mortality of both laboratory reared and wild *Anopheles* larvae. These results indicated the primary importance of palatability in the design of oral larvicide formulations. (340)

According to Lucantoni et al. (338), an insoluble baited insecticidal formulate should be: actively consumed by the larvae; an efficient and cost-effective employment of the PS; suitable for application in household water storages for drinking and other domestic purposes; unlikely to affect the organoleptic properties of the stored water; selected or manipulated on different porphyrin carriers in a way to standardize the particle dimension to a size range that is especially palatable for mosquito larvae (e.g., 5 – 50 µm), thus reducing the risks of uptake by non-target organisms.

**Table 7.2** List of porphyrinic derivatives used in non-clinical photodynamic inactivation experiments

| Porphyrin | Immobilized (Reference) |
|---|---|
| 5-(1-decilpyridinium-4-yl)-10,15,20-tris(1-methylpyridinium-4-yl)porphyrin | No (338) |
| 5-(1-dodecilpyridinium-4-yl)-10,15,20-tris(1-methylpyridinium-4-yl)porphyrin | No (340, 342, 358) |
| 5-(4-Aminophenyl)-10,15, 20-tris(1-methylpyridinium-4-yl)porphyrin | On filter paper (370) |
| 5-(4-aminophenyl)-10,15,20-trisarylporphyrin where aryl group can be neutral, anionic or cationic | On cotton fabric (374, 389) |
| 5-(4-carboxyphenyl)-10,15,20-tris(4-methylphenyl)porphyrin | On polysilsesquioxane plastic films (351) |
| 5-(4-ethynyloxiphenyl)-10,15,20-tris(4-methylphenyl)porphyrin | On cotton fabric (375) |
| 5-(4-ethynylphenyl)-10,15,20-tris(1-methylpyridinium-4-yl)porphyrinatozinc(II) tri-iodide | On azide-modified cellulose nanocrystals (334, 363) |
| 5-(4-methoxycarbonylphenyl)-10,15,20-tris(1-methylpyridinium-4-yl)porphyrin tri-iodide | No (359)<br>No (142) |
| 5-(pentafluorophenyl)-10,15,20-tris(1-methylpyridinium-4-yl)porphyrin tri-iodide | No (140-142, 359) and on silica coated $Fe_3O_4$ nanoparticles (198) |
| 5,10,15,20-tetrakis(1-decilpyridinium-4-yl)porphyrin | No (369) |
| 5,10,15,20-tetrakis(1-dodecilpyridinium-4-yl)porphyrin tetrabromide | No (233) |
| 5,10,15,20-tetrakis(1-methylpyridinium-4-yl)porphyrin (Tetra-$Py^+$-Me) | No (233, 331, 332, 359, 362, 369); entrapped into microporous silica gels (376) and into three alkylene-bridged polysilsesquioxanes (377) |
| 5,10,15,20-tetrakis(1-pentylpyridinium-4-yl)porphyrin tetra-iodide | No (233) |
| 5,10,15,20-tetrakis(4-(*N,N*-diphenyl)aminophenyl)porphyrin and Pd(II) complex (PdP) | On optically transparent indium tin oxide electrodes (352) |
| 5,10,15,20-tetrakis(4-aminophenyl)porphyrin | On chitosan membranes (360) |
| 5,10,15,20-tetrakis(4-hydroxyphenyl)-porphyrin | On chitosan membranes (360) |
| 5,10,15,20-tetrakis[2,3,5,6-tetrafluoro-4-(1-methylpyridinium-4-ylsulfanyl)phenyl]porphyrin tetra-iodide | No (233) |
| 5,10,15,20-tetrakis[2,3,5,6-tetrafluoro-4-(4-pyridylsulfanyl)phenyl]porphyrin | No (233) |
| 5,10,15,20-tetraphenylporphyrin | In hydrophilic polycaprolactone and polyurethane (TecophilicH) nanofibers (350); on electrospun polymeric nanofiber materials polyurethane Larithane™, polystyrene, polycaprolactone, and polyamide 6 (364); and into three alkylene-bridged polysilsesquioxanes (377) |
| 5,10,15-tris(4-methylphenyl)-20-(4-pyridyl)porphyrin | On chloroacetyl cellulose ester chlorides (366) |
| 5-[4-(10-carboxydecanoxy)phenyl]-10,15,20-tri(4-methylphenyl)porphyrin | On cellulose laurate esters plastic films (367) |
| 5-aminolevulinic acid, a precursor of Protoporphyrin IX | No (335, 343, 381, 382, 384) |
| Hematoporphyrin dimethyl ether | No (313, 314, 336, 381) |
| Pd(II) complex of 5,10,15,20-tetrakis(4-carboxyphenyl)porphyrin | On a polyurethane matrix (371) |
| Protoporphyrin IX | No (378); on acid-functionalized multi-walled carbon nanotubes (380, 388); on cellulose laurate esters plastic films (365); and on nylon fibers (361) |

**Table 7.2** List of porphyrinic derivatives used in non-clinical photodynamic inactivation experiments *(cont.)*

| | |
|---|---|
| Sodium chlorophyllin | No (346-348, 383-385) and on chitosan (387) |
| Sodium copper chlorophyllin (E-141) | On gelatin films and coatings (368) |
| Sodium magnesium chlorophyllin (E-140) | On gelatin films and coatings (368) |
| Zinc(II) complex of protoporphyrin IX | On nylon fibers (361) |

### 7.3.2 Water disinfection

The PDI of microorganisms in the context of water treatment goes back to the 1970s. (231) Even before it has been recognized as a potential therapeutic modality for microbial infections, the usage of PDI in disinfection and sterilization was already conceived. However, the use of porphyrin derivatives as PS for the purpose of treating water through the photodynamic process was only mentioned in scientific literature in the year 2000.

The possibility of treating wastewater for reuse in agriculture (crop irrigation) was mentioned in the research by Alouini and Jemli. (331, 332) Accordingly, the authors demonstrated the efficient PDI of helminth eggs by the tetracationic 5,10,15,20-tetrakis(1-methylpyridinium-4-yl)porphyrin (Tetra-$Py^+$-Me) under visible light illumination, in clear water and in secondary treated wastewater. In addition to different concentrations of PS and light intensities, the influence of turbidity (content of suspended solids), agitation (aeration), concentration of dissolved oxygen and the ultrastructural changes of two types of eggs of parasites was also investigated. Suspensions of *Ascaris lumbricoides* and *Taenia spp*. were irradiated with artificial white light (0 - 0.5 W $cm^{-2}$) with Tetra-$Py^+$-Me (5 - 30 µM) for 15 min in clear water and 30 min in wastewater. There was a destruction of around 28% of *Ascaris* eggs with 0.33 W $cm^{-2}$ and 10 µM of Tetra-$Py^+$-Me, after 15 min in clear water, and after 30 min in wastewater. The increase in the light fluence to 0.5 W $cm^{-2}$ caused 47% of destruction of *Ascaris* eggs in wastewater after 30 min of irradiation. This increase turned negligible the difference in the sensitivity of *Ascaris* eggs in clear and wastewater. An increase in the oxygenation of the wastewater and in the agitation process improved the photosensitivity of *Taenia* eggs. In fact, these effects were more evident when the concentration of PS was also increased. The process was optimized under the following conditions: dissolved oxygen was maintained at 7 mg $L^{-1}$, the Tetra-$Py^+$-Me concentration at 30 µM and the egg suspension was mixed at 300 rpm. The efficiency of the photoprocess was mainly controlled by the Tetra-$Py^+$-Me concentration, the irradiation time and the light intensity. Also, the dissolved oxygen concentration, water quality and the type of eggs can influence the sensitivity of helminth eggs to photosensitization. *Ascaris* eggs were found to be more sensitive to photosensitization than

*Taenia* eggs. The same authors also used Tetra-$Py^{+}$-Me in several concentration (1.0 μM, 5.0 μM e 10.0 μM) and sunlight irradiation (1235 mW $cm^{-2}$) up to 240 min to inactivate fecal coliforms and fecal streptococci on secondary wastewater samples. After 60 min, at 5.0 μM and 10.0 μM, a decrease of 2.94 and 2.4 logs in fecal bacteria counts was observed, respectively. After 240 min, a total cell survival reduction (> 4.0 log units) was achieved with both concentrations. The 5.0 μM concentration was considered to be more suitable to reduce fecal coliforms in wastewater since it allows obtaining a good treatment yield and it is more economic. (332) The suspended solids (turbidity) were the most influential solution parameter on the efficiency of the photochemical process. Turbidity reduces light penetration, which reduces the PS excitation and the absorption by the helminth eggs. (331) The decrease in log counts of fecal coliforms was ≈ 1.0 after 1 h of phototreatment by 5 μM Tetra-$Py^{+}$-Me when suspended solids reached 50 mg $L^{-1}$. (332)

Albeit these results were promising, the practical application of photodynamic treatment to disinfect microbiologically polluted waters depends on many factors: the removal of the PS after photodynamic treatment to avoid the release of PS to the environment; the use of photo-stable PS (i.e., PS which do not degradate under irradiation); the impact of this procedure on the structure of the natural non-pathogenic microbial communities; the toxicity of the PS to aquatic organisms at doses which induce marked mortality on microbial pathogens; the effect of physical and chemical properties of environmental waters; and the possibility of using sunlight as light source. (325, 328)

In a pioneering work, Bonnett et al. (360) incorporated *meso*-tetraarylporphyrins with amino and hydroxy substituents and also a tetra sulfonated zinc phthalocyanine ($ZnPcS_4$) into chitosan membranes for the specific purpose of water disinfection. Model reactors for a large-scale water-flow system were designed: a static photoreactor system with 7 mL of bacterial suspension (3500 cells $mL^{-1}$) and a circulating water photoreactor system with 455 mL of bacterial suspension ($10^5$ CFU - colony forming units- per mL), representing the significant levels of water contamination. After 30 min of irradiation with white light, the chitosan membrane containing the 5,10,15,20-tetrakis(4-aminophenyl)porphyrin (p-TAPP) caused a reduction to 1300 CFU $mL^{-1}$. However, the membrane prepared with $ZnPcS_4$, was much more effective and was able to completely inactivate the bacteria after 30 min. When the more efficient membrane was stored in the dark for nine months, the photodynamic action was still detectable demonstrating its thermodynamic stability. With that model system, the photoinactivation with immobilized PS can be used to lower microbial levels in water flow systems. (360)

Since 2004, our research group has developed a broad-spectrum of PS, namely cationic porphyrins, which can efficiently inactivate bacteria (77, 359), bacterial endospores (144), viruses (143, 199, 405) and fungi. (233) One of the most effective compounds, a tricationic porphyrin with a pentafluorophenyl group (Tri-$Py^+$-Me-PF), has been tested on bacteria and viruses to check the viability recovery and resistance development after repeated incomplete photoinactivation cycles. The bacteria and viruses that were inactivated to the detection limit with Tri-$Py^+$-Me-PF did not recover viability after one week and the resistance is not enhanced after ten sub-lethal photosensitization treatments. (119, 134) At the initial stage of our work, porphyrins were used to photoinactivate faecal coliforms and faecal enterococci in wastewater samples from a secondary-treated sewage plant. (142) Two of the cationic porphyrins used (Tri-$Py^+$-Me-PF and Tetra-$Py^+$-Me) inactivated 94 – 99.8% of the faecal coliforms at 5 μM upon white light at low light fluence (4 mW $cm^{-2}$) after 270 min of irradiation, demonstrating high efficiency. In this study, two rapid monitoring methods were used to oversee the bacterial photoinactivation: galactosidase activity as an indicator of the presence of faecal coliforms and leucine incorporation as an indicator of bacterial activity. The advantages of using these methods are their easier and faster performance against the determination of CFU, giving an excellent relation with faecal indicators abundance. (142) From these first studies, the experimental conditions were standardized for testing the antimicrobial photoinactivation *in vitro* of our porphyrins in further studies: cell cultures ranged from $10^7$ - $10^8$ CFU $mL^{-1}$, porphyrin concentrations ranged from 0.5 to 5.0 μM, white light irradiation had an irradiance of 4 mW $cm^{-2}$ and the maximum exposure time was 270 min (64.8 J $cm^{-2}$). The incubation time of the organisms with the porphyrins was 10 min in the dark, previously to irradiation, in accordance with the literature. (197) Specific conditions beyond these will be described on the text.

Later, seven synthetic cationic *meso*-substituted porphyrins with one to four charges were tested on *Enterococcus faecalis* and *Escherichia coli* ($10^7$ CFU $mL^{-1}$). The results showed that the tri- (Tri-$Py^+$-Me-PF and Tri-$Py^+$-Me-$CO_2$Me) and the tetra-cationic PS (Tetra-$Py^+$-Me) at 5.0 μM were the most efficient ones, reducing *E. coli* survival by 7 log CFU $mL^{-1}$ after 90 min with Tri-$Py^+$-Me-PF and Tri-$Py^+$-Me-$CO_2$Me and after 270 min with Tetra-$Py^+$-Me. (77) The complete photoinactivation of bacteria with low light intensity (4 mW $cm^{-2}$) suggests that PDI of fecal bacteria can be a possibility for wastewater disinfection under natural light conditions.

It was also reported the photoinactivation of a recombinant bioluminescent *E. coli* strain whose light emission decreased more than 4 log with the three porphyrins used (Tetra-$Py^+$-Me, Tri-$Py^+$-Me-PF and Tri-$Py^+$-Me-$CO_2$Me). These results were achieved both with artificial white light (4.0 mW $cm^{-2}$, 64.8 J $cm^{-2}$) and with sunlight (≈ 62 mW $cm^{-2}$, 1004.4 J $cm^{-2}$) after 90

to 270 min with 5.0 µM of PS but Tri-$Py^{+}$-Me-PF was the most efficient compound. (359) The same series of cationic porphyrins were also tested on bacteriophages isolated from wastewater, using white light and 5.0 µM of porphyrin. (143) Again, the tetra- and tricationic derivatives inactivated the T4-like phage to the limits of detection (reduction of ≈ 7 log).

As nanotechnology emerges as an opportunity for water treatment purposes (406-409), new materials based on magnetic nanoparticles with diferent porphyrins covalently immobilized have been recently developed, in order to be easily removed from the water matrix, for subsequent reuse. (198, 410) Three different hybrids have been prepared and tested in microcosm conditions, being the multi-charged nanomagnet hybrid based on Tri-$Py^{+}$-Me-PF quite effective against Gram-positive and Gram-negative faecal bacteria (5 log decrease for *E. faecalis* and *E. coli* at 20 µM of PS) when using white light irradiation (64.8 J $cm^{-2}$). This hybrid also presented antiviral activity, inactivating the T4-like bacteriophage to the detection limit (≈ 7 log of inactivation). (198)

In order to use this approach in operative field conditions, the multi-charged nanomagent-Tri-$Py^{+}$-Me-PF hybrid has been recently tested. Preliminary results showed that this hybrid was effective in *Vibrio fischeri* photoinactivation for at least 6 cycles, causing a cumulative bacterial reduction higher than 37 log under low light irradiance (4.0 mW $cm^{-2}$) (described in Chapter 10).

Another example of recovery and reuse of immobilized porphyrin used protoporphyrin IX (PPIX) attached to acid-functionalized multi-walled carbon nanotubes (NT-PPIX) as potent antiviral agents to be used on surface disinfection as a coating or in water treatment. (380) Influenza virus strain X-31, A/Aichi/2/68 (H3N2) was irradiated with visible light and 1 mg $mL^{-1}$ of NT-PPIX up to 90 min. This treatment caused more than a 250-fold reduction in the effective infectious viral dose after a 30 min exposure to light. The percentage of cells that could be infected by 200 ng of virus was only about 1%. A pre-exposure of NT-PPIX for 90 min showed a partial loss of photoactivity, but its effect on the virus was still equivalent to a reduction in the infectious viral dose by almost 50-fold. Reusability studies of NT-PPIX showed to be dependent on photobleaching of the porphyrin moiety and on the yield of recovery of NT-PPIX after each use. Besides being effective bactericidal agents as previously proved on *Staphylococcus aureus* (388), these conjugates may be applied as reusable antivirals in wastewater treatment, as they can be easily recovered without leaving any toxic by-products. (380)

Although there is a tremendous need for scientific knowledge on disinfection of hospital wastewater, there is only one report, from our group, on the use of photodynamic treatment on this type of effluent. The efficiency of photoinactivation on four multi-drug resistant isolated strains of *E. coli*, *Pseudomonas aeruginosa*, *S. aureus* and *Acinetobacter*

*baumannii* was evaluated in buffered solution and in hospital wastewater, using 5.0 μM of Tetra-$Py^+$-Me and white light (64.8 J $cm^{-2}$). (411) The results showed an efficient inactivation of multidrug-resistant (MDR) bacteria in buffered solution (reduction of 6 - 8 log CFU $mL^{-1}$) and in the wastewater, in which the photoinactivation of the four bacteria was also effective and the decrease in bacterial number occurred even sooner. This dissimilarity was assigned to dissolved compounds in the hospital wastewater, such as antibiotics.

### 7.3.3 Water disinfection in aquaculture

Aquaculture activity is increasing worldwide, motivated by the progressive reduction of natural fish stocks. This activity suffers, however, substantial financial losses resulting from fish infections by pathogenic microorganisms, including MDR strains. As a consequence, strategies to control fish pathogens are needed and PDI can be an option to treat diseases and to prevent the development of antibiotic resistance by pathogenic bacteria.

The photodynamic disinfection of water from fish farms as well as the prevention and treatment of localized fungal infections (saprolegniosis) in fish, with porphyrins as photosensitizing agents, was presented in 2006, demonstrating the inactivation *in vitro* of pathogenic fungi and bacteria, and the photo-treatment of spontaneously or artificially infected fish in a pilot aquaculture pond. (369) The PS chosen were Tetra-$Py^+$-Me and $C_{14}$ porphyrin (0.05 to 10 μM). The treatment of infected rainbow trout (*Oncorhynchus mykiss*) consisted in two protocols: preventive and curative. In the preventive protocol, artificially infected fish in 1000 L capacity tanks were dark incubated for 10 min with 0.2 μM of $C_{14}$ porphyrin and were not irradiated or were incubated for 10 min with 0.44 μM of Tetra-$Py^+$-Me and irradiated for 1 h with white light (50 mW $cm^{-2}$). The incubation and irradiation treatment was repeated daily, for ten consecutive days, starting from the first day after the infection. In the curative protocol, infected fish were dark incubated with 0.44 μM Tetra-$Py^+$-Me for 10 min in an 80 L pool, irradiated for 1 h and moved to a 1000 L tank (treatment repeated daily for six consecutive days); or dark incubated with 0.4 μM of $C_{14}$ porphyrin for 24 h in a 150 L tank, not irradiated and then moved to a 1000 L tank. (369)

Experiments with *Saprolegnia* (≈ $10^8$ zoospores $mL^{-1}$), indicated that $C_{14}$ porphyrin caused a decrease of the survival of the fungal cells survival by about 6 logs, after phototreatment with 10 μM. (369) The preventive protocol determined a reduction of the infected percentage to 10% and 13%, respectively, after one week, with irradiated Tetra-$Py^+$-Me and unirradiated $C_{14}$ porphyrin, respectively. After two weeks, all the infected individuals from all the experimental groups recovered from the infection. With the curative protocol, a

complete remission of the infection was induced within one week, followed by the complete healing of the ulcerated lesion. Gradual photobleaching of both porphyrins was observed but photodegradation products were not toxic. (369)

Studies carried out in our laboratory indicated that nine bacterial species (*Vibrio anguillarum*, *V. parahaemolyticus*, *Photobacterium damselae subsp. damselae*, *P. damselae subsp. piscicida*, *Aeromonas salmonicida*, *E. coli*, *Pseudomonas sp.*, *S. aureus* and *E. faecalis*) isolated from fish-farming plant water are effectively inactivated (up to 7 log) with the tricationic porphyrin Tri-Py$^{+}$-Me-PF at 5.0 μM, under a low light intensity (4.0 mW cm$^{-2}$). (141) The cultivable fraction of the heterotrophic bacteria of the same aquaculture plant, including pathogenic and non-pathogenic bacteria, was also inactivated by PDI, but the efficiency of the inactivation varied during the sampling period. The seasonal variation of photoinactivation efficiency can be due to differences in bacterial community structure but also due to variations of the water physico-chemical properties. The results clearly show that it is more difficult to photoinactivate the complex natural bacterial communities of aquaculture waters than pure cultures of bacteria isolated from these waters. (141) As PDI is not selective for pathogenic microorganisms, the non-pathogenic microbial community of aquaculture waters can also be affected. As non-pathogenic bacteria have an important ecological role in the biogeochemical cycles in aquaculture waters, namely in semi-intensive systems, a careful evaluation of the environmental impact must be conducted before PDI implementation in these systems. Preliminary results from our group showed that not all bacterial populations are affected by PDI. In aquaculture water treated with Tri-Py$^{+}$-Me-PF and exposed to light, a reduction on the number of bacterial genotypes relatively to the non-treated water samples has been observed, indicating that dominant bacterial populations were affected by PDI. However, bacterial population is also affected by simple light exposure. (141)

The effect of physico-chemical properties of aquaculture waters on PDI efficiency has also been evaluated. (140) The PDI assays were designed having into account the annual variability of pH (6.5 - 7.5), temperature (13 - 22 °C), salinity (10 - 35 g L$^{-1}$) and oxygen concentration (2 - 6 mg L$^{-1}$) values in the fish farms where the water was collected. To monitor the PDI kinetics, the bioluminescence of *V. fischeri* was measured. The variations in pH, temperature, salinity and $O_2$ did not significantly affect the PDI of *V. fischeri* (≈ 7 log reduction in all conditions) with 5.0 μM of Tri-Py$^{+}$-Me-PF under white light (4.0 mW cm$^{-2}$). The suspended solids in the aquaculture water reduced the efficiency of PDI in relation to clear aqueous solutions (buffered solution). On the other side, a good response was obtained in aquaculture water by increasing the porphyrin concentration to 20 μM. The kinetics of the photoinactivation of *V. fischeri* in aquaculture water using two different light sources (artificial

white light and solar light) was also tested. The inactivation of *V. fischeri* under solar light (40 mW $cm^{-2}$) was compared to that obtained with artificial white light, using the same total light dose. The results obtained with 20 μM of porphyrin showed that, using the same total light dose (64.8 J $cm^{-2}$), both light sources inactivate *V. fischeri* to the detection limit. As it is intended that this technology will be used in real aquaculture context, using solar irradiation as light source is expected to make this water disinfection approach economically sustainable in terms of energy demand. (140)

To overcome the enteric septicemia of catfish, columnaris disease and the presence of odor-producing cyanobacteria in ponds of catfish (*Ictalurus punctatus*) production, the antibacterial and algicidal activity of $C_{12}$ porphyrin has been evaluated on the fish pathogens *Edwardsiella ictaluri* and *Flavobacterium columnare* and on *S. aureus* for comparison. (358) The same PS was also used on the odor-producing planktonic cyanobacterium *Planktothrix perornata* and on a representative green alga *Selenastrum capricornutum*. $C_{12}$ porphyrin was used in concentrations ranging from 0.01 to 1000 μM and the samples were irradiated with fluorescent lamps at a photon flux density of 16 - 30 μE $m^{-2}$ $s^{-1}$. Minimal inhibitory concentrations were obtained as follows: 9.8 mg $L^{-1}$ for *E. ictaluri*, 0.5 - 1.0 mg $L^{-1}$ for *F. columnare* and 0.1 mg $L^{-1}$ for *S. aureus*. The growth inhibition after 96 h irradiation with 0.07 mg $L^{-1}$ and 0.2 mg $L^{-1}$ of $C_{12}$ porphyrin, inhibited 50% of both *P. perornata* and *S. capricornutum*, respectively (total inhibition was observed at 1.0 mg $L^{-1}$ in both cases). While *in vivo* tests or other toxicity test were not reported, the preliminary findings showed the broad spectrum activity of $C_{12}$ porphyrin and suggested applications include sanitizing empty tanks before restocking and treatment of other aquaculture systems dealing with similar disease outbreaks. (358)

$C_{12}$ porphyrin, already mentioned as an effective photoactivated antimicrobial agent for aquaculture (358) and disease-transmitting insect vectors (340), has also been tested on the protozoan Ciliophora *Colpoda inflata* and *Tetrahymena thermophile* and on the Crustacea Branchiopoda *Artemia franciscana* and *Daphnia magna*, which are used in routine toxicity assessment in freshwater ecosystems. (342) Following incubation with PS for 60 min (0.1 – 10 μM range) the organisms were irradiated with visible light (10 mW $cm^{-2}$) for 60 min as well. $C_{12}$ porphyrin caused a growth inhibition ≥ 90% against *C. inflata* cysts or trophozoites with 0.3 - 0.6 μM, 3 h after irradiation was ended. In turn, *T. thermophila* vegetative cells required 3 μM for a 50% inhibition of growth, 46 h after irradiation. The complete inactivation of *D. magna* was achieved with 0.6 μM of $C_{12}$ porphyrin while in *A. franciscana* photosensitivity was not detected up to 10 μM. Fluorescence microscopy analyses clearly revealed a damaged morphology induced on cysts of *C. inflata* by 1 μM of PS and on trophozoites of *C. inflata* by

0.6 μM. *T. termophila* also revealed damage with 6 μM of $C_{12}$ porphyrin. *D. magna* accumulated the PS in the digestive tract and exoskeleton and *A. fransciscana* revealed accumulation especially on the exoskeleton. The resistance of *A. franciscana* to the phototreatment was explained by the very low amount of the ingested PS along with its ability to adapt to extreme conditions. These findings emphasized the need for carefully tailored irradiation protocols, taking into account the nature of the specific water basin, particularly in what refers to its biotic characteristics. (342)

Recently, chlorophyllin-mediated PDI has been suggested as a new promising treatment to control ichthyophthiriosis, a white spot-causing disease in many freshwater fish species by the protozoan parasite *Ichthyophthirius mulftifiliis*. Different life stages of the parasite were tested: trophonts (encysted stage in the host) and tomites (motile, infective stage). Samples were incubated 60 min in the dark with 0.5 - 10 μg $mL^{-1}$, followed by irradiation with simulated sunlight (PAR 149.66 W $m^{-2}$, UV-A 32.67 W $m^{-2}$, and UV-B 0.77 W $m^{-2}$) for 30 min. The photodynamic effect on the cells was evaluated by fluorescence microscope after staining with the fluorescent dye acridine orange. Transmitted light microscopy showed that chlorophyllin completely filled the trophont and destroyed the nucleus and the cell wall. The $LC_{50}$ value, calculated for trophonts of *I. multifiliis*, was 0.67 μg $mL^{-1}$ with a maximum mortality of about 10% observed in dark conditions. Even at a chlorophyllin concentration of 2 μg $mL^{-1}$ in the medium, 100% of the tomites were dead. The results of the *in vitro* experiments showed that the photodynamically active chlorophyllin reduces the number of parasites already at very low concentrations. For the first time it was demonstrated that the photodynamic treatment of *I. multifiliis* with chlorophyllin is very effective against tomonts and tomites of these fish parasite. (379)

## 7.4 Elimination of food-borne pathogens

PDI of common food pathogens (yeasts, molds and bacteria) has been reported *in vitro*, and *in vivo* on foodstuff (sprouts, fruits, vegetables, meat products) by directly applying the PS or immobilizing it on edible solid supports and also on the surface of packaging material. In the last ten years, representative natural type porphyrins such as HPde, PPIX, sodium chlorophyllin (NaChl) or 5-ALA as prophyrin precursor, and also synthetic analogues, have been used in scientific research related with microbiological food control.

HPde (2.5 - 71 μM) has been tested on several strains of micromycetes with distinct morphological type: *Aspergillus flavus*, *Trichothecium roseum*, *Fusarium avenaceum*, *Rhizopus oryzae* (313), *Alternaria alternata* and *Acremonium strictum* (336), using visible light (30 mW

$cm^{-2}$) and 15 min of irradiation (27 J $cm^{-2}$), on $10^6$ spores $mL^{-1}$ suspensions, incubated for 20 min to 18 h before irradiation. After 18 h incubation with HPde, dark toxicity inhibited the conidia germination of the different microfungi. Concentrations of 51 µM caused 100% inhibition of spore germination after irradiation of *Aspergillus* (313), *R. oryzae* and *A. alternata.* (336) Dark toxicity percentages of ≈ 15% and 20% were observed at this concentration for both fungi, respectively. (336) The germination of microfungi *F. avenaceum* and *T. roseum* spores were inhibited by 71 µM up to 90 - 100% (with 30% of dark toxicity). (313) For *A. strictum*, only the highest concentration (108 µM) induced a photoinhibition of 90% with 9% of dark toxicity. (336) This dark toxicity was envisaged as a spore germination inhibitor which could prevent germination until they have been washed or diluted out of the surface. (313)

High inhibition of conidia germination was also observed after PDI when using PPIX (1 - 4 µM) on *Fusarium poae* and *Fusarium culmorum* isolated from infected barley seeds. The spores (≈ $10^5$ – $10^6$ $mL^{-1}$) incubated 30 min were irradiated with visible light at 150 W $m^{-2}$ (50 - 200 kJ $m^{-2}$). At a PS concentration of 1 µM and an illumination dose of 200 kJ $m^{-2}$, germination decreased to 40% for *F. poae* and 65% for *F. culmorum*. At 4 µM, 96% and 55% of conidia were eliminated for *F. poae* and *F. culmorum*, respectively. Also, at micromolar concentrations, PPIX sensitizes the photo-oxidation of proteins and lipids in hydrated conidia when illuminating the spore suspension with light doses of 50 – 200 kJ $m^{-2}$, disturbing the permeability of membranes and suppressing spore germination. (378)

5-ALA has been stated to improve the nutritive value of food and considered as a possible tool to decontaminate wheat seeds prior to their use into preparation of sprouts, with minimal damage to wheat germination and quality. Wheat (*Triticum aestivum* L. var. Zentos) seeds significantly contaminated with several microfungi were soaked and incubated with 6 mM 5-ALA for 4 h. After this time, the viability of *Mucor spp.*, *Penicillium spp.*, *Aspergillus spp.*, *Rhizopus spp.*, *Acremonium spp.*, *Fusarium spp.*, *Alternaria spp.*, *Mycelia sterilia* and other fungi significantly decreased ≈ 1.0 log CFU $g^{-1}$ of seeds. The sensitivity of fungi to 5-ALA treatment varied considerably among fungi. Besides antifungal activity, ALA demonstrated to be a growth stimulator of wheat seedlings and roots, without impairment of the vigor of germination and the viability of seeds. It also caused an increase of the chlorophyll content, favoring the rate of photosynthesis and of the activity of antioxidant enzymes, which can promote cellular detoxification from ROS. (335) The selection of this particular pro-drug took into account the fact that PS can interact with the food matrix. Being colorless and odorless, ALA would not change the organoleptic properties if sprayed on food. (343) Moreover, its water solubility, stable shelf-life, non-bleaching character, simplicity of production and the possibility to be a constituent or food additive, make ALA a potential candidate for the control

of food pathogens by photosensitization, without damage to food constituents and unwanted coloration. (412)

The efficiency of 5-ALA has been tested *in vitro* against *Salmonella enterica*, *Bacillus cereus* vegetative cells and spores, *Listeria monocytogenes* cells and biofilms and on packaging material (adhered cells/spores and biofilms). The approach of adherence to packaging consisted on soaking or submerging trays of polyolefin (a mixture of polyethylene and polypropylene) in $10^7$ - $10^8$ CFU $mL^{-1}$ cells or spores solutions for 30 min, followed by dark incubation up to 60 min, drying 20 min and irradiation with visible light (20 mW $cm^{-2}$) up to 20 min. *In vitro* results showed that *B. cereus* cells were inactivated by ≈ 6 logs with 3 mM, incubated 60 min and irradiated 20 min, and spores ≈ 3 logs with 7.5 mM after 30 min incubation and 15 min irradiation. Cells adhered to packaging material were inactivated by 4 logs after 10 min incubation with 3 mM porphyrin and 15 min irradiation. Increasing the concentration to 7.5 mM and the incubation time to 30 min caused 2.7 log decrease on spores adhered to packaging. (345) An efficient inactivation (6 log) of *Salmonella enterica* serovar Typhimurium resistant to tetracycline ($10^7$ CFU $mL^{-1}$) was achieved after 60 min incubation with 7.5 mM of 5-ALA and 20 min irradiation (24 J $cm^{-2}$). (344) In the case of *L. monocytogenes*, *in vitro* tests showed that cells were inactivated by 4 logs with 7.5 mM 5-ALA, incubated 120 min and irradiated 20 min. Cells adhered to packaging material were inactivated by 3.7 logs after 15 min incubation with 10 mM PS and 15 min irradiation (18 J $cm^{-2}$). With the same concentration, a 3.1 log decrease in viable cells was observed in biofilms formed in 48 h, incubated 30 min in the dark and irradiated for 15 min. Approximately 5.9 log CFU $cm^{-2}$ of biofilm-associated cells were adhered onto a plastic coupon. The different effectiveness between photosensitization of biofilms and the cells adhered to the surface of packaging material was explained by the polysaccharide matrix of biofilms acting as a diffusion barrier for PS and reducing its accumulation inside bacteria. (343) The fluorescence intensity analysis of endogenous PS in these three microorganisms revealed that *B. cereus* produces endogenous porphyrins ten times more efficiently than *L. monocytogenes* or *S. enterica* (344, 382), explaining its higher susceptibility to ALA-based photosensitization compared to the other two bacteria.

The photodynamic effect of chlorophyllins applied for inactivating food-borne pathogens was firstly reported by Lopez-Carballo et al. (368) In a way to improve food preservation, the authors developed and applied new antimicrobial PS-containing edible films and coatings based on gelatin incorporating sodium magnesium chlorophyllin (E-140) and sodium copper chlorophyllin (E-141). Cell suspensions of *S. aureus* and *L. monocytogenes* ($10^8$ CFU $mL^{-1}$) were spread on the surface of nutritive agar plates. E-140- and E-141-containing

gelatin films (80 μg $mL^{-1}$) were placed on the surface of the inoculated nutritive agar plates and irradiated for 5 or 15 min at several fluence rates: 10,000, 30,000 and 50,000 lx. Additionally, the inhibitory effect of 80 μg $mL^{-1}$ E-140 chlorophyllin-gelatin films on early-stationary phase cells of *S. aureus* and *L. monocytogenes* inoculated on slices of cooked frankfurters was tested. Frankfurter slices were inoculated with bacterial samples (50 μL, $10^6$ cells) and after inoculum penetration, the sample surfaces were wrapped in E-140 chlorophyllin edible films and exposed to 30,000 lx for 15 min. Chlorophyllin E-140 exerted a greater inhibiting effect than chlorophyllin E-141 on the bacterial viability. Differences in the antibacterial activity of the two chlorophyllins could be due to E-140 having a greater ability than E-141 to generate $^1O_2$ under the experimental conditions tested. Water soluble E-140 and E-141 reduced *S. aureus* and *L. monocytogenes* viability by 5 log and 4 log, respectively. Both procedures of wrapping or coating the food sample with E-140-containing gelatin films and coatings were successful, although the results of the antimicrobial studies were slightly different. The E-140 gelatin film was placed on the surface of a previously inoculated frankfurter sample, the combined treatment of wrapping with E-140 gelatin film and irradiation produced an approximately 1.5 log fall in the viability of *S. aureus* and *L. monocytogenes*. None of the PS treatments showed effect on the viability of *E. coli* or *Salmonella*. The antimicrobial films with potential application as wraps or castings to avoid contamination on the surface of fresh and processed products would increase their shelf-life and safety. Additionally, minimal impact on the visual sensory properties of the food has been observed with the low concentrations used of incorporated chlorophyllin. (368)

Besides immobilized chlorophyllin derivatives, sodium chlorophyllin (Na-Chl) has also been tested *in vivo* on the surface of fruits and vegetables. (348) The inactivation of *B. cereus* and aerobic mesophils on nectarines, iceberg lettuce, cherry tomatoes, cauliflowers and cherries, and the impact of the treatment on shelf-life (i.e., disease-free period) of the product were evaluated. *B. cereus* (≈ $10^7$ CFU $mL^{-1}$) were inoculated on the surface of these food products and they were soaked in the Na-Chl solution (0.15 mM) for 5 min, dried for 20 min and irradiated with the visible light (20 mW $cm^{-2}$) for 5 min. A 1.68 - 2.88 log reduction on bacterial survival was observed, depending on the surface structure and the light-surface interaction specificity. A reduction of 1.48 - 2.47 log of naturally distributed aerobic mesophils was also achieved. Also, the shelf-life of all treated products could be extended, in some cases, up to 70% compared to non-treated ones. (348) In another study, strawberries were inoculated with *L. monocytogenes* for 30 min, soaked in 1 mM Na-Chl for 5 min and irradiated for 20 min with visible light (12 mW $cm^{-2}$, 14.4 J $cm^{-2}$). Photosensitization decreased *Listeria* by 98% (1.8 log). Naturally occurring yeasts, microfungi and mesophils were inhibited by 86 (0.86

logs) and 97% (1.7 log), respectively. This photo-treatment extended the strawberry shelf-life by 2 days. The total antioxidant activity of treated strawberries increased 19%. No impact on the amount of phenols, anthocyanins or surface color was detected. The re-growth rate of yeast and fungal survivors slightly decreased. Furthermore, photosensitization did not affect strawberry color or taste. (385)

Na-Chl has also been tested *in vitro* and on surfaces of packaging material, with effective results on *B. cereus*, *Listeria* and *Salmonella enterica*. The experimental approach used in the studies below was the same already described for 5-ALA. (343-345) Na-Chl (0.075 µM to 75 µM) was tested against *B. cereus* ($10^7$ CFU $mL^{-1}$) vegetative cells and spores, *in vitro* or attached to the surface of packaging material, incubated 2 - 60 min and irradiated with visible light (20 mW $cm^{-2}$). *B. cereus* vegetative cells and spores were inactivated *in vitro* by 7 log with 0.75 µM after 2 and 5 min irradiation, respectively, after 2 min incubation in both cases. The 4-log photoinactivation of *B. cereus* cells on the surface of packaging materials required a concentration of Na-Chl 10-fold higher (7.5 µM). PDI with 75 µM of Na-Chl, 5 min of dark incubation and 5 min irradiation caused 5 log reductions in the concentration of attached endospores. Endospores are more resistant than vegetative cells to photoinactivation, since a higher concentration of Na-Chl is required than for vegetative cells for the same level of inactivation to be attained. (346) *Bacillus* spores were susceptible to ALA-based PDI as well. (345) The comparison of ALA and Na-Chl based photoinactivation of *B. cereus* indicates some advantages of the later PS; this means that using Na-Chl can shorten the dark incubation time from 20 to 2 min, reduce the irradiation time from 20 to 5 min and lower the optimal concentration (0.075 µM *versus* 7.5 mM for 5-ALA). (412)

*Listeria* biofilms were totally removed from the surface of packaging material at higher Na-Chl concentrations and after longer incubation times. *L. monocytogenes* cells were inactivated by 7 log using 0.75 µM of PS, and 30 min irradiation for a thermo-resistant strain and 5 min for a thermo-sensitive one. Decontamination of packaging material from thermo-resistant *L. monocytogenes* cells adhered to the surface reveals that a Na-Chl concentration of 0.15 µM is necessary to reduce the 4 log of bacteria with 15 min irradiation while the same reduction against the thermo-sensitive strain could be achieved within 5 min. With this irradiation time, *Listeria* biofilms were also susceptible to photosensitization and surfaces could be totally cleaned from them when 150 µM of Na-Chl is used (4.5 logs). (383) Additionally, a thermo-resistant strain of *Bacillus* was less susceptible to PDI than the thermo-resistant *Listeria* strain. (347)

A comparison between the antimicrobial efficiency of PDI with conventional surface cleaning products indicates that Na-Chl-based photosensitization is much more effective

against *B. cereus* attached to the surface of materials than washing with water or using 200 ppm of sodium hypochlorite. (346) In the case of *Listeria* strains (thermo-resistant or thermo-sensitive), washing with water diminishes pathogens by less than 1 log, 200 ppm of sodium hypochlorite by 1.7 log and Na-Chl-based photosensitization by 4.5 log. (383)

Chitosan, as a natural compound, may replace chemical preservatives and may be used to obtain eco-friendly products but it should not interact with food ingredients or alter food organoleptic features. (313) A chlorophyllin – chitosan complex (with 0.001% Na-Chl – 0.1% chitosan, Na-Chl–CHS) has been tested against *Salmonella enterica* (≈ $10^7$ CFU $mL^{-1}$) upon visible light irradiation (9.6 mW $cm^{-2}$) for 30 min. (387) The photoinactivation treatment (15 min of incubation with Na-Chl followed by irradiation) led to a 1.05 log reduction of *S. enterica*. The dark toxicity of the Na-Chl–CHS complex reduced cell viability by also 1.05 log. An extension of the incubation time to 120 min favored the inactivation of *Salmonella* to 1.39 log. An extremely high antibacterial efficiency was demonstrated after photoactivation with the Na-Chl–CHS complex (7.3 log reduction of microbial population) after 120 min irradiation. A photoactivated Na-Chl-CHS complex in a slightly acidic environment was suggested as a useful tool against *S. enterica*. The synergetic antibacterial effect of CHS and Na-Chl supposedly relies on the complexation of these two compounds governed by thermodynamic equilibrium and results in a uniform distribution of the short-chain component (Na-Chl) among the chains of the oppositely charged long-chain component (CHS) present in high excess. (387)

More recently, the photodynamic antimicrobial efficiency among 5-ALA, Na-Chl and a combined treatment of 5-ALA plus Na-Chl has been tested against *L. monocytogenes* and *S. enterica*. Cells were incubated with Na-Chl (75 µM – 0.075 µM) or 5-ALA (7.5 mM) and further irradiated with visible light (20 mW $cm^{-2}$). *Salmonella* was more sensitive to 5-ALA (≈ 6.6 log viability decrease with 7.5 mM, 40 min irradiation) than to Na-Chl (≈ 2.2 log viability decrease with 75 µM upon 40 min irradiation). *Listeria* was more sensitive to Na-Chl (7 log drop with 0.75 µM, 5 min irradiation) than to 5-ALA (≈ 3.8 log with 0.75 µM, 20 min irradiation and 60 min incubation). Both bacteria were inactivated to an undetectable level when combined treatment was applied (incubation time of 60 min, with 7.5 mM of 5-ALA and 0.15 µM of Na-Chl, 40 min of irradiation). (384)

Besides HPde, PpIX, 5-ALA and Na-Chl, novel cationic porphyrins were synthesized to be used on food contaminants. As such, the biological evaluation of five cationic porphyrins was tested on *Penicillium chrysogenum* conidia. Two different series of cationic porphyrin groups were prepared from 5,10,15,20-tetrakis(4-pyridyl)porphyrin and 5,10,15,20-tetrakis(pentafluorophenyl)porphyrin. A 50 µM of PS was used under white light at a fluence rate of 200 mW $cm^{-2}$ over 20 min showing that the most effective PS caused a 4.1 log (Tetra-

$Py^+$-Me) and a 3.4 log (Tetra-$Py^+$-Pe) reduction in the concentration of viable conidia. An increase of the porphyrin carbon chain led to a reduction of the inactivation of conidia, in both PS series. (233)

From these reports, one can detach the factors that influence the efficiency of PDI of food-borne pathogens:

- irradiation time (and consequently, light dose) (343-345, 348, 368);
- the surface specificity of food, as shown by *in vivo* studies (348);
- cell-bound PS concentration as shown in bacteria (348) and in fungi (336);
- the use of powerful light sources (light emitting diodes) (385);
- the size of the *N*-alkyl chain on the porphyrin structure as shown on the photoinactivation of fungi spores, mainly by affecting their binding to cellular material (233);
- initial concentration, in the case of 5-ALA (345), and incubation time (or concentration of endogenously produced porphyrins) (343-345).

## 7.5 Applications for domestic, industrial and healthcare settings

At a time when environmental protection, energy efficiency, sustainability and entrepreneurship are guiding principles of new technological solutions, it makes sense that the collaboration between researchers and businessmen / entrepreneurs is reinforced, combining innovation and creativity. In this partnership, which is an increasingly evident reality, the design, production and commercialization of multi-functional, reusable and durable products arise as emerging opportunities. Portuguese companies as Success Gadget and Revigrés are examples of this close collaboration. The first of these companies developed silica nanoparticles with different active ingredients (anti-mosquito, antimicrobial, antifungal) with applications in the textile industry (clothing and footwear), construction (paints) and health (antifungal socks, anti chilblain gloves and socks for diabetic foot). The innovation of these materials is linked to wash off resistance (they withstand up to 80 washes) and when applied in paints, varnishes or mortar their effect lasts up to five years. (413) The second company, Revigrés, sells self-cleaning tiles suitable for outdoor use (façade cladding and external cladding), since its titanium oxide coating, when in contact with sunlight, promotes the degradation of gaseous pollutants. Also, whenever the tile is wet, a wet film formed allows the removal of dirt. These properties reduce the maintenance costs and also promote cleaning in areas of difficult access. (414)

Despite these innovative examples, there is still a long way to go with regard to fast, effective and long-lasting elimination of microorganisms on surfaces, whether in the household, industrial or healthcare settings. The application of the photodynamic principle to this context seems to be a promising option, according to studies conducted in recent years. Table 7.3 gathers the potential non-clinical applications of porphyrin-based photoactive compounds/materials suggested by the referred literature.

**Table 7.3** Potential non-clinical applications of porphyrin-based photoactive compounds/materials

| | **References** |
|---|---|
| **Water and environment** | |
| Algicides | (358) |
| Control of fish infections in aquaculture systems | (369) |
| Control of insect pests around poultry-producing facilities, in barns, feedlots, manure storage areas, greenhouses | (381) |
| Disinfection of polluted waters from fish-farming ponds | (140, 141, 369) |
| Filters for water treatment | (373) |
| Larvicides/insecticides/pesticides | (321, 337-340, 349, 353-357, 381, 386, 390) |
| Wastewater treatment | (142, 198, 331, 332, 380) |
| Water disinfection | (342, 352, 360, 380) |
| **Food safety** | |
| Decontamination of food-related surfaces (packaging material) | (345-347, 363, 368, 383) |
| Decontamination of ready-to-eat fruits, frozen fruits, pastry products or similar | (348, 385) |
| Decontamination of sprouts | (335, 378) |
| Wraps or castings for fresh and processed products | (368) |
| **Domestic, industrial and healthcare settings** | |
| **Self-cleaning surfaces** | (334, 352, 363-365) |
| **More specifically:** | |
| Hygiene products or packaging materials | (370) |
| Polymeric materials (syringes, IV bags and tubing, catheters, hemodialysis filters and gloves) | (351, 361, 367) |
| Privacy curtains in hospital rooms | (361) |
| Protective clothes and masks | (361) |
| Sources of nosocomial infections textile (bedding, surgeons gowns, pillows) | (361, 367) |
| Walls, floors, instruments | (376) |
| **Other:** | |
| Hand hygiene | (362) |

### 7.5.1 Fabric

The thought of incorporating porphyrins into different textile materials to create protective clothing in the household, industrial and hospital settings, including masks, gowns, caps, bedding and other textiles, was suggested nearly 10 years ago. The first antimicrobial porphyrin textiles were reported by Bozja et al. (361), named as light-activated antimicrobial materials. Novel materials were synthesized by the grafting of PPIX and zinc protoporphyrin IX (Zn-PPIX) to nylon fibers and their antimicrobial effectiveness tested against *S. aureus* and *E.*

*coli*. Samples of the textiles were inoculated with bacteria and irradiated with incandescent light (at 10,000, 40,000, and 60,000 lx for 30 min or at 40,000 lx for 5, 15 and 30 min). At 40,000 lx, these fibers showed increased antimicrobial activity against *S. aureus* with increasing exposure time. The samples grafted with PPIX-ethylene diamine (PPIX-ED) were able to inactivate more than 95% of *S. aureus* after 30 min of irradiation upon 60,000 lx, but no reduction on *E. coli* survival was observed. The samples grafted with ZnPPIX-ED were able to eliminate 94% of *S. aureus* at 40,000 lx but a light intensity of 60,000 lx was required to attain a reduction of 30% on *E. coli* survival. The zinc samples were more effective than the corresponding free-base. With suitable changes, these materials have been suggested to be used for privacy curtains in hospital rooms, laboratory coats for medical personnel, or other fiber or plastic surfaces within the hospital environment considering that the normal rooms' illumination is approximately 30,000 lx. (361)

Other authors relied on the possibility of creating pioneering self-sterilizing fabrics from cotton fiber, due to its resistance to repeated washing or exposure to cleaning products. (374, 375, 389) Cotton fabrics, which essentially consist of cellulose fibers, can be easily modified by substitution of a relative small number of their numerous -OH nucleophilic groups. *Meso*-arylporphyrins bearing acetylenic units were grafted on cotton fabric with azide groups via "Click-Chemistry". Covalently attached porphyrin accounted for 70% of the total amount of PS and the remainder (around 30%) corresponded to porphyrins only sequestered in the cellulose fiber web. This material was impregnated with *E. coli* and *S. aureus* (≈ $10^6$ CFU per 10 cm Petri dish) and irradiated with white light (1000 lx) for 24 h. For both bacteria, a *c.a.* 0.74 log reduction was achieved after irradiation. (375) Soon afterwards, the same group reported a modification in porphyrin immobilization envisaging further industrial applications. In this way, covalently neutral, anionic and cationic 1,3,5-triazinylporphyrin derivatives were grafted on non-modified cotton fabrics using cyanuric chloride (2,4,6-trichloro-1,3,5-triazine) as linking agent. The photodynamic activity of these new cotton fabrics was tested *in vitro* against *S. aureus* with white light for 24 h (0.16 mW $cm^{-2}$). Sterile photosensitive textiles (3.5 × 3.5 cm), previously autoclaved for 15 min at 120 °C, impregnated with bacterial inoculum (≈ $10^6$ CFU $mL^{-1}$), deposited in a sterile Petri dish, were then incubated at 37 °C for 24 h under white light irradiation in wet atmosphere. All surfaces caused a photo-bactericidal effect at a quantity as low as ≈ 10 µmol of active compound per fabric square sample. After 24 h of light exposure, percentages of bacterial survival reduction were 37%, 93.7% and 100% for anionic, neutral and cationic surfaces respectively. The three materials did not show any photodynamic activity against Gram-negative bacteria. (374, 389)

Mosinger et al. (372) produced a novel polyurethane nanofabric using the Nanospider™ electrospinning industrial technology (415) which is used for the preparation of fibers with diameters ranging from nanometers to a few microns and for materials with a high surface area and porous structure. (416) The material was doped with 5,10,15,20-tetraphenylporphyrin (TPP). The nanofabrics, composed of polymeric nanofibers had 0.03 mm thickness (2 g $m^{-2}$) and contained 0.12% TPP. A hydrophilic variant was also produced, containing in addition 0.6% sodium dodecyl sulfate and the photodynamic function of this nanofabric variant was tested against *E. coli*. Small pieces of nanofabrics were inoculated with bacteria and illuminated with white light for 60 min. After irradiation and incubation on agar plates, no bacterial growth was observed on the nanofabric pieces. Daylight was at least as effective as artificial light. TPP incorporated in both nanofabrics variants were able to produce $^1O_2$ with high efficiency. Among the exceptional properties of these nanofabrics are the large specific surface area, light weight, chemical specificities, low cost and mechanical flexibility. The same authors studied three polyurethane nanofabrics containing respectively, 0.1% ZnPc, 0.1% ZnTPP and a mixture of PS (0.1% ZnPc and 0.1% ZnTPP). Another polyurethane nanofabrics was also prepared but containing two independent layers, one doped with 0.1% ZnPc and the other doped with 0.1% ZnTPP. All nanofabrics were placed on agar plates and inoculated with a suspension of *E. coli* in an undetermined concentration, and illuminated with white light for 30 min. All PS-doped nanofabrics were able to kill bacteria on their surfaces when exposed to white light. (373)

Later, Jesenska et al. (364) prepared electrospun polymeric nanofibers of polyurethane Larithane™ (PUR), polystyrene (POS), polycaprolactone (PCL), and polyamide 6 (PA6) doped with 1% TPP. The PUR, POS, and PCL nanofiber materials were able to inhibit completely the *E. coli* growth after 60 - 90 min of irradiation with white light, while lower antibacterial activity was found for PA6 nanofiber materials. The photodynamic effect was attributed to $^1O_2$ production and all tested nanofiber materials exhibit prolonged antibacterial properties after being treated with long-duration irradiation due to the formation of $H_2O_2$, even in the dark. The photoinactivation efficiency also depended on oxygen permeability and diffusion coefficients as on the diameter of the polymeric nanofibers. Soon after, the same group (350) selected another medical-grade nanofiber material, polyurethane Tecophilic® and also polycaprolactone (PCL) both loaded with TPP to study the photoinactivation of non-enveloped DNA viruses (mouse polyomaviruses, $10^5$ plaque forming units, PFU) and enveloped DNA viruses (baculoviruses pVLVP1, $10^4$ PFU). Viral suspensions were applied to the surface of small pieces of the nanofiber textiles doped with 1% TPP and were irradiated with white light for 30 min. The virus were retrieved from the surface of the textiles and used to infect 3T6 fibroblasts

(for the mouse polyomavirus) and the Sf9 insect cell line (for baculovirus). (350) Singlet oxygen released from the surface of doped polyurethane Tecophilic® and PCL upon irradiation efficiently inactivated both the non-enveloped and enveloped viruses and both types of polymer nanofibers are nontoxic to viruses in the absence of light. The results showed that baculovirus is more resistant to photoinactivation than the polyomavirus. The textiles were also tested after a year of storage at room temperature in the dark with the same results which indicate their long-term photovirucidal efficiency. (350)

### 7.5.2 Paper

Another possible application of microbial PDI is in hygiene products or packaging materials. Cellulose is thus envisaged as an exceptional sustainable material as it is degradable and renewable. (370) Paper or cardboard can thus be sanitized prior to use to avoid contamination. In this scope, a tricationic porphyrin, 5-(4-aminophenyl)-10,15,20-tris(1-methylpyridinium-4-yl)porphyrin was grafted on cellulose filter paper by using cyanuric chloride, without previous chemical modification of the cellulosic support, as already mentioned. (389) Sterile photosensitizing filter paper disks (0.5 cm diameter) impregnated with *E. coli* and with *S. aureus* ($10^5$ CFU $mL^{-1}$) were deposited on sterile Petri dishes, and then incubated at 37 °C for 24 h under white light irradiation (9.5 J $cm^{-2}$) in wet atmosphere. A strong photobactericidal effect was observed after light exposure, since no surviving bacteria were detected on grafted filter paper. (370)

### 7.5.3 Other support materials

Krouit et al. reported several works considering the preparation of plastic materials, based on natural and synthetic porphyrins, able to inactivate Gram-positive and Gram-negative bacteria. (365-367) Photobactericidal surfaces were prepared, containing different amounts of PPIX units (0.19% to 1.1%) covalently linked to cellulose esterified with lauric acid. (365) Besides, plastic material incorporating synthetic cationic porphyrin derivatives (0.14% to 0.57%), was also prepared in order to achieve a better photobactericidal activity. In this work the cellulose was derivatized with chloroacetyl groups. (366) Based on the first work the group prepared cellulose laurate esters plastic films grafted by different carbon-spacer arms (4- or 11- carbon) to synthetic porphyrins (0.08% to 0.58%). (367) The photodynamic activity of these polymers was tested against *E. coli* and *S. aureus*. Disks with 2 cm diameter were cut out of the porphyrinated plastic films and deposited onto nutrient agar seeded with the target strain and irradiated with visible light (1.7 mW $cm^{-2}$) for 24 h at 37 °C. The growth of the microorganisms

was examined visually under the porphyrinated disks. The cationic porphyrinic chloroacetyl cellulose chlorides, with porphyrin content higher than 0.20%, inactivated the two bacterial strains whereas films with lower porphyrin content were found more active against *S. aureus* than against *E. coli*. (366) In comparison, the films based on PPIX lauryl cellulose esters needed at least a porphyrin content value of 0.52% to photoinactivate *E. coli* (365). These results confirmed the higher photobactericidal effect of the cationic porphyrinic plastic films. (367)

The possibility of incorporating PS-modified-cellulose nanocrystals into paper, fabrics and plastics was highlighted by Feese et al. (363) who created a conjugate cellulose nanocrystals-cationic porphyrin (CNC-Por) with the aim to rapidly inactivate a range of bacteria, with minimal cost. As stated, cellulose nanocrystals have several advantages over amorphous cellulose ester: they have a particular degree of molecular control for precise functionalization due to their rigidity, defined surface, structure and dimensions; they are readily biodegradable; they represent a renewable resource, which eases the development of new advanced materials with photobactericidal activity. (363) To test the performance of these materials, a zinc(II) complex of a cationic water-soluble ethynylphenylporphyrin was covalently attached to azide-modified cellulose nanocrystals. Saline buffered suspensions of *E. coli*, *S. aureus* and *Mycobacterium smegmatis* (≈ $10^8$ CFU $mL^{-1}$) were incubated in the dark for different time intervals with 20 µM CNC-Por which refers to the concentration of the porphyrin on CNC-Por present in the suspension. Then they were illuminated with white light (60 mW $cm^{-2}$). Six log units reduction in viable cells were observed against *S. aureus* (5 min incubation, 30 min irradiation), 3.5 log units for *M. smegmatis* (45 min incubation, 30 min irradiation), and 2 log units for *E. coli* (60 min incubation, 30 min irradiation). (363)

The PDI of bacteria mediated by these same conjugates (20 µM) was further tested as a function of bacterial strain, incubation time and illumination time on *Acinetobacter baumannii*, multidrug resistant *A. baumannii* (MDRAB), methicillin-resistant *S. aureus* (MRSA) and *P. aeruginosa* (≈ $10^8$ CFU $mL^{-1}$) with visible light (65 mW $cm^{-2}$). (334) A 6 log units of reduction in viable cells was observed for MRSA (5 min incubation), 5 – 6 log units for *A. baumannii* (30 min incubation) and MDRAB (15 min incubation), and 2.5 log units for *P. aeruginosa* (60 min incubation) at a fluence of 118 J $cm^{-2}$ (30 min irradiation). Confocal laser scanning fluorescence microscopy of *A. baumannii* and *S. aureus* incubated with CNC-Por suggested a lack of internalization of the PS, supporting the hypothesis that direct binding and uptake of the PS are not necessary requirements for PDI by CNC-Por. On the other hand, the zinc(II) complex of a cationic water-soluble ethynylphenylporphyrin, when in solution and not bound to the cellulose nanocrystals, led to the fluorescence being localized on *A. baumannii*. Even though it was not determined whether the cationic PS was internalized by the bacterium,

or simply bound to the bacterial cell membrane. So the production of $^1O_2$ and other radical species in close proximity to the bacteria may be sufficient to result in cell inactivation or death. Despite forming an insoluble suspension, CNC-Por conjugate exhibited excellent antimicrobial activity for all strains examined with the exception of *P. aeruginosa*, which was only moderately inactivated. (334)

The efficient photodynamic effect of other photoactive surfaces was demonstrated by Funes et al. (352) The authors used two polymeric porphyrinated films formed by electrochemical polymerization of free-base 5,10,15,20-tetrakis(4-(*N,N*-diphenyl)aminophenyl)porphyrin (H2P-film) and its complex with Pd(II) (PdP-film) on optically transparent indium tin oxide (ITO) electrodes on microbial cell suspensions. The polymeric surfaces (0.7 × 3.0 × 2.1 $cm^2$) were placed inside of *E. coli* and *Candida albicans* suspensions (≈ $10^6$ CFU $mL^{-1}$) and irradiated with visible light (90 mW $cm^{-2}$) for different time periods. The viability of microbial cells irradiated with visible light depended on the light exposure. Both H2P- and PdP-films exhibited a photosensitizing activity causing a ≈ 3 log decrease of *E. coli* survival after 30 min of irradiation and a ≈ 2 log decrease in *C. albicans* viability. The advantages of these electrodes are that they represent an appropriated surface to obtain mechanically stable electropolymeric films, they are optically transparent to visible light, and also that they can be easily and quickly removed from the media after cell inactivation, avoiding permanent photodynamic effects. (352)

In another approach to photoinactivate *C. albicans* (351), novel photoactive flexible bridged polysilsesquioxane thin plastic films (SSO-P) doped with 5-(4-carboxyphenyl)-10,15,20-tris(4-methylphenyl)porphyrin (P-acid) were evaluated in aqueous suspensions (with 5 M free-base P-acid) and on two SSO-P films (with 2.6 x $10^{-4}$ w/w and 5.2 x $10^{-4}$ w/w concentration of P-acid in each film). The yeasts treated with 5 M of P-acid were incubated 30 min in dark at 37 °C later irradiated with visible light (90 mW $cm^{-2}$). In the case of polymeric films, their surfaces (0.7 x 2.5 = 1.75 $cm^2$) were inoculated with yeast suspension (≈ $10^6$ CFU $mL^{-1}$), irradiated, and then placed in saline buffer for serial diluting, plating and colony counting. With 5 M P-acid (non-cationic porphyrin), an expected small photoinactivation effect (0.5 log decrease) was observed after 60 min. The viability of *C. albicans* cells in irradiated SSO-P films depended on the light exposure although no differences were observed between the two SSO-P films. They caused a photosensitizing activity of ≈ 2.5 log decrease of *C. albicans* survival after 60 min of irradiation (324 J $cm^{-2}$). (351) Comparatively to the results obtained by Funes et al. (352), the main difference of the present SSO-P films is their versatility as plastic flexible materials at room temperature, easy obtention and ability to shape the surfaces. They also keep a higher antifungal activity against *C. albicans.*

Microporous silica gels prepared by sol–gel process from tetrakis(2-hydroxyethoxy)silane (THES) have been used to immobilize the cationic Tetra-$Py^{+}$-Me. (376) THES was used to ensure toughness and greater stability of silica-Tetra-$Py^{+}$-Me composites. The antimicrobial activity of these composites was compared with their tetramethoxysilane (TMOS) analogs against *E. coli*. Nutrient agar inoculated with *E. coli* ($10^{6}$ CFU $mL^{-1}$) was poured over the composites at the bottom of plastic plates and illuminated with visible light (10 klx for 0, 1.5, and 3 h, corresponding to a light dose of 0, 7.9 and 15.8 J $cm^{-2}$, respectively). Growth of *E. coli* in nutrient agar decreased with increasing light energy for all the composites. On the dense THES composites, the 15.8 J $cm^{-2}$ light energy led to the total growth inhibition (6 log). In the case of TMOS, the higher bactericidal effect was established for the weak composites (6 log reduction with the composite with PEG). In general, THES composites with the lower specific surface areas were more effective than TMOS analogs. The antimicrobial activity of these composites was mainly influenced by total Tetra-$Py^{+}$-Me content in the bulk, specific surface areas, and by the thicknesses of the composites. Among THES composites, their flexibility brought about by PEG 600, improved oxygen diffusion. All the composites showed good adhesion to glass, and THES ones have not shrunk at least for 3 months. These properties, along with a high shape stability of THES-Tetra-$Py^{+}$-Me composites, make them favorable photosensitive materials. (376)

The same microbiological method was applied to evaluate the antibacterial photodynamic effect of mesoporous organosilica – porphyrin composites obtained by entrapment of TPP and Tetra-$Py^{+}$-Me into three polysilsesquioxanes prepared by the sol – gel method from 1,2-bis(triethoxysilyl)ethane, 1,6-bis(triethoxysilyl)hexane, and 1,8-bis(triethoxysilyl)octane. The Si-matrices of the porphyrin composites under study are biocompatible and unresponsive to photosensitization. The pre-polymer-porphyrin mixtures were polymerized in a glass Petri dish and were inoculated with *E. coli* ($10^{5}$ CFU $mL^{-1}$) immobilized in nutrient agar. Irradiation was performed with visible light (with 5.5 klx for 0 h, 1.5 h, and 3 h corresponding to 0, 4.3, and 8.7 J $cm^{-2}$, respectively). The fluorescence and antibacterial effects of the TPP composites increased with increasing incident light energy and were dependent on the mesoporosity of the matrix. The composites with the higher mesoporosity are preferable since the matrix controls both oxygen diffusion through the material and quenching of the excited PS. For that reason, TPP – BTHP exerted the highest biocidal effect (≈ 5 log decrease with 8.7 J $cm^{-2}$) and the other TPP composites reduced cell viability to less than 1 log. Tetra-$Py^{+}$-Me – BTEP was less effective. The complete inactivation of the bacteria attained with TPP – BTH demonstrates that the photodynamic process takes place

in the whole volume of the agar layer (1000 µm thick) and not only on its contact surface with the TPP – BTH film. (377)

*In vitro* preliminary antimicrobial tests with palladium(II) complex of 5,10,15,20-tetrakis(4-carboxyphenyl)porphyrin)(PdTPPC) – Zn2Al/PU (polyurethane) composite films (0.4 wt% of PdTPPC for 1% of PdTPPC-Zn2Al filler loading) were able to totally inhibit two strains of *S. aureus* and *P. aeruginosa* seeded on nutrient agar (≈ $10^5$ CFU $mL^{-1}$) and incubated 24 h at 37 °C under continuous white light illumination at a fluence of 100 J $cm^{-2}$ $s^{-1}$. Considering the low amount of PS, the PdTPPC – Zn2Al/PU film proved to be a highly efficient light activated antimicrobial surface. (371)

According to Eicshner et al. (362), antimicrobial photodynamic treatment might become acceptable as a tool for hand hygiene procedures and also in other skin areas, as washing of the hands is of little use if, for example, a hospital environment is heavily contaminated. (417) So, the possibility of rapidly and efficiently inactivating MRSA, enterohemorrhagic *E. coli* (EHEC) and *C. albicans*, using the photodynamic approach, was revealed *in vitro* with different concentrations of Tetra-$Py^+$-Me illuminated with visible light (50 mW $cm^{-2}$) for 10 s and 60 s. A light dose of 0.5 J $cm^{-2}$ and 1 µM of Tetra-$Py^+$-Me achieved a PDI of ≥ 3 log of MRSA and EHEC. Incubation with higher concentrations (up to 100 µM) of Tetra-$Py^+$-Me caused bacterial inactivation by more than 5 log. Efficient *C. albicans* inactivation (≥ 5 log) was achieved at a light dose of 12 J $cm^{-2}$. Since Tetra-$Py^+$-Me has no clinical approval to be used as a medical drug, it was suggested that similar porphyrin molecules with similar properties that can be approved for use in humans should be developed in the near future. This rapid inactivation procedure may be useful for clinical, on industrial purposes, but it is also feasible in environmental technology. Processes with short application times, simplicity, efficacy and low costs are desirable and needed. (362)

In addition to testing the PDI of microorganisms, most of these studies tried to obtain a mechanistic explanation of the action of the PS immobilized on these supports, mainly based on the concept of 'photobactericidal surface', introduced by Midden and Wang who demonstrated that a light-induced flow of $^1O_2$ on the material surface was responsible for cell inactivation. (418) The scientific literature has disclosed distinctive forms of interaction between porphyrins and bacterial cells. If on one hand it has been argued that porphyrins can penetrate the cell wall to the periplasmic space and bind to the cytoplasmic membrane (62, 223, 224); on the other it has also been demonstrated that they can have a dual location (bound to the cell wall and to the nucleic acids) (76); or do not have to penetrate (51, 231) or even come into contact with the cells. (232)

When porphyrin molecules are immobilized in solid supports, their availability to bind and eventually penetrate into cells is reduced. Thus, to produce the same inactivation results, the concentration used in the supports must be higher than that which would be used in solution. (363) This fact supports the idea that direct binding and uptake of the PS are not necessary requirements for PDI. (363) This was justified by the production of ROS on the surface of the material, mainly $^1O_2$ during activation of the light-porphyrinated materials followed by their dissemination and possible interaction with the target cell. (365, 366) To interact against the cells and lead to cell death, these species would have to be longer-lived, and/or could be generated in close proximity to the bacteria. (334, 363, 371)

## 7.6 Final remarks and future perspective

Although not yet established as an antimicrobial therapeutic procedure, the photodynamic inactivation of microbes and other organisms within the environmental context continues being improved and increasingly optimized.

Among the main advantages of this approach are its nature of multi-target cellular damage and the possible use of a powerful and free light source, as sunlight. In the 1990s, when it was found that a photosensitizer with positive charges on its structure allowed the efficient inactivation of cells with complex structural features, such as Gram-negative bacteria, the research in photodynamic inactivation took a new breath.

In addition to being remarkably effective against a multitude of micro(organisms), the use of photosensitizers such as porphyrin derivatives, allows for the designing of an immense diversity of structurally different molecules that can be made more efficient and, in the non-clinical framework, also to be harmless to the environment and to humans and animals, if the photosensitizer molecules are immobilized on inert solid supports.

Likewise, the use of porphyrin concentrations in the micromolar range or from natural sources enables photodynamic inactivation to be used exclusively for its intended purpose without further impact.

The diversity of possible applications that have been proposed in recent years, as well as the progress made in this research demonstrate that PDI remains a method of disinfection/sterilization with promising practical application in the short term.

# Chapter 8. Bioluminescence and its application in the monitoring of antimicrobial photodynamic therapy

The content of this chapter has been published as:
Alves E, Costa L, Cunha Â, Faustino MAF, Neves MGPMS, Almeida A. Bioluminescence and its application in the monitoring of antimicrobial photodynamic therapy. Appl Microbiol Biotechnol. 2011;92(6):1115-28.

# 8 Bioluminescence and its application in the monitoring of antimicrobial photodynamic therapy

## 8.1 Abstract

Light output from bioluminescent microorganisms is a highly sensitive reporter of their metabolic activity and therefore can be used to monitor in real time the effects of antimicrobials. Antimicrobial photodynamic therapy (aPDT) is receiving considerable attention for its potentialities as a new antimicrobial treatment modality. This therapy combines oxygen, a nontoxic photoactive photosensitizer, and visible light to generate reactive oxygen species (singlet oxygen and free radicals) that efficiently destroy microorganisms. To monitor this photoinactivation process, faster methods are required instead of laborious conventional plating and overnight incubation procedures. The bioluminescence method is a very interesting approach to achieve this goal. This review covers recent developments on the use of microbial bioluminescence in aPDT in the clinical and environmental areas.

## 8.2 Introduction

In experimental systems, using natural or genetically engineered light-emitting microorganisms, a strong correlation between bioluminescence and viable counts can be demonstrated, configuring bioluminescence measurements as an alternative to the monitoring of microbial viability. As light production is noncumulative when the bioluminescent genes are regulated by constitutive promoters, light production reflects the actual metabolic rate of microbial cells. (419, 420) The measurement is direct, continuous, and nondestructive in high-throughput screening or continuous-culture models. (419) Thus, the use of naturally bioluminescent bacteria as well as the transformation of pathogenic microorganisms with bioluminescent genes from those bacteria turns out a fast, sensitive, and cost-effective methodology to evaluate the effect of antimicrobial agents.

The emergence of microbial resistance to many of the major classes of antimicrobials among several common pathogenic microbial strains is an increasing worldwide problem. The (a) increasing problems with resistance against antibiotics and other antimicrobials, (b) the concern about spreading of antibiotics in the environment due to the inappropriate or excessive prescription, (c) the more and more frequent dissemination of microorganisms due to global traveling, (d) the truly large variety of mechanisms adopted by microbial cells to increase their resistance to external threats, and (e) the diminishing investment of the pharmaceutical industry in research on new antibiotics, turning to more profitable drugs, bring

the need for the development of novel, effective, and inexpensive methods to circumvent microbial diseases.

Antimicrobials photodynamic therapy (aPDT) represents a potentially realistic alternative to antibiotics and to other antibacterial with applications both in the clinical and in the environmental areas. (13)

## 8.3 Bioluminescence

Bioluminescence refers to the process of visible light emission, by enzyme-catalyzed chemical reactions, in living organisms (421), and this production is directly dependent on the metabolic activity of the organism. (422) It can be distinguished from chemoluminescence because it occurs in living organisms and requires an enzyme catalyst. Light-emitting species can be found among bacteria, dinoflagellates, fungi, insects, shrimps, squids, and fish. This set of organisms includes terrestrial, freshwater, and marine species. (423)

There are no luminescent vertebrates (except for certain fish), higher plants, and viruses, except those created by recombinant technology.

### 8.3.1 Bioluminescent bacteria

Luminous bacteria are the most abundant and widely distributed of the light-emitting organisms and are found in marine, freshwater, and terrestrial environments as free-living species, saprophytes, symbionts, or parasites. (424) These bacteria are all Gram-negative motile rods and can function as facultative anaerobes. (425, 426) Almost all luminous bacteria have been assigned to three genera: *Vibrio*, *Photobacterium*, and *Photorhabdus* (formerly *Xenorhabdus*) with most of the species being found in the marine environment. (425, 427) Only *Photorhabdus* species infect terrestrial organisms. (428) Light-emitting *Vibrio harveyi*, *Vibrio fischeri*, *Photobacterium phosphoreum*, *Photobacterium leiognathi*, and *Photorhabdus luminescens* are the most exhaustively studied bacteria. Light production systems from luminescent strains can vary significantly among strains of the same species. (429) Nevertheless, all bacterial luciferases produce a blue-green light with emission peak at 490 nm. (430)

Luminescent bacteria found as symbionts in deepwater fish are primarily *P. phosphoreum*, whereas symbiotic luminescent bacteria of fish in shallow and temperate waters are mostly *P. leiognathi* or *V. fischeri*. (429)

Light production by bacterial symbionts of higher organisms may serve to attract prey, to intra-species communication or to escape from predators. (426) Luminescence provides a

direct benefit to the bacteria. Light emitted by large aggregates of bacteria may attract feeders which ingest them into the nutrient-rich environment of the gut tracts. Another possibility is that the luminescence system is used as a terminal oxidase which allows the cells to dispose of excess reductants at low oxygen concentration. (431) On the other hand, luminescence must have a positive selective value since as much as 20% of the bacterial cell energy is consumed by this process. (432, 433) Some hypotheses on the potential evolutionary origin and biochemical role of bacterial luminescence have been proposed. Bioluminescence has been related to alternative pathways for electron flow, detoxification of generated free radicals, and generation of photons necessary to the photoreactivation systems involving photolyase activity. (421, 426, 434)

## 8.4 Bioluminescence systems

Bioluminescent organisms produce energy that is released by a chemical reaction in the form of light emission. In general, the enzymes that catalyze the bioluminescent reaction are called luciferases and the substrates are luciferins. (435) The luciferin reacts with oxygen to produce light. The luciferase acts as a catalyst to accelerate the reaction, which is sometimes mediated by cofactors such as calcium ions or adenosine-5'-triphosphate (ATP). The structures of the luciferases and of the corresponding genes are not related from one luminescent organism to another. (421) There are also many types of luciferins, e.g., long chain of fatty aldehydes and a reduced form of flavin mononucleotide ($FMNH_2$) for bacteria, benzothiazole luciferin substrate along with ATP for the fireflies, and coelenterazine for the jellyfish *Aequorea*. Consequently, the light-emitting reactions are quite distinct among different organisms, with molecular oxygen as the only common requirement.

### 8.4.1 Bioluminescence systems in bacteria

The light-emitting reaction in bacteria involves the oxidation of a long chain fatty aldehyde and $FMNH_2$ with the emission of blue-green light. (436-440) The reaction is highly specific for $FMNH_2$. The natural aldehyde for the bioluminescence reaction is believed to be tetradecanal considering the identification of this compound in lipid extracts, the preference for tetradecanal by luciferases at low (nonsaturating) substrate concentrations, and the specificity of the *lux*-specific fatty acid reductase system, which catalyzes the synthesis of the fatty aldehyde substrate. (436-440) However, differences in aldehyde specificity do exist among different bacterial luciferases. Particularly important are the high luminescent responses of *V. harveyi* and *P. luminescens* luciferases to nonanal and decanal at saturating

substrate concentrations, whereas higher light intensity can be obtained with dodecanal for *P. phosphoreum*, *P. leiognathi*, and *V. fischeri* luciferases. (441-444) This property may be very important in terms of expression of light emission *in vivo* in cells lacking the aldehyde substrate because decanal appears to cross the cell membrane much more readily than longer chain aldehydes do. (429) Because the reaction involves reducing power ($FMNH_2$), it is dependent on metabolic activity of the bacteria. (422)

In both marine and terrestrial bioluminescent bacteria, a five-gene operon (*luxCDABE*) encodes the luciferase and biosynthetic enzymes (for the synthesis of the aldehyde substrate) necessary for light production. *luxA* and *luxB* genes encode the α and β subunits of the luciferase, with *luxC*, *luxD*, and *luxE* encoding proteins for aldehyde production. (429) Although a number of additional *lux* genes in bioluminescent bacteria have been identified, only *luxCDABE* is essential for the biosynthesis of light. The isolation of the *lux* genes from bioluminescent bacteria responsible for light production and the ability to transfer these genes to prokaryotic and to eukaryotic organisms have expanded the scope and potential uses of bacterial bioluminescence as a safe, rapid, and sensitive sensor for a wide variety of compounds and metabolic processes (421) thus allowing real-time detection of antimicrobial activity. (422)

## 8.5 Effects of chemicals on the bioluminescence encoded by the *lux* operon

Although a strong relation between the growth conditions and the light emission has been reported in the literature for bacterial strains, constitutively expressing the bacterial *lux* operon, some unexpected variations in the rate of light emission have been detected in the presence of different chemicals, even when naturally bioluminescent bacteria are used. (445) As the bacterial bioluminescence involves reducing power ($FMNH_2$), it is dependent of the metabolic activity of the bacteria. So, the presence of chemicals that direct or indirectly alter the concentration of the luciferase substrates, e.g., through changes of equivalents NADH and NADPH, can also enhance light emission or inhibit bioluminescence.

Compounds such as ethanol, trimethoprim, methotrexate, mutagenic compounds, and oxidants such as hydrogen peroxide ($H_2O_2$) enhance light emission. Ethanol is oxidized by the alcohol dehydrogenase enzyme, making bacterial cytoplasm more reduced (446) and enhancing light emission as observed for *Escherichia coli* and *Staphylococcus aureus* strains carrying the *lux* operon under constitutive or inducible control. (447) Trimethoprim and methotrexate inhibit the NADPH-dependent reduction of dihydrofolic acid, driving to the accumulation of NADPH (448), increasing bioluminescence. (447) This effect was observed for

the above mentioned *E. coli* and *S. aureus*. (447) Mutagenic compounds such as sodium azide, 2-methoxy-6-chloro-9-(3-(2-chloroethyl)aminopropylamino) acridine dihydrochloride, 4-nitro-*o*-phenylenediamine, 4-nitroquinolone-*N*-oxide, 2-aminofluorene, and benzo[α]pyrene caused DNA damage and enhanced bacterial bioluminescence of six strains of marine bacteria. (449) The interaction of these compounds with the DNA causes configurational changes of the double helix, resulting in derepression of transcription of the *lux* operon. (450) The presence of $H_2O_2$ may also enhance the activity of bacterial luciferase through a catalase-like reaction, in which the depletion of one atom of oxygen from intermediate II (luciferase-bound FMNH - OOH) by $H_2O_2$ leads to the formation of excited hydroxide (E-FMNH-OH×), $H_2O$, and $O_2$. (451) This effect was reported for various strains of luminescent bacteria and found that luminescence of the different strains was altered. (452)

Chemical compounds such as dimethyl sulfoxide (DMSO) inhibit light production by the *lux* operon. DMSO is metabolized by an NADH-dependent enzyme that reduces the NADH concentration of the bacteria (453), decreasing the light emission as observed once more in *E. coli* and *S. aureus* strains carrying the *lux* operon under constitutive or inducible control. (447)

For cationic porphyrins (e.g., Tri-$Py^+$-Me-PF and Tetra-$Py^+$-Me) tested against the recombinant bioluminescent *E. coli* transformed with *luxCDABE* genes from the marine bioluminescent bacterium *V. fischeri*, light emission in the dark was not affected. (359) In this study, the relation between light emission and colony-forming units was similar in the presence and in the absence of the porphyrin derivatives. However, upon irradiation, these porphyrins produce reactive oxygen species (ROS) that might stimulate the light emission as previously observed for $H_2O_2$. As far as it is known, information about the role of ROS on bioluminescence emission is not available from current literature.

## 8.6 Transformation of microorganisms with bioluminescence genes

The isolation, cloning, and expression of the genes coding for bioluminescence from different luminescent organisms, including marine (*Vibrio* spp.) and terrestrial (*P. luminescens*) bacteria (444, 454-461), fireflies and click beetles (462, 463), the jellyfish (*Aequorea* spp.) (464, 465), and the crustacean ostracod (*Vargula* spp.) (466) have provided the basis for the rapid expansion in the knowledge of the molecular biology of luminescence.

The luciferases from bacteria and from fireflies are now well characterized and cloned, being routinely used in the laboratory. The genes encoding bacterial luciferase of *V. fischeri* and of *P. luminescens* (*luxCDABE* operon) have been expressed successfully in a wide range of Gram-negative bacteria and a redesigned operon has also been used to transform Gram-

positive bacteria (see section 8.7 - Transformation of bacteria). They are generally used to provide autonomous luminescence in bacterial systems, but, ordinarily, they are not useful for analysis in mammalian cells. The gene-encoding firefly luciferase has been optimized for mammalian expression. Luciferase genes from thermolabile bioluminescent bacteria of marine origin which have adapted to a cooler environment (the ocean) emit light preferentially at temperatures below 30 °C (467), while those from terrestrial bacteria *P. luminescens* and from fireflies have the advantage of functioning at higher temperatures (up to 45 °C). (468) Consequently, transformed organisms with the *lux* operon from *P. luminescens* and with the *lux* operon from firefly are ideally suited for the study of pathogens in mammalian animal models as the enzyme retains significant activity at 37 °C. (421)

As the entire *lux* gene operon encoding both the bacterial luciferase and the biosynthetic enzymes for substrate synthesis is transfected, the resulting bacteria are bioluminescent without the need for exogenous administration of luciferin. (469) Contrarily, organisms transformed with firefly genes only emit light when provided with luciferin.

The recognition by researchers in different scientific fields of the ease and sensitivity of detecting light emission from the mentioned organisms has led to the widespread and expanding application of genes coding for luciferases as reporters of gene expression and regulation, as well as sensors of metabolic function in the diverse cells of prokaryotic and eukaryotic organisms.

## 8.7 Transformation of bacteria

The *lux* operon can be easily transferred to a variety of Gram-negative bacteria in order to confer a bioluminescent phenotype. However, because all identified species of naturally occurring marine and terrestrial bioluminescent bacteria are Gram-negative, the transformation of Gram-positive bacteria to a light-emitting phenotype has been somewhat limited due to the differing genetics of these two bacterial groups. Moreover, most bioluminescent Gram-positive bacteria have been generated using bacterial luciferase genes that encode enzymes that are unstable at temperatures above 30 °C. (470) Although such bacteria are useful for environmental studies (as for the assessment of food products contamination), *luxAB* constructs that only allow bioluminescence to occur below 30° C are of limited use for experimentation on pathogenicity carried out at 35 °C and above *in vivo*. (471)

It is possible to generate bioluminescent Gram-positive bacteria capable of producing high levels of light at 37 °C without the addition of an exogenous substrate. The construction of a novel modified *P. luminescens lux* operon involved the introduction of a Gram-positive

ribosome-binding site (Shine–Dalgarno sites) at the start of each *lux* gene for optimal expression and bioluminescence at temperatures above 35 °C. The gene sequence had also to be changed from *luxCDABE* to *luxABCDE* in these constructs. (471) The plasmid DNA with the redesigned operon is functional in both Gram-negative and Gram-positive bacteria (including *S. aureus*, *Streptococcus pneumoniae*, and *Listeria monocytogenes*) allowing several highly bioluminescent strains to be generated.

Among the *lux* operons from bioluminescent bacteria, that from *P. luminescens* (472, 473) appears to be ideally suited for use in mammalian animal models, given that mammalian body temperatures lie within the optimum temperature for the bioluminescent enzymes from this bacterium. (444, 460, 474) This is in contrast to the low optimum temperature for firefly luciferases (luc) and other characterized bacterial luciferases, such as those from *Vibrio* species. (421, 470) Although a large variety of Gram-negative bacteria can be labeled with the *P. luminescens lux* operon, the introduction of this or other bacterial *lux* operons into Gram-positive bacteria results in low or no light emission, regardless of the strength of the promoter controlling this operon.

## 8.8 Antimicrobial photodynamic therapy

aPDT is a new approach to inactivate microorganisms. This methodology is an alternative to conventional antimicrobials and has already proved to be effective *in vitro* against bacteria, viruses, fungi, and protozoa. (10, 13, 136, 197, 326, 475-477) Antimicrobial photodynamic therapy combines a non-toxic photosensitizer (PS) with visible light to generate ROS (singlet oxygen and free radicals) that destroy microbial cells. (211, 238)

Although the main use of PDT has been focused on cancer treatment, the worldwide emergence of antimicrobial resistance among pathogenic microorganisms has led to a major research effort to find alternative antimicrobial therapeutics. (13, 475, 478) The aPDT relies on the accumulated experience in the treatment of malignant tumors by PDT. However, as the delivery of light is a localized process, this application in the clinical area is restricted to localized infections. (218) Contrarily to anti-tumor PDT, where the PS is usually injected into the bloodstream, in aPDT for localized infections, the PS is applied in the infected area by topical application, instillation, interstitial injection, or aerosol delivery. (218)

The research conducted until the present brings forward some of the positive aspects of the use of aPDT in the clinical area: (1) the efficiency of the PS has been proved for different microorganisms at micromolar and nanomolar concentration under different light conditions; (2) PS have, in general, no significant effects on the cells of the infected tissues, the inhibition

of microorganisms occurs, frequently, at concentrations lower that those found to elicit cytotoxic responses in mammalian cells; (3) the effectiveness of the PS depends on the characteristics of the medium where aPDT is intended to occur, therefore whenever planning aPDT *in vivo*, the "sample" type should be specified in order to enable the proper adjustment of concentration and exposure time; (4) the PS are effective to inactivate microbial strains resistant to antimicrobial drugs; and (5) the regrowth of the pathogens after aPDT with different PS, in general, has not been observed. (13, 218)

Although only few studies using the photodynamic process have been conducted in the environmental area, preliminary results obtained at both laboratory and pilot station levels suggest that this photochemical technique has a great potential for field application, namely for use in water disinfection in treatment plants (77, 142, 143, 332, 359, 360) and in fish-farming plants. (140, 141, 369) To implement this technology in the environment, some other aspects less relevant to aPDT in the clinic area need to be taken into consideration, namely: (1) the removal of the PS after photodynamic action to avoid its release to the water output; (2) the determination of the stability of the PS conjugates under solar irradiation conditions; (3) the assessment of the impact of this procedure on the natural non-pathogenic microbial community structure, for instance when this technology is applied in extensive and semi-intensive fish-farming plants; (4) the toxicity of the PS on aquatic organisms (e.g., fish and shellfish) at doses which induce marked mortality of microbial pathogens; (5) the effect of physical and chemical properties of environmental waters on the photodynamic process; and (6) the possibility of using solar light as light source. (13, 140, 141, 369)

### 8.8.1 Advantages of aPDT relatively to conventional antimicrobials

The main advantages of aPDT relatively to conventional antimicrobials are the non-target action and the lack of development of resistance mechanisms due to the mode of action and type of biochemical targets (multi-target process). (136, 479)

The two oxidative mechanisms of photoinactivation involved in the inactivation of the target cells, type I and type II pathways (10, 480), lead to highly ROS such as singlet oxygen, hydrogen peroxide, superoxide, and hydroxyl radical which are able to irreversibly oxidize microorganism vital constituents resulting in lethal damage. (481, 482) Although antioxidant enzymes such as superoxide dismutase, catalase, and peroxidase give protection against some ROS, they do not act against singlet oxygen (483) that, according to the literature, is the main ROS through which the PS exert their photodynamic action. (151, 484-487) Moreover, singlet oxygen has been shown to inactivate these enzymes. (125)

The main targets of the antibacterial and antiviral photodynamic activity are the external microbial structures, as cell walls, cell membranes, protein capsids, lipid envelopes, as well as nucleic acids. (218, 237, 238, 488-492) The damages of the external microbial structures can involve leakage of cellular contents or inactivation of membrane transport systems and enzymes. (227, 228) Some damages produced in the nucleic acid chain can be repaired by the action of DNA repairing systems. (217) It has been concluded that although nucleic acid damage occurs, it cannot be the main cause of microbial photodynamic inactivation. (90, 218, 493)

As in most microorganisms, the main targets of aPDT are the external structures, the PS does not need to enter the microorganism and, consequently, target microorganisms cannot develop resistance by blocking uptake, increasing metabolic detoxification or increasing export of the drug. (479) The studies that tested the possible development of microbial resistance to aPDT (117, 119, 134) proved, as first hypothesized (172, 251, 494-498), that microorganisms are not able to do so. Besides, studies regarding the inactivation of antimicrobial resistant microorganisms by aPDT showed that these microorganisms are equally as susceptible as their native counterparts. (10, 151, 499-504)

## 8.9 Applications of bioluminescence in aPDT

New approaches to evaluate candidate antimicrobials both *in vitro* and *in vivo* are essential to accelerate the development of new drugs. To this end, bioluminescence can provide a sensitive and innocuous way to detect live or viable microorganisms. Furthermore, *in vivo* detection of bioluminescent microorganisms is non-invasive, allowing rapid monitoring of the infective state of eukaryotic cells both in culture and in animals. (471, 505) The *in vivo* monitoring of bioluminescence organisms in living animals has been described for bacteria and for fungi. (471, 506, 507) This approach has been used to screen new PS, to assess the efficiency of aPDT, namely in bacteria, to evaluate the regrowth of microorganisms after aPDT, and to assess the toxicity of the PS in the cells of the infected tissues.

### 8.9.1 Bioluminescent bacteria in aPDT

The efficiency of aPDT for the inactivation of bacteria has been tested using naturally bioluminescent bacteria and also bacteria transformed with the *lux* operon from *V. fischeri* and *P. luminescens*.

In the beginning of 2000, genetically engineered bioluminescent bacteria began to be used as a rapid method of control in studies involving targeted PDT of wound infections in

mice. (508) For preliminary *in vitro* studies, bioluminescence can be measured in a tube luminometer or on a 96-well plate reader. For *in vivo* studies, the light emitted by bacteria can be imaged by optical techniques, namely by the use of an intensified charge-coupled device (ICCD) camera. All of these three techniques allow a real-time measurement of the bioluminescence, therefore monitoring infection status.

Hamblin et al. (508) used *E. coli* transformed with the *lux* operon from *P. luminescens*. (460) After topical application of a polycationic PS (pL-$ce_6$ conjugate, covalently formed between poly-L-lysine and chlorin $e_6$), penetration in the Gram-negative outer bacterial membrane, and the subsequent activation with 660 nm laser light, rapidly killed *E. coli* in infected excisional wounds. There was a light dose-dependent loss of luminescence in the wound treated with conjugate and light, not seen in untreated wounds. Treated wounds healed as well as control wounds, showing that the photodynamic treatment did not damage the host tissue. A similar work used a bioluminescent *P. aeruginosa* transformed by electroporation with the plasmid pCGLS1, an expression vector containing the entire *P. luminescens lux* operon (460), thus allowing again the infection in excisional mouse wounds to be imaged by the use of an ICCD camera. (509)

Demidova et al. (510) monitored the PDT of localized infections in wounds and soft tissue abscesses in mice through bioluminescence imaging, using two Gram-negative bioluminescence strains, *E. coli* and *P. aeruginosa*, and a Gram-positive bioluminescent *S. aureus*. The later was transformed using a *luxABCDE* transposon cassette (Tn4001 *luxABCDE* $Km^r$) that allows random integration of *lux* genes on the bacterial chromosome. (511) Bioluminescent bacteria treated with PDT *in vitro* lost luminescence in parallel with the loss of colony-forming ability. *In vivo*, the size and intensity of the infection could be sequentially monitored in a noninvasive fashion in individual mice in real time. When the PS (pL-$ce_6$ conjugate) was introduced in the infected tissue and illuminated with red light, a light dose-dependent loss of luminescence was observed. With invasive bacteria, the loss of luminescence correlated with increased survival of the mice, in comparison with control animals. The authors concluded that this approach allows the monitoring of localized infections of various animal models and provides an accurate estimate of the efficiency of the PDT treatment.

The photodynamic inactivation of the mouse pathogen *S. aureus* 8325–4 (XEN8.1) transformed with a modified *P. luminescens lux* operon using the Gram-positive *lux* transposon plasmid pAUL-Atn4001 *luxABCDE* $Km^r$ (511), was tested by Lambrechts et al. (512) The therapy mediated by 5-phenyl-10,15,20-tris(1-methylpyridinium-4-yl)porphyrin was used to treat burn wounds in mice with established *S. aureus* infections. Third degree burn wounds were infected

with the bioluminescent *S. aureus* and PS was applied after 1 day of bacterial growth followed by illumination with red light and periodic imaging of the mice using an ICCD camera to detect light emission. The results showed that more than 98% of the bacteria were eradicated after a light dose of 211 J $cm^{-2}$ in the presence of the porphyrin. However, bioluminescent bacterial regrowth was observed, indicating that the treatment needs to be optimized to prevent recurrence.

The efficiency of aPDT to eliminate bacterial biofilms was also evaluated (135) using *P. aeruginosa* (XEN5) and *Proteus mirabilis* (XEN44) that had been engineered by transformation with a transposon containing the entire *P. luminescens lux* operon in order to be stably bioluminescent. (513) aPDT combined with conventional endodontic treatment was used to eliminate root canal biofilm infection. Single-rooted freshly extracted human teeth were inoculated with the mentioned bioluminescent strains to form 3-day biofilms in prepared root canals. Bioluminescence imaging was used to serially quantify bacterial burdens. aPDT employed a conjugate between polyethylenimine and chlorin ($ce_6$) as PS and a 660-nm diode laser light delivered into the root canal, using a light energy of 9.6 J $cm^{-2}$. Endodontic therapy alone reduced bacterial bioluminescence by 90%, while aPDT alone reduced bioluminescence by 95%. The combination reduced bioluminescence by 98%, and the bacterial regrowth observed 24 h after treatment was much less for the combination than for either single treatment. Bioluminescence imaging was considered an efficient way to monitor endodontic therapy and aPDT to possibly have a role to play in optimized endodontic therapy.

For the evaluation of aPDT against *Acinetobacter baumannii* burn infections in mice (514), a new mouse model of infected full-thickness thermal burns and a bioluminescent derivative of a clinical multi-drug resistant isolate of *A. baumannii* transformed with the plasmid pMF 385 containing *P. luminescens luxCDABE* operon were used. (474) The covalent conjugation chlorin ($ce_6$) with polyethylenimine was topically applied, followed by illumination of the burn surface with red light. A remarkably stable bacterial bioluminescence indicated that a chronic infection was established lasting, on average, 22 days. aPDT carried out on day 0, soon after application of the bacteria, gave over 3 $\log_{10}$ units loss of bacterial luminescence in a light exposure-dependent manner, while aPDT carried out on days 1 and 2 gave an approximately 1.7 $\log_{10}$ reduction. The application of PS without light gave only a modest reduction in the bacterial luminescence from mouse burns. A modest regrowth of the bioluminescent bacteria was observed in the treated burn wound.

More recently, bioluminescent bacteria have been used in studies focused on the application of photodynamic process in the environment, namely in water disinfection. A recombinant bioluminescent *E. coli* was used to evaluate its *in vitro* photoinactivation by three

cationic *meso*-substituted porphyrins under artificial (40 W $m^{-2}$) and solar irradiation (≈ 620 W $m^{-2}$). (359) Plasmids pHK724 and pHK555 which contained *lux* genes (*luxCDABE* operon and *luxR* gene) from *V. fischeri* (515, 516) were cloned in *E. coli* cells. Photoinactivation of *E. coli* was detected by a decrease of more than 4 $\log_{10}$ in bioluminescence (the detection limit of the method used) using the three porphyrins, being the tricationic porphyrin 5-(pentafluorophenyl)-10,15,20-tris(1-methylpyridinium-4-yl)porphyrin tri-iodide (Tri-$Py^{+}$-Me-PF) the most effective PS. The results obtained showed that the photoinactivation process is faster and more efficient with solar irradiation than with artificial light. The authors concluded that the bioluminescence-based method is effective and sensitive and also simpler, faster, more cost effective, and much less laborious than the conventional plating method with interest as a screening method for *in vitro* studies of bacterial photoinactivation.

The naturally bioluminescent marine bacterium *V. fischeri* was also used to evaluate the efficiency of the same porphyrin, Tri-$Py^{+}$-Me-PF, in the disinfection of aquaculture water. (140) The influence of temperature, pH, salinity, oxygen concentration, and suspended solids on the photoinactivation process was studied *in vitro* and the efficiency of *in situ* inactivation was assessed using samples of aquaculture water. The process was monitored by measuring *V. fischeri* light emission during the experiments. The variations in pH, temperature, salinity, or oxygen concentration in aquaculture waters did not affect the efficiency of the photoinactivation of *V. fischeri*, since the detection limit of the method (≈ 7 $\log_{10}$ bioluminescence decrease) was reached. The bioluminescence monitoring during the assays using aquaculture water indicate that the complete inactivation of *V. fischeri* is dependent on water composition (suspended matter), PS concentration, and light fluence. (140) Once more, the measurement of bacterial bioluminescence proved to be a useful tool in the monitoring of the photoinactivation process.

## 8.10 Conclusions

The considerable efforts put in the study of the molecular biology of bioluminescence during the last three decades have led to a great advance in the discovery of luciferase coding genes, their regulation and expression. This knowledge associated with the advances on the genetic engineering provided bioluminescent microorganisms which have been used in aPDT.

The *lux* system has been used to monitor aPDT in bacteria and the firefly luciferase-coding genes for study aPDT in viruses. The *P. luminescens lux* operon has been the most used in aPDT studies. Although this operon has been referred as inadequate for experiments with mammalian cells, aPDT assays using several models of infections caused by bacteria

transformed with this operon in wounds and soft tissue abscesses in mice has been successful monitored by bioluminescence imaging. The size and intensity of the infection after aPDT can be sequentially monitored in a non-invasive approach in individual mice in real time.

Although the presence of chemicals affects light emission in bacteria, photosensitizers do not seem to interfere with the bioluminescence emission in dark conditions. However, during the photoinactivation process, in the presence of light, $H_2O_2$ can enhance light emission. As the main ROS involved in the photoinactivation of microorganisms is the singlet oxygen, which has not been reported as interfering with light emission, the bioluminescent method can still be regarded as a valuable tool in the evaluation of the efficiency of the aPDT approaches.

# Chapter 9. Photodynamic antimicrobial chemotherapy in aquaculture: photoinactivation studies of *Vibrio fischeri*

The content of this chapter has been published as:
Alves E, Faustino MAF, Tomé JPC, Neves MGPMS, Tomé AC, Cavaleiro JAS, et al. Photodynamic antimicrobial chemotherapy in aquaculture: photoinactivation studies of *Vibrio fischeri*. PLoS One. 2011;6(6):e20970.

# 9 Photodynamic antimicrobial chemotherapy in aquaculture: photoinactivation studies of *Vibrio fischeri*

## 9.1 Abstract

Photodynamic antimicrobial chemotherapy (PACT) combines light, a light-absorbing molecule that initiates a photochemical or photophysical reaction, and oxygen. The combined action of these three components originates reactive oxygen species that lead to microorganisms' destruction. The aim was to evaluate the efficiency of PACT on *Vibrio fischeri*: 1) with buffer solution, varying temperature, pH, salinity and oxygen concentration values; 2) with aquaculture water, to reproduce photoinactivation (PI) conditions *in situ*.

To monitor the PI kinetics, the bioluminescence of *V. fischeri* was measured during the experiments. A tricationic *meso*-substituted porphyrin (Tri-Py$^{+}$-Me-PF) was used as photosensitizer (5 μM in the studies with buffer solution and 10 - 50 μM in the studies with aquaculture water); artificial white light (4 mW cm$^{-2}$) and solar irradiation (40 mW cm$^{-2}$) were used as light sources; and the bacterial concentration used for all experiments was ≈ $10^{7}$ CFU mL$^{-1}$ (corresponding to a bioluminescence level of $10^{5}$ relative light units - RLU). The variations in pH (6.5 - 8.5), temperature (10 - 25 °C), salinity (20 - 40 g L$^{-1}$) and oxygen concentration did not significantly affect the PI of *V. fischeri*, once in all tested conditions the bioluminescent signal decreased to the detection limit of the method (≈ 7 log reduction). The assays using aquaculture water showed that the efficiency of the process is affected by the suspended matter. Total PI of *V. fischeri* in aquaculture water was achieved under solar light in the presence of 20 μM of Tri-Py$^{+}$-Me-PF.

If PACT is to be used in environmental applications, the matrix containing target microbial communities should be previously characterized in order to establish an efficient protocol having into account the photosensitizer concentration, the light source and the total light dose delivered. The possibility of using solar light in PACT to treat aquaculture water makes this technology cost-effective and attractive.

## 9.2 Introduction

Aquaculture is an important and rapidly growing industry of intensive seafood production that contributes to global supplies of fish, crustaceans and mollusks. (517) It has grown faster than all other food animal-producing sectors. Modern aquaculture has been threatened by mass mortality due to several bacterial and viral infections in larvae, juveniles

(518) and in fish, namely vibriosis, photobacteriosis, furunculosis, among others (519-523), and also due to lack of control of the microbiota in rearing systems. (517)

To prevent diseases, antibiotics and/or vaccines are administrated to fish, but the use of antibiotics in aquatic ecosystems is presently kept to a minimum, and commercially available vaccines are still very limited in the aquaculture field. (524-526) Vaccinated fishes appear to grow and survive better than their unvaccinated counterparts, however the exact nature of the immunity provided is not clear. (517, 525) Moreover, vaccination is not possible in the case of fish larvae, which generally are most susceptible to disease, because it is practically unfeasible to handle these small animals and also because it is believed that fish larvae do not have the ability to develop specific immunity. (527) On the other side, the use of large amounts of a wide variety of antibiotics, including non-biodegradable ones, results in their accumulation in the aquatic environment which exerts a selective pressure for long periods of time. (528) This process has raised several problems: a) the emergence of antibiotic-resistant bacteria in aquaculture environments; b) the increase of antibiotic resistance in fish pathogens; c) the transfer of these resistance determinants to bacteria of land animals and to human pathogens; and d) in alterations of the bacterial flora both in sediments and in water column. (528)

Alternatives to antibiotics and vaccines in the prevention of fish diseases include phage therapy (529), the use of short-chain fatty acids (530), polyhydroxyalkanoates (531), quorum-sensing disruption (532), probiotics (521), and the addition of microalgae to the water system as an enhancement, not as a direct food source. (533) Recently, photodynamic antimicrobial chemotherapy (PACT) was mentioned as an alternative technology for the disinfection of polluted waters from fish-farming ponds. (369) This technology combines light, a light-absorbing molecule called photosensitizer (PS) that initiates a photochemical or photophysical reaction, and oxygen. These three components are responsible for the formation of reactive oxygen species (singlet oxygen and/or free radicals) that lead to microorganism photoinactivation (PI). (197) The efficiency of PACT to disinfect drinking (360) and wastewaters (326, 332) has been proved by laboratory tests using microbial faecal pollution indicators. If PACT is to be applied in the environment, solar light can be used as light source. Furthermore, with respect to aquacultures, it has been demonstrated that porphyrins used as PS show no significant toxicity toward higher organisms (as fishes) at photochemically active doses (namely, in the micromolar concentration range) (369), once they were approved as food additives (401) or phototherapeutic agents for some human diseases. (534-537) Another advantage of using porphyrins is that their excessive accumulation in the environment is unlikely to occur, because of their gradual photobleaching by solar light. (538) However, the

idea is to use solar light and functional cationic nanomagnet-porphyrin hybrids (198) to disinfect the water from aquacultures previously to its contact with fish, preventing the disturbance on the balance between microbial communities (517), or the proliferation of opportunistic bacteria or unpredictable development of bacterial communities. (517) The immobilization of the porphyrin allows its recovery and reuse, avoiding the ingestion by fish and also the release to the water output.

Although it has been shown that PI by porphyrins appears to represent a very useful and flexible tool for the decontamination of microbiologically polluted waters (369), the effect of physical and chemical properties of aquaculture waters on the efficiency of this technology, as well as the use of aquaculture water samples for microbial PI studies, have never been reported. On the other hand, most of the studies about the influence of physical-chemical parameters on the PI of cells are clinically oriented (539-541), and those which are applied to the environment use different cell types (331) or methods of water treatment. (542)

This study aimed to evaluate a) the influence of the pH, temperature, salinity, and oxygen concentration on the PI of the light emitting Gram-negative bacterium *Vibrio fischeri* under controlled experimental conditions, and b) how the PI of *V. fischeri* is affected by using aquaculture water samples, under artificial white light and solar light.

The tricationic *meso*-substituted porphyrin 5,10,15-tris(1-methylpyridinium-4-yl)-20-(pentafluorophenyl)porphyrin tri-iodide (Tri-Py$^{+}$-Me-PF) was selected as PS. This porphyrin, already described by our group, has shown promising results on the PI of several types of microorganisms. (326)

## 9.3 Material and Methods

### 9.3.1 Photosensitizer

5,10,15-tris(1-methylpyridinium-4-yl)-20-(pentafluorophenyl)porphyrin tri-iodide, Tri-Py$^{+}$-Me-PF (Figure 9.1) was prepared according to the literature. (172, 173) A stock solution of Tri-Py$^{+}$-Me-PF in DMSO at 500 µM was prepared, divided into aliquots of 1.5 mL and maintained at 4 °C. Before each PI assay, the porphyrin aliquot to be used was stirred at 120 rpm, until room temperature (25 °C) was reached.

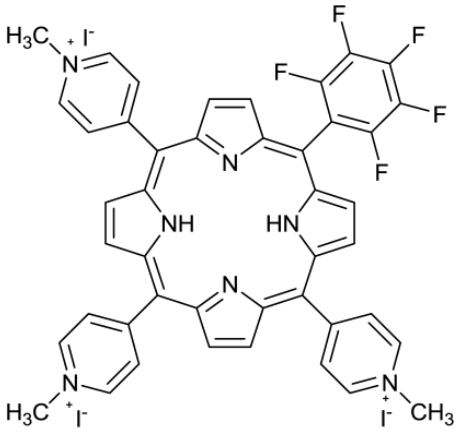

**Figure 9.1** Structure of the 5,10,15-tris(1-methylpyridinium-4-yl)-20-(pentafluorophenyl)porphyrin tri-iodide.

### 9.3.2 Bacterial strain and growth conditions

The bacterial model used in this work was the marine bioluminescent bacterium *V. fischeri* ATCC 49387 (USA). Cells were stored at -80 °C in 10% glycerol. Fresh plate cultures of *V. fischeri* were maintained in solid BOSS medium at 4 °C (BOSS medium: 1% peptone, 0.3% beef extract, 0.1% glycerol, 3% NaCl, 1.5% agar, pH 7.3). (543) A concentration of 20 - 40 g $L^{-1}$ of NaCl is necessary to maintain the osmotic pressure of cells required to natural light emission to occur.

Before each assay, one isolated colony was aseptically inoculated in 30 mL of liquid BOSS medium and grew for one day at 25 °C under stirring (120 rpm). An aliquot of this culture (240 µL) was subcultured in 30 mL of BOSS medium and grew overnight at 25 °C under stirring (120 rpm) to reach an optical density ($OD_{620}$) of ≈ 1.0, corresponding to ≈ $10^8$ cells $mL^{-1}$.

### 9.3.3 Correlation between bioluminescence and colony-forming units

To evaluate the correlation between the colony-forming units (CFU) and the bioluminescent signal (in relative light units, RLU) of *V. fischeri*, the assays were carried out in dark conditions, with and without Tri-$Py^+$-Me-PF. These correlations are similar in the presence and in the absence of Tri-$Py^+$-Me-PF, and the bioluminescence results reflect the viable bacterial abundance as it is shown in Figure 9.2. These results were already demonstrated in a previous work. (119) In this study, BOSS medium was used instead of tryptic soy medium supplemented with 30 g $L^{-1}$ NaCl because the growth rate of *V. fischeri* in BOSS medium is slightly higher.

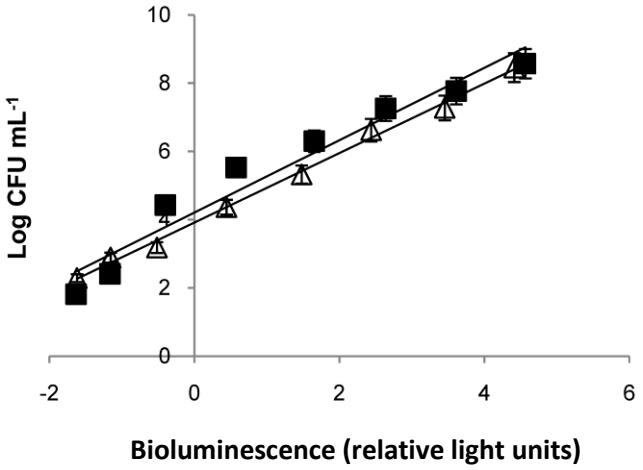


**Figure 9.2** Relationship between the bioluminescence signal and viable counts of an overnight culture of *V. fischeri* (≈ $10^9$ CFU $mL^{-1}$) serially diluted in PBS with 3% of NaCl. Bioluminescence is expressed in relative light units (RLU) and viable counts in CFU $mL^{-1}$. Bacterial suspension in the absence of PS (unfilled triangle), $R^2$=0,9957; bacterial suspension with 5 µM of Tri-$Py^+$-Me-PF incubated 4h in the dark (black square), $R^2$=0,9495. Values represent the mean of two independent experiments; error bars indicate the standard deviation.

### 9.3.4 Irradiation conditions

In the assays using artificial light, the samples were exposed to white light (photosynthetically active radiation, i.e., the spectral range of solar irradiation from 380 to 700 nm, consisting in 13 OSRAM lamps 21 - 840, of 18 W each) with a fluence rate of 4 mW $cm^{-2}$, for 270 min (total light dose of 64.8 J $cm^{-2}$), under 100 rpm.

The assays using solar light were carried out outside the laboratory. Samples were exposed to solar light in two autumn sunny days, where the averaged light fluence rate was 40 mW $cm^{-2}$ measured with a laser power and energy meter (FieldMaxII-TOP, Coherent Inc., USA), for 27 min (total light dose of 64.8 J $cm^{-2}$), under 100 rpm. Ultraviolet radiation was not filtered in order to test the real field conditions. The beakers were only protected by cling film, except the dark controls.

As *V. fischeri* emits light at temperatures below 30 °C, the beakers with the samples were always placed in a water bath in order to maintain a constant temperature (25 °C), except when the effect of temperature was addressed.

### 9.3.5 Photoinactivation assays in buffer solution

In all assays, an overnight culture of *V. fischeri* was used after a tenfold dilution in phosphate buffered saline (PBS) with 30 g $L^{-1}$ of NaCl (PBS: 30 g NaCl, 0.2 g KCl, 1.44 g $Na_2HPO_4$ and 0.24 g $KH_2PO_4$ per litre; pH 7.4) to achieve a final concentration of $10^7$ CFU $mL^{-1}$. This

bacterial suspension was equally distributed in 100 mL sterilized and acid-washed glass beakers. Then, appropriate amounts of the porphyrin Tri-$Py^{+}$-Me-PF were added to achieve a final concentration of 5 μM (total volume was 20 mL per beaker). After distribution in the beakers and after adding the porphyrin, all the samples were wrapped with aluminium foil to protect from light exposure and incubated for 10 min under 100 rpm stirring, at 25 °C, to promote the porphyrin binding to *Vibrio* cells (pre-irradiation incubation procedure). Then, the mixtures were exposed to artificial white light (4 mW $cm^{-2}$) for 270 min. Aliquots of treated and control samples were collected at time 0 and after 30, 60, 90, 120, 150, 180 and 270 min of light exposure and the bioluminescence signal was measured in a luminometer (peak wavelength detected at 420 nm, standard range: 300 - 650 nm) (TD-20/20 Luminometer, Turner Designs, Inc., USA). All experiments were done in duplicate and the results were averaged.

Light and dark controls were carried out simultaneously during the experiments. The light control corresponded to the bacterial suspension without porphyrin that was exposed to similar irradiation conditions as the tests. The dark control corresponded to the bacterial suspension plus 5 μM of porphyrin but protected from light during the irradiation time by wrapping the beaker with aluminium foil. Both controls followed the pre-irradiation incubation procedure.

Having into account the annual variability of pH (6.5 - 7.5), temperature (13 - 22 °C), salinity (10 - 35 g $L^{-1}$) and oxygen concentration (2 - 6 mg $L^{-1}$) values in the fish-farm Corte das Freiras (Aveiro, Portugal, 40°N; 8°W) (personal data), and the optimum light emission conditions for *V. fischeri in vitro* (25 °C, pH 7.4 and 30 g $L^{-1}$ NaCl), the PI assays were designed to independently test each of the mentioned parameters.

#### 9.3.5.1 pH

In order to evaluate the pH effect in the PI assays, overnight cultures of *V. fischeri* were tenfold diluted in PBS solutions with pH ranging from 6.5 to 8.5. During these experiments, the temperature of the samples was kept at 25 °C and the NaCl concentration of PBS was 30 g $L^{-1}$.

#### 9.3.5.2 Temperature

To evaluate the effect of temperature in the PI assays, the samples were maintained in a refrigerated recirculation bath (FRIGITERM-10, JP Selecta S.A., Spain). During the exposure to irradiation, temperature was kept constant at 10, 15, 20 and 25 °C. The pH of the suspension during experiments was 7.4 and the NaCl concentration of PBS was 30 g $L^{-1}$.

#### 9.3.5.3 Salinity

To assess the effect of salinity, the concentration of NaCl in the PBS used for the bacterial suspension ranged from 20 to 40 g $L^{-1}$ (or 2% - 4% of NaCl). During these experiments the temperature of the samples was kept at 25 °C and pH was 7.4.

#### 9.3.5.4 Oxygen concentration

To evaluate the effect of oxygen concentration in the PI kinetics, PI assays were carried out with and without stirring. Oxygen concentration was measured with a portable oximeter (Oxi 340i/SET, WTW GmbH, Germany). During the experiments, temperature was kept at 25 °C, NaCl concentration was 30 g $L^{-1}$ and pH was 7.4.

### 9.3.6 Photoinactivation assays in aquaculture water with artificial white light

In the assays using aquaculture water, the water samples were collected in a fish-farm tank in different occasions (May and June 2010). Temperature, salinity (Cond 330i/SET, WTW, Germany) and oxygen concentration (Oxi 197, WTW GmbH, Germany) were directly measured in the tank. Water samples were collected with a bucket and transferred to sterilized 600 mL Duran® reagent bottles (Schott, UK) (ca. 400 mL per bottle). The pH value was measured later in the laboratory (pH meter Orion Model 290A, Orion Research Inc, USA).

In the laboratory, water samples were treated as previously described for PBS assays (i.e., as suspension medium for *V. fischeri*), in order to assess the influence of the suspended solids on the PI of this strain. The samples were divided into fractions, from which particulate material was selectively removed: one fraction (100 mL) was kept intact without removal of particles (non-filtered water); a second fraction (200 mL) was filtered through a 0.7 µm porosity GF glass microfiber filter (Whatman, England), and a third fraction was obtained by further filtering 100 mL from the 0.7 µm-filtered water through a 0.2 µm porosity GE polycarbonate membrane filter (Osmonics Labstore, USA). The non-filtered fraction contained the total suspended solids in the aquaculture water as well as the microbial community. From the 0.7 µm-filtered fraction particulate organic matter was removed and the 0.2 µm-filtered fraction did not contain neither particulate organic matter nor bacterial cells. To each of the fractions, the *V. fischeri* culture was added ($10^7$ CFU $mL^{-1}$ as mentioned above) and the PI was tested using the following concentrations of porphyrin: 5 µM, 10 µM, 20 µM and 50 µM. Cell suspensions were exposed to artificial white light (4 mW $cm^{-2}$) for 270 min. Aliquots of the different treatments and controls were collected at different time intervals of light exposure and the bioluminescence signal was measured in the luminometer. All experiments were

performed in duplicate and the results were averaged. Light and dark controls, prepared as described for the PBS experiments, were included.

### 9.3.7 Photoinactivation assays in aquaculture water with different light sources

In order to compare the kinetics of the PI of *V. fischeri* in aquaculture water using two different light sources (artificial white light and solar light), PI experiments were carried out with non-filtered aquaculture water, under solar light. The kinetics of *V. fischeri* inactivation on a non-filtered matrix was compared with that obtained with artificial white light, using the same total light dose.

For these studies, the water samples were collected in October 2010, following the same procedure mentioned above, using 20 μM of porphyrin. The cell suspensions were exposed to the light sources and aliquots of treated and control samples were collected at time intervals corresponding to total light doses of 7.2, 14.4, 21.6, 43.2 and 64.8 J $cm^{-2}$ for measurement of the bioluminescence signal. Experiments were performed in duplicate and the results were averaged. Light and dark controls were included.

### 9.3.8 Statistical analysis

All experiments were conducted in duplicate and averaged. Statistical analysis was performed by using SPSS (SPSS 15.0 for Windows, SPSS Inc., USA). Normal distributions were assessed by Kolmogorov-Smirnov test and homogeneity of variances was assessed by Levene test. The significance of difference in *V. fischeri* PI in each experimental condition was assessed by one-way analysis of variance (ANOVA) model with the Bonferroni post-hoc test. A value of $p < 0.05$ was considered significant.

## 9.4 Results

### 9.4.1 Photoinactivation assays in buffer solution

In order to evaluate the influence of the pH, temperature, salinity and oxygen concentration on the PI of *V. fischeri*, light and dark controls were carried out for all the experiments including for each value of the variables. These control samples showed no variability on the bioluminescence during all the PI process. This means that, for each parameter tested, the bioluminescence light emission from *V. fischeri* cells is not affected, neither when cells are suspended in PBS and irradiated for 270 min (light control), nor when cells are suspended in PBS in the presence of PS but protected from light for 270 min. It is

worth to refer that the bioluminescent method only detects the presence or absence of viable *Vibrio* cells. To facilitate the interpretation of the results in the figures, light and dark controls are represented for only one value, within each variable (6.5 for pH assays, 15 °C for temperature assays, and 20 g $L^{-1}$ NaCl for salinity assays). Data from the other control values are not shown, but are similar.

#### 9.4.1.1 pH

The photodynamic inactivation of *V. fischeri* is not affected by pH within the range of 6.5 to 8.5 (Figure 9.3). After 90 min of irradiation, the decrease of the bioluminescence signal to the detection limit of the method was achieved for all pH values tested. However, at physiological pH value (7.4), the PI is slightly faster (≈ 7 log decrease after 60 min of irradiation) than for other pH values, and statistically different from pH 8.0 ($p < 0.05$, ANOVA).

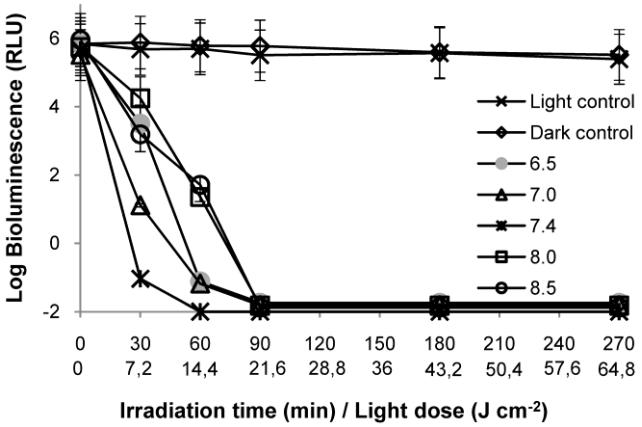


**Figure 9.3** Photoinactivation of *V. fischeri* with 5 µM of Tri-$Py^{+}$-Me-PF at different pH values of the suspension medium, under 4 mW $cm^{-2}$ irradiation. Values represent the mean of two independent experiments; error bars indicate the standard deviation.

#### 9.4.1.2 Temperature

At 25 °C, the PI process occurred faster than for the other incubation temperatures, reaching the limit of detection after 30 min of irradiation (Figure 9.4). However, at 20 °C the decrease in cell survival is slightly faster than for the lower incubation temperatures 10 °C and 15 °C (≈ 4.5 log reduction after 60 min of irradiation), being this difference statistically significant ($p < 0.05$, ANOVA). The decrease of the *V. fischeri* bioluminescence signal reached the detection limit of the method (≈ 7 log reduction) after 180 min of irradiation for all the temperatures tested (10 - 25 °C).

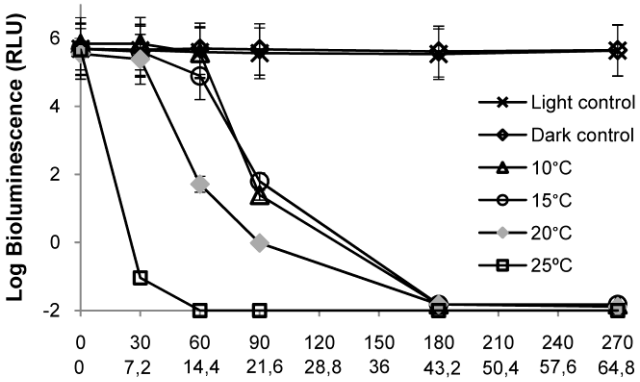


**Figure 9.4** Photoinactivation of *V. fischeri* with 5 µM of Tri-Py$^{+}$-Me-PF at different temperatures of the suspension medium, under 4 mW cm$^{-2}$ irradiation. Values represent the mean of two independent experiments; error bars indicate the standard deviation.

#### 9.4.1.3 Salinity

The photodynamic assays in different concentrations of NaCl (20 and 40 g L$^{-1}$) showed that, after 60 min of irradiation, a reduction of ≈ 7 log on the *V. fischeri* bioluminescence was achieved (Figure 9.5). In fact, significant differences in the PI of cell suspensions for different salinity values were not detected ($p > 0.05$, ANOVA).

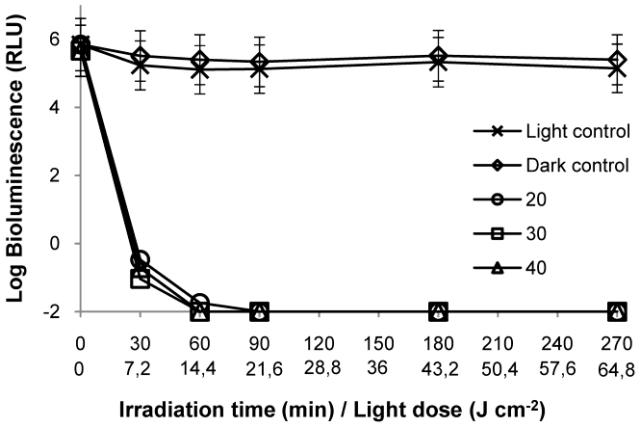


**Figure 9.5** Photoinactivation of *V. fischeri* with 5 µM of Tri-Py$^{+}$-Me-PF at different concentrations of NaCl (in g L$^{-1}$) in the suspension medium, under 4 mW cm$^{-2}$ irradiation. Values represent the mean of two independent experiments; error bars indicate the standard deviation.

#### 9.4.1.4 Oxygen concentration

The values of oxygen concentration found during the PI experiments showed that the range is realistic and compatible with that measured in the fish farm tanks (2 - 6 mg L$^{-1}$). The average value of oxygen concentration during the PI assays at 5 µM of PS with stirring was 5.9 mg L$^{-1}$ and without stirring was 5.3 mg L$^{-1}$. This difference does not affect the PI efficiency, being the decreasing profile of bioluminescence signal similar under stirring (Figure 9.3, pH 7.4, 25 °C and 30 g L$^{-1}$) and without stirring (data not shown).

### 9.4.2 Photoinactivation assays in aquaculture water

#### 9.4.2.1 Assays with artificial white light

In the first assay using water samples from the aquaculture, 5 µM of PI was not sufficient to inactivate *V. fischeri* after 270 min of irradiation, even in filtered sub-samples (the obtained results at this porphyrin concentration are very similar to control samples, so they are not shown). Consequently, higher porphyrin concentrations (10 µM, 20 µM and 50 µM) were used in the following assays.

The values of the physical-chemical parameters measured in the field (May and June, respectively) were: temperature (17.2 °C and 21.1 °C); salinity (33.3 g $L^{-1}$ and 34.3 g $L^{-1}$); dissolved oxygen (7.8 mg $L^{-1}$ and 6.0 mg $L^{-1}$); and pH (8.42 and 8.39).

For all the water matrices used (non-filtered and filtered), light controls showed that the light emission from bacteria was not affected by the suspended solids present in the water. Dark controls showed that the concentration of 50 µM of PS was not toxic for this bacterium, once the bioluminescence values were not affected during all these experiments (Figure 9.6 and Figure 9.7).

The results of PI of *V. fischeri* using non-filtered water as suspension medium showed that bioluminescence only decreased to the detection limit of the method after 270 min of irradiation with artificial white light (4 mW $cm^{-2}$) and using the highest concentration of PS (50 µM) (Figures 9.6A and 9.7A). This concentration was ten times higher than that used in the assays with PBS. Under these conditions, the other two concentrations of PS (10 µM and 20 µM) were not sufficient to destroy all *V. fischeri* cells, in the presence of suspended solids ($p < 0.05$, ANOVA).

The results of the PI of *V. fischeri* using aquaculture water filtered by a 0.7 µm membrane as suspension medium revealed that a decrease of ≈ 7 log on bioluminescence signal was achieved for a concentration of 50 µM of PS after 270 min of irradiation (Figures 9.6B and 9.7B). At the lower PS concentrations (10 µM and 20 µM), the efficiency of the PI was variable between assays. In the May assay, the PS was able to inactivate by more than 7 log after 270 min of irradiation without significant difference between the three concentrations ($p > 0.05$, ANOVA). In the June assay (Figure 9.7B), there are still significant differences ($p < 0.05$, ANOVA) among the three concentrations, after 270 min of irradiation, being the lowest ones inefficient for the total inactivation of *V. fischeri*.

The results obtained from the PI assays using aquaculture water filtered by a 0.2 µm membrane as suspension medium indicated that, for the highest concentration of PS (50 µM), the PI kinetics was similar in the two assays (Figures 9.6C and 9.7C). For the lowest

concentrations (10 µM and 20 µM), the bioluminescence signal decreased to the detection limit of the method after 270 min of irradiation, although the PI profile was steeper in the June sampling (Figures 9.6C and 9.7C).

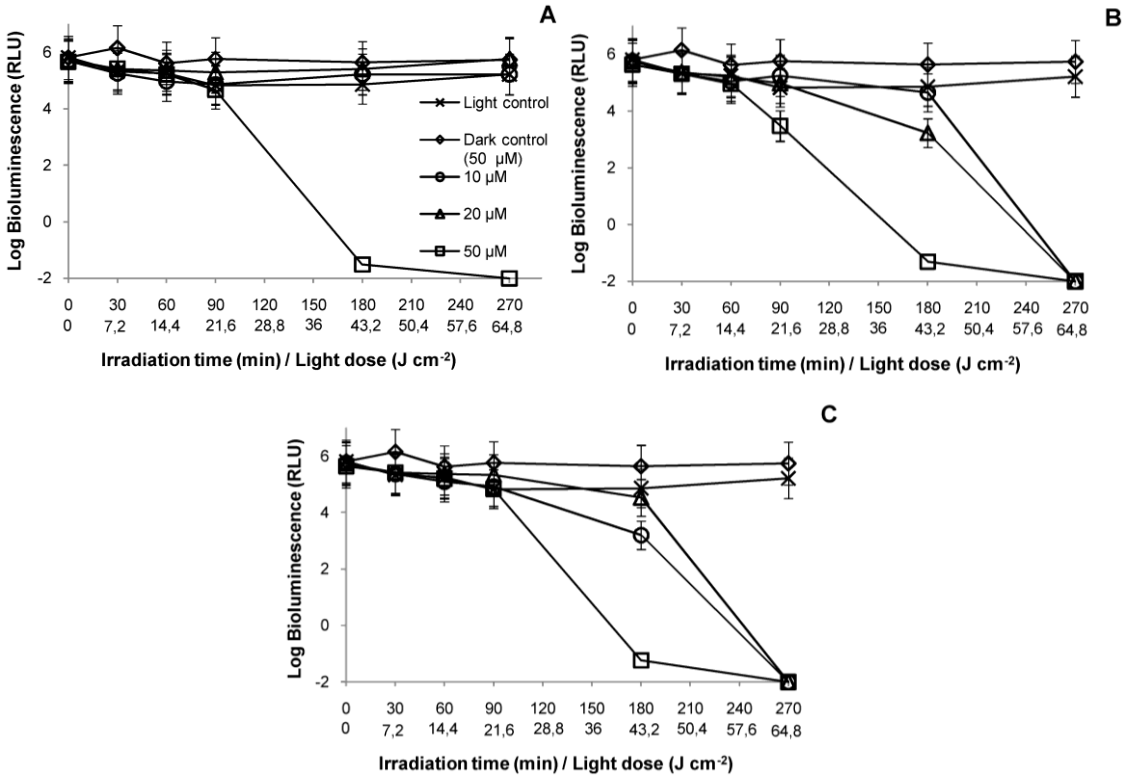


**Figure 9.6** Photoinactivation of *V. fischeri* with Tri-Py$^{+}$-Me-PF at 10, 20 and 50 µM, in an aquaculture water sample collected in May 2010, under 4 mW cm$^{-2}$ irradiation. **A**: non-filtered portion; **B**: portion filtered by 0.7 µm membrane; **C**: portion filtered by 0.2 µm membrane. Values represent the mean of two replicates of the same sample; error bars indicate the standard deviation.

The highest PS concentration (50 µM) of PS was necessary to completely inactivate *V. fischeri* cells in all sample fractions (between 180 and 270 min). For the water fractions without particulate matter (samples filtered by a 0.7 µm membrane), and without particulate matter and bacterial cells (samples filtered by 0.2 µm membrane), the complete PI of *V. fischeri* using 10 µM or 20 µM was variable but achievable after 270 min and a total light dose of 64.8 J cm$^{-2}$ (except for the case seen in Figure 9.7B).

#### 9.4.2.2 Assays with artificial light sources

The physical-chemical properties of the aquaculture water collected for the PI experiments conducted with solar light (≈ 40 mW cm$^{-2}$, between 10:00 a.m. and 11:30 a.m., with the sun at the azimuth and elevation range of [130°; 160°] and [30°; 40°], respectively) and with artificial white light (4 mW cm$^{-2}$) (for comparison) were: temperature, salinity, oxygen concentration, and pH values were, respectively: 18.1°C; 34.1 g L$^{-1}$, 5.3 mg L$^{-1}$ and 7.8.

The results obtained with 20 µM of porphyrin show that, using the same total light dose (64.8 J $cm^{-2}$), both light sources (artificial white light or solar light) can inactivate *V. fischeri* to the detection limit (Figure 9.8). However, for lower light doses (e.g., 43.2 J $cm^{-2}$), the PI rate was higher with artificial white light. As it can be seen, there is a significant difference ($p < 0.05$, ANOVA) between the PI profiles at the light dose 43.2 J $cm^{-2}$. Control samples did not showed variation in the emission of bioluminescence, indicating that only solar light alone (including total spectrum) or the presence of the 20 µM of PS in the dark do not affect *V. fischeri* viability.

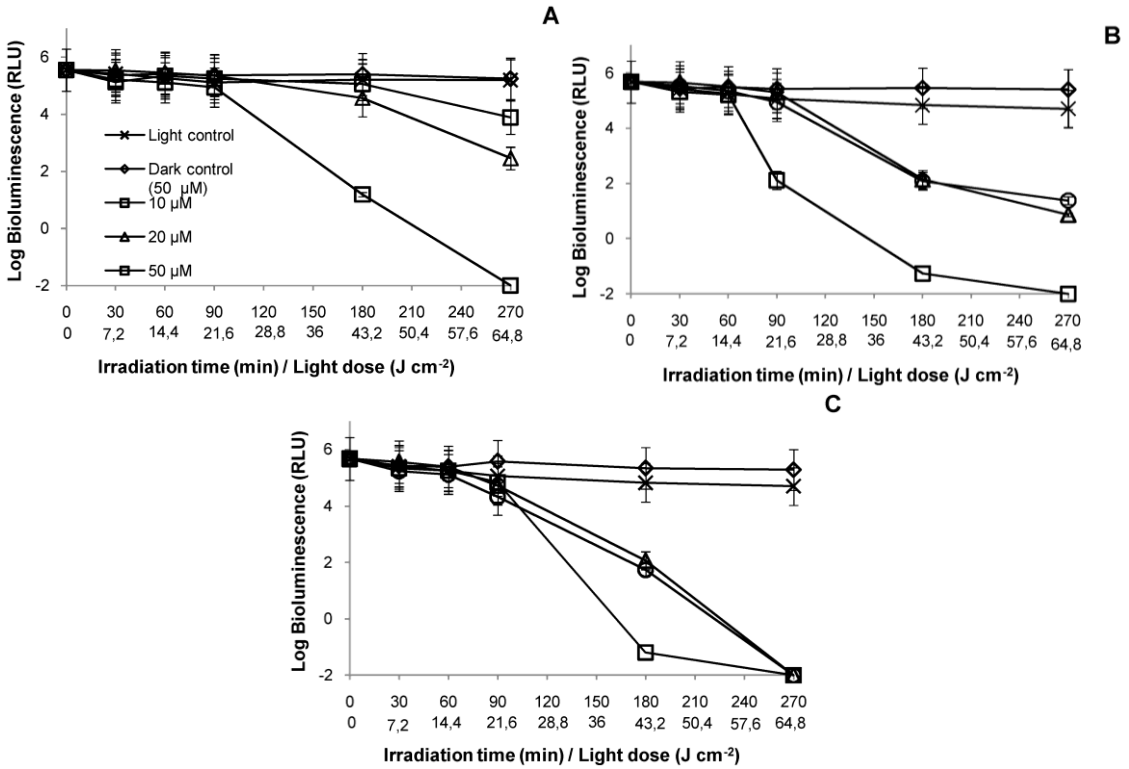


**Figure 9.7** Photoinactivation of *V. fischeri* with Tri-$Py^{+}$-Me-PF at 10, 20 and 50 µM, in an aquaculture water sample collected in June 2010, under 4 mW $cm^{-2}$ irradiation. **A**: Assays with non-filtered water portion; **B**: Assays with water filtered by 0.7 µm membrane; **C**: Assays with water filtered by 0.2 µm membrane. Values represent the mean of two replicates of the same sample; error bars indicate the standard deviation.

## 9.5 Discussion

Photodynamic antimicrobial chemotherapy has been proved to be a promising alternative to treat human diseases. (534-537) The idea of applying it to treat aquaculture waters is recent. (369) Considering that this activity, when conducted in out-door facilities, is exposed to the natural variability of physical and chemical parameters of the water matrix, thorough investigations addressing real field conditions are needed for the design and implementation of effective PACT approaches.

The results show that the efficiency of photodynamic inactivation of *V. fischeri* is not affected by the variation of pH, temperature, salinity, or oxygen concentration within the characteristic ranges of aquaculture waters in temperate climate. In addition, the data points out that solar irradiation can be used as a light source to efficiently photoinactivate microorganisms in aquaculture in the presence of the adequate PS concentration.

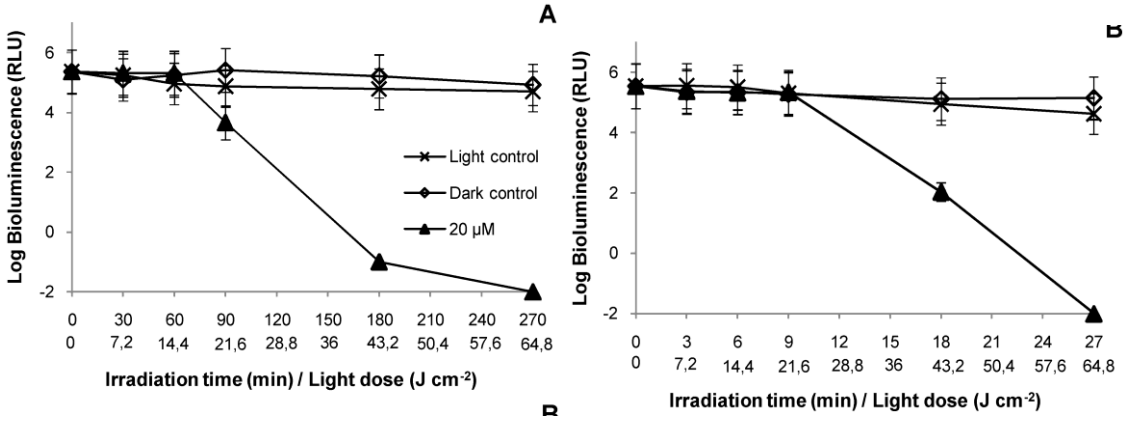


**Figure 9.8** Photoinactivation of *V. fischeri* with 20 µM of Tri-Py$^{+}$-Me-PF, in an aquaculture sample collected in October 2010 using different light sources. A: Assays with artificial white light (4 mW cm$^{-2}$). 64.8 J cm$^{-2}$ was the total light dose applied after 270 min of irradiation; B: Assays with solar light (40 mW cm$^{-2}$). 64.8 J cm$^{-2}$ was the total light dose applied after 27 min of irradiation. Values represent the mean of two replicates of the same sample; error bars indicate the standard deviation.

All the studies performed in controlled experimental conditions using a buffer solution (PBS) to evaluate how the mentioned parameters can affect the PI of *V. fischeri* were carried out in the presence of the porphyrin Tri-Py$^{+}$-Me-PF. In fact, with this PS at 5 µM and under a low light fluence rate (4 mW cm$^{-2}$), the decrease of the bioluminescence signal reached the detection limit of the method (i.e., total reduction in the metabolic rate of bacteria) for all the tested conditions.

The results illustrate that pH variations in the range of 6.5 - 8.5 do not affect the complete inactivation of *V. fischeri* after 90 min of irradiation. Similar conclusions were reached in a study (539), when using PDT to destroy *C. albicans* cells. The authors referred that the pH of the irradiation medium did not significantly affect cell survival in the pH range of 5 - 8. For a similar pH range, another study using photocatalysis against coliform bacteria and poliovirus 1 concluded that PI was not affected by the pH of the solution. (542)

The results of the present study show a total inactivation of *V. fischeri* after 180 min of irradiation with different temperature values, in the range 10 - 25 °C. Nevertheless, the data indicate that increasing the incubation temperature to 20 °C (or 25 °C) the photodynamic process is accelerated, although similar patterns of inactivation were obtained within the tested temperature range. A previous study with human colon adenocarcinoma cells refers

that a reduction in light irradiation temperature (4 - 8 °C) lead to an enhancement on cell survival. (541) In addition, PI of *C. albicans* showed increasing efficiency with increasing irradiation temperature (20 - 24 °C) and it was suggested that this temperature dependence is possibly related to a temperature-induced enhancement of the cell membrane fluidity. (539) However, the different experimental conditions used in different studies, restricts the comparability of the results.

It is well known that the salt concentration in aquaculture waters varies slightly during the year. The results obtained in PBS with different concentrations of salt (range 20 - 40 g $L^{-1}$) show that the efficiency on the PI of *V. fischeri* was not significantly affected by salt concentration. In fact, a total inactivation of light emission is attained after 60 min for all the tested salt concentrations.

Significant differences were observed between pH values 7.4 and 8, and temperature values between 10 °C and 15 °C and 20 °C - 25 °C. In the assays to monitor the PI of *V. fischeri*, the method of bacterial bioluminescence was used. With this method, the metabolic state of bacteria can be assessed in real-time. Given the fact that the ideal *in vitro* conditions for the light emission of these bacteria to be high are 25 °C, pH 7.4 and 30 g $L^{-1}$ NaCl, the explanation for such differences is most likely due to this fact.

Molecular oxygen is one of the requirements for the photodynamic effect. The results show that the concentration of dissolved oxygen, although slightly lower without stirring (5.3 mg $L^{-1}$), does not restrict the PI efficiency at 5 μM of PS. In fact, it was previously referred (331) that the dissolved oxygen concentration in water plays an important role in the production of the oxidative species required for the photodisinfection process to occur and the effect of oxygenation was more evident with higher PS concentration. In the present work, the concentration of oxygen was always higher than 2 mg $O_2$ $L^{-1}$, the minimum concentration of dissolved oxygen considered necessary for an efficient photodisinfection. (544)

The results of photoinactivation of *V. fischeri* in aquaculture water show that it is affected by: 1) the content of the suspended solids in the medium; 2) the concentration of PS; and 3) the light fluence rate. In fact, the first set of PI assays using artificial white light (4 mW $cm^{-2}$) show that the presence of suspended solids (organic matter, bacteria, viruses, and undetermined particles in water) affect the photodynamic process itself, requiring an higher concentrations of PS (10 - 50 μM) to achieve the same efficiency than that obtained in PBS (5 μM). In fact, the results show that when the major fraction of suspended solids is removed (water filtered by 0.2 μm membrane), a concentration of 10 μM of porphyrin is sufficient to inactivate *V. fischeri* cells after 270 min of irradiation with mild light fluence. However, when using non-filtered water, only the concentration of 50 μM was able to totally inactivate

bioluminescent bacteria. The light emission of the bacterium suspended in non-filtered water was not affected by light alone (light control) or by the presence of 50 µM of Tri-$Py^{+}$-Me-PF in the dark (dark control). So, the photodynamic effect at low PS concentrations (10 - 20 µM) seems to be insufficient to inactivate $10^{7}$ CFU $mL^{-1}$ of *V. fischeri* in non-filtered aquaculture water samples. As already demonstrated, one of the water parameters which largely affects the efficiency of photosensitization is the content of suspended solids, which can compete with the microorganisms for the PS, decreasing the real concentration of PS available for their photoinactivation, and can also absorb light and protect microorganisms. (331) It is well known that specific organic and inorganic compounds in wastewater absorb energy at wavelengths in the range 400 - 800 nm, affecting the intensity of radiation. On other hand, visible light is unable to penetrate the aggregates of microorganisms in suspended matter preventing the cells photosensitization. The possibility of a portion of the PS to be bound to the organic and mineral matter present in the water was also suggested as affecting the efficiency of the photosensitization process. (331)

The results obtained in the first set of assays in natural aquaculture water, lead to verify the efficacy of the PI of *V. fischeri* in real field conditions (non-filtered aquaculture water samples) using solar irradiation as light source. Because the fluence rate of solar light is approximately ten times higher than the one used in laboratory conditions, it is possible to achieve the same total light dose in an exposure time around ten times lower. Using 20 µM of porphyrin, both light sources (artificial and solar light) caused complete PI of *V. fischeri* when a total energy dose of 64.8 J $cm^{-2}$ was delivered. However, the two light sources show a different pattern of PI when lower energy doses are compared, being the PI of *V. fischeri* less efficient with solar irradiation. This effect can be explained by the fact that when a high fluence rate is used, the PS in the suspension is not able to absorb all photons. Although the concentration of the PS used is the same, the emission spectra of the light sources are different and, consequently, the energy available to excite the PS is different. Since the absorption wavelengths for the porphyrin derivatives range from 400 to 650 nm, most of the energy provided by solar irradiation ($\lambda > 650$ nm) is not used to excite the PS. On the contrary, for the fluorescent lamps, most of the energy is emitted at 545 and 611 nm which coincides with the Q bands of the PS (Figure 9.9). Similar results were reported for the photodynamic inactivation of T4-like bacteriophages. (199) The authors reported that the PI efficiency is affected by the fluence rate when lower light doses are delivered. At higher light doses, the fluence rate effect is not significant. (199) Identical results were found on the PI of *Escherichia coli* and *Enterococcus hirae*, and yeast cells. (237, 545)

The differences obtained in the PI patterns when using artificial white light to irradiate the water samples collected in May, June and October samplings point out that the PI efficiency of *V. fischeri* is most likely affected by the seasonal variation of water properties, namely in relation to plankton seasonal dynamics and also by the variation of solar light intensity.

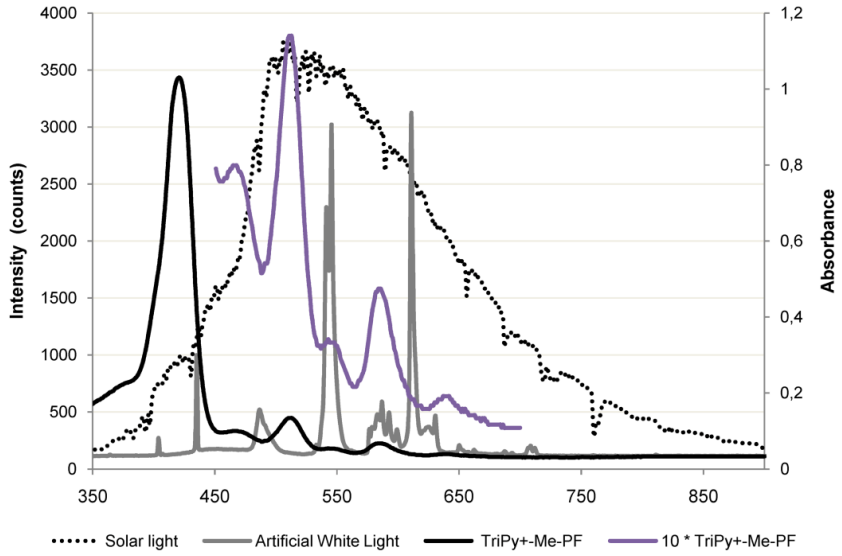


**Figure 9.9** Absorption spectrum of the tricationic *meso*-subtituted porphyrin and emission spectra of the two light sources used in the photoinactivation studies.

The use of artificial white light of low intensity (4 mW $cm^{-2}$) aims to simulate the weather for this region of Portugal during dark days in winter. It is intended that this technology will be used in real context, using only solar irradiation as light source which is, at least, around ten times more intense than the artificial white light tested in laboratory studies (an annual average of 34.1 mW $cm^2$ in the city of Aveiro, going up to 42.8 mW $cm^2$ in August – data from year 2010). As it happened in this study, but also in another two studies of our group, solar irradiation was tested in the PI of bacteria (359) and T4-like phages (199) with efficient results as well. Therefore, considering natural light conditions, this photodynamic approach applied to water disinfection makes it economically feasible in terms of light source.

The overall analysis of the results obtained show that the presence of suspended solids, photosensitizer concentration and light fluence are the major determinants of the PI efficiency.

It can be concluded that temperature, salinity and dissolved oxygen are not likely to affect the success of photoinactivation of *V. fischeri* in aquaculture conditions. On the contrary, water suspended solids considerably affect the efficiency of the process. Although PI of microorganisms in environmental waters with high loads of suspended matter is not as effective as in clear aquatic matrices, a good response can be obtained in aquaculture waters

by adjusting the PS concentration and light dose. As the effectiveness of PACT in environmental waters depends on the suspended matter content, whenever planning for PACT in field conditions, the water should be previously characterized. The use of solar irradiation in PACT can be regarded as a suitable option for the establishment of environmentally efficient cost-effective antimicrobial protocols.

# Chapter 10. Nanomagnet-porphyrin hybrids for the photodynamic inactivation of microorganisms: further developments

The content of this hapter has been submitted for peer-review:
Alves E, Rodrigues JMM, Faustino MAF, Neves MGPMS, Cavaleiro JAS, Lin Z, et al. Nanomagnet-porphyrin hybrids for the photodynamic inactivation of microorganisms: further developments. ChemSusChem. submitted.

# 10 Nanomagnet-porphyrin hybrids for the photodynamic inactivation of microorganisms: further developments

## 10.1 Abstract

Cationic porphyrin [5-(pentafluorophenyl)-10,15,20-tris(1-methylpyridinium-4-yl)porphyrin tri-iodide] **1a** coupled to cationized silica-coated magnetic nanoparticles (NPs) of $Fe_3O_4$ (hybrid **6**) has demonstrated a remarkable antimicrobial activity for water/wastewater disinfection through the photodynamic process. In this study, such cationic nanomagnet-porphyrin hybrid and also a new nanomagnet hybrid with a $CoFe_2O_4$ core (hybrid **7**) were synthesized, characterized and their recovery and reuse/recycling capability were tested on a small scale laboratory model. The photochemical stability of the hybrids and of porphyrin **1a** in solution was also evaluated. *Vibrio fischeri*, a naturally bioluminescent Gram-negative bacterium was used in the biological experiments (reuse/recycling of the hybrids) to monitor the photoinactivation kinetics in real-time.

Both hybrids showed similar photochemical and photophysical properties, maintaining magnetite stable during the photoinactivation experiments (irradiance of 40 W $m^{-2}$ with a total light dose of 345 J $cm^{-2}$). Recycling experiments with both hybrids revealed a loss of photobiocidal activity from cycle to cycle probably due to the loss of small NPs containing the active porphyrin, which can disaggregate from the nanoclusters, during water removal. The cumulative values of bacterial inactivation (in colony forming units per milliliter, CFU $mL^{-1}$) after a six-cycle reuse were ≈ 32 $\log_{10}$ in 7h30 with non-supported porphyrin **1a**, ≈ 42 $\log_{10}$ in 21h30 with hybrid **6** and ≈ 38 $\log_{10}$ in 27h with hybrid **7**. The increasing time needed to photoinactivate all viable bacteria was due to the increasing amount of organic matter present in the medium and, when using the hybrids, to the competitive effect of NPs in relation to reactive oxygen species.

The reuse and recycling capability of cationic nanomagnet-porphyrin hybrids for water disinfection is for the first time reported and discussed in this work. The results suggest that particles with suitable size should be prepared in a larger scale, to allow their use in environmental applications and turn their recycling process easier and more efficient.

## 10.2 Introduction

Water is an essential resource whose reuse starts to become an essential requirement. Even in developed countries, the treatment of drinking water and wastewater faces many challenges nowadays. The chlorine-based agents are still the most widely used for disinfection,

and although they are effective against bacteria and viruses, inexpensive and easy to use, the lack of effectiveness against parasites and the formation of toxic by-products (e.g., trihalomethanes, haloacetic acids, bromate, and chlorite) are a major concern. Alternatives to chlorine such as chloramines, chlorine dioxide, ozone and UV irradiation, have pros and cons with respect to cost, efficiency, stability, ease of application, and nature of formed by-products. Ozone is the most efficient disinfectant in terms of microbial inactivation but it is expensive, leads to toxic compounds and requires an *in situ* generation due to its unstable nature. Chloramines, although producing fewer by-products than chlorine, are less efficient. Chlorine dioxide is efficient against parasites but it entails highly specialized operators, high cost and sometimes some odor and taste problems may occur. UV irradiation inactivates organisms that are resistant to chlorination but it does not offer residual protection. (407, 546)

In order to overcome the problems of microbial inactivation and formation of toxic by-products, new technologies had emerged. In recent years, nanotechnology has been identified as a promising alternative for the improvement of the water treatment process with useful features for different applications. (408) As regards disinfection and decontamination, bioactive nanoparticles (NPs) have been developed (408), consisting of NPs associated with, for example, photosensitizers (PS) that, in the presence of molecular oxygen and light, lead to the effective elimination of different biological entities. In this process, termed photodynamic inactivation (PDI), various processes of energy transfer and electronic state transition take place with further production of reactive oxygen species (singlet oxygen and/or free radical species). The aggressive action of these species, especially singlet oxygen, causes irreversible effects at the level of lipids, proteins and nucleic acids, leading to cell inactivation. (547) Furthermore, the development of resistance has not been observed in repeated cycles of PDI in semi-lethal conditions using tetrapyrrolic macrocyles. (119, 120, 134)

The use of this approach in the environmental context has been explored by some research groups who believe it is an interesting alternative for the decontamination of wastewater (60, 142, 331, 332, 360) and water of fish farms. (140, 141, 369) The idea of using PDI for this purpose is intended to overcome economic, ecological and public health issues, with minimal environmental impact.

There is obviously a myriad of aspects to consider before using PDI for water treatment, such as physical, chemical and microbiological properties of water (140, 141, 331, 332); turbidity (presence of suspended solids) (140, 331); thickness of the water column (related to the depth of light penetration); dissolved oxygen concentration (331); light source and light dose (140, 199, 359, 369); irradiation time (331, 332); photophysical and photochemical properties of the PS (60, 369); and concentration of the PS. (141)

Porphyrin-based PS have been commonly used in PDI, even in environmentally oriented approaches, specifically cationic *meso*-substituted compounds. (60, 140, 141, 331, 332, 342, 359, 360, 369) The potential benefits of this therapy include the use of sunlight as energy source (the most economic option) (140, 340, 359); the decreased or absent toxicity of the PS, specifically porphyrins, towards higher organisms at photochemically active doses (369); the gradual photobleaching of porphyrins by solar light (538), which prevents their accumulation in the environment; the reuse of the PS (360); and the possibility of water recycling after disinfection (for agricultural and landscape irrigation, for example). (332)

In order to achieve the actual field implementation and to diminish the potential environmental impact, PS have been covalently linked/grafted or incorporated into inert solid supports such as silica powders or beads (548), chitosan membranes (360), chitosan NPs (549), silica-coated magnetite NPs (198) or multi-walled carbon nanotubes (380), and tested upon Gram-negative bacteria, bacteriophages, yeasts and viruses, with significant antimicrobial activity. The immobilization of the PS aims to allow both the efficient elimination of microorganisms during several cycles of use and the complete PS removal from the treated medium.

The synthesis of different silica based nanomagnet-porphyrin hybrids and their use in PDI of *Escherichia coli* and T4-like bacteriophages has been described. (198) These hybrids consist of porphyrin covalently linked to silica-coated iron oxide NPs. The major advantages of these NPs is their magnetic behavior provided by the metal core (550), the prevention of the intrinsic tendency of aggregation and oxidation by the silica shell, as well as the ability to be functionalized (551) with a very effective broad-spectrum PS. (77, 140, 141, 143, 144, 359) The PDI with the cationic porphyrin [5-(pentafluorophenyl)-10,15,20-tris(1-methylpyridinium-4-yl)porphyrin tri-iodide] **1a** coupled on cationized NPs (hybrid **6**) led to a reduction in viability of 4.8 $\log_{10}$ of *E. coli* at 20 µM (PS concentration in the hybrid) and 43.2 J $cm^{-2}$ (180 min of irradiation with white light at an irradiance of 40 W $m^{-2}$), and 6.8 $\log_{10}$ of T4-like phage at the same concentration and 14.4 J $cm^{-2}$. (198) A reduction in cellular viability of 1.0 $\log_{10}$ corresponds to a reduction in 10 colony forming units per milliliter (CFU $mL^{-1}$).

The promising results obtained with this hybrid in biological experiments as well as the potential advantages of using magnetic NPs sparked an interest in pursuing the studies on the reuse/recycling of these materials. Firstly on a small scale, the goal has concerned variables as PS photostability and integrity of the hybrid nanomagnetic core that can affect the PDI process during the reuse/recycling cycles. In this way, the influence of these variables on the reuse/recycling of the nanomaterials and also the PDI efficiency, the lifetime of the active materials, and the bioavailability of singlet oxygen were evaluated.

Accordingly to this aim, it was tested, on a small scale: a) the recovery of these hybrids after three PDI cycles (recycling), applying either a permanent magnetic field or centrifugation to compare these two recovery approaches; and b) the chemical stability and biological efficiency of the hybrids after several cycles of reuse (six cycles) in order to determine their practical application.

Herein, a strain of the marine bacterium *Vibrio* (*Aliivibrio) fischeri* was used as a model of Gram-negative bacteria. Being a naturally bioluminescent bacterium (emits green light at ≈ 490 nm), its viability can be quickly and easily monitored during the laboratory PDI tests using a device (luminometer) that records the light emission/light loss in real-time, instead of the conventional pour plate method.

## 10.3 Material and Methods

### 10.3.1 Synthesis of the porphyrin photosensitizer

The synthesis and the full characterization of 5-pentafluorophenyl-10,15,20-tri(4-pyridyl)porphyrin (**1**) and the corresponding cationic 5,10,15-tris(1-methylpyridinium-4-yl)-20-(pentafluorophenyl)porphyrin tri-iodide (**1a**, Scheme 10.1) were already described in the literature. (142, 173, 198)

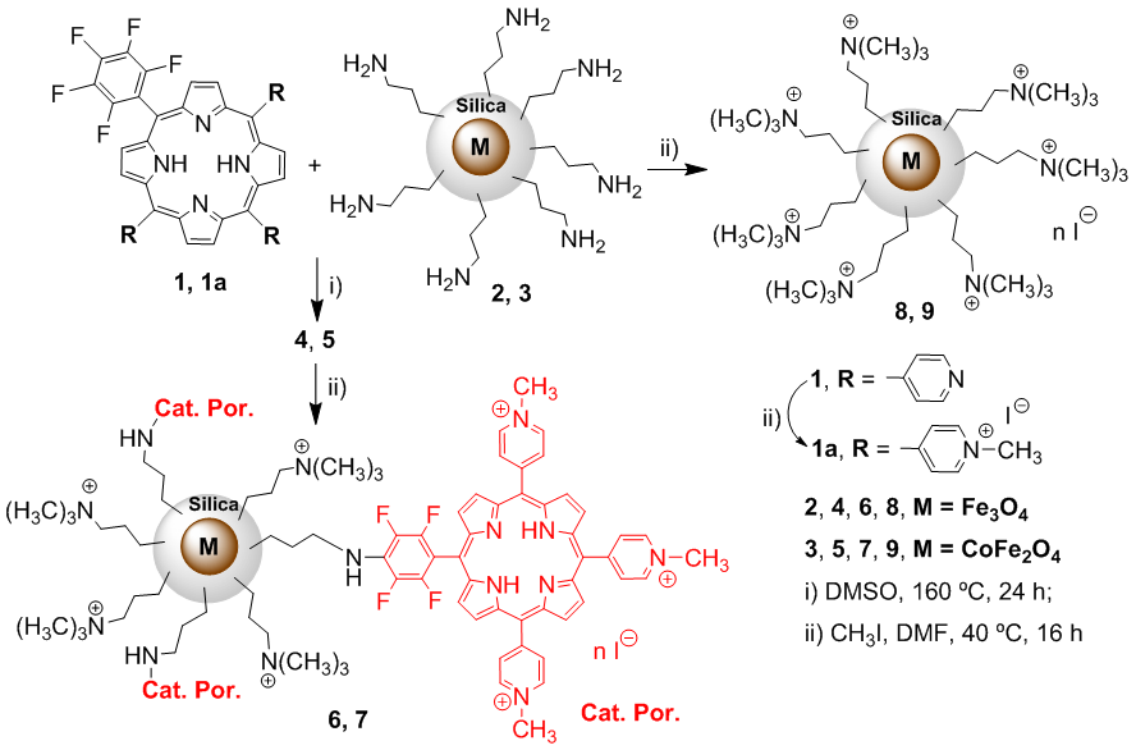


**Scheme 10.1** Synthesis procedure of the two cationic nanomagnet materials and the corresponding porphyrin hybrids.

### 10.3.2 Preparation and characterization of magnetic silica nanoparticles

The $Fe_3O_4$ silica core-shell NPs **2** were prepared by the same procedure described by Liu et al. (552) with small modifications already described. (198)

The $CoFe_2O_4$ silica core-shell NPs **3** were also prepared according to the literature. (553) The $CoFe_2O_4$ core was obtained by the conventional co-precipitation method, where $CoCl_2 \cdot 6H_2O$ (0.24 g) and $FeCl_3$ (0.33 g) were dissolved in deionized water (10 mL at 80 °C) with vigorous stirring. NaOH (1.20 g) were then slowly added to the solution, forming immediately black particles. This mixture was kept under stirring at 70 - 85 °C for 1 h and then washed twice with deionized water. Sodium metasilicate (7.92 g) was dissolved in deionized water and the pH value of the solution adjusted to 12 - 13 by addition of concentrated hydrochloric acid (37%). The sodium metasilicate solution and the prepared $CoFe_2O_4$ nanocores were poured into a beaker equipped with a mechanical stirrer and heated to *ca.* 70 °C. The mixture was ultrasonicated for 15 min. Then, the temperature of the mixture was increased to 75 - 80 °C. A HCl solution was added dropwise to adjust the pH value to 6 - 7. The particles formed were washed several times with deionized water and then dispersed in ethanol (160 mL). 3-aminopropyl)triethoxysilane (APTS, 1.33 mL*)* was added to the suspension and the resulting mixture was magnetically stirred at room temperature for 72 h. The precipitate was washed several times with ethanol, the magnetic NPs were purified by magnetic decantation and then dispersed in the same solvent (150 mL).

Powder X-ray diffraction (XRD) was performed between 10 - 80° in 2θ on a Philips X'pert MPD diffractometer using CuK$\alpha$ radiation. The Fe/Co and Si/(Fe+Co) ratios were analyzed using energy dispersive X-ray spectrometry (EDS) carried out by Römteck EDS system attached to the scanning electron microscope Hitachi S-4100.

### 10.3.3 Synthesis of nanomagnet-porphyrin hybrids – General procedure

Previously prepared ethanol suspensions of magnetic silica NPs **2** and **3** (11.5 mL, corresponding to 190 mg), were filtered through a polyamide membrane, washed several times with DMSO and then resuspended in DMSO (1 - 2 mL). A solution of porphyrin **1** (10.0 mg, 14.1 μmol) in DMSO (4 - 5 mL) was added to that suspension and the resulting mixture was magnetically stirred during 24 h at 160 °C. In both cases, red insoluble hybrid materials **4** and **5** were obtained (Scheme 10.1). The immobilization of **1** was easily monitored by thin-layer chromatography, by the disappearance of the band corresponding to unbound porphyrin **1**. The resulting hybrid materials **4** and **5** were washed several times with appropriate solvent, $CHCl_3$/MeOH (95:5), until no Soret band of compound **1** was observed in the rinse solvent. In

the washing process the materials were firstly decanted by using a magnetic field and then filtered through a polyamide membrane. The amount of unreacted/adsorbed porphyrin **1** was calculated by UV-Vis spectrophotometry (Shimadzu UV-2101PC Spectrophotometer, International Equipment Trading Ltd., Illinois, USA), and then discounted from the amount used initially. The hybrids **4** (7.5 mg, 10.6 μmol of **1**) and **5** (8.1 mg, 11.4 μmol of **1**) were then resuspended in dry DMF (6 mL) and subsequently treated with a large excess of methyl iodide (2 mL). The reaction mixtures were kept under stirring at 40 °C for 16 h. After this period the suspensions were cooled down in ice and the corresponding cationic hybrids **6** and **7** were filtered and washed with methanol and water (Scheme 10.1). These final hybrid nanomaterials **6** and **7** were resuspended in water (50 mL), which correspond to stock suspensions of approximately 212 μM and 230 μM of PS (Cat. Por **1a**), respectively, used on the bacterial photoinactivation assays. Both cationic nanomagnet-porphyrin hybrids were characterized by liquid and solid-state UV-Vis spectrophotometry.

### 10.3.4 Synthesis of the cationic magnetic silica nanoparticles - General procedure

Using similar procedure for the preparation of the cationic hybrids **6** (M = $Fe_3O_4$) and **7** (M = $CoFe_2O_4$), both amino functionalized NPs **2** and **3**, without PS, were quaternized in order to get the fully cationized NPs **8** (M = $Fe_3O_4$) and **9** (M = $CoFe_2O_4$), respectively. For that, silica NPs **2** and **3** (11.5 mL, corresponding to 190 mg), kept in ethanol, were filtered through a polyamide membrane, washed several times with DMF and then resuspended in DMF (6 mL) and subsequently treated with a large excess of methyl iodide (2 mL). The reaction mixtures were kept under stirring at 40 °C for 16 h. After this period the suspensions were cooled down in ice and the corresponding cationic NPs **8** and **9** were filtered and washed with methanol and water (Scheme 10.1). These final nanomaterials **8** and **9** were resuspended in water (50 mL), which correspond to stock suspensions of approximately 18 mg $mL^{-1}$ used as controls on the bacteria photoinactivation assays.

### 10.3.5 Experimental setup for the photoinactivation of bacteria

#### 10.3.5.1 Bacterial strain and growth conditions

*V. fischeri* ATCC® 49387™ (VA, USA) was stored at −80 °C in 10% glycerol. Fresh plate cultures were maintained in solid BOSS medium with 3% of NaCl at 4 °C (BOSS medium: 1% peptone, 0.3% beef extract, 0.1% glycerol, 3% NaCl, 1.5% agar, pH 7.3). (543) A concentration of 20 - 40 g $L^{-1}$ of NaCl is necessary to maintain the osmotic pressure of cells required for natural light emission to occur. Before each experiment, one isolated colony was aseptically

inoculated in 30 mL of liquid BOSS medium and grown for one day at 25 °C under stirring (120 rpm). An aliquot of this culture (240 µL) was subcultured in 30 mL of BOSS medium and grown overnight at 25 °C under stirring (120 rpm) to reach an optical density ($OD_{620}$) of ≈ 1.0, corresponding to ≈ 8 $\log_{10}$ CFU $mL^{-1}$. As *V. fischeri* emits light at temperatures below 30 °C, in all the experiments, the containers with the samples were always placed in contact with water (22 - 26 °C) to prevent the heating of the sample.

#### 10.3.5.2 Correlation between bioluminescence and colony-forming units

Starting from an overnight culture of *V. fischeri*, serial dilutions of 1:10 were made in phosphate buffered saline (PBS) with 30 g $L^{-1}$ of NaCl (30 g NaCl, 0.2 g KCl, 1.44 g $Na_2HPO_4$ and 0.24 g $KH_2PO_4$ per liter; pH 7.4). From each dilution, the bioluminescent signal was measured (100 µL in a tube luminometer; peak wavelength detected at 420 nm; standard range: 300 - 650 nm; TD − 20/20 Luminometer, Turner Designs, Inc., USA) and 100 µL were plated by spreading on the surface of BOSS solid medium followed by incubation for 36 h at 25 °C. The correlation between the two methods was set as the value of bioluminescence in relative light units (RLU) *versus* the number of CFU per mL. The bioluminescence values represent the viable bacterial abundance. This procedure was performed three separate times and the values were averaged. Previously, it was also demonstrated that the presence of 5 µM of porphyrin **1a** does not affect the bacterial bioluminescence (and so, bacterial viability) in the absence of light. (140)

#### 10.3.5.3 Irradiation conditions

The artificial white light system used in the photoinactivation and photo-oxidation experiments consisted in 13 parallel placed OSRAM 21 lamps (Munich, Germany) of 18 W each, with an irradiance of 40 W $m^{-2}$ (emitting in the 380 - 700 nm range).

#### 10.3.5.4 Recycling of hybrids

The term recycling refers to a new use of the hybrid after recovery by applying a magnetic field, removal of the treated liquid (i.e., when the bioluminescent signal reaches the detection limit) followed by the addition of a new volume of bacterial suspension (Scheme 10.2).

From an overnight culture of *V. fischeri*, 1 mL was removed and centrifuged 5 min at 13,000 x *g*. The bacterial pellet was washed twice and resuspended in PBS with 3% NaCl. The cell suspension was transferred to a luminometer tube (3 mL, 11 x 55 mm) as well as the tested hybrids at the selected amount (20 µM of PS), making a final volume of 1 mL. To each

test tube, a sterile magnetic bar was added. The bottom of the tube was immersed in water in a well of a 12 wells tissue culture test plate (Orange Scientific, Belgium) and this was placed on a magnetic stir plate, under the light system. For each hybrid, one photoinactivation experiment (1 cycle) ended up when the luminometer reached 0.01 RLU (detection limit), which means that total bacterial load was photoinactivated. Then, the hybrids were collected at the bottom of the tube with a strong permanent magnetic field, using a neodymium magnet; the supernatant was centrifuged for 30 min at 39,788 x *g* (Avanti® J-25, Beckman Coulter, Inc.) to check the presence or absence of small hybrid NPs. Then, a new bacterial suspension was added to the luminometer tube containing the hybrid and the irradiation restarted. For each hybrid, three cycles of photoinactivation were performed (i.e., the hybrids were recycled twice). Three independent experiments, of three cycles each, were done and the results were averaged. A light control (bacteria exposed to irradiation without hybrid) and a dark control (bacteria exposed to hybrid without irradiation) were done simultaneously under the same experimental conditions to check the bacterial viability and the potential hybrid toxicity during the experiments.

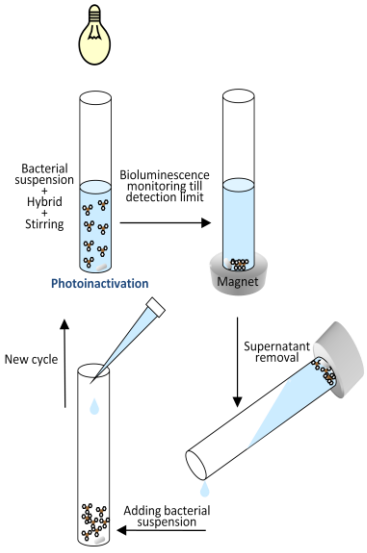


**Scheme 10.2** Schematic illustration of the hybrids recycling.

#### 10.3.5.5 Reuse of free porphyrin and hybrids

The term reuse refers to the repeated addition of inoculum (bacterial mass, ≈ 7 $\log_{10}$ CFU $mL^{-1}$) either to non-supported porphyrin **1a** (5 µM) or to hybrids **6** or **7** (20 µM), after the bioluminescent signal of the previous suspension reaches the detection limit (Scheme 10.3). From an overnight culture of *V. fischeri*, 1 mL was removed and centrifuged 5 min at 13,000 x *g*. The bacterial pellet was washed two times and resuspended in PBS with 3% NaCl. The cell suspension was transferred to a luminometer tube and porphyrin **1a** or hybrid was added (suitable volumes which corresponded to 20 and 5 µM of supported porphyrin (PS) and **1a**,

respectively), making a final volume of 1 mL. The bottom of the tube was immersed in water in a well of a 12 wells tissue culture test plate (Orange Scientific, Belgium) and this was placed on a magnetic stir plate, under the light system. For each hybrid (**6** and **7**) and **1a**, one photoinactivation experiment (1 cycle) ended up when the luminometer reached 0.01 RLU (detection limit), which means that the total bacterial load was photoinactivated. Three independent experiments, of six cycles each, were done and the results were averaged. Light and dark controls were also done simultaneously.

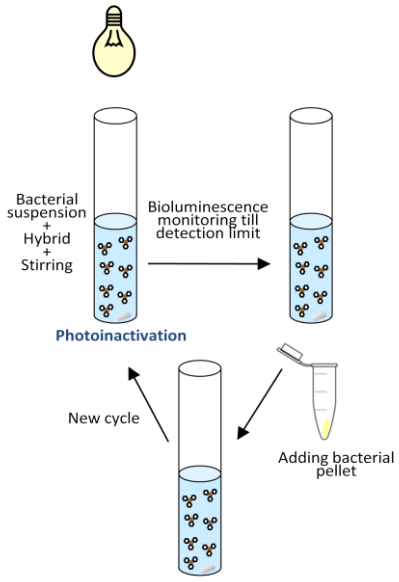


**Scheme 10.3** Schematic illustration of free porphyrin and hybrids reuse.

### 10.3.6 Photobleaching of porphyrin and hybrids

The aim of this task was to check the photostability of the non-supported porphyrin **1a** and the possible oxidation of the magnetic core of the NPs by reactive oxygen species generated during 24 h of irradiation at the same conditions as in the photoinactivation experiments (white light and an irradiance of 40 W $m^{-2}$). The strategy consisted of irradiating the hybrids **6** and **7** in parallel with the respective cationic magnetic NPs **8** and **9**, and porphyrin **1a**, suspended/dissolved in PBS (see composition above), for 24 h, in crystallizing dishes (1 L capacity) and every four hours check for loss/maintenance of the magnetic properties of the NPs, their sedimentation time (placing the containers with the NPs/hybrid on a magnetic plate) and record the UV-Vis spectra of the supernatants after magnetic sedimentation.

The stock solutions of hybrids **6** and **7**, NPs **8** and **9** and of the non-supported **1a** were sonicated 30 min to disperse the NPs and/or disaggregate the non-supported porphyrin **1a**, respectively. Appropriate volumes of hybrids/NPs/**1a** were added to each crystallizing dish in order to have final: i) hybrid suspensions of 20 μM based on PS supported); ii) NPs suspensions

(17.9 mg); and iii) non-supported **1a** (5 μM) in a final volume of about 280 mL for hybrids **6** and **7** and NPs **8** and **9**, and 50 mL for the cationic water soluble **1a**. A magnetic bar was placed in each of the crystallizing dishes with hybrid/NPs; they were carefully homogenized and placed on a magnetic stirring plate under irradiation at room temperature. The beaker with the porphyrin **1a** solution was stirred in the same conditions.

Every 4 h, the glass containers were placed on a magnetic plate and the deposition time of the NPs and the visual changes were recorded with a camera. After sedimentation, 2 mL of supernatant were used to record the UV-Vis spectrum. After 24 h of irradiation, the hybrids/NPs were filtered, completely dried under vacuum and analyzed by XRD. The solution containing **1a** was also filtered. The color of the filtrates and their UV-Vis spectra were recorded.

## 10.4 Results and Discussion

### 10.4.1 Synthesis of porphyrin and nanomagnet-porphyrin hybrids

Porphyrins 5,10,15-tri(4-pyridyl)-20-(pentafluorophenyl)porphyrin (**1**) and the corresponding cationic water soluble 5,10,15-tris(1-methylpyridinium-4-yl)-20-(pentafluorophenyl)porphyrin tri-iodide (**1a**, Scheme 10.1) were prepared following previously described procedures. (142, 173, 198) Both structures were confirmed by $^{1}$H NMR and mass spectrometry. Hybrids **4** (M = $Fe_3O_4$) and **5** (M = $CoFe_2O_4$) were obtained from the reaction of porphyrin **1** with the magnetic silica NPs **2** (M = $Fe_3O_4$) and **3** (M = $CoFe_2O_4$) in 75 and 80% yield, respectively. The reaction was carried out in DMSO at 160 °C during 24 h. After this time, TLC of each reaction mixture showed that most of the starting porphyrin **1** was converted into a new red-colored material that remains in the baseline. The resulting solids were filtered and washed with the appropriate solvent until no Soret band was detected in the rinse solvent, confirming the removal of residual non-reacted **1**. The successful coupling of **1** to the magnetic silica NPs was confirmed by UV-Vis spectroscopy (Figure 10.1).

Both magnetic silica NPs **2** and **3** and also the hybrid materials **4** and **5** were fully cationized. The cationization process was carried out with a large excess of methyl iodide in DMF at 40 °C. After 16 h, the cationic hybrids **6** and **7**, and the cationic nanomaterials **8** and **9**, were filtered and washed several times with water and methanol and then resuspended in water.

For hybrids **6** and **7**, it was possible to confirm the characteristic Soret band of the porphyrin derivative at *ca.* 420 nm (Figure 10.1). This signal clearly indicates the success of the immobilization process and the preservation of the structural features of the PS.

Due to the magnetic nature, these small particles are easy to aggregate. The dynamic light scattering (DLS) analyses of these two hybrids showed aggregates/clusters with a range of 240 nm (NPs **6**) and 1600 nm (NPs **7**) formed by smaller particles of around 20 nm.

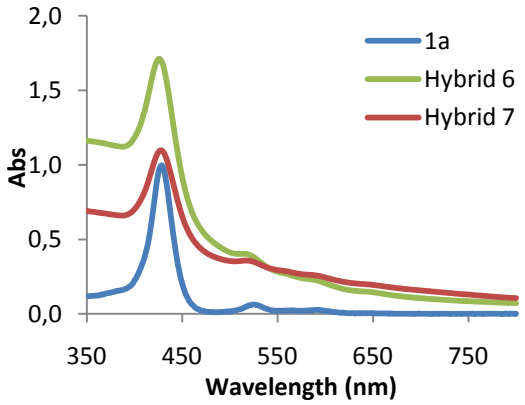


**Figure 10.1** UV-Vis spectra of the hybrids 6 and 7 and cationic porphyrin 1a in water.

### 10.4.2 Preliminary recycling experiments with hybrid 6 ($Fe_3O_4$)

The preliminary experiments, carried out in glass beakers with final volumes between 50 and 250 mL (Figure 10.2A), demonstrated that: i) from cycle to cycle, there was a diminished photoinactivation ability of the PS (data not shown); ii) there was a visible change of color after the experiments in the supernatant of the sample (hybrid **6** with bacterial suspension subjected to irradiation) not seen in the supernatant of the dark control sample (hybrid **6** with bacterial suspension protected from light) (Figure 10.2B and 10.2C); iii) leaving the beaker with the supernatant on a magnetic plate for several hours, there was sedimentation of hybrid on the magnets (Figure 10.2D); iv) the filtration of supernatants showed the presence of hybrid, being the amount greater in the first cycle (first use) relatively to the following recycling cycles (Figure 10.2E).

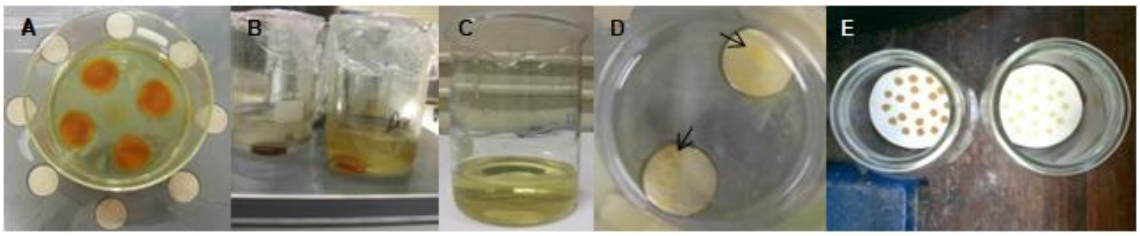


**Figure 10.2** Preliminary recycling experiments with hybrid 6 ($Fe_3O_4$). From left to right: **A**) appearance of the sample (hybrid and bacterial suspension) after sedimentation of the hybrid on a magnetic plate at the end of an experiment; **B**) appearance of the supernatant from the dark control (left) and the test sample (right); **C**) appearance of supernatant removed after an experiment; **D**) the beaker of the previous image was left on the magnetic plate for 12 h. On the magnets, the "orange powder" that has sedimented can be seen, denoting the presence of hybrid or nanoparticles; **E**) the beaker on the left has the filtrate resulting from filtration (0.22 µm membrane filter) of the supernatant from the first

inactivation cycle and the one on the right has the supernatant from the second inactivation, confirming the presence of hybrid or nanoparticles that remained in suspension and did not sediment.

Given these results, it was suspected that photo-oxidation of the magnetic core of the NPs by reactive oxygen species generated during the photodynamic process and/or photobleaching of the porphyrin from the hybrid during the experiments could occur. In addition, the loss of photoinactivation ability could be due to the strategy of hybrid recovery: the magnetic force of the neodymium disks on the magnetic plate used is not sufficient to achieve full sedimentation; the settling time is not sufficient to recover all the hybrid; the removal of supernatant with an automatic pipette leaving only residual liquid enough for the NPs not to dry out or aggregate can remove some volume of hybrid; and inherent to these factors, the size of the NPs *versus* the volume of liquid to be treated. Furthermore, to check whether it could be photo-oxidation of the iron oxide magnetic core of the NPs, new cationic silica NPs with a cobalt iron oxide core (NPs **9**) and the NPs-porphyrin hybrid **7**, much less susceptible to oxidation, were synthesized and tested. The new hybrid **7** ($CoFe_2O_4$) was prepared using the same general procedure, showing similar photochemical and photophysical properties to hybrid 6.

### 10.4.3 Recycling of hybrids

In order to discard the variables related to hybrid recovery, the recycling studies were redesigned to a final volume of 1 mL. This volume was placed in a polypropylene luminometer tube. The bacterium used (*V. fischeri*) is Gram-negative and naturally bioluminescent. This last feature allows monitoring the photoinactivation kinetics in real-time and also prevents losses of volume that would be required to perform serial dilutions and plating by the conventional pour plating method. As performed in previous studies (140, 183), in which this strain was used as a model of Gram-negative bacteria, the correlation between CFU per mL and bioluminescence (in RLU) of a *V. fischeri* culture in the early stationary phase was established. The results show a linear correlation between the viable bacterial abundance and bioluminescence (Figure 10.3).

Recycling experimental procedure with hybrids **6** and **7** is illustrated in Scheme 10.2. The results of these experiments are shown in Figure 10.4. In addition to the test samples, two controls were carried out simultaneously (light control and dark control) and showed that bioluminescence remained stable throughout the experiment, which means that irradiation itself does not affect the bacterial viability nor the concentration of PS used (in the absence of light) is toxic for bacteria.

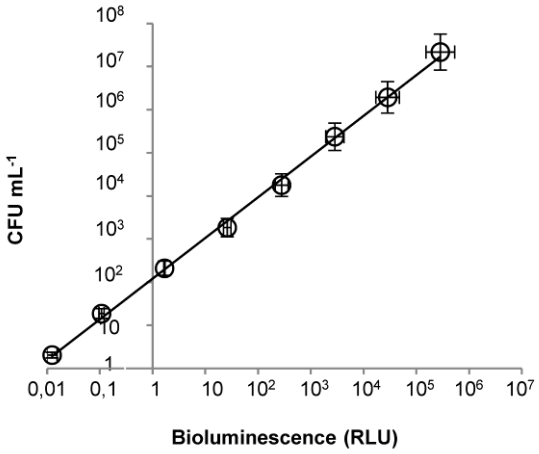


**Figure 10.3** Relationship between the bioluminescence signal and viable counts of an overnight culture of *V. fischeri* (≈ $10^7$ CFU $mL^{-1}$) serially diluted in PBS with 3% of NaCl. Bioluminescence is expressed in relative light units (RLU) and viable counts in CFU $mL^{-1}$; $R^2$ = 0.9984. Values represent the mean of three independent experiments; error bars indicate the standard deviation.

After three cycles, the experiments with hybrid **6** ($Fe_3O_4$) were concluded because of the observed results (Figure 10.4A), which agreed with the results of the preliminary recycling experiments with this hybrid (Figure 10.2). Again, there was an apparent loss of photoinactivation efficiency by the hybrid over the cycles, and differences between the supernatants of the irradiated hybrid (sample) and the non-irradiated hybrid (dark control) were detected (Figure 10.5). The loss of photoinactivation efficiency may be due to losses of hybrid from cycle to cycle due to the size of the NPs that remain adsorbed to all material with which they contact. On the other side, from the DLS data, most probably the smaller active NPs could be disaggregated from the big hybrid cluster due to the sonication before each cycle, causing a continuous loss of these most active particles. The different colors from the supernatants observed after each cycle were another concern. The supernatants of the dark controls were translucent but the supernatants from the irradiated samples were yellowish (inspected visually and shown by spectroscopy in Figure 10.5A and 10.5C).

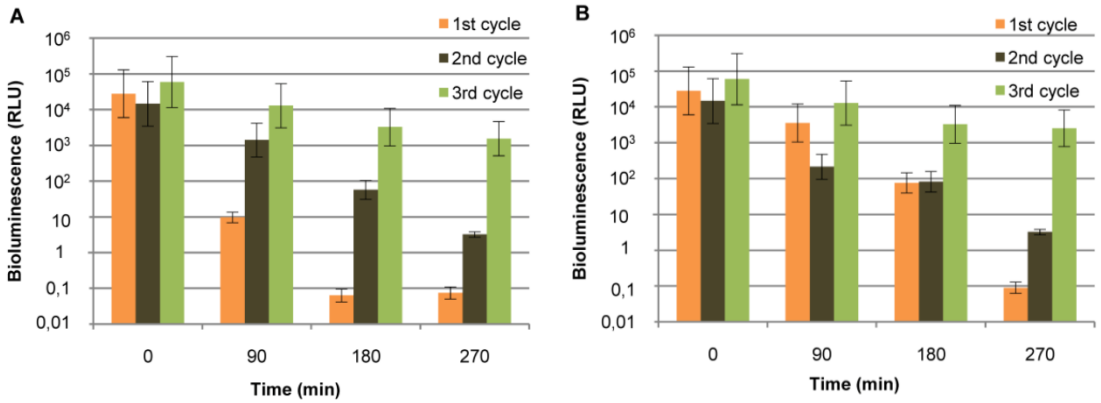


**Figure 10.4** Photoinactivation experiments of *V. fischeri* (initial concentration of $10^7$ CFU $mL^{-1}$) with recycling of 20 µM of hybrid 6 (**A**) and hybrid 7 (**B**) under a permanent magnetic field (bars represent mean ± standard deviation of three photoinactivation cycles of 270 min each with an irradiance of 40 W $m^{-2}$, and a light dose of 64.8 J $cm^{-2}$).

With hybrid **6**, it was first suspected that during the photodynamic process the magnetic core ($Fe^{2+}/Fe^{3+}$) could suffer some demagnetization. In fact, singlet oxygen, being a strong oxidizing agent and the main reactive oxygen species formed during the photodynamic process with this PS, could diffuse through the amorphous silica shell and promote the oxidation of $Fe^{2+}$ to $Fe^{3+}$. This could justify the typical yellow color of $Fe_2O_3$ observed in the samples during the PDI cycles, contrarily to what happened in the dark control. The core of the irradiated NP would then be constituted by non-magnetic $Fe_2O_3$ core which limited the magnetic deposition. So, during supernatant removal, suspended non-magnetic active hybrid would be discarded/lost, which could explain the decreasing of photoinactivation efficiency.

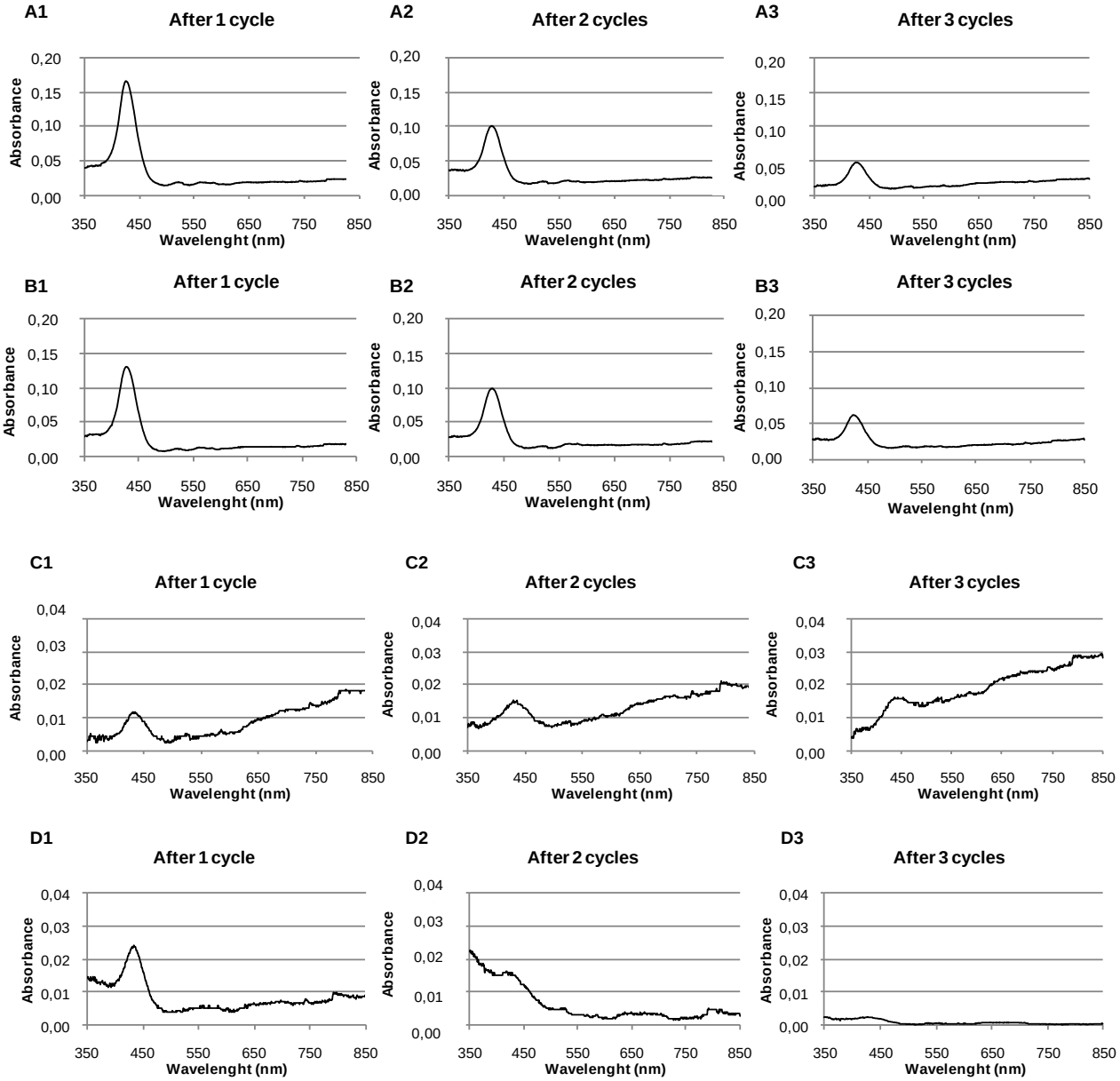


**Figure 10.5** UV-Vis spectra of the supernatant of the samples centrifuged 30 min at 39,788 x *g*, after each photoinactivation cycle (recycling) with hybrids **6** ($Fe_3O_4$) (**A1-A3**, irradiated samples; **C1-C3**, dark controls) and **7** ($CoFe_2O_4$) (**B1-B3**, irradiated samples; **D1-D3**, dark controls).

However, the UV-Vis spectra and the recycling studies with the hybrid **7** ($CoFe_2O_4$) samples and dark controls (Figures 10.5B and 10.5D and 10.4B) show similar behavior as hybrid **6**. These results discarded the hypothesis of iron core oxidation and supported the disaggregation of superficial smaller active NPs (decorated with the PS) from the big hybrid cluster as the most probable hypothesis to explain the decrease in the photoinactivation efficiency.

### 10.4.4 Porphyrin and hybrids photobleaching experiments

The two nanomagnet-porphyrin hybrids **6** and **7** (20 μM of PS) and the respective cationic NPs **8** and **9** (435 mg $dm^{-3}$ and 518.5 mg $dm^{-3}$, respectively) were used in photo-oxidation experiments to check the loss of magnetic properties (by reactive oxygen species formed during irradiation) and/or if there was photobleaching of porphyrin. These experiments were done simultaneously with the cationic porphyrin **1a** in solution (5 μM) in a final volume of 50 mL in a glass beaker of 600 mL, and irradiated under the same conditions (Figure 10.6).

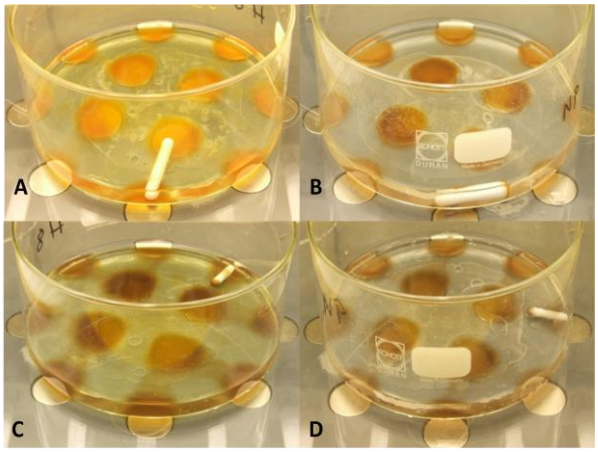


**Figure 10.6** Suspensions of cationic hybrids **6** ($Fe_3O_4$) and **7** ($CoFe_2O_4$) (**A** and **C**) irradiated for 24 hours with visible light (40 W $m^{-2}$), and the corresponding magnetic nanoparticles **8** (**B**) and **9** (**D**).

The UV-Vis spectra of the non-supported porphyrin **1a** (Figure 10.7) in PBS confirmed its high stability after 24 h of irradiation at an irradiance of 40 W $m^{-2}$. No significant alterations were detected in the initial and final UV-Vis spectrum.

A different situation was observed with the UV-Vis spectra of the supernatant PBS from hybrid suspensions which showed a gradual increase of disaggregated hybrid throughout the irradiation time/cycles (Figure 10.8A1 and 10.8B1). After 24 h of irradiation, the absorption intensity was very similar between hybrids (Figure 10.8A2 and 10.8B2). The spectra of the

irradiated NP **8** and **9** show no absorption peaks in the UV-Vis region as expected (Figure 10.8A2 and 10.8B2).

The UV-Vis spectra of the filtrates of hybrid suspensions showed absorption bands consistent with the presence of nanomagnet-porphyrin hybrids (Figure 10.8A3 and 10.8B3). Figure 10.9 (A and C) also shows the yellowish color of the filtrates evidencing the presence of hybrids.

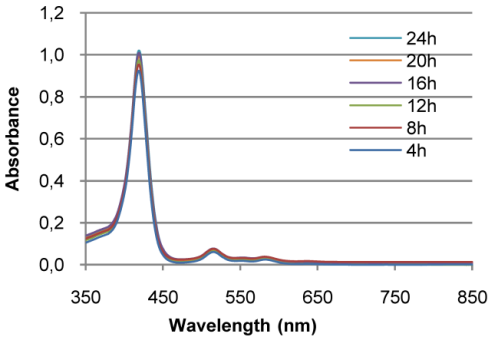


**Figure 10.7** UV-Vis spectra of free Tri-Py$^{+}$-Me-PF (5.0 µM) recorded every 4 h during 24 h of irradiation at 40 W m$^{-2}$.

It is worth to mention that Barnejee et al. also reported activity loss during their studies involving the recovery and recycling of protoporphyrin IX (PPIX) attached to acid-functionalized multi-walled carbon nanotubes (NT-P) against influenza virus. (380) The authors justify that the recycling of NT-P was dependent on both photobleaching of the porphyrin moiety as well as on the yield of recovery of NT-P after each use. (380) In the experiments, the loss of hybrid during removal seems to be the main cause of activity loss and not the photobleaching of the porphyrin.

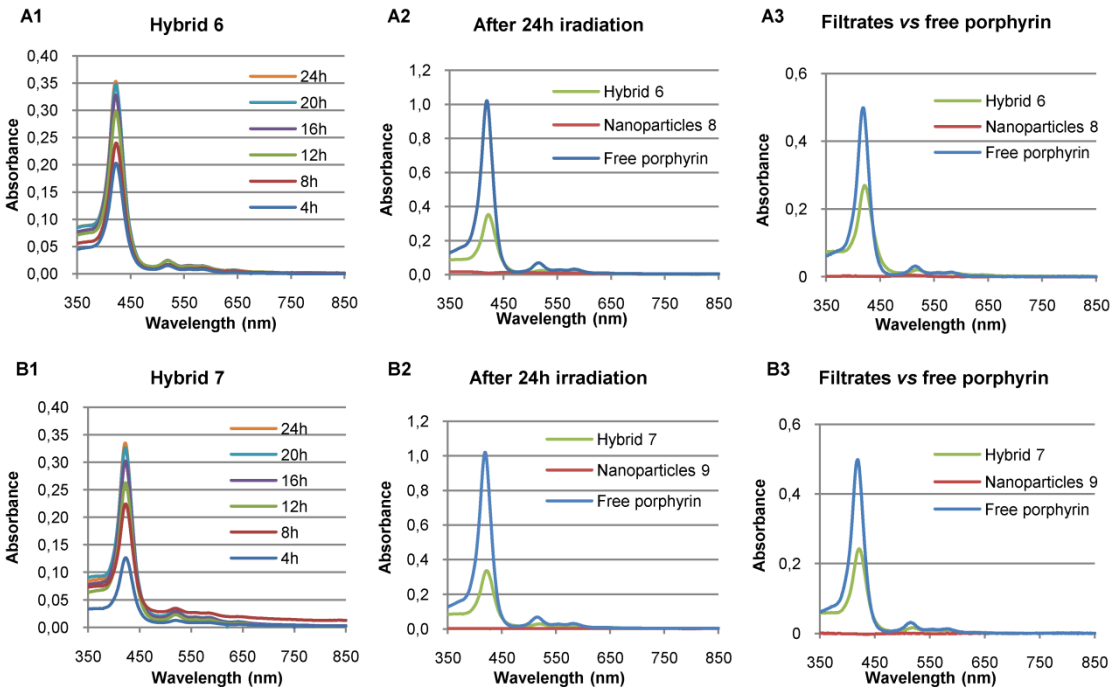

**Figure 10.8** UV-Vis spectra of the hybrids **6** ($Fe_3O_4$) and **7** ($CoFe_2O_4$) and the respective cationic nanoparticles **8** and **9**: recorded in the supernatant liquid after magnetic sedimentation on a magnetic plate, every 4 h during 24 h of irradiation with an irradiance of 40 W $m^{-2}$ (**A1**, **B1**); comparison among the supernatants from the suspensions of hybrids, the respective cationic magnetic nanoparticles and the cationic porphyrin **1a** after 24 h of irradiation (**A2**, **B2**); comparison among the filtered suspensions of hybrids, of the respective nanoparticles and cationic porphyrin **1a** after 24 h of irradiation (**A3**, **B3**).

### 10.4.5 X-ray diffraction analysis of the hybrids after 24 h irradiation

The powder XRD pattern of the NPs **8** confirmed the maintenance of magnetite. The powder XRD pattern of the NPs **9** after 24 h irradiation contains the peaks at *ca.* 30.1, 35.5, 43.1, 57.1 and 62.7° 2θ, which match the peaks of magnetite, indicating that $CoFe_2O_4$ is crystallized as Co-Fe mixed metal magnetite (Figures 10.10 and 10.11). The XRD patterns also indicated that both materials are stable under irradiation. These peaks are broad, which is due to the small size of crystallites. The hump between 17 and 26° 2θ results from amorphous $SiO_2$ shell. The peaks due to porphyrinic PS do not appear in powder XRD pattern, which may be due to two reasons: the amount of porphyrin is low and/or the molecules are well separated on the NP surface. The powder XRD patterns of the samples after 24 h irradiation have, not only those broad magnetite peaks, but also sharp peaks at 27.3, 31.7 and 45.5° 2θ. These sharp peaks are from NaCl residues from the PBS used in the test solution. The EDS indicates that the Fe/Co ratio is *ca.* 2, which is in accordance with composition of Co-Fe mixed metal magnetite by assuming $Co^{2+}$ and $Fe^{3+}$ in the material. The Si/(Fe+Co) ratio of NP **9** is *ca.* 16, which can be used to estimate the $SiO_2$ shell. The Si/Fe ratio of NPs **8** is *ca.* 18, which indicated that the $SiO_2$ shell of NP **8** is very similar to that of NP **9**.

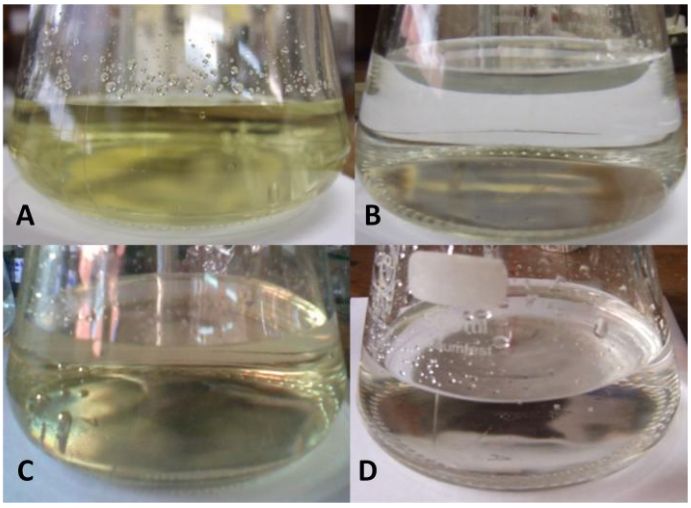


**Figure 10.9** Filtrates of cationic hybrids suspensions **6** ($Fe_3O_4$, **A**) and **7** ($CoFe_2O_4$, **C**) irradiated for 24 h with an irradiance of 40 W $m^{-2}$, and the corresponding cationic magnetic nanoparticles **8** (**B**) and **9** (**D**).

### 10.4.6 Reuse of free porphyrin and hybrids 6 and 7

In order to evaluate the efficiency of the photoactive nanomaterials, without loss of any of the active NPs, even knowing that this would not be the best practical protocol, the reuse of these compounds/materials was tested without supernatant removal (Scheme 10.3). The results of the six cycles of non-supported porphyrin **1a** reuse (Figure 10.12A) show the ability of producting reactive oxygen species, capable to cumulatively inactivate ≈ 32 $\log_{10}$ bacteria in 7h30, at least. From cycle to cycle, the time needed to inactivate all the viable cells increases (from 30 to 90 min). This should be due to the increasing organic matter from the successive addition of bacteria, since there was no removal of the supernatant between cycles. From the first cycle to the next cycles, **1a** is not so available to bind to the cells because the main cell binding should occur in the first cycle. However, between the second and third cycles, some aggregates can be seen, suggesting that the organic matter is largely increasing. With the continuous stirring, the aggregates gradually dissolve, and it seems that the **1a** previously bonded to the cells is released, being available to produce singlet oxygen and inactivate new bacteria. The presence of organic matter in the medium has a scavenger effect on reactive oxygen species and may bind to the photosensitizer, thus affecting the photoinactivation process. (554)

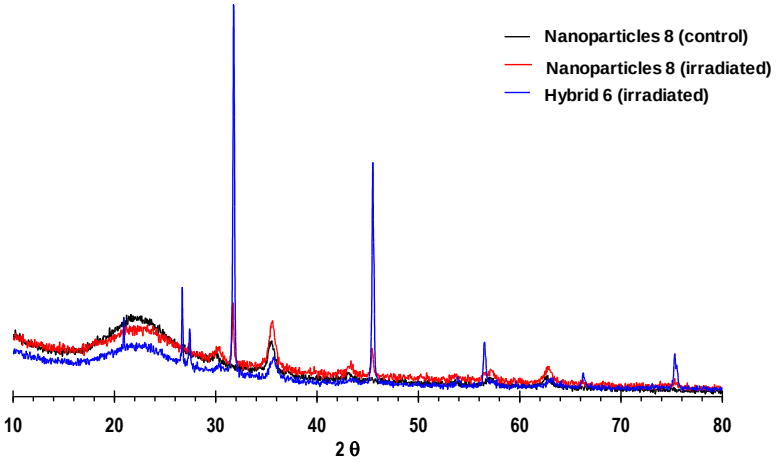


**Figure 10.10** X-ray diffraction analysis of magnetic nanoparticles **8** and hybrid **6** ($Fe_3O_4$) after 24 h of irradiation (40 W $m^{-2}$). Non-irradiated nanoparticles **8** (black line) were used as control.

The results from the reuse of hybrid **6** ($Fe_3O_4$) in six cycles (Figure 10.12B) show that 2h30 are required to inactivate ≈ 7 $\log_{10}$ of bacteria (first cycle) and that the produced reactive oxygen species are able to cumulatively inactivate ≈ 42 $\log_{10}$ of bacteria in 21h30, at least.

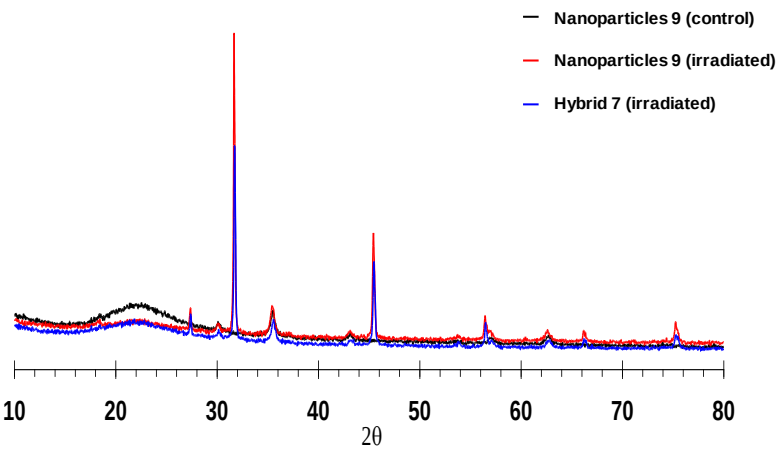


**Figure 10.11** X-ray diffraction analysis of magnetic nanoparticles **9** and hybrid **7** ($CoFe_2O_4$) after 24 h of irradiation (40 W $m^{-2}$). Non-irradiated nanoparticles 9 (black line) were used as control.

Relatively to hybrid **7** ($CoFe_2O_4$) (Figure 10.12C), it was shown that 4h30 are necessary to cumulatively inactivate ≈ 7 $log_{10}$ of bacteria (first cycle) and that the produced reactive oxygen species are able to inactivate at least ≈ 38 $log_{10}$ of bacteria in 27 h.

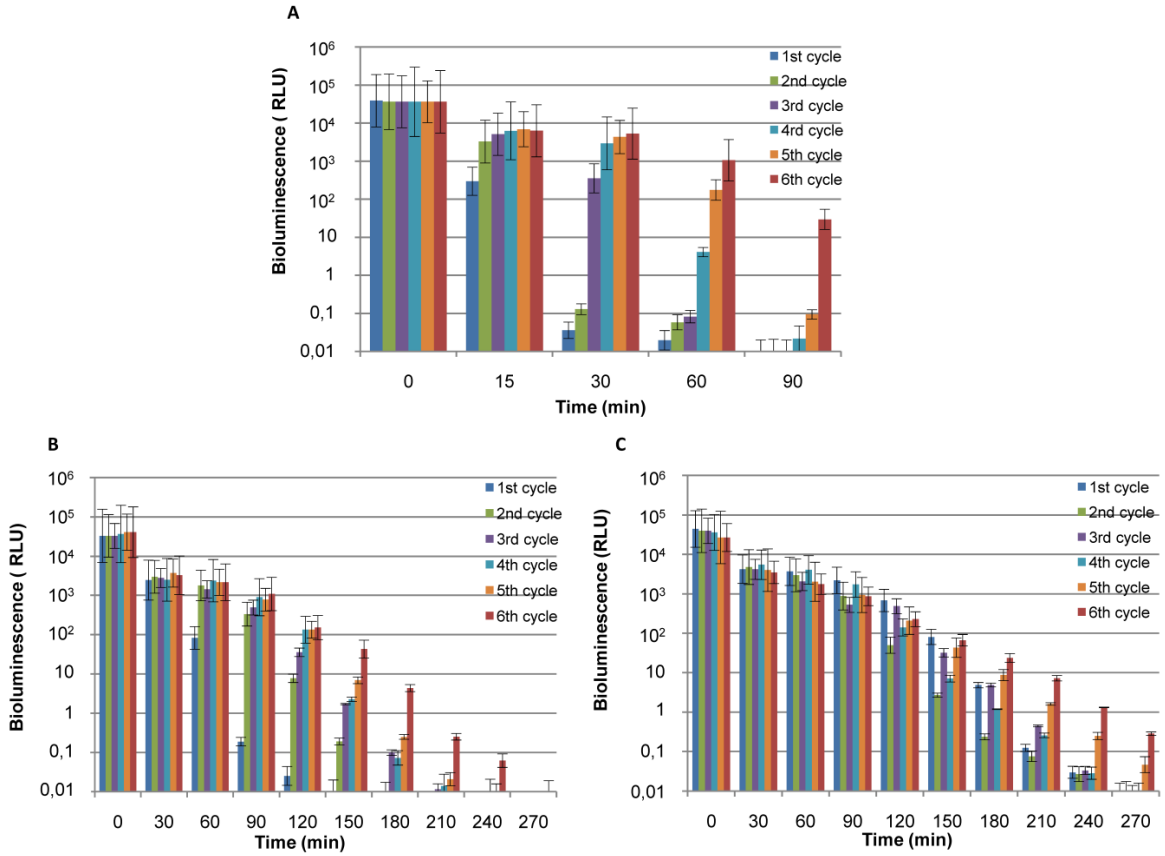


**Figure 10.12** Reuse of cationic porphyrin **1a** at 5 µM (**A**) and hybrids **6** (**B**) and **7** (**C**) at 20 µM of PS, by successive addition of bacteria for 6 cycles (bars represent mean ± standard deviation of 6 photoinactivation cycles with an irradiance of 40 W $m^{-2}$).

## 10.5 Conclusions

Considering the preliminary results obtained with hybrid **6** ($Fe_3O_4$), a new nanomagnet-porphyrin hybrid based on a $CoFe_2O_4$ core was prepared and tested. This new core, more resistant to oxidation processes, could clarify the hypothesis of the $Fe_3O_4$ core oxidation during the recycling experiments. However, the XRD data of the photobleaching studies of both hybrids did not present considerable changes.

Although for a real application in water disinfection of these photoactive magnetic nanoparticles, they should be easily and completely retained by a permanent magnetic field, allowing their recycling, herein two different approaches were tested (recycling and reuse protocols) to understand why the PDI efficiency of the studied materials decreases after several cycles.

The results point out that in the recycling approach, a portion of the most active hybrid is lost when the supernatant is discarded due to the disaggregation of small hybrid nanoparticles from the functionalized clusters. The reuse approach shows that these materials maintain their activity but the inactivation time required is dependent on the organic matter.

In future experiments, it is mandatory to prepare bigger particles, with suitable size to allow the recycling process to b easier and more efficient.

# Chapter 11. General conclusions and future perspective

# 11 General conclusions and future perspective

Photodynamic inactivation (PDI) is considered a valuable alternative to the conventional antimicrobial approaches. In the clinical area, PDI is intended to be used for the treatment of superficial and localized infections of the skin and oral cavity, given the accessibility of these infection sites and the susceptibility of microorganisms. Since it does not act on a specific cell target, as it is a multi-target process, its mechanism of action is still unclear. Beyond the clinical field, PDI offers a range of potential applications, including water disinfection. Since there is the possibility to immobilize the photosensitizer and to use sunlight to carry out the treatment, research is required to evaluate the impact of this methodology in this area.

This thesis sought to address the PDI of bacteria with cationic porphyrins in two ways: in studying the cellular targets and evaluating the potential application in water disinfection. Accordingly, in the first part of the thesis, the oxidative effects of PDI were evaluated in the major phospholipid classes, in total proteins and in intracellular nucleic acids of *S. warneri* and *E. coli*, using conventional methodologies and a rapid method.

Photosensitization with porphyrin Tri-Py$^{+}$-Me-PF induces changes in the phospholipid profile of bacteria, in particular by varying the relative abundance in some of the major phospholipid classes and also by the formation of oxidized molecular species from unsaturated fatty acids, most frequently in the cardiolipins from Gram-positive bacteria and phosphatidylethanolamines from Gram-negative bacteria. These oxidized species were identified as hydroxy and hydroperoxy derivatives (in *E. coli*) and also as bearing carbonyl groups (in *S. warneri*).

These studies contain the first scientific evidence that phospholipids are important targets of oxidative damage caused by PDI of bacteria. Given the structural difference of the bacterial cell wall, these damages have a different degree of importance in the inactivation process, depending if the bacterium is Gram-negative or Gram-positive.

The decrease in the nucleic acid content of bacteria decreases as the photoinactivation occurs, in a parallel fashion. Porphyrins Tri-Py$^{+}$-Me-PF and Tetra-Py$^{+}$-Me are efficient photosensitizers in inactivating *S. warneri* and *E. coli* causing reductions in cell viability much higher (> 99.99999%) than the minimum bactericidal concentration (99.9 %) at relatively low doses (0.5 - 5 μM) and low light doses (up to 64.8 J cm$^{-2}$). However, the inactivation is faster

with the tricationic porphyrin on both bacteria. In the case of *E. coli*, a hierarchy of degradation of the nucleic acids could be established, being 23S RNA degraded firstly, followed by 16S rRNA and then, genomic DNA. This degradation of nucleic acids occurs when cells are already inactivated and, therefore, these are not the primary target of attack by reactive oxygen species.

The greater efficiency of the tricationic porphyrin towards Tetra-$Py^+$-Me is associated with higher production of singlet oxygen, with its cellular localization and its amphiphilic character. Tri-$Py^+$-Me-PF has shown to have greater affinity for *E. coli* and Tetra-$Py^+$-Me for *S. warneri*, but this feature does not determine *per se* the porphyrin efficiency.

Total bacterial proteins are largely affected after photoinactivation (after half reduction of bacterial viability), the effects being faster and more drastic with Tri-$Py^+$-Me-PF on both bacteria, since most of the proteins are degraded during light exposure.

In *E. coli* photosensitized with Tri-$Py^+$-Me-PF, the most evident results suggest increased expression of a protein presumably corresponding to Dps, a protein that non-specifically binds to DNA, acting as a protection from exposure to toxicity, and the appearance of new proteins assigned to stress response (YggX, UspG, OsmC). With Tetra-$Py^+$-Me, the most obvious results suggest increased expression of proteins presumably involved in stress response (YgiN or GrcA), and disappearance of several proteins assigned to proteins involved in metabolic or biosynthetic processes (MdoG or PPSA) as well as in response to cellular stress (DnaK or GroL).

In *S. warneri*, besides degradation of proteins in large scale, some new proteins with high molecular weight appear, associated with the possible formation of cross-linked complexes, immediately after irradiation with Tri-$Py^+$-Me-PF and more slowly with Tetra-$Py^+$-Me. Other proteins are detected after treatment and may be associated with specific functions of response to PDI.

Evidence of this work showed that the bacterial proteins are important targets of PDI. The results suggest that even though the attempt to respond to cell injury by upregulation or synthesis of new proteins of response to stress, the damage is lethal and can inhibit cellular response both during and after treatment.

The infrared spectroscopy analysis of the oxidative effects induced by PDI on bacteria is corroborated by the results obtained by conventional methods and allows studying the cellular changes at a molecular level. With this methodology, it was demonstrated that the difference between the two porphyrins occurs at the level of kinetics of photoinactivation,

both in the inactivation of *E. coli* and *S. warneri*, since the cellular targets are the same with both porphyrins on each strain.

In *E. coli*, the analysis of infrared spectra evidenced that most of the induced changes are associated with proteins, lipids and nucleic acids, with both porphyrins. The presence of carbonyl groups is associated with lipid oxidation and protein oxidation. A more detailed analysis of the spectra showed changes in the protein conformation (disordered structures, exposure of amino acids) and in the protein composition (modification of amino acid side chains). The increase of the bands corresponding to methyl groups and esters of fatty acids in the lipid region and can be associated with a change in the composition of phospholipids. The increase of phosphate groups and bonds associated with the ribose are assigned to nucleic acid damage.

In *S. warneri*, the main changes were detected in proteins, namely changes in their conformation, degradation, and presence of glycosylated proteins. Degradation of nucleic acids was also suggested by analysis of spectra. Some changes in spectral peaks assigned to polysaccharides suggest that oxidative damage affects these molecules but probably in a later stage of photosensitization, when major alterations have already occur, as a consequence of the attack of secondary and radical species formed from singlet oxygen activity.

Infrared spectroscopy has the advantage of being a reliable tool, less time-consuming, less expensive and much less laborious than conventional methodologies, enabling the study of bonding types, functional groups and molecular conformations.

The results reflected that the modifications induced by photosensitization on bacteria, in the experimental conditions, are not target-specific but global, with major consequences on proteins.

From the actual scientific knowledge on the mode of action and cellular targets of bacterial PDI, and from the results obtained in the first part of this thesis, some assumptions can be addressed:

- Interactions between photosensitizers and cellular constituents rely on their affinity for cell wall components. The photosensitizer chemical structures, namely the number of positive charges, degree of hydrophobicity and spatial distribution of substituents are important features to have in account;
- The amount of photosensitizer that binds to bacteria depends, at least and simultaneously, on its amphiphilic character and on its affinity for the cellular components;

- Shrunken and constricted cells with irregular surfaces observed at early PDI stages are associated with structural changes at the outer membrane and alterations in the inner membrane integrity;
- Decrease of membrane integrity during PDI is a function of photosensitizer concentration and light dose, observed by leakage of cytoplasmic constituents, increase in β-galactosidase activity and in protein amounts;
- Cationic porphyrins appear to inhibit membrane potential by inhibiting respiration and xanthene dyes by increasing membrane permeability in early stages of PDI;
- Efficient photoinactivation of biofilms is affected by their structural, biochemical and metabolic features, and to improve efficiency synergistic effects using PDI and other therapeutic approaches are being sought;
- Oxidative damage on nucleic acids occurs when cells are extensively photoinactivated and is influenced by the photosensitizer structure and its features;
- PDI induces lipid peroxidation, changes in the amount of phospholipids and formation of oxidized molecular species;
- Oxidative damage on proteins involved in metabolic activities, response to oxidative stress, cell division and sugar uptake suggest an underlying specific mechanism;
- Although some proteins and enzymes involved in the oxidative stress response are overexpressed upon PDI, singlet oxygen can inactivate them as well as can inactivate virulence factors, and there is no recognized mechanism of resistance to PDI;
- Infrared spectroscopy, supported by complementary approaches such as mass spectrometry-based lipidomics and proteomics analyses, will help to provide further insight into the response mechanism to this type of oxidative stress as well as in optimizing the treatment protocol, by evaluating the effects on specific strains, the efficiency of different photosensitizers, and irradiation conditions.

PDI has been shown to have a very broad range of applications that go beyond the medical scope. In fact, this methodology is being explored in water and foodstuff decontamination, to control insect pests and also fish infection in aquaculture ponds, or to disinfect surfaces, objects, or materials in a self-cleaning way. The research in "non-clinical PDI" has had great development in recent years, particularly owing to the huge development in the area of materials chemistry, nanotechnology, and of new classes of photosensitizers, but also due to the search for economically, environmentally and humanly sustainable alternatives to currently available options. It also shows promising results, not only in terms of the

photosensitizing materials, but also on the efficiency of inactivation of a vast range of microbes and other organisms.

The use of sunlight provides this methodology the advantage of being cost-effective in relation to the light source. Photosensitizers of natural origin or easily accessible synthetically, are also a cost-effective possibility as, for instance, in developing countries where the use of expensive photosensitizers is not economically feasible.

As new photoinactivation experiments are being designed and tested, new methods of monitoring the efficiency of photoinactivation are needed. The use of naturally or genetically modified bioluminescent strains of microorganisms, represents a simple, fast, reliable and economic way to achieve this goal, both in *in vitro* and *in vivo*.

In the second part of the experimental work of this thesis, a bioluminescent bacterium from marine origin, *Vibrio fischeri*, representing Gram-negative bacteria, was used for environmentally-oriented experiments.

In aquaculture waters, as demonstrated herein, the efficiency of photoinactivation is determined by the content of suspended solids, the photosensitizer concentration and light fluence. Factors such as temperature, salinity and dissolved oxygen are not likely to affect the efficiency of PDI of bacteria in aquaculture conditions. In environmental aqueous matrices carrying high loads of suspended matter, as in aquaculture waters, it is necessary to adjust the concentration of PS and light dose in order to achieve an efficient photoinactivation. The use of solar irradiation not only accelerates the process but also minimizes or avoids the costs associated with the use of an artificial energy source.

The immobilization of Tri-Me-$Py^{+}$-PF on magnetic nanoparticles ($Fe_3O_4$ and $CoFe_2O_4$) allows the recycling of photosensitizer, without loss of efficiency by photodegradation.

The porphyrin used in the free form is photostable and highly effective in inactivating *V. fischeri* in several cycles. The organic matter accumulation slows down the process, due to the competitive effect of the nanoparticles in relation to reactive oxygen species, although more than 38 $\log_{10}$ of bacterial inactivation are achieved after, at least, 27 h of irradiation with very mild irradiance (4.0 mW $cm^{-2}$).

In the nanomagnet-porphyrin hybrids, the magnetite from the nanoparticles remains stable during the photoinactivation experiments and during the recycling process. The observed loss of photobiocidal activity can be assigned to the loss of small nanoparticles containing the active porphyrin, which can disaggregate from the nanoclusters, during water removal.

This work presents the first evidence of reuse and recycling capability of cationic nanomagnet-porphyrin hybrids for water disinfection. The results suggest the need of using bigger nanoparticles to immobilize the photosensitizer in order to facilitate the recovery and recycling and make the process even more efficient.

PDI is a promising strategy for infection treatment and further studies should concern the specificity of PDI by the way the photosensitizer interacts with cell components (main cellular components and virulence factors) and damages specific targets, development of resistance mechanisms, efficient inactivation of biofilms and multi-drug resistant strains, photosensitizer and light delivery strategies and parameters, and host cell response to infection.

For water disinfection by PDI, further studies should consider optimizing the support material, testing the ability of recovery and recycling of the immobilized photosensitizer, adjusting its concentration and light dose to the aqueous matrix.

## References

1. The evolving threat of antimicrobial resistance: options for action. Geneva: World Health Organization; 2012.

2. Leung E, Weil DE, Raviglione M, Nakatani H. The WHO policy package to combat antimicrobial resistance. Bull World Health Organ. 2011;89(5):390-2.

3. Wang J-F, Chou K-C. Metallo-beta-lactamases: structural features, antibiotic recognition, inhibition, and inhibitor design. Curr Top Med Chem. 2013;13(10):1242-53.

4. Liu Y, Imlay JA. Cell death from antibiotics without the involvement of reactive oxygen species. Science. 2013;339(6124):1210-3.

5. Thakor NS, Wilson KS, Scott PG, Taylor DE. An improved procedure for expression and purification of ribosomal protection protein Tet (O) for high-resolution structural studies. Protein Expression Purif. 2007;55(2):388-94.

6. Witte W, Cuny C, Klare I, Nübel U, Strommenger B, Werner G. Emergence and spread of antibiotic-resistant Gram-positive bacterial pathogens. Int J Med Microbiol. 2008;298(5):365-77.

7. Wainwright M, Amaral L. Photobactericides—a local option against multi-drug resistant bacteria. Antibiotics. 2013;2(2):182-90.

8. Foote CS. Definition of type I and type II photosensitized oxidation. Photochem Photobiol. 1991;54(5):659.

9. Girotti AW. Photosensitized oxidation of membrane lipids: reaction pathways, cytotoxic effects, and cytoprotective mechanisms. J Photochem Photobiol B. 2001;63(1-3):103-13.

10. Wainwright M. Photodynamic antimicrobial chemotherapy (PACT). J Antimicrob Chemother. 1998;42(1):13-28.

11. Dai T, Huang Y-Y, Hamblin MR. Photodynamic therapy for localized infections—state of the art. Photodiagn Photodyn Ther. 2009;6(3):170-88.

12. Kharkwal GB, Sharma SK, Huang Y-Y, Dai T, Hamblin MR. Photodynamic therapy for infections: clinical applications. Lasers Surg Med. 2011;43(7):755–67.

13. Almeida A, Cunha Â, Faustino M, Tomé A, Neves M. Porphyrins as antimicrobial photosensitizing agents. In: Hamblin M, Jori G, editors. Photodynamic inactivation of microbial pathogens: medical and environmental applications. Cambridge: Royal Society of Chemistry; 2011. p. 83-160.

14. Wainwright M. Photodynamic medicine and infection control. J Antimicrob Chemother. 2012;67(4):787-8.

15. Agostinis P, Berg K, Cengel KA, Foster TH, Girotti AW, Gollnick SO, et al. Photodynamic therapy of cancer: an update. CA Cancer J Clin. 2011;61(4):250-81.

16. Juzeniene A, Nielsen KP, Moan J. Biophysical aspects of photodynamic therapy. J Environ Pathol Toxicol Oncol. 2006;25(1-2).

17. Sharman WM, Allen CM, van Lier JE. [35] Role of activated oxygen species in photodynamic therapy. Methods Enzymol. 2000;319:376-400.

18. Bronshtein I, Afri M, Weitman H, Frimer AA, Smith KM, Ehrenberg B. Porphyrin depth in lipid bilayers as determined by iodide and parallax fluorescence quenching methods and its effect on photosensitizing efficiency. Biophys J. 2004;87(2):1155-64.

19. Krasnovsky Jr A. Singlet molecular oxygen in photobiochemical systems: IR phosphorescence studies. Membr Cell Biol. 1998;12(5):665.

20. Moan J. On the diffusion length of singlet oxygen in cells and tissues. J Photochem Photobiol B. 1990; 6:343-4.

21. Ochsner M. Photophysical and photobiological processes in the photodynamic therapy of tumours. J Photochem Photobiol B. 1997;39(1):1-18.

22. Bergamini CM, Gambetti S, Dondi A, Cervellati C. Oxygen, reactive oxygen species and tissue damage. Curr Pharm Des. 2004;10(14):1611-26.

23. Plaetzer K, Krammer B, Berlanda J, Berr F, Kiesslich T. Photophysics and photochemistry of photodynamic therapy: fundamental aspects. Lasers Med Sci. 2009;24(2):259-68.

24. Pushpan SK, Venkatraman S, Anand VG, Sankar J, Parmeswaran D, Ganesan SC, T.K. Porphyrins in photodynamic therapy - a search for ideal photosensitizers. Curr Med Chem Anticancer Agents. 2002;2:187-207.

25. Silhavy TJ, Kahne D, Walker S. The bacterial cell envelope. Cold Spring Harbor Perspect Biol. 2010;2(5).

26. Vollmer W, Seligman SJ. Architecture of peptidoglycan: more data and more models. Trends Microbiol. 2010;18(2):59-66.

27. Wang X, Quinn PJ. Lipopolysaccharide: biosynthetic pathway and structure modification. Prog Lipid Res. 2010;49(2):97-107.

28. Jori G. Photodynamic therapy of microbial infections: state of the art and perspectives. J Environ Pathol Toxicol Oncol. 2006;25(1-2):505-20.

29. Costa L, Faustino MAF, Neves MGP, Cunha Â, Almeida A. Photodynamic inactivation of mammalian viruses and bacteriophages. Viruses. 2012;4(7):1034-74.

30. St. Denis TG, Dai T, Izikson L, Astrakas C, Anderson RR, Hamblin MR, et al. All you need is light: antimicrobial photoinactivation as an evolving and emerging discovery strategy against infectious disease. Virulence. 2011;2(6):509-20.

31. Wainwright M. Methylene blue derivatives—suitable photoantimicrobials for blood product disinfection? Int J Antimicrob Agents. 2000;16(4):381-94.

32. Usacheva MN, Teichert MC, Biel MA. Comparison of the methylene blue and toluidine blue photobactericidal efficacy against gram-positive and gram-negative microorganisms. Lasers Med Sci. 2001;29(2):165-73.

33. Usacheva M, Teichert M, Usachev Y, Sievert C, Biel M. Interaction of the photobactericides methylene blue and toluidine blue with a fluorophore in *Pseudomonas aeruginosa* cells. Lasers Surg Med. 2008;40(1):55-61.

34. Usacheva MN, Teichert MC, Sievert CE, Biel MA. Effect of $Ca^{+}$ on the photobactericidal efficacy of methylene blue and toluidine blue against gram-negative bacteria and the dye affinity for lipopolysaccharides. Lasers Med Sci. 2006;38(10):946-54.

35. Cronan JE. Bacterial membrane phospholipids: where do we stand? Annu Rev Microbiol. 2003;57(1):203-24.

36. Domingues MM, Castanho MA, Santos NC. rBPI21 promotes lipopolysaccharide aggregation and exerts its antimicrobial effects by (hemi) fusion of PG-containing membranes. PLoS One. 2009;4(12):e8385.

37. Shireen T, Singh M, Dhawan B, Mukhopadhyay K. Characterization of cell membrane parameters of clinical isolates of *Staphylococcus aureus* with varied susceptibility to alpha-melanocyte stimulating hormone. Peptides. 2012;37(2):334-9.

38. Epand RM, Epand RF. Lipid domains in bacterial membranes and the action of antimicrobial agents. Biochim Biophys Acta, Biomembr. 2009;1788(1):289-94.

39. Cordeiro RM, Miotto R, Baptista MS. Photodynamic efficiency of cationic *meso*-porphyrins at lipid bilayers: insights from molecular dynamics simulations. J Phys Chem B. 2012;116(50):14618-27.

40. de Sousa Neto D, Hawe A, Tabak M. Interaction of meso-tetrakis (4-*N*-methylpyridyl) porphyrin in its free base and as a Zn (II) derivative with large unilamellar phospholipid vesicles. Eur Biophys J. 2013;42:267–79.

41. Pashkovskaya A, Maizlish V, Shaposhnikov G, Kotova E, Antonenko Y. Role of electrostatics in the binding of charged metallophthalocyanines to neutral and charged phospholipid membranes. Biochim Biophys Acta, Biomembr. 2008;1778(2):541-8.

42. Fiel RJ, Datta-Gupta N, Mark EH, Howard JC. Induction of DNA damage by porphyrin photosensitizers. Cancer Res. 1981;41(9 Part 1):3543-5.

43. Lang K, Mosinger J, Wagnerová D. Photophysical properties of porphyrinoid sensitizers non-covalently bound to host molecules; models for photodynamic therapy. Coord Chem Rev. 2004;248(3):321-50.

44. Viola G, DallAcqua F. Photosensitization of biomolecules by phenothiazine derivatives. Curr Drug Targets. 2006;7(9):1135-54.

45. Dutikova I, Borisova O, Shchelkina A, Lin J, Huang S, Shtil A, et al. [5, 10, 15, 20-Tetra-(N-methyl-3-pyridyl) porphyrin destabilizes the anti-parallel telomeric quadruplex d (TTAGGG) 4]. Molekuliarnaia biologiia. 2009;44(5):929-37.

46. Sari MA, Battioni JP, Dupré D, Mansuy D, Le Pecq JB. Interaction of cationic porphyrins with DNA: importance of the number and position of the charges and minimum structural requirements for intercalation. Biochemistry. 1990;29(17):4205-15.

47. Kovaleva OA, Tsvetkov VB, Shchyolkina AK, Borisova OF, Ol'shevskaya VA, Makarenkov AV, et al. The role of carboxymethyl substituents in the interaction of tetracationic porphyrins with DNA. Eur Biophys J. 2012;41(9):723-32.

48. Epe B. DNA damage spectra induced by photosensitization. Photochem Photobiol Sci. 2012;11(1):98-106.

49. Cadet J, Douki T, Badouard C, Favier A, Ravanat J-L. Oxidatively generated damage to cellular DNA: mechanistic aspects. In: Evans MD, Cooke MS, editors. Oxidative damage to nucleic acids: Landes Bioscience and Springer Science; 2007. p. 1-13.

50. Redmond RW, Gamlin JN. A compilation of singlet oxygen yields from biologically relevant molecules. Photochem Photobiol. 1999;70(4):391-475.

51. Preuß A, Zeugner L, Hackbarth S, Faustino MAF, Neves MGPMS, Cavaleiro JAS, et al. Photoinactivation of *Escherichia coli* (SURE2) without intracellular uptake of the photosensitizer. J Appl Microbiol. 2013;114(1):36-43.

52. Strakhovskaya M, Antonenko YN, Pashkovskaya A, Kotova E, Kireev V, Zhukhovitsky V, et al. Electrostatic binding of substituted metal phthalocyanines to enterobacterial cells: its role in photodynamic inactivation. Biochemistry (Moscow). 2009;74(12):1305-14.

53. Jin H, Huang X, Chen Y, Zhao H, Ye H, Huang F, et al. Photoinactivation effects of hematoporphyrin monomethyl ether on Gram-positive and -negative bacteria detected by atomic force microscopy. Appl Microbiol Biotechnol. 2010;88(3):761-70.

54. Pudziuvyte B, Bakiene E, Bonnett R, Shatunov PA, Magaraggia M, Jori G. Alterations of *Escherichia coli* envelope as a consequence of photosensitization with tetrakis(N-ethylpyridinium-4-yl)porphyrin tetratosylate. Photochem Photobiol Sci. 2011;10(6):1046-55.

55. Yow C, Tang HM, Chu ES, Huang Z. Hypericin-mediated photodynamic antimicrobial effect on clinically isolated pathogens. Photochem Photobiol. 2012;88(3):626-32.

56. Alves E, Faustino MAF, Tomé JPC, Neves MGPMS, Tomé AC, Cavaleiro JAS, et al. Nucleic acid changes during photodynamic inactivation of bacteria by cationic porphyrins. Bioorg Med Chem. 2013;21(14):4311–8.

57. Kato H, Komagoe K, Nakanishi Y, Inoue T, Katsu T. Xanthene dyes induce membrane permeabilization of bacteria and erythrocytes by photoinactivation. Photochem Photobiol. 2012;88(2):423-31.

58. George S, Kishen A. Influence of photosensitizer solvent on the mechanisms of photoactivated killing of *Enterococcus faecalis*. Photochem Photobiol. 2008;84(3):734-40.

59. Caminos DA, Spesia MB, Pons P, Durantini EN. Mechanisms of *Escherichia coli* photodynamic inactivation by an amphiphilic tricationic porphyrin and 5,10,15,20-tetra(4-N,N,N-trimethylammoniumphenyl) porphyrin. Photochem Photobiol Sci. 2008;7(9):1071-8.

60. Ergaieg K, Seux R. A comparative study of the photoinactivation of bacteria by *meso*-substituted cationic porphyrin, rose Bengal and methylene blue. Desalination. 2009;246(1):353-62.

61. Gomes MC, Silva S, Faustino MA, Neves MG, Almeida A, Cavaleiro JA, et al. Cationic galactoporphyrin photosensitisers against UV-B resistant bacteria: oxidation of lipids and proteins by $^1O_2$. Photochem Photobiol Sci. 2013;12(2):262-71.

62. Komagoe K, Kato H, Inoue T, Katsu T. Continuous real-time monitoring of cationic porphyrin-induced photodynamic inactivation of bacterial membrane functions using electrochemical sensors. Photochem Photobiol Sci. 2011;10(7):1181-8.

63. Spesia MB, Caminos DA, Pons P, Durantini EN. Mechanistic insight of the photodynamic inactivation of *Escherichia coli* by a tetracationic zinc(II) phthalocyanine derivative. Photodiagnosis Photodyn Ther. 2009;6(1):52-61.

64. George S, Hamblin MR, Kishen A. Uptake pathways of anionic and cationic photosensitizers into bacteria. Photochem Photobiol Sci. 2009;8(6):788-95.

65. Nitzan Y, Gutterman M, Malik Z, Ehrenberg B. Inactivation of Gram-negative bacteria by photosensitized porphyrins. Photochem Photobiol. 1992;55(1):89-96.

66. Minnock A, Vernon DI, Schofield J, Griffiths J, Parish JH, Brown SB. Mechanism of uptake of a cationic water-soluble pyridinium zinc phthalocyanine across the outer membrane of *Escherichia coli*. Antimicrob Agents Chemother. 2000;44(3):522-7.

67. Hancock RE. The bacterial outer membrane as a drug barrier. Trends Microbiol. 1997;5(1):37-42.

68. Rose RK, Matthews SP, Hall RC. Investigation of calcium-binding sites on the surfaces of selected gram-positive oral organisms. Arch Oral Biol. 1997;42(9):595-9.

69. Fresno S, Jiménez N, Izquierdo L, Merino S, Corsaro MM, De Castro C, et al. The ionic interaction of *Klebsiella pneumoniae* K2 capsule and core lipopolysaccharide. Microbiology. 2006;152(6):1807-18.

70. Wiese A, Münstermann M, Gutsmann T, Lindner B, Kawahara K, Zähringer U, et al. Molecular mechanisms of polymyxin B-membrane interactions: direct correlation between surface charge density and self-promoted transport. J Membr Biol. 1998;162(2):127-38.

71. Banfi S, Caruso E, Buccafurni L, Battini V, Zazzaron S, Barbieri P, et al. Antibacterial activity of tetraaryl-porphyrin photosensitizers: an *in vitro* study on Gram negative and Gram positive bacteria. J Photochem Photobiol B. 2006;85(1):28-38.

72. Boyle RW, Dolphin D. Structure and biodistribution relationships of photodynamic sensitizers. Photochem Photobiol. 1996;64(3):469-85.

73. Caminos DA, Spesia MB, Durantini EN. Photodynamic inactivation of *Escherichia coli* by novel *meso*-substituted porphyrins by 4-(3-N,N,N-trimethylammoniumpropoxy)phenyl and 4-(trifluoromethyl)phenyl groups. Photochem Photobiol Sci. 2006;5(1):56-65.

74. Grancho J, Pereira M, Miguel MdG, Gonsalves A, Burrows H. Synthesis, spectra and photophysics of some free base tetrafluoroalkyl and tetrafluoroaryl porphyrins with potential applications in imaging. Photochem Photobiol. 2002;75(3):249-56.

75. Spesia MB, Lazzeri D, Pascual L, Rovera M, Durantini EN. Photoinactivation of *Escherichia coli* using porphyrin derivatives with different number of cationic charges. FEMS Immunol Med Microbiol. 2005;44(3):289-95.

76. Ragàs X, Agut M, Nonell S. Singlet oxygen in *Escherichia coli*: new insights for antimicrobial photodynamic therapy. Free Radical Biol Med. 2010;49(5):770-6.

77. Alves E, Costa L, Carvalho CM, Tomé JP, Faustino MA, Neves MG, et al. Charge effect on the photoinactivation of Gram-negative and Gram-positive bacteria by cationic *meso*-substituted porphyrins. BMC Microbiol. 2009;9:70.

78. Walther J, Bröcker MJ, Wätzlich D, Nimtz M, Rohde M, Jahn D, et al. Protochlorophyllide: a new photosensitizer for the photodynamic inactivation of Gram-positive and Gram-negative bacteria. FEMS Microbiol Lett. 2009;290(2):156-63.

79. Spesia MB, Durantini EN. Photodynamic inactivation mechanism of *Streptococcus mitis* sensitized by zinc (II) 2, 9, 16, 23-tetrakis [2-(*N*,*N*,*N*-trimethylamino) ethoxy] phthalocyanine. J Photochem Photobiol B. 2013;125:179–87.

80. Du W, Sun C, Liang Z, Han Y, Yu J. Antibacterial activity of hypocrellin A against *Staphylococcus aureus*. World J Microbiol Biotechnol. 2012;28(11):3151-7.

81. Webb HK, Truong VK, Hasan J, Crawford RJ, Ivanova EP. Physico-mechanical characterisation of cells using atomic force microscopy—current research and methodologies. J Microbiol Methods. 2011;86(2):131-9.

82. Wright CJ, Shah MK, Powell LC, Armstrong I. Application of AFM from microbial cell to biofilm. Scanning. 2010;32(3):134-49.

83. Sahu K, Bansal H, Mukherjee C, Sharma M, Gupta PK. Atomic force microscopic study on morphological alterations induced by photodynamic action of toluidine blue O in *Staphylococcus aureus* and *Escherichia coli*. J Photochem Photobiol B. 2009;96(1):9-16.

84. Lin S-l, Hu J-m, Tang S-s, Wu X-y, Chen Z-q, Tang S-z. Photodynamic inactivation of methylene blue and tungsten-halogen lamp light against food pathogen *Listeria monocytogenes*. Photochem Photobiol. 2012;88(4):985-91.

85. Núñez SC, Ribeiro MS, Garcez AS, Miyakawa W. Assessment of photodynamic damage on *Escherichia coli* via atomic force microscopy. In: Popp J, Drexler W, Tuchin VV, Matthews DL, editors. Biophotonics: Photonic Solutions for Better Health Care II Proceedings of the SPIE Photonics Europe: International Society for Optics and Photonics (SPIE), Bellingham, Washington; 2010. p. 77151L-L-8.

86. Boulos L, Prevost M, Barbeau B, Coallier J, Desjardins R. LIVE/DEAD® *Bac* Light™: application of a new rapid staining method for direct enumeration of viable and total bacteria in drinking water. J Microbiol Methods. 1999;37(1):77-86.

87. Chen CZ, Cooper SL. Interactions between dendrimer biocides and bacterial membranes. Biomaterials. 2002;23(16):3359-68.

88. Romanova NA, Brovko LY, Moore L, Pometun E, Savitsky AP, Ugarova NN, et al. Assessment of photodynamic destruction of *Escherichia coli* O157:H7 and *Listeria monocytogenes* by using ATP bioluminescence. Appl Environ Microbiol. 2003;69(11):6393-8.

89. von Ballmoos C, Wiedenmann A, Dimroth P. Essentials for ATP synthesis by $F_1F_0$ ATP synthases. Annu Rev Biochem. 2009;78(1):649-72.

90. Valduga G, Breda B, Giacometti GM, Jori G, Reddi E. Photosensitization of wild and mutant strains of *Escherichia coli* by meso-Tetra (N-methyl-4-pyridyl)porphine. Biochem Biophys Res Commun. 1999;256(1):84-8.

91. Kato H, Komagoe K, Inoue T, Katsu T. *In situ* monitoring of photodynamic inactivation of the membrane functions of bacteria using electrochemical sensors. Anal Sci. 2010;26(10):1019-21.

92. Davies MJ. Singlet oxygen-mediated damage to proteins and its consequences. Biochem Biophys Res Commun. 2003;305(3):761-70.

93. Pattison DI, Rahmanto AS, Davies MJ. Photo-oxidation of proteins. Photochem Photobiol Sci. 2012;11(1):38-53.

94. Segalla A, Borsarelli CD, Braslavsky SE, Spikes JD, Roncucci G, Dei D, et al. Photophysical, photochemical and antibacterial photosensitizing properties of a novel octacationic Zn(ii)-phthalocyanine. Photochem Photobiol Sci. 2002;1(9):641-8.

95. Dosselli R, Millioni R, Puricelli L, Tessari P, Arrigoni G, Franchin C, et al. Molecular targets of antimicrobial photodynamic therapy identified by a proteomic approach. J Proteomics. 2012;77:329-43.

96. Tseng S, Teng L, Chen C, Lo T, Hung W, Chen H, et al. Toluidine blue O photodynamic inactivation on multidrug-resistant *Pseudomonas aeruginosa*. Lasers Surg Med. 2009;41(5):391-7.

97. Bertoloni G, Lauro FM, Cortella G, Merchat M. Photosensitizing activity of hematoporphyrin on *Staphylococcus aureus* cells. Biochim Biophys Acta, General Subjects. 2000;1475(2):169-74.

98. Stark G. Functional consequences of oxidative membrane damage. J Membr Biol. 2005;205(1):1-16.

99. Imlay JA. Pathways of oxidative damage. Annu Rev Microbiol. 2003;57(1):395-418.

100. Usacheva MN, Teichert MC, Biel MA. The interaction of lipopolysaccharides with phenothiazine dyes. Lasers Med Sci. 2003;33(5):311-9.

101. Alves E, Melo T, Simões C, Faustino MAF, Tomé JPC, Neves MGPMS, et al. Photodynamic oxidation of *Staphylococcus warneri* membrane phospholipids: new insights based on lipidomics. Rapid Commun Mass Spectrom. 2013;27(14):1607-18.

102. Alves E, Santos N, Melo T, Maciel E, Dória L, Faustino MAF, et al. Photodynamic oxidation of *Escherichia coli* membrane phospholipids: new insights based on lipidomics. Rapid Commun Mass Spectrom. in press.

103. Salmon-Divon M, Nitzan Y, Malik Z. Mechanistic aspects of *Escherichia coli* photodynamic inactivation by cationic tetra-*meso*(*N*-methylpyridyl)porphine. Photochem Photobiol Sci. 2004;3(5):423-9.

104. Ruiz-González R, White JH, Agut M, Nonell S, Flors C. A genetically-encoded photosensitiser demonstrates killing of bacteria by purely endogenous singlet oxygen. Photochem Photobiol Sci. 2012;11(9):1411-3.

105. Taraszkiewicz A, Fila G, Grinholc M, Nakonieczna J. Innovative strategies to overcome biofilm resistance. Biomed Res Int. 2013;2013(Article ID 150653):13 pages.

106. Kishen A, Haapasalo M. Biofilm models and methods of biofilm assessment. Endod Topics. 2010;22(1):58-78.

107. Li X, Guo H, Tian Q, Zheng G, Hu Y, Fu Y, et al. Effects of 5-aminolevulinic acid–mediated photodynamic therapy on antibiotic-resistant staphylococcal biofilm: an *in vitro* study. J Surg Res. 2013;184(2):1013-21.

108. Saino E, Sbarra MS, Arciola CR, Scavone M, Bloise N, Nikolov P, et al. Photodynamic action of Tri-meso (*N*-methylpyridyl), meso (*N*-tetradecyl-pyridyl) porphine on *Staphylococcus epidermidis* biofilms grown on Ti6Al4V alloy. Int J Artif Organs. 2010;33(9):636-45.

109. Sbarra MS, DL POTO A, Arciola CR, Saino E, Sharma M, Bragheri F, et al. Photodynamic action of merocyanine 540 on *Staphylococcus epidermidis* biofilms. Int J Artif Organs. 2008;31(9):848-57.

110. Di Poto A, Sbarra MS, Provenza G, Visai L, Speziale P. The effect of photodynamic treatment combined with antibiotic action or host defence mechanisms on *Staphylococcus aureus* biofilms. Biomaterials. 2009;30(18):3158-66.

111. Eick S, Markauskaite G, Nietzsche S, Laugisch O, Salvi GE, Sculean A. Effect of photoactivated disinfection with a light-emitting diode on bacterial species and biofilms associated with periodontitis and peri-implantitis. Photodiagn Photodyn Ther. 2013;10(2):156–67.

112. Sharma M, Visai L, Bragheri F, Cristiani I, Gupta PK, Speziale P. Toluidine blue-mediated photodynamic effects on staphylococcal biofilms. Antimicrob Agents Chemother. 2008;52(1):299-305.

113. Collins TL, Markus EA, Hassett DJ, Robinson JB. The effect of a cationic porphyrin on *Pseudomonas aeruginosa* biofilms. Curr Microbiol. 2010;61(5):411-6.

114. Kishen A, Upadya M, Tegos GP, Hamblin MR. Efflux pump inhibitor potentiates antimicrobial photodynamic inactivation of *Enterococcus faecalis* biofilm. Photochem Photobiol. 2010;86(6):1343-9.

115. Fontana C, Abernethy A, Som S, Ruggiero K, Doucette S, Marcantonio R, et al. The antibacterial effect of photodynamic therapy in dental plaque-derived biofilms. J Periodontal Res. 2009;44(6):751-9.

116. Gad F, Zahra T, Hasan T, Hamblin MR. Effects of growth phase and extracellular slime on photodynamic inactivation of gram-positive pathogenic bacteria. Antimicrob Agents Chemother. 2004;48(6):2173-8.

117. Lauro FM, Pretto P, Covolo L, Jori G, Bertoloni G. Photoinactivation of bacterial strains involved in periodontal diseases sensitized by porphycene–polylysine conjugates. Photochem Photobiol Sci. 2002;1(7):468-70.

118. Pedigo LA, Gibbs AJ, Scott RJ, Street CN. Absence of bacterial resistance following repeat exposure to photodynamic therapy. 2009:73803H-H.

119. Tavares A, Carvalho CMB, Faustino MA, Neves MGPMS, Tomé JPC, Tomé AC, et al. Antimicrobial photodynamic therapy: study of bacterial recovery viability and potential development of resistance after treatment. Mar Drugs. 2010;8(1):91-105.

120. Giuliani F, Martinelli M, Cocchi A, Arbia D, Fantetti L, Roncucci G. *In vitro* resistance selection studies of RLP068/Cl, a new Zn(II) phthalocyanine suitable for antimicrobial photodynamic therapy. Antimicrob Agents Chemother. 2010;54(2):637-42.

121. Nitzan Y, Ashkenazi H. Photoinactivation of *Acinetobacter baumannii* and *Escherichia coli* B by a cationic hydrophilic porphyrin at various light wavelengths. Curr Microbiol. 2001;42(6):408-14.

122. Nitzan Y, Ashkenazi H. Photoinactivation of *Deinococcus radiodurans*: an unusual Gram-positive microorganism. Photochem Photobiol. 1999;69(4):505-10.

123. Grinholc M, Szramka B, Kurlenda J, Graczyk A, Bielawski KP. Bactericidal effect of photodynamic inactivation against methicillin-resistant and methicillin-susceptible *Staphylococcus aureus* is strain-dependent. J Photochem Photobiol, B. 2008;90(1):57-63.

124. Nakonieczna J, Michta E, Rybicka M, Grinholc M, Gwizdek-Wiśniewska A, Bielawski K. Superoxide dismutase is upregulated in *Staphylococcus aureus* following protoporphyrin-mediated photodynamic inactivation and does not directly influence the response to photodynamic treatment. BMC Microbiol. 2010;10(1):323.

125. Kim SY, Kwon OJ, Park J-W. Inactivation of catalase and superoxide dismutase by singlet oxygen derived from photoactivated dye. Biochimie. 2001;83(5):437-44.

126. Tubby S, Wilson M, Nair S. Inactivation of staphylococcal virulence factors using a light-activated antimicrobial agent. BMC Microbiol. 2009;9(1):211.

127. Bolean M, Paulino TdP, Thedei Jr G, Ciancaglini P. Photodynamic therapy with rose bengal induces GroEL expression in *Streptococcus mutans*. Photomed Laser Surg. 2010;28(S1):S-79-S-84.

128. St Denis TG, Huang L, Dai T, Hamblin MR. Analysis of the bacterial heat shock response to photodynamic therapy-mediated oxidative stress. Photochem Photobiol. 2011;87(3):707-13.

129. Park HJ, Moon YH, Yoon HE, Park YM, Yoon JH, Bang IS. Agr function is upregulated by photodynamic therapy (PDT) for *Staphylococcus aureus* and is related to resistance against PDT. Microbiol Immunol. 2013;57(8):547-52.

130. Tegos GP, Hamblin MR. Phenothiazinium antimicrobial photosensitizers are substrates of bacterial multidrug resistance pumps. Antimicrob Agents Chemother. 2006;50(1):196-203.

131. Tegos GP, Masago K, Aziz F, Higginbotham A, Stermitz FR, Hamblin MR. Inhibitors of bacterial multidrug efflux pumps potentiate antimicrobial photoinactivation. Antimicrob Agents Chemother. 2008;52(9):3202-9.

132. von Tappeiner H, Jodlbauer A. Uber die Wirkung der photodynamischen (fluorescierenden) Stoffe auf Protozoen und Enzyme. Dtsch Arch Klin Med. 1904;80:427-87.

133. Foote CS. Photosensitized oxidation and singlet oxygen: consequences in biological systems. In: Pryor WA, editor. Free radicals in biology. New York: Academic Press; 1976. p. 85-133.

134. Costa L, Tomé JPC, Neves MGPMS, Tomé AC, Cavaleiro JAS, Faustino MAF, et al. Evaluation of resistance development and viability recovery by a non-enveloped virus after repeated cycles of aPDT. Antiviral Res. 2011;91(3):278-82.

135. Garcez AS, Ribeiro MS, Tegos GP, Núñez SC, Jorge AOC, Hamblin MR. Antimicrobial photodynamic therapy combined with conventional endodontic treatment to eliminate root canal biofilm infection. Lasers Surg Med. 2007;39(1):59-66.

136. Merchat M, Bertolini G, Giacomini P, Villanueva A, Jori G. *Meso*-substituted cationic porphyrins as efficient photosensitizers of gram-positive and gram-negative bacteria. J Photochem Photobiol B. 1996;32(3):153-7.

137. Reddi E, Ceccon M, Valduga G, Jori G, Bommer JC, Elisei F, et al. Photophysical properties and antibacterial activity of *meso*-substituted cationic porphyrins. Photochem Photobiol. 2002;75(5):462-70.

138. Friedrich CL, Moyles D, Beveridge TJ, Hancock REW. Antibacterial action of structurally diverse cationic peptides on gram-positive bacteria. Antimicrob Agents Chemother. 2000;44(8):2086-92.

139. Bertoloni G, Rossi F, Valduga G, Jori G, Ali H, van Lier J. Photosensitizing activity of water- and lipid-soluble phthalocyanines on prokaryotic and eukaryotic microbial cells. Microbios. 1992;71(286):33-46.

140. Alves E, Faustino MAF, Tomé JPC, Neves MGPMS, Tomé AC, Cavaleiro JAS, et al. Photodynamic antimicrobial chemotherapy in aquaculture: photoinactivation studies of *Vibrio fischeri*. PLoS One. 2011;6(6):e20970.

141. Arrojado C, Pereira C, Tomé JPC, Faustino MAF, Neves MGPMS, Tomé AC, et al. Applicability of photodynamic antimicrobial chemotherapy as an alternative to inactivate fish pathogenic bacteria in aquaculture systems. Photochem Photobiol Sci. 2011;10(10):1691-700.

142. Carvalho CMB, Gomes ATPC, Fernandes SCD, Prata ACB, Almeida MA, Cunha MA, et al. Photoinactivation of bacteria in wastewater by porphyrins: bacterial beta-galactosidase activity and leucine-uptake as methods to monitor the process. J Photochem Photobiol B. 2007;88(2-3):112-8.

143. Costa L, Alves E, Carvalho CMB, Tomé JPC, Faustino MAF, Neves MGPMS, et al. Sewage bacteriophage photoinactivation by cationic porphyrins: a study of charge effect. Photochem Photobiol Sci. 2008;7:415 - 22.

144. Oliveira A, Almeida A, Carvalho CMB, Tomé JPC, Faustino MAF, Neves MGPMS, et al. Porphyrin derivatives as photosensitizers for the inactivation of *Bacillus cereus* endospores. J Appl Microbiol. 2009;106(6):1986-95.

145. Ramstad S, Futsaether CM, Johnsson A. Porphyrin sensitization and intracellular calcium changes in the prokaryote *Propionibacterium acnes*. J Photochem Photobiol B. 1997;40(2):141-8.

146. Geiger O, González-Silva N, López-Lara IM, Sohlenkamp C. Amino acid-containing membrane lipids in bacteria. Prog Lipid Res. 2010;49(1):46-60.

147. Moan J, Berg K. Photochemotherapy of cancer: experimental research. Photochem Photobiol. 1992;55(6):931-48.

148. Bielski BH, Arudi RL, Sutherland MW. A study of the reactivity of $HO_2/O_2^-$ with unsaturated fatty acids. J Biol Chem. 1983;258(8):4759-61.

149. Dai T, Tegos GP, Zhiyentayev T, Mylonakis E, Hamblin MR. Photodynamic therapy for methicillin-resistant *Staphylococcus aureus* infection in a mouse skin abrasion model. Lasers Surg Med. 2010;42(1):38-44.

150. Grinholc M, Szramka B, Kurlenda J, Graczyk A, Bielawski KP. Bactericidal effect of photodynamic inactivation against methicillin-resistant and methicillin-susceptible *Staphylococcus aureus* is strain-dependent. J Photochem Photobiol B. 2008;90(1):57-63.

151. Maisch T, Bosl C, Szeimies R-M, Lehn N, Abels C. Photodynamic effects of novel XF porphyrin derivatives on prokaryotic and eukaryotic cells. Antimicrob Agents Chemother. 2005;49(4):1542–52.

152. Venkatesh MP, Placencia F, Weisman LE. Coagulase-negative staphylococcal infections in the neonate and child: an update. Semin Pediatr Infect Dis. 2006;17(3):120-7.

153. Mack D, Davies AP, Harris LG, Jeeves R, Pascoe B, Knobloch JK-M, et al. *Staphylococcus epidermidis* in biomaterial-associated infections. In: Moriarty TF, Zaat SAJ, Busscher HJ, editors. Biomaterials associated infection - immunological aspects and antimicrobial strategies. New York: Springer New York; 2013. p. 25-56.

154. Otto M. *Staphylococcus epidermidis* - the 'accidental' pathogen. Nat Rev Microbiol. 2009;7(8):555-67.

155. Widerström M, Wiström J, Sjöstedt A, Monsen T. Coagulase-negative staphylococci: update on the molecular epidemiology and clinical presentation, with a focus on *Staphylococcus epidermidis* and *Staphylococcus saprophyticus*. Eur J Clin Microbiol Infect Dis. 2012;31(1):7-20.

156. Huebner M, Johannes, Goldmann M, Donald A. Coagulase-negative staphylococci: role as pathogens. Annu Rev Med. 1999;50(1):223-36.

157. Kloos WE, Schleifer KH. Isolation and characterization of staphylococci from human skin II. Descriptions of four new species: *Staphylococcus warneri*, *Staphylococcus capitis*, *Staphylococcus hominis*, and *Staphylococcus simulans*. Int J Syst Bacteriol. 1975;25(1):62-79.

158. Leighton PM LJ. Identification of coagulase-negative Staphylococci isolated from urinary tract infections. Am J Clin Pathol. 1986;85(1):92-5.

159. Wood CA, Sewell DL, Strausbaugh LJ. Vertebral osteomyelitis and native valve endocarditis caused by *Staphylococcus warneri*. Diagn Microbiol Infect Dis. 1989;12(3):261-3.

160. Kamath U, Singer C, Isenberg HD. Clinical significance of *Staphylococcus warneri* bacteremia. J Clin Microbiol. 1992;30(2):261-4.

161. Incani RN, Hernández M, Cortez J, González ME, Dorel Salazar Y. *Staphylococcus warneri* meningitis in a patient with *Strongyloides stercoralis* hyperinfection and lymphoma: first report of a case. Rev Inst Med Trop Sao Paulo. 2010;52:169-70.

162. Legius B, Van Landuyt K, Verschueren P, Westhovens R. Septic arthritis due to *Staphylococcus warneri*: a diagnostic challenge. Open Rheumatol J. 2012;6:310-1.

163. Ivic I, Karanovic J, Pavicic-Ivelja M. Sepsis with multiple abscesses caused by *Staphylococcus warneri*: a case report. centeurjmed. 2013;8(1):45-7.

164. Arslan F, Saltoglu N, Mete B, Mert A. Recurrent *Staphylococcus warnerii* prosthetic valve endocarditis: a case report and review. Ann Clin Microbiol Antimicrob. 2011;10(1):14.

165. Stöllberger C, Wechsler-Fördös A, Geppert F, Gulz W, Brownstone E, Nicolakis M, et al. *Staphylococcus warneri* endocarditis after implantation of a lumbar disc prosthesis in an immunocompetent patient. J Infect. 2006;52(1):e15-e8.

166. Torre D, Ferraro G, Fiori GP, Martegani R, Speranza F, Tambini R, et al. Ventriculoatrial shunt infection caused by *Staphylococcus warneri*: case report and review. Clin Infect Dis. 1992;14(1):49-52.

167. Cimiotti JP, Haas JP, Della-Latta P, Wu F, Saiman L, Larson EL. Prevalence and clinical relevance of *Staphylococcus warneri* in the neonatal intensive care unit. Infect Control Hosp Epidemiol. 2007;28(3):326–30.

168. Hira V, Sluijter M, Goessens WHF, Ott A, de Groot R, Hermans PWM, et al. Coagulase-negative staphylococcal skin carriage among neonatal intensive care unit personnel: from population to infection. J Clin Microbiol. 2010;48(11):3876-81.

169. Center KJ, Reboli AC, Hubler R, Rodgers GL, Long SS. Decreased vancomycin susceptibility of coagulase-negative staphylococci in a neonatal intensive care unit: evidence of spread of *Staphylococcus warneri*. J Clin Microbiol. 2003;41(10):4660-5.

170. Drucker D, Abdullah N. Polar lipids of *Staphylococcus* strains analysed by fast atom bombardment mass spectrometry. J Appl Bacteriol. 1995;79(2):219-24.

171. Nahaie MR, Goodfellow M, Minnikin DE, Hájek V. Polar lipid and isoprenoid quinone composition in the classification of *Staphylococcus*. J Gen Microbiol. 1984;130(9):2427-37.

172. Maestrin APJ, Ribeiro AO, Tedesco AC, Neri CR, Vinhado FS, Serra OA, et al. A novel chlorin derivative of *Meso*-tris(pentafluorophenyl)-4-pyridylporphyrin: synthesis, photophysics and photochemical properties. J Braz Chem Soc. 2004;15:923-30.

173. Tomé JPC, Neves MGPMS, Tomé AC, Cavaleiro JAS, Soncin M, Magaraggia M, et al. Synthesis and antibacterial activity of new poly-*S*-lysine-porphyrin conjugates. J Med Chem. 2004;47(26):6649-52.

174. Shah MM, Iihara H, Noda M, Song SX, Nhung PH, Ohkusu K, et al. *dnaJ* gene sequence-based assay for species identification and phylogenetic grouping in the genus *Staphylococcus*. Int J Syst Evol Microbiol. 2007;57(1):25-30.

175. Henriques IS, Fonseca F, Alves A, Saavedra MJ, Correia A. Occurrence and diversity of integrons and beta-lactamase genes among ampicillin-resistant isolates from estuarine waters. Res Microbiol. 2006;157(10):938-47.

176. Oursel D, Loutelier-Bourhis C, Orange N, Chevalier S, Norris V, Lange CM. Lipid composition of membranes of *Escherichia coli* by liquid chromatography/tandem mass spectrometry using negative electrospray ionization. Rapid Commun Mass Spectrom. 2007;21(11):1721-8.

177. Bartlett EM, Lewis DH. Spectrophotometric determination of phosphate esters in the presence and absence of orthophosphate. Anal Biochem. 1970;36(1):159-67.

178. Fuchs B, Süß R, Teuber K, Eibisch M, Schiller J. Lipid analysis by thin-layer chromatography - a review of the current state. J Chromatogr A. 2011;1218(19):2754-74.

179. Wolff SP. Ferrous ion oxidation in presence of ferric ion indicator xylenol orange for measurement of hydroperoxides. Methods Enzymol. 1994;233:182-9.

180. Schwalbe-Herrmann M, Willmann J, Leibfritz D. Separation of phospholipid classes by hydrophilic interaction chromatography detected by electrospray ionization mass spectrometry. J Chromatogr A. 2010;1217(32):5179-83.

181. Hsu F-F, Turk J. Electrospray ionization with low-energy collisionally activated dissociation tandem mass spectrometry of glycerophospholipids: mechanisms of fragmentation and structural characterization. J Chromatogr B Analyt Technol Biomed Life Sci. 2009;877(26):2673-95.

182. Maciel E, Domingues P, Domingues MRM. Liquid chromatography/tandem mass spectrometry analysis of long-chain oxidation products of cardiolipin induced by the hydroxyl radical. Rapid Commun Mass Spectrom. 2011;25(2):316-26.

183. Tavares A, Dias SRS, Carvalho CMB, Faustino MAF, Tomé JPC, Neves MGPMS, et al. Mechanisms of photodynamic inactivation of a Gram-negative recombinant bioluminescent bacterium by cationic porphyrins. Photochem Photobiol Sci. 2011;10(10):1659-69.

184. Kim J, Rodriguez ME, Oleinick NL, Anderson VE. Photo-oxidation of cardiolipin and cytochrome c with bilayer-embedded Pc 4. Free Radical Biol Med. 2010;49(5):718-25.

185. Tyurin VA, Tyurina YY, Feng W, Mnuskin A, Jiang J, Tang M, et al. Mass-spectrometric characterization of phospholipids and their primary peroxidation products in rat cortical neurons during staurosporine-induced apoptosis. J Neurochem. 2008;107(6):1614-33.

186. Tyurin VA, Tyurina YY, Jung M-Y, Tungekar MA, Wasserloos KJ, Bayır H, et al. Mass-spectrometric analysis of hydroperoxy- and hydroxy-derivatives of cardiolipin and phosphatidylserine in cells and tissues induced by pro-apoptotic and pro-inflammatory stimuli. J Chromatogr B. 2009;877(26):2863-72.

187. Shadyro O, Yurkova I, Kisel M, Brede O, Arnhold J. Radiation-induced fragmentation of cardiolipin in a model membrane. Int J Radiat Biol. 2004 80(3):239-45.

188. Epand RF, Mowery BP, Lee SE, Stahl SS, Lehrer RI, Gellman SH, et al. Dual mechanism of bacterial lethality for a cationic sequence-random copolymer that mimics host-defense antimicrobial peptides. J Mol Biol. 2008;379(1):38-50.

189. Epand RF, Schmitt MA, Gellman SH, Epand RM. Role of membrane lipids in the mechanism of bacterial species selective toxicity by two alpha/beta-antimicrobial peptides. Biochim Biophys Acta, Biomembr. 2006;1758(9):1343-50.

190. Jean-François F, Castano S, Desbat B, Odaert B, Roux M, Metz-Boutigue MH, et al. Aggregation of cateslytin beta-sheets on negatively charged lipids promotes rigid membrane domains. A new mode of action for antimicrobial peptides? Biochemistry. 2008;47(24):6394-402.

191. Coppellotti O, Fabris C, Soncin M, Magaraggia M, Camerin M, Jori G, et al. Porphyrin photosensitised processes in the prevention and treatment of water- and vector-borne diseases. Curr Med Chem. 2012;19(6):808-19.

192. Kim J, Minkler PE, Salomon RG, Anderson VE, Hoppel CL. Cardiolipin: characterization of distinct oxidized molecular species. J Lipid Res. 2011;52(1):125-35.

193. Rodriguez ME, Kim J, Santos GBD, Azizuddin K, Berlin J, Anderson VE, et al. Binding to and photo-oxidation of cardiolipin by the phthalocyanine photosensitizer Pc 4. J Biomed Opt. 2010;15(5):051604.

194. Dowhan W. Genetic analysis of lipid-protein interactions in *Escherichia coli* membranes. Biochim Biophys Acta, Rev Biomembr. 1998;1376(3):455-66.

195. Raetz C. Enzymology, genetics, and regulation of membrane phospholipid synthesis in *Escherichia coli*. Microbiol Rev. 1978;42(3):614-59.

196. Ames GF. Lipids of *Salmonella typhimurium* and *Escherichia coli*: structure and metabolism. J Bacteriol. 1968;95(3):833-43.

197. Jori G, Fabris C, Soncin M, Ferro S, Coppellotti O, Dei D, et al. Photodynamic therapy in the treatment of microbial infections: basic principles and perspective applications. Lasers Surg Med. 2006;38(5):468-81.

198. Carvalho CMB, Alves E, Costa L, Tomé JPC, Faustino MAF, Neves MGPMS, et al. Functional cationic nanomagnet-porphyrin hybrids for the photoinactivation of microorganisms. ACS Nano. 2010;4(12):7133-40.

199. Costa L, Carvalho CMB, Faustino MAF, Neves MGPMS, Tome JPC, Tome AC, et al. Sewage bacteriophage inactivation by cationic porphyrins: influence of light parameters. Photochem Photobiol Sci. 2010;9(8):1126-33.

200. Aued-Pimentel S, Lago JH, Chaves MH, Kumagai EE. Evaluation of a methylation procedure to determine cyclopropenoids fatty acids from *Sterculia striata* St. Hil. Et Nauds seed oil. J Chromatogr A. 2004;1054(1-2):235-9.

201. Oursel D, Loutelier-Bourhis C, Orange N, Chevalier S, Norris V, Lange CM. Identification and relative quantification of fatty acids in *Escherichia coli* membranes by gas chromatography/mass spectrometry. Rapid Commun Mass Spectrom. 2007;21(20):3229-33.

202. Teuber K, Riemer T, Schiller J. Thin-layer chromatography combined with MALDI-TOF-MS and $^{31}$P-NMR to study possible selective bindings of phospholipids to silica gel. Anal Bioanal Chem. 2010;398(7-8):2833-42.

203. da Silva RN, Tomé AC, Tomé JPC, Neves MGPMS, Faustino MAF, Cavaleiro JAS, et al. Photo-inactivation of *Bacillus* endospores: inter-specific variability of inactivation efficiency. Microbiol Immunol. 2012;56(10):692-9.

204. Gidden J, Denson J, Liyanage R, Ivey DM, Lay Jr JO. Lipid compositions in *Escherichia coli* and *Bacillus subtilis* during growth as determined by MALDI-TOF and TOF/TOF mass spectrometry. Int J Mass Spectrom. 2009;283(1-3):178-84.

205. Hsu FF, Turk J. Characterization of cardiolipin from *Escherichia coli* by electrospray ionization with multiple stage quadrupole ion-trap mass spectrometric analysis of $[M-2H+Na]^-$ ions. J Am Soc Mass Spectrom. 2006;17(3):420-9.

206. Kol MA, Kuster DWD, Boumann HA, de Cock H, Heck AJR, de Kruijff B, et al. Uptake and remodeling of exogenous phosphatidylethanolamine in *E. coli*. Biochim Biophys Acta, Mol Cell Biol Lipids. 2004;1636(2–3):205-12.

207. Reis A, Spickett CM. Chemistry of phospholipid oxidation. Biochim Biophys Acta, Biomembr. 2012;1818(10):2374-87.

208. Jori G, Camerin M, Soncin M, Guidolin L, Coppellotti O. Antimicrobial photodynamic therapy: basic principles. In: Hamblin MR, Jori G, editors. Photodynamic inactivation of microbial pathogens: medical and environmental applications. Cambridge: RSC Publishing; 2011. p. 1-18.

209. Sharma SK, Mroz P, Dai T, Huang YY, St. Denis TG, Hamblin MR. Photodynamic therapy for cancer and for infections: what is the difference? Isr J Chem. 2012;52(8-9):691-705.

210. Carvalho C, Tomé J, Faustino M, Neves M, Tomé A, Cavaleiro J, et al. Antimicrobial photodynamic activity of porphyrin derivatives: potential application on medical and water disinfection. J Porphyrins Phthalocyanines. 2009;13:574-7.

211. Minnock A, Vernon DI, Schofield J, Griffiths J, Howard Parish J, Brown SB. Photoinactivation of bacteria. Use of a cationic water-soluble zinc phthalocyanine to photoinactivate both Gram-negative and Gram-positive bacteria. J Photochem Photobiol B. 1996;32(3):159-64.

212. Wilson M. Photolysis of oral bacteria and its potential use in the treatment of caries and periodontal disease. J Appl Bacteriol. 1993;75(4):299-306.

213. Malik Z, Ladan H, Nitzan Y. Photodynamic inactivation of Gram-negative bacteria: problems and possible solutions. J Photochem Photobiol B. 1992;14(3):262-6.

214. Bertoloni G, Lauro FM, Cortella G, Merchat M. Photosensitizing activity of hematoporphyrin on *Staphylococcus aureus* cells. Biochim Biophys Acta, Gen Subj. 2000;1475(2):169-74.

215. Malik Z, Babushkin T, Sher S, Hanania J, Ladan H, Nitzan Y, et al. Collapse of $K^+$ and ionic balance during photodynamic inactivation of leukemic cells, erythrocytes and *Staphylococcus aureus*. Int J Biochem. 1993;25(10):1399-406.

216. Schäfer M, Schmitz C, Horneck G. High sensitivity of *Deinococcus radiodurans* to photodynamically-produced singlet oxygen. Int J Radiat Biol. 1998;74(2):249-53.

217. Imray FP, MacPhee DG. The role of DNA polymerase I and the *rec* system in survival of bacteria and bacteriophages damaged by the photodynamic action of acridine orange. Mol Gen Genet. 1973 (123):289-98.

218. Hamblin MR, Hasan T. Photodynamic therapy: a new antimicrobial approach to infectious disease? Photochem Photobiol Sci. 2004;3:436 - 50.

219. Gong X, Tao R, Li Z. Quantification of RNA damage by reverse transcription polymerase chain reactions. Anal Biochem. 2006;357(1):58-67.

220. Liu M, Gong X, Alluri RK, Wu J, Sablo T, Li Z. Characterization of RNA damage under oxidative stress in *Escherichia coli*. Biol Chem. 2012;393(3):123-32.

221. Nir U, Ladan H, Malik Z, Nitzan Y. *In vivo* effects of porphyrins on bacterial DNA. J Photochem Photobiol B. 1991;11(3–4):295-306.

222. Caminos DA, Durantini EN. Interaction and photodynamic activity of cationic porphyrin derivatives bearing different patterns of charge distribution with GMP and DNA. J Photochem Photobiol A. 2008;198(2–3):274-81.

223. Bertoloni G, Salvato B, Dall'Acqua M, Vazzoler M, Jori G. Hematoporphyrin-sensitized photoinactivation of *Streptococcus faecalis*. Photochem Photobiol. 1984;39:811-6.

224. Nitzan Y, Gozhansky S, Malik Z. Effect of photoactivated hematoporphyrin derivative on the viability of *Staphylococcus aureus*. Curr Microbiol. 1983;8(5):279-84.

225. Boye E, Moan J. The photodynamic effect of hematoporphyrin on DNA. Photochem Photobiol. 1980;31(3):223-8.

226. Kubat P, Lang K, Anzenbacher Jr P, Jursikova K, Kral V, Ehrenberg B. Interaction of novel cationic meso-tetraphenylporphyrins in the ground and excited states with DNA and nucleotides. J Chem Soc Perkin Trans I. 2000;0(6):933-41.

227. Li H, Fedorova OS, Grachev AN, Trumble WR, Bohach GA, Czuchajowski L. A series of meso-tris(N-methyl-pyridiniumyl)-(4-alkylamidophenyl) porphyrins: synthesis, interaction with DNA and antibacterial activity. Biochim Biophys Acta, Gene Struct Expr. 1997;1354(3):252-60.

228. Mettath S, Munson BR, Pandey RK. DNA interaction and photocleavage properties of porphyrins containing cationic substituents at the peripheral position. Bioconjugate Chem. 1998;10(1):94-102.

229. Munson BR, Fiel RJ. DNA intercalation and photosensitization by cationic meso substituted porphyrins. Nucleic Acids Res. 1992;20(6):1315-9.

230. Vergeldt FJ, Koehorst RBM, van Hoek A, Schaafsma TJ. Intramolecular interactions in the ground and excited states of tetrakis(N-methylpyridyl)porphyrins. J Phys Chem. 1995;99(13):4397-405.

231. Bezman SA, Burtis PA, Izod TPJ, Thayer MA. Photodynamic inactivation of *E. coli* by rose Bengal immobilized on polystyrene beads. Photochem Photobiol. 1978;28(3):325-9.

232. Dahl T, Midden R, Hartman P. Pure singlet oxygen cytotoxicity for bacteria. Photochem Photobiol. 1987;46(3):345-52.

233. Gomes MC, Woranovicz-Barreira SM, Faustino MAF, Fernandes R, Neves MGPMS, Tome AC, et al. Photodynamic inactivation of *Penicillium chrysogenum* conidia by cationic porphyrins. Photochem Photobiol Sci. 2011;10(11):1735-43.

234. Alves E, Melo T, Simões C, Faustino MAF, Tomé JPC, Neves MGPMS, et al. Photodynamic oxidation of *Staphylococcus warneri* membrane phospholipids: new insights based on lipidomics. Rapid Commun Mass Spectrom. 2013;27(1):1607–18.

235. Demidova TN, Hamblin MR. Effect of cell-photosensitizer binding and cell density on microbial photoinactivation. Antimicrob Agents Chemother. 2005;49(6):2329-35.

236. Sheridan GEC, Masters CI, Shallcross JA, Mackey BM. Detection of mRNA by reverse transcription-PCR as an indicator of viability in *Escherichia coli* cells. Appl Environ Microbiol. 1998;64(4):1313-8.

237. Gábor F, Szocs K, Maillard P, Csík G. Photobiological activity of exogenous and endogenous porphyrin derivatives in *Escherichia coli* and *Enterococcus hirae* cells. Radiat Environ Biophys. 2001;40(2):145-51.

238. Merchat M, Spikes JD, Bertoloni G, Jori G. Studies on the mechanism of bacteria photosensitization by meso-substituted cationic porphyrins. J Photochem Photobiol B. 1996;35(3):149-57.

239. Ito T. Cellular and subcellular mechanisms of photodynamic action: the $^1O_2$ hypothesis as a driving force in recent research. Photochem Photobiol. 1978;28(4-5):493-506.

240. Shacter E. Quantification and significance of protein oxidation in biological samples. Drug Metab Rev. 2000;32(3-4):307-26.

241. Davies MJ. Reactive species formed on proteins exposed to singlet oxygen. Photochem Photobiol Sci. 2004;3(1):17-25.

242. Afonso SG, Enríquez de Salamanca R, Batlle AMdC. The photodynamic and non-photodynamic actions of porphyrins. Braz J Med Biol Res. 1999;32:255-66.

243. Clarke SR, Foster SJ. Surface adhesins of *Staphylococcus aureus*. Adv Microb Physiol. 2006;51:187-224.

244. Dramsi S, Magnet S, Davison S, Arthur M. Covalent attachment of proteins to peptidoglycan. FEMS Microbiol Rev. 2008;32(2):307-20.

245. Buettner GR. Molecular targets of photosensitization - some biological chemistry of singlet oxygen ($^1O_2$) [Internet]. American Society for Photobiology; 2011 [updated 5 Jul 2013; cited 2013 15 Feb]; Available from: http://www.photobiology.info/Buettner.html.

246. Booth L, Redmond RW. Can lipid peroxidation of plasma membranes induce DNA strand breaks. Free Radical Biol Med. 2002;33(suppl. 2):S390.

247. Ouédraogo GD, Redmond RW. Secondary reactive oxygen species extend the range of photosensitization effects in cells: DNA damage produced via initial membrane photosensitization. Photochem Photobiol. 2003;77(2):192-203.

248. Bose B, Dube A. Interaction of Chlorin p6 with bovine serum albumin and photodynamic oxidation of protein. J Photochem Photobiol B. 2006;85(1):49-55.

249. Silvester JA, Timmins GS, Davies MJ. Protein hydroperoxides and carbonyl groups generated by porphyrin-induced photo-oxidation of bovine serum albumin. Arch Biochem Biophys. 1998;350(2):249-58.

250. Tamarit J, Cabiscol E, Ros J. Identification of the major oxidatively damaged proteins in *Escherichia coli* cells exposed to oxidative stress. J Biol Chem. 1998;273(5):3027-32.

251. Bhatti M, MacRobert A, Meghji S, Henderson B, Wilson M. A study of the uptake of toluidine blue O by *Porphyromonas gingivalis* and the mechanism of lethal photosensitization. Photochem Photobiol. 1998;68(3):370-6.

252. Bhatti M, Nair SP, Macrobert AJ, Henderson B, Shepherd P, Cridland J, et al. Identification of photolabile outer membrane proteins of *Porphyromonas gingivalis*. Curr Microbiol. 2001;43(2):96-9.

253. Packer S, Bhatti M, Burns T, Wilson M. Inactivation of proteolytic enzymes from *Porphyromonas gingivalis* using light-activated agents. Lasers Med Sci. 2000;15(1):24-30.

254. Laemmli UK. Cleavage of structural proteins during the assembly of the head of bacteriophage T4. Nature. 1970;227(5259):680-5.

255. O'Connell KL, Stults JT. Identification of mouse liver proteins on two-dimensional electrophoresis gels by matrix-assisted laser desorption/ionization mass spectrometry of *in situ* enzymatic digests. Electrophoresis. 1997;18(3-4):349-59.

256. Neuhoff V, Stamm R, Eibl H. Clear background and highly sensitive protein staining with Coomassie Blue dyes in polyacrylamide gels: a systematic analysis, modified by A. Posch. Electrophoresis. 1985;6(9):427-48.

257. Lemos MF, Soares AM, Correia AC, Esteves AC. Proteins in ecotoxicology – how, why and why not? Proteomics. 2010;10(4):873-87.

258. Fu F, Cheng VW, Wu Y, Tang Y, Weiner JH, Li L. Comparative proteomic and metabolomic analysis of *Staphylococcus warneri* SG1 cultured in the presence and absence of butanol. J Proteome Res. 2013;12(10)*:*4478–89.

259. Han M-J, Lee SY. The *Escherichia coli* proteome: past, present, and future prospects. Microbiol Mol Biol Rev. 2006;70(2):362-439.

260. Altuvia S, Almiron M, Huisman G, Kolter R, Storz G. The dps promoter is activated by OxyR during growth and by IHF and σS in stationary phase. Mol Microbiol. 1994;13(2):265-72.

261. Wenning M, Scherer S. Identification of microorganisms by FTIR spectroscopy: perspectives and limitations of the method. Appl Microbiol Biotechnol. 2013:1-10.

262. Duygu DY, Baykal T, Açikgoz İ, Yildiz K. Fourier transform infrared (FT-IR) spectroscopy for biological studies. GU J Sci. 2010;22(3):117-21.

263. Naumann D. Infrared spectroscopy in microbiology. In: Meyers RA, editor. Encyclopedia of analytical chemistry. Chichester: John Wiley & Sons Ltd; 2000. p. 102-31.

264. Hotze EM, Badireddy AR, Chellam S, Wiesner MR. Mechanisms of bacteriophage inactivation via singlet oxygen generation in UV illuminated fullerol suspensions. Environ Sci Technol. 2009;43(17):6639-45.

265. Kiwi J, Nadtochenko V. New evidence for $TiO_2$ photocatalysis during bilayer lipid peroxidation. J Phys Chem B. 2004;108(45):17675-84.

266. Nadtochenko V, Rincon A, Stanca S, Kiwi J. Dynamics of *E. coli* membrane cell peroxidation during $TiO_2$ photocatalysis studied by ATR-FTIR spectroscopy and AFM microscopy. J Photochem Photobiol A Chem. 2005;169(2):131-7.

267. Santos AL, Moreirinha C, Lopes D, Esteves AC, Henriques I, Almeida A, et al. Effects of UV radiation on the lipids and proteins of bacteria studied by mid-infrared spectroscopy. Environ Sci Technol. 2013;47:6306−15.

268. Barros A . Contribution à la sélection et la comparaison de variables caractéristiques [Ph.D. Thesis]. Paris, France: Institut national agronomique Paris-Grignon; 1999.

269. Manoharan R, Baraga JJ, Rava RP, Dasari RR, Fitzmaurice M, Feld MS. Biochemical analysis and mapping of atherosclerotic human artery using FT-IR microspectroscopy. Atherosclerosis. 1993;103(2):181-93.

270. Ansari NA, Dash D. Biochemical studies on methylglyoxal-mediated glycated histones: implications for presence of serum antibodies against the glycated histones in patients with type 1 diabetes mellitus. ISRN Biochemistry. 2013;2013:5.

271. Dovbeshko GI, Gridina NY, Kruglova EB, Pashchuk OP. FTIR spectroscopy studies of nucleic acid damage. Talanta. 2000;53(1):233-46.

272. Schulz H, Baranska M. Identification and qualification of valuable plant substances by IR and Raman spectroscopy. Vib Spectrosc. 2007;43(13-25).

273. Fujioka N, Morimoto Y, Arai T, Kikuchi M. Discrimination between normal and malignant human gastric tissues by Fourier transform infrared spectroscopy. Cancer Detect Prev. 2004;28(1):32-6.

274. Paluszkiewicz C, Kwiatek WM. Analysis of human cancer prostate tissues using FTIR microscopy and SXIXE techniques. J Mol Struct. 2001;565-566:329-34.

275. Richter T, Steiner G, Abu-Id MH, Salzer R, Bergmann R, Rodig H, et al. Identification of tumor tissue by FTIR spectroscopy in combination with positron emission tomography. Vib Spectrosc. 2002;28(1):103-10.

276. Dovbeshko G, Chegel V, Gridina NY, Repnytska O, Shirshov Y, Tryndiak V, et al. Surface enhanced IR absorption of nucleic acids from tumor cells: FTIR reflectance study. Biopolymers. 2002;67(6):470-86.

277. Chiriboga L, Xie P, Yee H, Vigorita V, Zarou D, Zakim D, et al. Infrared spectroscopy of human tissue. I. Differentiation and maturation of epithelial cells in the human cervix. Biospectroscopy. 1998;4(1):47-53.

278. Wong P, Papavassiliou E, Rigas B. Phosphodiester stretching bands in the infrared spectra of human tissues and cultured cells. Appl Spectrosc. 1991;45(9):1563-7.

279. Yang Y, Sulé-Suso J, Sockalingum GD, Kegelaer G, Manfait M, El Haj AJ. Study of tumor cell invasion by Fourier transform infrared microspectroscopy. Biopolymers. 2005;78(6):311-7.

280. Fabian H, Jackson M, Murphy L, Watson PH, Fichtner I, Mantsch HH. A comparative infrared spectroscopic study of human breast tumors and breast tumor cell xenografts. Biospectroscopy. 1995;1(1):37-45.

281. Shetty G, Kedall C, Shepherd N, Stone N, Barr H. Raman spectroscopy: evaluation of biochemical changes in carcinogenesis of oesophagus. Br J Cancer. 2006;94:1460-4.

282. Yoshida S, Miyazaki M, Sakai K, Takeshita M, Yuasa S, Sato A, et al. Fourier transform infrared spectroscopic analysis of rat brain microsomal membranes modified by dietary fatty acids: possible correlation with altered learning behavior. Biospectroscopy. 1997;3(4):281-90.

283. Gazi E, Dwyer J, Gardner P, Ghanbari-Siahkali A, Wade A, Miyan J, et al. Applications of Fourier transform infrared microspectroscopy in studies of benign prostate and prostate cancer. A pilot study. J Pathol. 2003;201(1):99-108.

284. Yang WH, Zhang WC, Lu XM, Jiang GS, Gao PJ. Characterization of a novel antibacterial glycopeptide produced by *Penicillium sp*. M03. Lett Appl Microbiol. 2009;48(4):393-7.

285. Fukuyama Y, Yoshida S, Yanagisawa S, Shimizu M. A study on the differences between oral squamous cell carcinomas and normal oral mucosas measured by Fourier transform infrared spectroscopy. Biospectroscopy. 1999;5(2):117-26.

286. Wood BR, Quinn MA, Tait B, Ashdown M, Hislop T, Romeo M, et al. FTIR microspectroscopic study of cell types and potential confounding variables in screening for cervical malignancies. Biospectroscopy. 1998;4(2):75-91.

287. Andrus PG, Strickland RD. Cancer grading by Fourier transform infrared spectroscopy. Biospectroscopy. 1998;4(1):37-46.

288. Benning LG, Phoenix V, Yee N, Tobin M. Molecular characterization of cyanobacterial silicification using synchrotron infrared micro-spectroscopy. Geochim Cosmochim Acta. 2004;68(4):729-41.

289. Fung MFK, Senterman MK, Mikhael NZ, Lacelle S, Wong PT. Pressure-tuning fourier transform infrared spectroscopic study of carcinogenesis in human endometrium. Biospectroscopy. 1996;2(3):155-65.

290. Movasaghi Z, Rehman S, ur Rehman DI. Fourier transform infrared (FTIR) spectroscopy of biological tissues. Appl Spectrosc Rev. 2008;43(2):134-79.

291. Li Q-B, Sun X-J, Xu Y-Z, Yang L-M, Zhang Y-F, Weng S-F, et al. Diagnosis of gastric inflammation and malignancy in endoscopic biopsies based on Fourier transform infrared spectroscopy. Clin Chem. 2005;51(2):346-50.

292. Wu JG, Xu YZ, Sun CW, Soloway RD, Xu DF, Wu QG, et al. Distinguishing malignant from normal oral tissues using FTIR fiber-optic techniques. Biopolymers. 2001;62(4):185-92.

293. Zang X. Investigating the role of extracellular phosphate groups in bacterial adhesion to soil minerals [Fellowship Report]. Davies, CA, USA: University of California; 2009.

294. Jiang W, Saxena A, Song B, Ward BB, Beveridge TJ, Myneni SC. Elucidation of functional groups on gram-positive and gram-negative bacterial surfaces using infrared spectroscopy. Langmuir. 2004;20(26):11433-42.

295. Santhiya D, Subramanian S, Natarajan K. Surface chemical studies on galena and sphalerite in the presence of *Thiobacillus thiooxidans* with reference to mineral beneficiation. Miner Eng. 2000;13(7):747-63.

296. Choo-Smith L-P, Maquelin K, Van Vreeswijk T, Bruining H, Puppels G, Thi NN, et al. Investigating microbial (micro) colony heterogeneity by vibrational spectroscopy. Appl Environ Microbiol. 2001;67(4):1461-9.

297. Wang H, Wang H-C, Huang Y-J. Microscopic FTIR studies of lung cancer cells in pleural fluid. Sci Total Environ. 1997;204(3):283-7.

298. Wang Y, Zhou Q, Li B, Liu B, Wu G, Ibrahim M, et al. Differentiation in MALDI-TOF MS and FTIR spectra between two closely related species *Acidovorax oryzae* and *Acidovorax citrulli*. BMC Microbiol. 2012;12(1):182.

299. Dennis K, Shibamoto T. Gas chromatographic analysis of reactive carbonyl compounds formed from lipids upon UV-irradiation. Lipids. 1990;25(8):460-4.

300. Gault N, Rigaud O, Poncy J-L, Lefaix J-L. Infrared microspectroscopy study of γ-irradiated and $H_2O_2$-treated human cells. Int J Radiat Biol. 2005;81(10):767-79.

301. Lasch P, Petras T, Ullrich O, Backmann J, Naumann D, Grune T. Hydrogen peroxide-induced structural alterations of RNAse A. J Biol Chem. 2001;276(12):9492-502.

302. Demple B. Regulation of bacterial oxidative stress genes. Annu Rev Genet. 1991;25(1):315-37.

303. Reynaud E. Protein misfolding and degenerative diseases. Nature Education. 2010;3(9):28.

304. Mariño K, Bones J, Kattla JJ, Rudd PM. A systematic approach to protein glycosylation analysis: a path through the maze. Nature chemical biology. 2010;6(10):713-23.

305. Roth J, Zuber C, Park S, Jang I, Lee Y, Kysela KG, et al. Protein N-glycosylation, protein folding, and protein quality control. Mol Cells. 2010;30(6):497-506.

306. Baglo Y, Sousa MM, Slupphaug G, Hagen L, Håvåg S, Helander L, et al. Photodynamic therapy with hexyl aminolevulinate induces carbonylation, posttranslational modifications and changed expression of proteins in cell survival and cell death pathways. Photochem Photobiol Sci. 2011;10(7):1137-45.

307. Hsieh Y, Chien K, Lin S, Sabu S, Hsu R, Chi L, et al. Photofrin binds to procaspase-3 and mediates photodynamic treatment-triggered methionine oxidation and inactivation of procaspase-3. Cell Death Dis. 2012;3(7):e347.

308. Vollmer W, Blanot D, De Pedro MA. Peptidoglycan structure and architecture. FEMS Microbiol Rev. 2008;32(2):149-67.

309. Min D, Boff J. Chemistry and reaction of singlet oxygen in foods. Compr Rev Food Sci Food Saf. 2002;1(2):58-72.

310. Dougherty TJ, Gomer CJ, Henderson BW, Jori G, Kessel D, Korbelik M, et al. Photodynamic therapy. J Natl Cancer Inst. 1998;90(12):889-905.

311. Perlin M, Mao JCH, Otis ER, Shipkowitz NL, Duff RG. Photodynamic inactivation of influenza and herpes viruses by hematoporphyrin. Antiviral Res. 1987;7(1):43-51.

312. Nitzan Y, Wexler HM, Finegold SM. Inactivation of anaerobic bacteria by various photosensitized porphyrins or by hemin. Curr Microbiol. 1994;29(3):125-31.

313. Luksiene Z, Peciulyte D, Lugauskas A. Inactivation of fungi *in vitro* by photosensitization: preliminary results. Ann Agric Environ Med. 2004;11:215-20.

314. Luksiene Z, Peciulyte D, Lugauskas A. Photodynamic inactivation of harmful and pathogenic microorganisms. Vet Med Zootechn. 2004;26:58-60.

315. Giese AC. Protozoa in photobiological research. Physiol Zool. 1953;26(1):1-22.

316. Goble FC, Boyd JL. Action of certain tetrapyrrole derivatives in experimental *Trypanosoma congolense* infections. Exp Biol Med. 1959;100(4):745-50.

317. Tosk J, Sherif A, Hall R, Lau B. Phototoxicity of hematoporphyrin derivative in larvae of *Culex quinquefasciatus*. Proc Pap Annu Conf Calif Mosq Control Assoc. 1986;54:70-3.

318. Bliss JM, Bigelow CE, Foster TH, Haidaris CG. Susceptibility of *Candida* species to photodynamic effects of photofrin. Antimicrob Agents Chemother. 2004;48(6):2000-6.

319. Maisch T, Hackbarth S, Regensburger J, Felgenträger A, Bäumler W, Landthaler M, et al. Photodynamic inactivation of multi-resistant bacteria (PIB) – a new approach to treat superficial infections in the 21st century. J Dtsch Dermatol Ges. 2011;9(5):360-6.

320. Ormond A, Freeman H. Dye sensitizers for photodynamic therapy. Materials (Basel). 2013;6(3):817-40.

321. Erzinger G, Wohllebe S, Vollrath F, Souza S, Richter P, Lebert M, et al. Optimizing conditions for the use of chlorophyll derivatives for photodynamic control of parasites in aquatic ecosystems. Parasitol Res. 2011;109(3):781-6.

322. Milgrom LR, Warren MJ. The colours of life: an introduction to the chemistry of porphyrins and related compounds. Oxford: Oxford University Press, Inc.; 1997. 225 p.

323. Allison RR, Bagnato VS, Sibata CH. Future of oncologic photodynamic therapy. Future Oncol. 2010;6(6):929-40.

324. Darlenski R, Fluhr JW. Photodynamic therapy in dermatology: past, present, and future. J Biomed Opt. 2012;18(6):061208.

325. Almeida A, Cunha Â, Gomes NC, Alves E, Costa L, Faustino MA. Phage therapy and photodynamic therapy: low environmental impact approaches to inactivate microorganisms in fish farming plants. Mar Drugs. 2009;7(3):268-313.

326. Carvalho C, Tomé J, Faustino M, Neves M, Tomé A, Cavaleiro J, et al. Antimicrobial photodynamic activity of porphyrin derivatives: potential application on medical and water disinfection. J Porphyr Phthalocyanines. 2009;13:574-7.

327. Jori G, Magaraggia M, Fabris C, Soncin M, Camerin M, Tallandini L, et al. Photodynamic inactivation of microbial pathogens: Disinfection of water and prevention of water-borne diseases. J Environ Pathol Toxicol Oncol. 2011;30(3).

328. Magaraggia M, Coppellotti O, Fabris C, Guidolin L, Jori G. Inactivation of microbial pathogens by photosensitized processes: environmental applications. In: Hamblin M, Jori G, editors. Photodynamic inactivation of microbial pathogens: medical and environmental applications. Cambridge: Royal Society of Chemistry; 2011. p. 403-23.

329. National Office of Forests, Bull. Tech., Dec 1997, No. (34), p. 167.

330. Fies TS, Mathers M. The basics of efficient lighting - a reference manual for training in efficient lighting principles. National Framework for Energy Efficiency. Australian, State and Territory and New Zealand Governments; 2009. 152 p.

331. Alouini Z, Jemli M. Destruction of helminth eggs by photosensitized porphyrin. J Environ Monitor. 2001;3:548 - 51.

332. Jemli M, Alouini Z, Sabbahi S, Gueddari M. Destruction of fecal bacteria in wastewater by three photosensitizers. J Environ Monitor. 2002;4(4):511-6.

333. Lacombe S, Pigot T. New materials for sensitized photo-oxygenation. In: Albini A, editor. Photochemistry: specialist periodical reports. Cambridge: RSC Publishing; 2010. p. 307-29.

334. Carpenter BL, Feese E, Sadeghifar H, Argyropoulos DS, Ghiladi RA. Porphyrin-cellulose nanocrystals: a photobactericidal material that exhibits broad spectrum antimicrobial activity. Photochem Photobiol. 2012;88(3):527-36.

335. Luksiene Z, Danilčenko H, Tarasevičienė Ž, Anusevičius Ž, Marozienė A, Nivinskas H. New approach to the fungal decontamination of wheat used for wheat sprouts: effects of aminolevulinic acid. Int J Food Microbiol. 2007;116(1):153-8.

336. Luksienė Z, Pečiulytė D, Jurkonienė S, Puras R. Inactivation of possible fungal food contaminants by photosensitization. Food Technol Biotechnol. 2005;43(4):1-7.

337. Dondji B, Duchon S, Diabate A, Herve JP, Corbel V, Hougard JM, et al. Assessment of laboratory and field assays of sunlight-induced killing of mosquito larvae by photosensitizers. J Med Entomol. 2005;42(4):652-6.

338. Lucantoni L, Magaraggia M, Lupidi G, Ouedraogo RK, Coppellotti O, Esposito F, et al. Novel, *meso*-substituted cationic porphyrin molecule for photo-mediated larval control of the dengue vector *Aedes aegypti*. PLoS Negl Trop Dis. 2011;5(12):e1434.

339. El-Tayeb TA, El-Aziz NMA, Awad HH. A study on the dynamics of *Aedes caspius* larval uptake and release of novel haematoporphyrin. Afr Entomol. 2013;21(1):15-23.

340. Fabris C, Ouédraogo RK, Coppellotti O, Dabiré RK, Diabaté A, Di Martino P, et al. Efficacy of sunlight-activatable porphyrin formulates on larvae of *Anopheles gambiae* M and S molecular forms and *An. arabiensis*: a potential novel biolarvicide for integrated malaria vector control. Acta Trop. 2012;123(3):239-43.

341. Mukwaya L. Photo-biological control of mosquito larvae. Entebbe, Uganda: Uganda Virus Reseacht Instituti, 2008 21 Nov 2008. Available from: http://www.inradcorp.com/photos/letter.pdf.

342. Fabris C, Soncin M, Jori G, Habluetzel A, Lucantoni L, Sawadogo S, et al. Effects of a new photoactivatable cationic porphyrin on ciliated protozoa and branchiopod crustaceans, potential components of freshwater ecosystems polluted by pathogenic agents and their vectors. Photochem Photobiol Sci. 2012;11(2):294-301.

343. Buchovec I, Paskeviciute E, Luksiene Z. Photodynamic inactivation of food pathogen *Listeria monocytogenes*. Food Technol Biotechnol. 2010;48(2):207 - 13.

344. Buchovec I, Vaitonis Z, Luksiene Z. Novel approach to control *Salmonella enterica* by modern biophotonic technology: photosensitization. J Appl Microbiol. 2009;106(3):748-54.

345. Luksiene Z, Buchovec I, Paskeviciute E. Inactivation of food pathogen *Bacillus cereus* by photosensitization *in vitro* and on the surface of packaging material. J Appl Microbiol. 2009;107(6):2037-46.

346. Luksiene Z, Buchovec I, Paskeviciute E. Inactivation of *Bacillus cereus* by Na-chlorophyllin-based photosensitization on the surface of packaging. J Appl Microbiol. 2010;109(5):1540-8.

347. Luksiene Z, Paskeviciute E. Microbial control of food-related surfaces: Na-Chlorophyllin-based photosensitization. J Photochem Photobiol B. 2011;105(1):69-74.

348. Paskeviciute E, Luksiene Z. Photosensitization as a novel approach to decontaminate fruits and vegetables. Časopis za procesnu tehniku i energetiku u poljoprivredi/PTEP. 2009;13(1):50-3.

349. Ben Amor T, Tronchin M, Bortolotto L, Verdiglione R, Jori G. Porphyrins and related compounds as photoactivatable insecticides I. Phototoxic activity of hematoporphyrin toward *Ceratitis capitata* and *Bactrocera oleae*. Photochem Photobiol. 1998;67(2):206-11.

350. Lhotáková Y, Plíštil L, Morávková A, Kubát P, Lang K, Forstová J, et al. Virucidal nanofiber textiles based on photosensitized production of singlet oxygen. PLoS One. 2012;7(11):e49226.

351. Alvarez MG, Gómez ML, Mora SJ, Milanesio ME, Durantini EN. Photodynamic inactivation of *Candida albicans* using bridged polysilsesquioxane films doped with porphyrin. Bioorg Med Chem. 2012;20(13):4032-9.

352. Funes MaD, Caminos DA, Alvarez MG, Fungo F, Otero LA, Durantini EN. Photodynamic properties and photoantimicrobial action of electrochemically generated porphyrin polymeric films. Environ Sci Technol. 2009;43(3):902-8.

353. Pujol-Lereis LM, Massaldi A, Rabossi A, Quesada-Allué LA. Photosensitizing effect of hematoporphyrin IX on immature stages of *Ceratitis capitata* (Diptera: Tephritidae). Photochem Photobiol. 2010;86(3):639-44.

354. Wohllebe S, Ulbrich C, Grimm D, Pietsch J, Erzinger G, Richter R, et al. Photodynamic treatment of *Chaoborus crystallinus* larvae with chlorophyllin induces necrosis and apoptosis. Photochem Photobiol. 2011;87(5):1113-22.

355. Wohllebe S, Richter R, Richter P, Häder DP. Photodynamic control of human pathogenic parasites in aquatic ecosystems using chlorophyllin and pheophorbid as photodynamic substances. Parasitol Res. 2009;104(3):593-600.

356. Awad HH, El-Tayeb TA, Abd El-Aziz NM, Abdelkader MH. A semi-field study on the effect of novel hematoporphyrin formula on the control of *Culex pipiens* larvae. J Agri Soc Sci. 2008;4:85-8.

357. El-Tayeb TA. The use of photoactivable photopesticides for the control of potentially noxious insects [MSc Thesis]. Cairo, Egypt: Cairo University; 1999.

358. Schrader KK, Bommer JC, Jori G. *In vitro* evaluation of the antimicrobial agent AquaFrin as a bactericide and selective algicide for use in channel catfish aquaculture. N Am J Aquac. 2010;72(4):304-8.

359. Alves E, Carvalho CMB, Tome JPC, Faustino MAF, Neves MGPMS, Tome AC, et al. Photodynamic inactivation of recombinant bioluminescent *Escherichia coli* by cationic porphyrins under artificial and solar irradiation. J Ind Microbiol Biot. 2008;35(11):1447 - 54.

360. Bonnett R, Krysteva MA, Lalov IG, Artarsky SV. Water disinfection using photosensitizers immobilized on chitosan. Water Res. 2006;40(6):1269-75.

361. Bozja J, Sherrill J, Michielsen S, Stojiljkovic I. Porphyrin-based, light-activated antimicrobial materials. J Polym Sci A Polym Chem. 2003;41(15):2297-303.

362. Eichner A, Gonzales FP, Felgentrager A, Regensburger J, Holzmann T, Schneider-Brachert W, et al. Dirty hands: photodynamic killing of human pathogens like EHEC, MRSA and *Candida* within seconds. Photochem Photobiol Sci. 2013;12(1):135-47.

363. Feese E, Sadeghifar H, Gracz HS, Argyropoulos DS, Ghiladi RA. Photobactericidal porphyrin-cellulose nanocrystals: synthesis, characterization, and antimicrobial properties. Biomacromolecules. 2011;12(10):3528-39.

364. Jesenská S, Plíštil L, Kubát P, Lang K, Brožová L, Popelka Š, et al. Antibacterial nanofiber materials activated by light. J Biomed Mater Res A. 2011;99A(4):676-83.

365. Krouit M, Granet R, Branland P, Verneuil B, Krausz P. New photoantimicrobial films composed of porphyrinated lipophilic cellulose esters. Bioorg Med Chem Lett. 2006;16(6):1651-5.

366. Krouit M, Granet R, Krausz P. Photobactericidal plastic films based on cellulose esterified by chloroacetate and a cationic porphyrin. Bioorg Med Chem. 2008;16(23):10091-7.

367. Krouit M, Granet R, Krausz P. Photobactericidal films from porphyrins grafted to alkylated cellulose – synthesis and bactericidal properties. Eur Polym J. 2009;45(4):1250-9.

368. López-Carballo G, Hernández-Muñoz P, Gavara R, Ocio MJ. Photoactivated chlorophyllin-based gelatin films and coatings to prevent microbial contamination of food products. Int J Food Microbiol. 2008;126(1–2):65-70.

369. Magaraggia M, Faccenda F, Gandolfi A, Jori G. Treatment of microbiologically polluted aquaculture waters by a novel photochemical technique of potentially low environmental impact. J Environ Monitor. 2006;8(9):923-31.

370. Mbakidi J-P, Herke K, Alvès S, Chaleix V, Granet R, Krausz P, et al. Synthesis and photobiocidal properties of cationic porphyrin-grafted paper. Carbohydr Polym. 2013;91(1):333-8.

371. Merchán M, Ouk TS, Kubát P, Lang K, Coelho C, Verney V, et al. Photostability and photobactericidal properties of porphyrin-layered double hydroxide–polyurethane composite films. J Mater Chem B Mater Biol Med. 2013;1(16):2139-46.

372. Mosinger J, Jirsak O, Kubat P, Lang K, Mosinger B. Bactericidal nanofabrics based on photoproduction of singlet oxygen. J Mater Chem. 2007;17(2):164-6.

373. Mosinger J, Lang K, Kubát P, Sýkora J, Hof M, Plíštil L, et al. Photofunctional polyurethane nanofabrics doped by zinc tetraphenylporphyrin and zinc phthalocyanine photosensitizers. J Fluoresc. 2009;19(4):705-13.

374. Ringot C, Sol V, Barrière M, Saad Nm, Bressollier P, Granet R, et al. Triazinyl porphyrin-based photoactive cotton fabrics: preparation, characterization, and antibacterial activity. Biomacromolecules. 2011;12(5):1716-23.

375. Ringot C, Sol V, Granet R, Krausz P. Porphyrin-grafted cellulose fabric: new photobactericidal material obtained by “Click-Chemistry” reaction. Mater Lett. 2009;63(21):1889-91.

376. Rychtarikova R, Sabata S, Hetflejs J, Kuncova G. Composites with photosensitive 5,10,15,20-tetrakis(N-methylpyridinium-4-yl)porphyrin entrapped into silica gels. J Sol-Gel Sci Technol. 2012;61(1):119-25.

377. Rychtarikova R, Sabata S, Hetflejs J, Kuncova G. Photodynamic efficiency of porphyrins encapsulated in polysilsesquioxanes. Chem Pap. 2012;66(4):269-77.

378. Vorobey AV, Pinchuk SV. Photodamage to spores of *Fusarium* fungi sensitized by protoporphyrin IX. Biophysics. 2008;53(5):386-9.

379. Wohllebe S, Richter P, Häder D-P. Chlorophyllin for the control of *Ichthyophthirius multifiliis* (Fouquet). Parasitol Res. 2012;111(2):729-33.

380. Banerjee I, Douaisi MP, Mondal D, Kane RS. Light-activated nanotube-porphyrin conjugates as effective antiviral agents. Nanotechnology. 2012;23(10):105101.

381. Luksiene Z, Kurilcik N, Jursenas S, Radziute S, Buda V. Towards environmentally and human friendly insect pest control technologies: photosensitization of leafminer flies *Liriomyza bryoniae*. J Photochem Photobiol B. 2007;89(1):15-21.

382. Buchovec I, Paskeviciute E, Luksiene Z. Photosensitization-based inactivation of food pathogen *Listeria monocytogenes* in vitro and on the surface of packaging material. J Photochem Photobiol B. 2010; 99(9-14).

383. Luksiene Z, Buchovec I, Paskeviciute E. Inactivation of several strains of *Listeria monocytogenes* attached to the surface of packaging material by Na-Chlorophyllin-based photosensitization. J Photochem Photobiol B. 2010;101(3):326-31.

384. Luksiene Z, Kokstaite R, Katauskis P, Skakauskas V. Novel approach for effective and uniform inactivation of Gram-positive *Listeria monocytogenes* and Gram-negative *Salmonella enterica* by photosensitization. Food Technol Biotechnol. in press.

385. Luksiene Z, Paskeviciute E. Novel approach to the microbial decontamination of strawberries: chlorophyllin-based photosensitization. J Appl Microbiol. 2011;110(5):1274-83.

386. El-Tayeb TA, Gharib MM, Al-Gendy AM. Preliminary study to investigate the optimum parameters of using hematoporphyrin IX to control flesh fly (*Parasarcophaga argyrostoma*). J Entomol. 2011;8:384-90.

387. Buchovec I, Kokstaite R, Luksiene Z, Pamedytyte V, Makuska R. Antimicrobial efficiency of photoactivated chlorophyllin-chitosan complex. Chemical Technology. 2012;61(3):54-7.

388. Banerjee I, Mondal D, Martin J, Kane RS. Photoactivated antimicrobial activity of carbon nanotube−porphyrin conjugates. Langmuir. 2010;26(22):17369-74.

389. Ringot C, Saad N, Granet R, Bressollier P, Sol V, Krausz P. Meso-functionalized aminoporphyrins as efficient agents for photo-antibacterial surfaces. J Porphyr Phthalocyanines. 2010;14:925-31.

390. Ben Amor T, Bortolotto L, Jori G. Porphyrins and related compounds as photoactivatable insecticides. 3. Laboratory and field studies. Photochem Photobiol. 2000;71(2):124-8.

391. Barbieri A. Sensibilizadores fluorescentes como larvicidas. Action fotodynamica de la luz. Riv Malariol. 1928(7):456-63.

392. Robinson J. Photodynamic insecticides: a review of studies on photosensitizing dyes as insect control agents, their practical application, hazards, and residues. Residue Rev. 1983:69-100.

393. Rebeiz CA, Juvick JA, Rebeiz CC. Porphyric insecticides. I. Concepts and phenomenology. Pestic Biochem Physiol. 1988(30):11-27.

394. Rebeiz CA, Juvik JA, Rebeiz CC, Bouton CE, Gut LT. Porphyric insecticides 2. 1,10 phenanthroline, a potent porphyric insecticide modulator. Pestic Biochem Physiol. 1990;36:201-7.

395. Rebeiz CA, Montazer-Zouhoor A, Mayasich IM, Tripathy BC, Wu SM, Rebeiz CC. Photodynamic herbicides. Recent developments and molecular basis of selectivity. CRC Crit Rev Plant Sci. 1988;6:385-434.

396. Rebeiz CA, Reddy KN, Nandihalli UB, Velu J. Tetrapyrrole-dependent photodynamic herbicides. Photochem Photobiol. 1990;52:1099-1 117.

397. Snow K, Ramsdale C. Distribution chart for European mosquitoes. European Mosquito Bulletin Journal of the European Mosquito Control Association. 1999(3):14-31.

398. Directorate-General of Health from the Portuguese Ministry of Health. Monthly updates on outbreak of dengue in Madeira, situation in 07/04/2013 [Internet]. 2013 [updated 2013 Sep 1; cited 2013 May 11]; Available from: http://www.dgs.pt/?cn=683368347243AAAAAAAAAAAA.

399. Schaffner F AP, Medlock J, eds. European Mosquito Bulletin Journal of the European Mosquito Control Association. [place unknown]: [publisher unknown]; [cited 2013 28 Apr 2013]. Available from: http://e-m-b.org/.

400. European Comission. Union list of food additives. Brussels: Official Journal of the European Union; 11/11/2011. Commission Regulation (EU) No 1129/2011.

401. European Union. Food additives authorized for use in foodstuffs intended for human consumption. Geneva; 21/12/1989. Council Directive 89/107/EEC.

402. Brandis A, Salomon Y, Scherz A. Chlorophyll sensitizers in photodynamic therapy. In: Grimm B, Porra R, Rüdiger W, Scheer H, editors. Chlorophylls and bacteriochlorophylls: Springer The Netherlands; 2006. p. 461-83.

403. Ben Amor T, Bortolotto L, Jori G. Porphyrins and related compounds as photoactivatable insecticides. 2. Phototoxic activity of meso-substituted porphyrins. Photochem Photobiol. 1998;68(3):314-8.

404. Ben Amor T, Jori G. Sunlight-activated insecticides: historical background and mechanisms of phototoxic activity. Insect Biochem Mol Biol. 2000;30(10):915-25.

405. Costa L, Tomé JP, Neves MG, Tomé AC, Cavaleiro JA, Cunha Â, et al. Susceptibility of non-enveloped DNA-and RNA-type viruses to photodynamic inactivation. Photochem Photobiol Sci. 2012;11(10):1520-3.

406. Brame J, Alvarez PJJ. Challenges and opportunities in the use of nanotechnology for water treatment and wastewater reuse. In: Korhonen-Kurki K, Fox M, editors. Towards new solutions in managing environmental crisis, Proceedings of the USA - Iran - Finland Environmental Workshop; 2009 Sep 14-15; Haikko, Finland; Helsinki: Helsinki University Printing House; 2010. p. 84-92.

407. Ngwenya N, Ncube E, Parsons J. Recent advances in drinking water disinfection: successes and challenges. In: Whitacre DM, editor. Reviews of Environmental Contamination and Toxicology. New York: Springer New York; 2013. p. 111-70.

408. Qu X, Brame J, Li Q, Alvarez PJJ. Nanotechnology for a safe and sustainable water supply: enabling integrated water treatment and reuse. Acc Chem Res. 2013;46(3):834-43.

409. Theron J, Walker JA, Cloete TE. Nanotechnology and water treatment: applications and emerging opportunities. Crit Rev Microbiol. 2008;34(1):43-69.

410. Almeida A, Cavaleiro, J.A.S., Rocha J, Carvalho CMB, Costa LAS, Alves E, et al., inventors; Nanomagnet-porphyrin hybrid materials: synthesis and water disinfection application. Portuguese Patent PT103828, Portugal2009.

411. Almeida J. Multidrug resistant bacteria inactivation by photodynamic therapy [MSc Thesis]. Aveiro, Portugal: University of Aveiro; 2011.

412. Luksiene Z, Zukauskas A. Prospects of photosensitization in control of pathogenic and harmful micro-organisms. J Appl Microbiol. 2009;107(5):1415-24.

413. Pelicano S. Portuguese company creates anti mosquito nanoparticle [Internet]. Success Gadget©; [cited 2013 29 Apr]; Available from: http://www.success-gadget.com/news/empresa-portuguesa-cria-nanoparticula-antimosquitos-1?set_language=en.

414. Self-cleaning tiles [Internet]. Revigres® Lab; 2013 [cited 2013 4 May]; Available from: http://www.revigres.pt/microsite.php?id=4&lg=gb.

415. Jirsák O, Sanetrník F, Lukáš D, Kotek V, Martinová L, Chaloupek J, inventors. CZ Patent 294274 (2003); PCT/CZ2004/000056 (2004), Czech Republic2004.

416. Greiner A, Wendorff JH. Electrospinning: a fascinating method for the preparation of ultrathin fibers. Angew Chem Int Ed Engl. 2007;46(30):5670-703.

417. Dancer S. How do we assess hospital cleaning? A proposal for microbiological standards for surface hygiene in hospitals. J Hosp Infect. 2004;56(1):10-5.

418. Midden WR, Wang SY. Singlet oxygen generation for solution kinetics: clean and simple. J Am Chem Soc. 1983;105(13):4129-35.

419. Beard S, Salisbury V, Lewis R, Sharpe J, MacGowan A. Expression of *lux* genes in a clinical isolate of *Streptococcus pneumoniae*: using bioluminescence to monitor gemifloxacin activity. Antimicrob Agents Chemother. 2002;46(2):538-42.

420. Koga K, Harada T, Shimizu H, Tanaka K. Bacterial luciferase activity and the intracellular redox pool in *Escherichia coli*. Mol Genet Genomics. 2005;274(2):180-8.

421. Meighen EA. Bacterial bioluminescence: organization, regulation, and application of the *lux* genes. FASEB J. 1993;7(11):1016-22.

422. Vesterlund S, Paltta J, Laukova A, Karp M, Ouwehand AC. Rapid screening method for the detection of antimicrobial substances. J Microbiol Meth. 2004;57(1):23-31.

423. Harveyi E. Bioluminescence. New York: Academic Press, Inc.; 1952.

424. Hastings J. Bioluminescence in bacteria and dinoflagellates. In: Govindjee A, Fork D, editors. Light emission by plants and bacteria. New York: Academic Press, Inc.; 1986. p. 363-98.

425. Baumann L, Baumann L, Woolkalis M, Bang S. Evolutionary relationships in *Vibrio* and *Photobacterium*. A basis for a natural classification. Annu Rev Microbiol. 1983(37):369-98.

426. Nealson K, Hastings J. Bacterial bioluminescence: its control and ecological significance. Microbiol Rev. 1979(43):496-518.

427. Campbell A. Living light: biochemistry, function and biomedical applications. Essays Biochem. 1989(24):41-76.

428. Farmer JI, Jorgensen J, Grimont P, Akhurst R, Poinar GJ, Ageron E, et al. *Xenorhabdus luminescens* (DNA hybridization group 5) from human clinical specimens. J Clin Microbiol. 1989(27):1594-600.

429. Meighen EA. Molecular biology of bacterial bioluminescence. Microbiol Mol Biol Rev. 1991;55(1):123-42.

430. Hastings J. Chemistries and colors of bioluminescent reactions: a review. Gene. 1996(173):5–11.

431. Makemson JC, Hastings JW. Iron represses bioluminescence and affects catabolite repression of luminescence in *Vibrio harveyi*. Curr Microbiol. 1982;7(3):181-6.

432. Bassler B, Silverman M. Intercellular communication in marine *Vibrio* species: density-dependent regulation of the expression of bioluminescence. In: Silhavy JAHTJ, editor. Two-component signal transduction. Washington DC: American Society for Microbiology; 1995. p. 431-45.

433. Makemson J. Luciferase-dependent oxygen consumption by bioluminescent *Vibrio*. J Bacteriol 1986(165):461-6.

434. Szpilewska H, Czyz A, Wegrzyn G. Experimental evidence for the physiological role of bacterial luciferase in the protection of cells against oxidative stress. Curr Microbiol. 2003;47(5):379-82.

435. Ziegler M, Baldwin T. Biochemistry of bacterial bioluminescence. Curr Top Bioenerg. 1981(12):65-113.

436. Meighen E, Grant G. Bioluminescence analysis of long chain aldehydes: detection of insect pheromones. In: Dyke KV, editor. Bioluminescence and chemiluminescence: instruments and applications. Boca Raton, Florida: CRC Press, Inc.; 1985. p. 253-68.

437. Meighen E, Slessor K, Grant G. Development of a bioluminescence assays for aldehyde pheromones of insects. I. Sensitivity and specificity. J Chem Ecol. 1982(8):911-21.

438. Rodriguez A, Nabi I, Meighen E. ATP turnover by the fatty acid reductase complex of *Photobacterium phosphoreum*. Can J Biochem Cell Biol. 1985(63):1106-11.

439. Shimomura O, Johnson F, Morise H. The aldehyde content of luminous bacteria and of an "aldehydeless" dark mutant. Proc Natl Acad Sci USA. 1974(71):4666-9.

440. Ulitzur S, Hastings J. Evidence for tetradecanal as the natural aldehyde in bacterial bioluminescence. Proc Natl Acad Sci USA. 1979(76):265-7.

441. Colepicolo P, Cho K-W, Poinar G, Hastings J. Growth and luminescence of the bacterium *Xenorhabdus luminescens* from a human wound. Appl Environ Microbiol. 1989(55):2601-6.

442. Meighen E, Bartlet I. Complementation of subunits from different bacterial luciferases. Evidence for the role of the P subunit in the bioluminescent mechanism. J Biol Chem. 1980(255):11181-7.

443. Schmidt T, Kopecky K, Nealson K. Bioluminescence of the insect pathogen *Xenorhabdus luminescens*. Appl Environ Microbiol. 1989(55):2607-12.

444. Szittner R, Meighen E. Nucleotide sequence, expression and properties of luciferase coded by *lux* genes from a terrestrial bacterium. J Biol Chem. 1990(265):16581-7.

445. Watanabe H, Hastings J. Expression of bacterial bioluminescence is stimulated by nalidixic acid in a nalidixic acid resistent mutant. Arch Microbiol 1990;154:239-43.

446. Clark D. The fermentation pathways of *Escherichia coli*. FEMS Microbiol Rev 1989;5:223-34.

447. Galluzzi L, Karp M. Intracellular redox equilibrium and growth phase affect the performance of luciferase-based biosensors. J Biotechnol. 2007;127(2):188-98.

448. Scholar EM, Pratt WB. The antimicrobial drugs. 2nd ed. New York: Oxford University Press, Inc.; 2000.

449. Czyz A, Plata K, Wegrzyn G. Induction of light emission by luminescent bacteria treated with UV light and chemical mutagens. J App Gen. 2002;43(3):377-89.

450. Ulitzur S, Weiser I. Acridine dyes and other DNA-intercalating agents induce the luminescence system of luminous bacteria and their dark variants. Proc Natl Acad Sci USA. 1981;78(6):3338-42.

451. Watanabe H, Nagoshi T, Inaba H. Luminescence of a bacterial luciferase intermediate by reaction with $H_2O_2$: the evolutionary origin of luciferase and source of endogenous light emission. Biochim Biophys Acta - Bioenergetics. 1993;1141(2-3):297-302.

452. Katsev AM, Węgrzyn G, Szpilewska H. Effects of hydrogen peroxide on light emission by various strains of marine luminescent bacteria. J Basic Microbiol. 2004;44(3):178-84.

453. Weiner JH, MacIsaac DP, Bishop RE, Bilous PT. Purification and properties of *Escherichia coli* dimethyl sulfoxide reductase, an iron-sulfur molybdoenzyme with broad substrate specificity. J Bacteriol. 1988;170(4):1505-10.

454. Baldwin T, Berends T, Bunch T, Holzman T, Rausch S, Shamansky L, et al. Cloning of the luciferase structural genes from *Vibrio harveyi* and expression of bioluminescence in *Escherichia coli*. Biochemistry. 1984;16(23):3663-7.

455. Belas R, Mileham A, Cohn D, Hilman M, Simon M, Silverman M. Bacterial bioluminescence: isolation and expression of the luciferase genes from *Vibrio harveyi*. Science. 1982;218(4574):791-3.

456. Cohn D, Ogden R, Abelson J, Baldwin T, Nealson K, Simon M, et al. Cloning of the *Vibrio harveyi* luciferase genes: use of a synthetic oligonucleotide probe. Proc Natl Acad Sci USA. 1983;1(80):120-3.

457. Delong E, Steinhauer D, Israel A, Nealson K. Isolation of the *lux* genes from *Photobacterium leiognathi* and expression in *Escherichia coli*. Gene. 1987;2-3(54):203-10.

458. Engebrecht J, Silverman M. Nucleotide sequence of the regulatory locus controlling expression of bacterial genes for bioluminescence. Nucl Acids Res. 1987;15(24):10455-67.

459. Evans JF, McCracken S, Miyamoto CM, Meighen EA, Graham AF. *In vitro* synthesis of subunits of bacterial luciferase in an *Escherichia coli* system. J Bacteriol. 1983;153(1):543-5.

460. Frackman S, Anhalt M, Nealson KH. Cloning, organization, and expression of the bioluminescence genes of *Xenorhabdus luminescens*. J Bacteriol 1990;172(10):5767-73.

461. Mancini JA, Boylan M, Soly RR, Graham AF, Meighen EA. Cloning and expression of the *Photobacterium phosphoreum* luminescence system demonstrates a unique *lux* gene organization. J Biol Chem. 1988;263(28):14308-14.

462. de Wet JR, Wood KV, Helinski DR, DeLuca M. Cloning of firefly luciferase cDNA and the expression of active luciferase in *Escherichia coli*. Proc Natl Acad Sci U S A. 1985;82(23):7870-3.

463. Wood KV, Lam YA, Seliger HH, McElroy WD. Complementary DNA coding click beetle luciferases can elicit bioluminescence of different colors. Science. 1989;244(4905):700-2.

464. Kurose K, Inouye S, Sakaki Y, Tsuji FI. Bioluminescence of the $Ca^{2+}$-binding photoprotein aequorin after cysteine modification. Proc Natl Acad Sci USA. 1989;86(1):80-4.

465. Prasher D, McCann C, Longlaru M, Cormier M. Sequence comparisons of complementary DNAs encoding aequorin isotypes. Biochemistry 1987(26):1326-32.

466. Thompson EM, Nagata S, Tsuji FI. Cloning and expression of cDNA for the luciferase from the marine ostracod *Vargula hilgendorfii*. Proc Natl Acad Sci USA. 1989;86(17):6567-71.

467. Slock J. Molecular biology experiments utilizing the *lux* genes of *Vibrio fischeri* and gfp gene of *Aequoria victoria* [Internet]. Wilkes Barre: Biology Department, King's College; 2000 [cited 2007 7 Aug]; Available from: http://departments.kings.edu/biology/lux/bacterial.html.

468. Chatterjee J, Meighen E. Biotechnological applications of bacterial bioluminescence genes. Photochem Photobiol. 1995(62):641-50.

469. Rocchetta HL, Boylan CJ, Foley JW, Iversen PW, LeTourneau DL, McMillian CL, et al. Validation of a noninvasive, real-time imaging technology using bioluminescent *Escherichia coli* in the neutropenic mouse thigh model of infection. Antimicrob Agents Chemother. 2001;45(1):129-37.

470. Hill P, Rees C, Winson M, Stewart G. The application of *lux* genes. Biotechnol Appl Biochem. 1993(17):3-14.

471. Francis KP, Joh D, Bellinger-Kawahara C, Hawkinson MJ, Purchio TF, Contag PR. Monitoring bioluminescent *Staphylococcus aureus* infections in living mice using a novel *luxABCDE* construct. Infect Immun. 2000;68(6):3594-600.

472. Boemare N, Akhurst R, Mourant R. DNA relatedness between *Xenorhabdus* spp. (*Enterobacteriaceae*), symbiotic bacteria of entomopathogenic nematodes, and a proposal to transfer *Xenorhabdus* luminescens to a new genus, *Photorhabdus* gen. nov. Int J Bacteriol. 1993(43):249-55.

473. Rainey FA, Ehlers RU, Stackebrandt E. Inability of the polyphasic approach to systematics to determine the relatedness of the genera *Xenorhabdus* and *Photorhabdus*. Int J Syst Bacteriol. 1995;45(2):379-81.

474. Xi L, Cho KW, Tu SC. Cloning and nucleotide sequences of *lux* genes and characterization of luciferase of *Xenorhabdus luminescens* from a human wound. J Bacteriol. 1991;173(4):1399-405.

475. Huang L, Dai T, Hamblin M. Antimicrobial photodynamic inactivation and photodynamic therapy for infections. Methods Mol Biol. 2010;635:155-73.

476. Kosaka S, Akilov OE, O'Riordan K, Hasan T. A mechanistic study of [delta]-aminolevulinic acid-based photodynamic therapy for cutaneous leishmaniasis. J Invest Dermatol. 2007;127(6):1546-9.

477. Lambrechts SAG, Aalders MCG, Van Marle J. Mechanistic study of the photodynamic inactivation of *Candida albicans* by a cationic porphyrin. Antimicrob Agents Chemother. 2005;49(5):2026-34.

478. Cassell GH, Mekalanos J. Development of antimicrobial agents in the era of new and reemerging infectious diseases and increasing antibiotic resistance. J Am Med Assoc. 2001;285(5):601-5.

479. Winckler KD. Special section: focus on anti-microbial photodynamic therapy (PDT). J Photochem Photobiol B. 2007;86(1):43-4.

480. Calin M, Parasca S. Light sources for photodynamic inactivation of bacteria. Lasers Med Sci. 2009;24(3):453-60.

481. DeRosa MC, Crutchley RJ. Photosensitized singlet oxygen and its applications. Coord Chem Rev 2002;233-234:351-71.

482. Ergaieg K, Chevanne M, Cillard J, Seux R. Involvement of both type I and type II mechanisms in gram-positive and gram-negative bacteria photosensitization by a *meso*-substituted cationic porphyrin. Sol Energy. 2008;82(12):1107-17.

483. Wainwright M, Crossley KB. Photosensitising agents - circumventing resistance and breaking down biofilms: a review. Int Biodeterior Biodegrad. 2004;53(2):119-26.

484. Hadjur C, Lange N, Rebstein J, Monnier P, Bergh Hvd, Wagnières G. Spectroscopic studies of photobleaching and photoproduct formation of meta(tetrahydroxyphenyl) chlorin (m-THPC) used in photodynamic therapy. The production of singlet oxygen by m-THPC. J Photochem Photobiol B. 1998;45 170-8.

485. Maclean M, MacGregor SJ, Anderson JG, Woolsey GA. The role of oxygen in the visible-light inactivation of *Staphylococcus aureus*. J Photochem Photobiol B. 2008;92(3):180-4.

486. Müller-Breitkreutz K, Mohr H, Briviba K, Sies H. Inactivation of viruses by chemically and photochemically generated singlet molecular oxygen. J Photochem Photobiol B. 1995;30(1):63-70.

487. Nitzan Y, Shainberg B, Malik Z. The mechanism of photodynamic inactivation of *Staphylococcus aureus* by deuteroporphyrin. Curr Microbiol. 1989;19(4):265-9.

488. Allen CM, Weber JM, van Lier JE. Sulfophthalocyanines for photodynamic inactivation of viruses in blood products: effect of structural modifications. Photochem Photobiol. 1995;62(1):184-9.

489. Egyeki M, Turóczy G, Majer Z, Tóth K, Fekete A, Maillard P, et al. Photosensitized inactivation of T7 phage as surrogate of non-enveloped DNA viruses: efficiency and mechanism of action. Biochim Biophys Acta-Gen Subj. 2003;1624(1-3):115-24.

490. Käsermann F, Kempf C. Photodynamic inactivation of enveloped viruses by buckminsterfullerene. Antiviral Res. 1997;34(1):65-70.

491. Vzorov AN, Dixon DW, Trommel JS, Marzilli LG, Compans RW. Inactivation of human immunodeficiency virus type 1 by porphyrins. Antimicrob Agents Chemother. 2002;46(12):3917-25.

492. Zupán K, Egyeki M, Tóth K, Fekete A, Herényi L, Módos K, et al. Comparison of the efficiency and the specificity of DNA-bound and free cationic porphyrin in photodynamic virus inactivation. J Photochem Photobiol B. 2008;90(2):105-12.

493. Durantini EN. Photodynamic inactivation of bacteria. Curr Bioact Compd. 2006;2:127-42.

494. Bagchi B, Basu S. Role of dye molecules remaining outside the cell during photodynamic inactivation of *Escherichia coli* in the presence of acriflavine. Photochem Photobiol. 1979;29(2):403-5.

495. Carre V, Gaud O, Sylvain I, Bourdon O, Spiro M, Biais J, et al. Fungicidal properties of *meso*-arylglycosylporphyrins: influence of sugar substituents on photoinduced damage in the yeast *Saccharomyces cerevisiae*. J Photochem Photobiol B. 1999;48(1):57-62.

496. Cassidy CM, Tunney MM, McCarron PA, Donnelly RF. Drug delivery strategies for photodynamic antimicrobial chemotherapy: from benchtop to clinical practice. J Photochem Photobiol B. 2009;95(2):71-80.

497. Ehrenberg B, Malik Z, Nitzan Y, Ladan H, Johnson F, Hemmi G, et al. The binding and photosensitization effects of tetrabenzoporphyrins and texaphyrin in bacterial cells. Lasers Med Sci. 1993;8(3):197-203.

498. Ito T, Kobayashi K. *In vivo* evidence for the photodynamic membrane damage as a determining step of the inactivation of yeast cells sensitized by toluidine blue. Photochem Photobiol. 1977;25(4):399-401.

499. Bombelli C, Bordi F, Ferro S, Giansanti L, Jori G, Mancini G, et al. New cationic liposomes as vehicles of m-tetrahydroxyphenylchlorin in photodynamic therapy of infectious diseases. Mol Pharm. 2008;5(4):672-9.

500. Grinholc M, Szramka B, Olender K, Graczyk A. Bactericidal effect of photodynamic therapy against methicillin-resistant *Staphylococcus aureus* strain with the use of various porphyrin photosensitizers. Acta Biochim Pol. 2007;54(3):665-70.

501. Maisch T, Baier J, Franz B, Maier M, Landthaler M, Szeimies R-M, et al. The role of singlet oxygen and oxygen concentration in photodynamic inactivation of bacteria. Proc Natl Acad Sci USA. 2007;104(17):7223-8.

502. North J, Coombs R, Levy J. Photodynamic inactivation of free and cell-associated HIV-1 using the photosensitizer, benzoporphyrin derivative. JAIDS. 1994;7(9):891-8.

503. Trannoy LL, Terpstra FG, De Korte D, Lagerberg JWM, Verhoeven AJ, Brand A, et al. Differential sensitivities of pathogens in red cell concentrates to Tri-P(4)-photoinactivation. Vox Sang. 2006;91(2):111-8.

504. Wilson M, Yianni C. Killing of methicillin-resistant *Staphylococcus aureus* by low-power laser light. J Med Microbiol. 1995(42):62-6.

505. Contag C, Contag P, Mullins J, Spilman S, Stevenson D, Benaron D. Photonic detection of bacterial pathogens in living hosts. Mol Microbiol. 1995 4(18):593-603.

506. Brock M, Jouvion G, Droin-Bergere S, Dussurget O, Nicola M, Ibrahim-Granet O. Bioluminescent *Aspergillus fumigatus*, a new tool for drug efficiency testing and *in vivo* monitoring of invasive aspergillosis. Appl Environ Microbiol. 2008;74(22):7023.

507. Doyle TC, Nawotka KA, Kawahara CB, Francis KP, Contag PR. Visualizing fungal infections in living mice using bioluminescent pathogenic *Candida albicans* strains transformed with the firefly luciferase gene. Microb Pathog. 2006;40(2):82-90.

508. Hamblin MR, O'Donnell DA, Murthy N, Contag CH, Hasan T. Rapid control of wound infections by targeted photodynamic therapy monitored by *in vivo* bioluminescence imaging. Photochem Photobiol. 2002;75:51 - 7.

509. Hamblin MR, Zahra T, Contag CH, McManus AT, Hasan T. Optical monitoring and treatment of potentially lethal wound infections *in vivo*. J Infect Dis. 2003;187(11):1717-26.

510. Demidova TN, Gad F, Zahra T, Francis KP, Hamblin MR. Monitoring photodynamic therapy of localized infections by bioluminescence imaging of genetically engineered bacteria. J Photochem Photobiol B. 2005;81(1):15-25.

511. Francis KP, Yu J, Bellinger-Kawahara C, Joh D, Hawkinson MJ, Xiao G, et al. Visualizing pneumococcal infections in the lungs of live mice using bioluminescent *Streptococcus pneumoniae* transformed with a novel Gram-positive *lux* transposon. Infect Immun. 2001;69(5):3350-8.

512. Lambrechts SAG, Demidova TN, Aalders MCG, Hasan T, Hamblin MR. Photodynamic therapy for *Staphylococcus aureus* infected burn wounds in mice. Photochem Photobiol Sci. 2005;4(7):503-9.

513. Maoz A, Mayr R, Bresolin G, Neuhaus K, Francis KP, Scherer S. Sensitive *in situ* monitoring of a recombinant bioluminescent *Yersinia enterocolitica* reporter mutant in real time on camembert cheese. Appl Environ Microbiol. 2002;68(11):5737-40.

514. Dai T, Tegos GP, Lu Z, Zhiyentayev T, Franklin MJ, Baer DG, et al. Photodynamic therapy for *Acinetobacter baumannii* burn infections in mice. Antimicrob Agents Chemother. 2009.

515. Kaplan HB, Greenberg EP. Overproduction and purification of the *luxR* gene product: transcriptional activator of the *Vibrio fischeri* luminescence system. Proc Natl Acad Sci USA. 1987;84(19):6639-43.

516. Slock J, VanRiet D, Kolibachuk D, Greenberg EP. Critical regions of the *Vibrio fischeri luxR* protein defined by mutational analysis. J Bacteriol. 1990;172(7):3974-9.

517. Olafsen JA. Interactions between fish larvae and bacteria in marine aquaculture. Aquaculture. 2001;200(1-2):223-47.

518. Muroga K. Viral and bacterial diseases of marine fish and shellfish in Japanese hatcheries. Aquaculture. 2001;202(1-2):23-44.

519. Defoirdt T, Boon N, Sorgeloos P, Verstraete W, Bossier P. Alternatives to antibiotics to control bacterial infections: luminescent vibriosis in aquaculture as an example. Trends Biotechnol. 2007;25(10):472-9.

520. Moriarty DJW. Control of luminous *Vibrio* species in penaeid aquaculture ponds. Aquaculture. 1998;164(1-4):351-8.

521. Moriarty DJW. Disease control in shrimp aquaculture with probiotic bacteria. Microbial biosystems: new frontiers. In: Bell CR, Brylinsky M, Johnson-Green P, editors. Proceeding of the 8th International Symposium on Microbial Ecology. Canada: Microbial Interactions in Aquaculture; 1999.

522. Shao ZJ. Aquaculture pharmaceuticals and biologicals: current perspectives and future possibilities. Adv Drug Deliver Rev. 2001;50(3):229-43.

523. Toranzo AE, Magariños B, Romalde JL. A review of the main bacterial fish diseases in mariculture systems. Aquaculture. 2005;246(1-4):37-61.

524. Arijo S, Rico R, Chabrillon M, Diaz-Rosales P, Martínez-Manzanares E, Balebona MC, et al. Effectiveness of a divalent vaccine for sole, *Solea senegalensis* (Kaup), against *Vibrio harveyi* and *Photobacterium damselae* subsp. *piscicida*. J Fish Dis. 2005;28(1):33-8.

525. Reed PA, Francis-Floyd R. *Vibrio* infections of fish. FA-31, Department of fisheries and aquatic sciences, Florida cooperative extension service, Institute of Food and Agricultural Sciences. Gainesville: University of Florida; 1996.

526. Romalde J. *Photobacterium damselae* subsp. *piscicida*: an integrated view of a bacterial fish pathogen. Int Microbiol. 2002;5(1):3-9.

527. Vadstein O. The use of immunostimulation in marine larviculture: possibilities and challenges. Aquaculture. 1997;155(1-4):401-17.

528. Cabello FC. Heavy use of prophylactic antibiotics in aquaculture: a growing problem for human and animal health and for the environment. Environ Microbiol. 2006;8(7):1137-44.

529. Shivu MM, Rajeeva BC, Girisha SK, Karunasagar I, Krohne G. Molecular characterization of *Vibrio harveyi* bacteriophages isolated from aquaculture environments along the coast of India. Environ Microbiol. 2007;9(2):322-31.

530. Defoirdt T, Halet D, Sorgeloos P, Bossier P, Verstraete W. Short-chain fatty acids protect gnotobiotic *Artemia franciscana* from pathogenic *Vibrio campbellii*. Aquaculture. 2006;261(2):804-8.

531. Halet D, Defoirdt T, Van Damme P, Vervaeren H, Forrez I, Van de Wiele T, et al. Poly-beta-hydroxybutyrate-accumulating bacteria protect gnotobiotic *Artemia franciscana* from pathogenic *Vibrio campbellii*. FEMS Microbiology Ecology. 2007;60(3):363-9.

532. Defoirdt T, Boon N, Bossier P. Can bacteria evolve resistance to quorum sensing disruption? PLoS Pathog. 2010;6(7).

533. Lio-Po GD, Leaño EM, Peñaranda MMD, Villa-Franco AU, Sombito CD, Guanzon JNG. Anti-luminous *Vibrio* factors associated with the green water grow-out culture of the tiger shrimp *Penaeus monodon*. Aquaculture. 2005;250(1-2):1-7.

534. Maisch T. A new strategy to destroy antibiotic resistant microorganisms: antimicrobial photodynamic treatment. Mini-Rev Med Chem. 2009;9:974-83.

535. O'Connor AE, Gallagher WM, Byrne AT. Porphyrin and nonporphyrin photosensitizers in oncology: preclinical and clinical advances in photodynamic therapy. Photochem Photobiol. 2009;85(5):1053-74.

536. Ortner M-A. Photodynamic therapy for cholangiocarcinoma: overview and new developments. Curr Opin Gastroen. 2009;25(5):472-6.

537. Smits T, Moor ACE. New aspects in photodynamic therapy of actinic keratoses. J Photochem Photobiol B. 2009;96(3):159-69.

538. Rotomskis R, Streckyte G, Bagdonas S. Phototransformations of sensitizers 2. Photoproducts formed in aqueous solutions of porphyrins. J Photochem Photobiol B. 1997;39(2):172-5.

539. Bertoloni G, Reddi E, Gatta M, Burlini C, Jori G. Factors influencing the haematoporphyrin-sensitized photoinactivation of *Candida albicans*. J Gen Microbiol. 1989;135(4):957-66.

540. Carvalho G, Felipe M, Costa M. The photodynamic effect of methylene blue and toluidine blue on *Candida albicans* is dependent on medium conditions. J Microbiol. 2009;47(5):619-23.

541. West CML, Moore JV. Cell survival characteristics of a human colon adenocarcinoma cell line after photodynamic treatment: a comparison of photofrin II and TPPS. Int J Radiat Biol. 1988;54(4):621-34.

542. Watts RJ, Kong S, Orr MP, Miller GC, Henry BE. Photocatalytic inactivation of coliform bacteria and viruses in secondary wastewater effluent. Water Res. 1995;29(1):95-100.

543. Klein G, Zmijewski M, Krzewska J, Czeczatka M, Lipinska B. Cloning and characterization of the *dnaK* heat shock operon of the marine bacterium *Vibrio harveyi*. Mol Gen Genet. 1998;259:179-89.

544. Acher AJ, Fischer E, Manor Y. Sunlight disinfection of domestic effluents for agricultural use. Water Res. 1994;28(5):1153-60.

545. Prates R, da Silva E, Yamada A, Suzuki L, Paula C, Ribeiro M. Light parameters influence cell viability in antifungal photodynamic therapy in a fluence and rate fluence-dependent manner. Laser Phys. 2009;19(5):1038-44.

546. Somani S, Ingole N, Principal I, Ghatkhed A. Alternative approach to chlorination for disinfection of drinking water - an overview. Int J Adv Eng Res Stud. 2011;1(1):47-50.

547. Oleinick NL. Basic photosensitization [Internet]. American Society for Photobiology; 2011 [updated 2011 Sep 9; cited 2011 13 Nov]; Available from: http://www.photobiology.info/Oleinick.html.

548. Benabbou AK, Guillard C, Pigeot-Rémy S, Cantau C, Pigot T, Lejeune P, et al. Water disinfection using photosensitizers supported on silica. J Photochem Photobiol A. 2011;219(1):101-8.

549. Chen C-P, Chen C-T, Tsai T. Chitosan nanoparticles for antimicrobial photodynamic inactivation: characterization and *in vitro* investigation. Photochem Photobiol. 2012;88(3):570-6.

550. Laurent S, Forge D, Port M, Roch A, Robic C, Vander Elst L, et al. Magnetic iron oxide nanoparticles: synthesis, stabilization, vectorization, physicochemical characterizations, and biological applications. Chem Rev 2008;108(6):2064-110.

551. Figueira F, Cavaleiro JAS, Tomé JPC. Silica nanoparticles functionalized with porphyrins and analogs for biomedical studies. J Porphyr Phthalocyanines. 2011;15(07n08):517-33.

552. Liu X, Ma Z, Xing J, Liu H. Preparation and characterization of amino–silane modified superparamagnetic silica nanospheres. J Magn Magn Mater. 2004;270(1–2):1-6.

553. Zhao S-Y, Qiao R, Zhang XL, Kang YS. Preparation and reversible phase transfer of $CoFe_2O_4$ nanoparticles. J Phys Chem C Nanomater Interfaces. 2007;111(22):7875-8.

554. Orlandi VT, Caruso E, Banfi S, Barbieri P. Effect of organic matter on the *in vitro* photoeradication of *Pseudomonas aeruginosa* by means of a cationic tetraaryl-porphyrin. Photochem Photobiol. 2012;88(3):557-64.